THE UNIVERSITY *of* EDINBURGH

Characterisation of a Model of ALS8 in the Rat

Brenda Murage B.Sc. (Hons), M.Sc.

A thesis submitted for the degree of Doctor of Philosophy at the University of Edinburgh

November 2022

Declaration

I hereby declare that I have solely completed this thesis with the exception of the following:

1. CLICK (CRISPR with lssDNA inducing conditional knockout alleles) generation of rats and establishment of initial colony from founding individuals, completed by Professor Tomoji Mashimo and colleagues
2. Protocol for extracting cerebrospinal fluid developed in conjunction with Dr Mosi Li, becoming a University of Edinburgh Bioresearch and Veterinary Services Standard Operating Procedure 19_014
3. Production of antisera against vapB and vapA carried out by Dr Paul Skehel
4. Analysis of CatWalk gait data aided by Han Tan
5. Iba-1 immunofluorescence for individual 502 completed by Dr Paul Skehel
6. Immunoblots of lumbar spinal cord homogenate for Iba-1, Ceramide Transfer Protein (CERT), Glucose-Regulated Protein 78 (GRP78/BiP), and Protein tyrosine phosphatase interacting protein 51 (PTPIP51), were carried out by Dr Paul Skehel
7. Preparation of hippocampal cultures for Seahorse mitochondrial stress experiments was carried out by Dr Paul Skehel

This body of work has not been submitted for any other degree or professional qualification.

Signed: Dated: 20/11/2022

Acknowledgements

First and foremost, I would like to thank the Euan Macdonald Centre for funding my work. I would also like to thank my extremely patient and ever-supportive supervisors, Dr Paul Skehel and Dr Mandy Jackson for their swift constructive feedback, understanding, and generosity which I appreciate more than they know. Thank you to Professor Tomoji Mashomo and colleagues for the generation of the founders of the colony.

Thank you to Professor Ian Duguid and his team for obtaining and setting up the CatWalk apparatus, especially Sarah Giachetti who worked extremely hard to get the apparatus set up initially. Thanks also to Dr Mosi Li for helping to develop the protocol for collecting cerebrospinal fluid from rats. Thanks to Han Tan for rationalising the CatWalk analysis, and to Marie Bowers who taught me so much about working with rats. Thanks to Neil Odey, Christopher Lockheart, and all of the animal technicians for constant vigilance over the colony, and for being so helpful and kind over my requests.

I would also like to thank the wonderful people at the Hugh Robson building, from the Telfer group (special thanks to Yvonne for dealing with a torrent of questions with a smile), the Gillingwater and Murray groups for constant technical and emotional support over coffee (thanks to Ines and Dinja for the many wise words) the Wishart group (Rachel and her fantastic enthusiasm), and the wider PhD and postdoctoral community who have been the most wonderful people to have met and worked with (thanks to Sean, Paul, Alison, Liz, Tina, Christina, and Jini).

Finally, I would like to thank my family who have gone above and beyond to get me here. It is a debt that can never be repaid.

Dedicated to my beloved grandfather, Simon Wanjohi, and his inexhaustible drive to learn about the world around him.

Abstract

Amyotrophic lateral sclerosis 8 (ALS8) is a late-onset slow-progressing form of motor neurone disease caused by a missense mutation replacing cytosine with thymine in the VAMP-associated protein B (vapB) gene, leading to a proline to serine replacement at position 56 (P56S) in the protein. The vapB protein is ubiquitously expressed in humans and located on the endoplasmic reticulum (ER). It is involved in intracellular signalling through two phenylalanine in a fatty acidic tract (FFAT)-like motifs on target proteins binding the major sperm protein domain (MSP) which can also cleave for extracellular signalling. The vapB^{P56S} mutation interferes with MSP cleavage and vapB function by preventing cleavage of the MSP domain. CRISPR with long single stranded DNA inducing conditional knockout alleles (CLICK) was used to generate founders of a colony, with heterozygous (vapB$^{P56S/+}$), homozygous (vapB$^{P56S/P56S}$), and knockout (vapB$^{-/-}$) offspring. A cohort was aged to 17-18 months in a longitudinal study with gait being assessed at 6, 12, and 18 months. Male vapB$^{P56S/P56S}$, female vapB$^{P56S/P56S}$ and female vapB$^{-/-}$ exerted less pressure on their paws at 18 months. Tissue was collected at 18 months and analysed. There were fewer motor neurons (MN) in the lumbar spinal cord of vapB$^{P56S/+}$ and vapB$^{P56S/P56S}$, and MN were smaller in vapB$^{P56S/P56S}$. TDP-43 pathology was present in vapB$^{-/-}$ motor neurons, and syntaxin 1A signal was reduced in lumbar spinal homogenates, but glial activation was absent. These results show that this rat model could help to provide insight into the initiation and propagation of ALS8.

Lay Summary

Motor neuron disease is an umbrella term for a group of diseases affecting the central nervous system and muscles involved in voluntary movement, leading to a deterioration of muscle control over time. One of these diseases, amyotrophic lateral sclerosis 8 (ALS8), is caused by a mutation in the vapB gene which changes the function of the protein created from that gene. The mutation linked to ALS8 was introduced into the rat version of the gene to see how it affected movement and the cells that send signals to muscles for movement which are called motor neurons. Rats that carried the mutation had smaller and fewer motor neurons than rats without the mutation. They also used tiptoe-like gait when walking, which indicates a significant change in their movement, and a cellular marker of ALS was present in cells where vapB was not functional. These results indicate that this rat model could offer clues into how motor neuron diseases start and progress over time.

Table of Contents

List of Figures

List of Tables

List of Abbreviations

ATP	Adenosine triphosphate
AD	Alzheimer's Disease
ALS	Amyotrophic lLateral sSclerosis
ALS8	Amyotrophic lLateral sSclerosis 8
APOE	Apolipoprotein E
βA	β-amyloid
BBB	Blood-brain barrier
BoS	Base of sSupport
C9orf72	Chromosome 9 open reading frame 72
CCD	Coiled cCoil dDomain
CD8+	Cytotoxic T-lymphocytes
CLICK	CRISPR with lssDNA inducing conditional knockout alleles
CSF	Cerebrospinal fFluid
CSMN	Corticospinal motor neuron
EAAT	Excitatory amino acid transporter
ECAR	Extracellular acidification rate
ECGGlut4	ElectrocardiogramGlucose-4-transporter
Eph	Ephrin
ER	Endoplasmic rReticulum
ERAD	ER-associated protein degradation
ERAD	Endoplasmic reticulum-associated degradation
ETC	Electron transport chain
FALS	Familial ALS
FCCP	Carbonilcyanide p-triflouromethoxyphenylhydrazone
FFAT	Two phenylalanines in an acidic tract
FIP200	FAK family-interacting protein of 200kDa
FTLD	Frontotemporal lLobe Dementiademention
FUS	Fused in sSarcoma
GFP	Green fluorescent protein
GLT-1	Glutamate transporter 1
GLT-1	Glutamate receptors

GLUT1	Glucose transporter 1
Glut4	Glucose-4-transporter
gRNA	Guide RNA
HD	Huntington's Disease
HGB	Haemoglobin
HGBAc1	Haemoglobin Ac1
Hsc70	Heat shock cognate 70
iNOS	Induced nitric oxide synthase
iPSC	Induced pluripotent stem cell
LAR	Leukocyte common antigen-related-like receptors
LSC	Lumbar sSpinal cCord
lssDNA	Long single stranded DNA
MCT	monocarboxylate transporter
MN	Motor neuron
MOSPD	Motile perm domain-containing protein
mRNA	Messenger RNA
MSP	Major sSperm pProtein
Nir	Phosphatidylinositol-transfer proteins
Nir1, Nir2, Nir3	Phosphatidylinositol-transfer proteins (Near Infrared)
NMJ	Neuromuscular jJunction
OCR	Oxygen consumption rate
Osbp	Oxysterol binding protein
OSBP	Oxysterol binding protein (OSBP
P56S	Proline to Serine replacement at amino acid position 56
P62	Sequestosome 1
PD	Parkinson's Disease
PLS	Primary lateral sclerosis
PTPIP51	Protein tyrosine phosphatase interacting protein 51
RBC	Red blood cell/erythrocyte
ROS	Reactive oxygen species
SALS	Sporadic ALS
SMA	Spinal muscular atrophy
SMN	Spinal motor neuron

SMN 1, SMN 2	Survival motor neuron proteins 1 and 2
SOD1	Copper/zZinc s Superoxide dDismutase
TARDBP/TDP-43	Transactive responseAR DNA-binding protein
TCA	Tricarboxylic Acid cycle
TMD	Transmembrane dDomain
Tregs	Regulatory T cells
TUBB1	Tubulin β1
UBQLN2	Ubiquilin 2
ULK	Unk 51-like autophagy activating kinase
UPR	Unfolded protein response
UPS	Ubiquitin-proteasome system
VAMP	Vesicle-associated membrane protein
VAP-33	VAMP-associated protein of 33 kilo Daltons
vapA	VAP-associated protein A (vapB homologue)
vapB	VAP-associated protein B
$vapB^{-/-}$	Rats homozygous for the knockout of exon 2 of vapB
$vapB^{P56S/+}$	Rats heterozygous for the P56S mutation
$vapB^{P56S/P56S}$	Rats homozygous for the P56S mutation
vapC	VAP-associated protein C (vapB splice variant)
VEGF	Vascular endothelial growth factor

1 Introduction

1.1 Neurodegeneration and Motor Neuron Diseases

Neurodegeneration refers to the progressive loss of cells in the central and/or peripheral nervous system. Some cellular mechanisms have been studied as potential culprits of neurodegeneration.

1.1.1 Protein Misfolding and Aggregation

Of all transcribed proteins, around 30% are misfolded (Schubert et al., 2000), affecting the tertiary structure of the protein and modifying or eliminating sites that would usually interact with cellular targets, and ultimately modifying or eliminating the protein's role with adverse downstream effects. Aggregation of misfolded proteins is a common hallmark of neurodegenerative diseases due to regions of the protein, usually hidden away in its native tertiary structure, being exposed and forming bonds with similarly exposed regions in other copies of misfolded protein. This leads to the build-up of oligomers of various lengths, which have been shown to induce apoptosis in cells (Demuro et al., 2005, Simoneau et al., 2007).

Famously, β-amyloid (βA) and tau proteins form plaques and neurofibrillary tangles respectively in the cortex of patients diagnosed with Alzheimer's disease (AD) (Masters et al., 1985, Grundke-Iqbal et al., 1987), with misfolding of the former occurring up to 14 years before clinical symptoms emerge (Stocker et al., 2020). Parkinson's disease (PD) is characterised histologically by the presence of Lewy bodies and Lewy Neurites composed of alpha-synuclein aggregates (Polymeropoulos et al., 1997). Mutations in the huntingtin gene leads to the production of misfolded protein in Huntington's disease (HD) (Neueder et al., 2017).

The aggregation of misfolded proteins is thought to progress through seeding nucleation where small oligomers of misfolded protein grow to a thermodynamically-favourable size, and increase in size at a faster rate (Chothia and Janin, 1975). As post-mitotic cells, neurons heavily rely on mechanisms that clear misfolded proteins and protect cells from aggregate formation. Proteins are folded in the endoplasmic reticulum (ER) before translocation to their target site, and misfolded proteins are cleared by the ER-associated degradation pathway (ERAD), which transports proteins out of the ER for degradation by processes such as the

ubiquitin-proteasome system (UPS) or the autophagy-lysosome system (Halbleib et al., 2017, Baldridge and Rapoport, 2016).

Molecular chaperones, such as heat shock cognate 70 (Hsc70), recognise exposed hydrophobic domains of misfolded proteins and can aid their refolding, or assist in their degradation through the UPS, or the autophagy-lysosome system (Bercovich et al., 1997, Ciechanover et al., 1995). UPS degrades proteins by tagging them with chains of ubiquitin, which are recognised by the proteasome which degrades target proteins into peptides (Arrigo et al., 1988), which are then further degraded to their constituent amino acids by peptidases (Reits et al., 2003, Reits et al., 2004). The autophagy-lysosome system involves lysosomes taking in targets through a transmembrane translocation complex (Cuervo and Dice, 1996), or through invagination (Sattler and Mayer, 2000). Lysosomes can also take part in macroautophagy where targets are enveloped in membrane to form a phagophore (Suzuki et al., 2001), which develops into an autophagosome (Abeliovich et al., 2000), which fuses with lysosomes (Nguyen et al., 2016), which use their acidic environment filled with hydrolases to degrade material in the autophagosome (G.M., 2000). This fusion is enabled through proteins involved in the SNARE complex (soluble N-ethylmaleimide-sensitive factor attachment protein receptor), which also has roles in vesicle recycling (Mori et al., 2021) and neurotransmitter release (Xu et al., 1999).

1.1.2 Neuroinflammation

Neuroinflammation is also implicated in neurodegeneration, primarily enacted by glial cells, which are non-neuronal populations of cells in the nervous system. Whilst important for promoting tissue repair and removing cellular debris (Albrecht et al., 2003, Miron et al., 2013), persistent inflammatory responses can lead to damage and progressive neurodegeneration.

Microglia are the innate immune cells of the nervous system, and can release neuroprotective or neurotoxic factors, as well as phagocytose and clear debris (Sierra et al., 2010, Chen et al., 2019, Zhou et al., 2020). Whilst morphology varies (Lawson et al., 1990), microglia constantly monitor their microenvironment for any sign of damage or infection (Wake et al., 2009), can change morphology from ramified to amoeboid (Das Sarma et al., 2013, Nimmerjahn et al., 2005), and are able to translocate to target sites (Davalos et al., 2005a). They can release anti-inflammatory cytokines and growth factors to aid repair (Park et al., 2007), and can release

toxic factors to kill invading pathogens and recruit help via the release of pro-inflammatory cytokines (Fenn et al., 2014). In the event of prolonged exposure to stressors such as physical injury, excessive heat, or ageing, long-lasting activation of microglia could become damaging to surrounding tissue and contribute to neurodegenerative diseases (Baniasadi et al., 2020, Barcia et al., 2011). Their morphology and activity can be location-dependent, such as βA plaque adjacent microglia in AD undergo major changes whereas plaque-distant microglia show only minor changes (Plescher et al., 2018). Pro-inflammatory cytokines were significantly elevated in patients with PD (Qin et al., 2016). Microglia were shown to release elevated levels of reactive oxygen species in pluripotent stem cells from HD patients (O'Regan et al., 2021).

Astrocytes are star-shaped glial cells that have key roles in maintaining the central nervous system blood-brain barrier (BBB), providing energy through metabolites to neurons, modulating synaptic activity, and in glial scar formation (Wolburg et al., 2009, Pellerin and Magistretti, 1994, Magistretti and Chatton, 2005, Wanner et al., 2013). Astrocytes, like microglia, activate when exposed to stress or injury by changing morphology and releasing neurotoxic or neuroprotective factors, depending on the microenvironment (Hayakawa et al., 2014, Lian et al., 2015). They also upregulate glial fibrillary acidic protein (GFAP), which could potentially have neuroprotective effects in pathological conditions (Wilhelmsson et al., 2004, Liedtke et al., 1998). There is also cross talk between astrocytes and microglia, which can activate or alleviate each other depending on the environment (Saijo et al., 2009, Liddelow et al., 2017).

1.1.3 Metabolism

Astrocytes play a key role in metabolism in the CNS as neurons are isolated from blood supply through the BBB (Ehrlich, 1885). They have a higher capacity for glucose utilisation (Jakoby et al., 2012), and provide neurons with lactate through the astrocyte-neuron lactate shuttle. Glucose transporters such as glucose transporter 1 (GLUT1) translocate glucose from capillaries to astrocytes where it is converted to pyruvate and then lactate, or is used to generate ATP. Lactate is transported to neurons via monocarboxylate transporters (MCTs) where it is converted back to pyruvate, and used for the production of cellular energy in the form of adenosine triphosphate (ATP) through aerobic respiration (Brooks, 1985). In events of increased neurotransmission, glutamate, an excitatory neurotransmitter, is taken up by

astrocytes via excitatory amino acid transporters (EAATs) and converted to glutamine, which is transported into neurons for conversion back into glutamate and re-used (Hertz and Rothman, 2016). This recycling mechanism also clears the synapse of excess glutamate which can excite post-synaptic neurons and lead to excitotoxicity (Olney, 1971, Choi et al., 1988). Astrocytes can also synthesize glutamate *de novo* from glucose through pyruvate carboxylase (Gamberino et al., 1997), and glutamate in astrocytes has been shown to be oxidised to generate ATP (McKenna, 2012, Hertz and Hertz, 2003, Sonnewald et al., 1993).

Changes to the glycolytic pathway and tricarboxylic acid (TCA) cycle have been observed in models of AD (Arias et al., 2002, van Gijsel-Bonnello et al., 2017). Plasma samples from PD patients contained significantly reductions of fatty acids, elevation of bile acids and alterations in steroid hormones compared to controls (Shao et al., 2021). Early positron emission tomography scans revealed reduced glucose metabolism in the cerebral cortex and striatum of HD patients before the emergence of clinical symptoms (Kuwert et al., 1990, Antonini et al., 1996)

Cholesterol and unsaturated fatty acids are enriched at the synaptic membrane and play key roles in membrane fluidity, vesicle formation, synaptogenesis, and ion channel function and clustering (Pani et al., 2008, Bolotina et al., 1989, Zhang et al., 2009, Mauch et al., 2001). Astrocytes provide cholesterol via the apolipoprotein E (APOE) complex to neurons to utilise, and also play a role in defending fatty acid toxicity by taking up lipoproteins carrying peroxidated lipids secreted by overstimulated neurons and storing them in lipid droplets and breaking them down (Ioannou et al., 2018).

Glucose metabolism is linked to lipid metabolism through the synthesis of cholesterol from acetyl CoA, which is a derivative of glucose (Gould et al., 1953). Therefore, changes to glucose metabolism can affect lipid metabolism. For example, glucose metabolism is altered in carriers of APOE*E4 before the appearance of symptoms of Alzheimer's disease (Reiman et al., 2004). APOE also increases calcium excitability in astrocytes (Larramona-Arcas et al., 2020). Increasing the presence of cholesterol in astrocytes has been shown to be neuroprotective (Fagan et al., 1996, Berghoff et al., 2021). Altered cholesterol metabolites found in blood and CSF (Griffiths et al., 2021, Segatto et al., 2014).

Mitochondria provide energy in the form of ATP that enables cellular processes to occur. In stress or pathological conditions, the ability to provide this energy alters to a malfunctioning

state. Less ATP is produced, more reactive oxygen species (ROS) are generated, and calcium regulation is negatively affected, causing further stress and cellular dysfunction (Cha et al., 2015, McManus et al., 2011, Peterson et al., 1985). Mitochondrial dysfunction has been implicated in neurodegeneration through these mechanisms, in conjunction with other malfunctioning cellular processes.

1.1.4 Motor Neuron Diseases

The term motor neuron disease (MND) encompass a group of diseases in which the degeneration of either upper, lower or both upper and lower motor neurons are linked with muscular atrophy and/ or weakness. With ongoing study, diagnostic criteria enable clinicians to discern MNDs from potential mimic diseases, allowing for suitable therapeutic steps to take, and enabling patients to understand their prognosis.

Primary lateral sclerosis (PLS) has been characterised as an adult- to late-onset slowly progressive upper motor neuron disease with mild or lack of lower motor neuron deficiency (Sorenson et al., 2002). Symptoms initially tend to emerge in lower limbs, but upper motor signs predominate, including hyperreflexia and pseudobulbar effect (Turner et al., 2020). PLS is sporadic, with diagnosis requiring a lack of familial history of the disease (Pringle et al., 1992), however cases of PLS patients with a family history of other motor neurons diseases have been described (Brugman et al., 2005). Underlying mechanisms are unknown due to the rarity of the disease, but TDP-43 pathology has been identified in post-mortem motor cortex (Mackenzie and Briemberg, 2020, Singer et al., 2005).

Spinal muscular atrophy (SMA) is characterised by the homozygous deletion of survival motor neuron 1 protein (SMN1) in 95% of SMN cases, and mutation in the remaining 5% of cases (Lefebvre et al., 1995). Incidence is 1 in 11,000 live births (Sugarman et al., 2012). This results in the death of alpha motor neurons in the spinal cord (Powis and Gillingwater, 2016). Subsequently, patients present with lower motor signs including muscle weakness and atrophy, although clinical presentation is heterogeneous from foetal death to mild presentation in adulthood and are classified according to age of onset and clinical severity (Finkel et al., 2014, Swoboda et al., 2005, Kaufmann et al., 2011, Oskoui et al., 2017). Although homozygous deletion of SMN1 is the key cause of the disease, heterogeneity may arise from the various number of copies of SMN2 that individuals carry (Prior et al., 2004). SMN2 cannot

fully compensate for the lost SMN protein expressed by SMN1, and a single C-T substitution in SMN2 promotes splicing of exon 7, resulting in dysfunctional truncated SMN protein (Burnett et al., 2009). SMN is thought to have roles in spliceosome formation (Chari et al., 2008), actin dynamics (Antoine et al., 2020), vesicle release (Kong et al., 2009), and mRNA transport (Fallini et al., 2011). However, precise understanding of how reduced availability of SMN leads to SMA is not completely understood.

1.2 Amyotrophic Lateral Sclerosis

The prevalence of motor neuron diseases varies geographically, but the most globally common form of motor neuron disease is amyotrophic lateral sclerosis (ALS), also known as Lou Gehrig's disease in North America, named after the famous baseball player diagnosed in 1939.

1.2.1 A Brief History

Whilst multiple clinical descriptions of progressive muscular atrophy had been described (Duchenne de Boulogne, 1851, Aran, 1850), the disease was described by Jean-Martin Charcot in 1829 after longitudinal observation of similar clinical symptoms in multiple patients (Charcot, 1869). This led to him coining the term Amyotrophic Lateral Sclerosis (ALS) after linking clinical symptoms of progressive muscular atrophy with the loss of large cells in the anterior horn and sclerosis of the lateral columns of the spinal cord. This was built upon by subsequent groups identifying the loss of Betz cells in the motor cortex (Hammer et al., 1979), which are large pyramidal motor neurons in layer Vb of the primary motor cortex, and synapse with motor neurons in the ventral horn of the spinal cord (Nieuwenhuys et al., 2008). This forms part of the link between ALS with frontotemporal lobar dementia (FDLD) (Hudson, 1981, Kiernan and Hudson, 1994), and the presence of ubiquitin-positive tau-negative protein aggregates in neurons (Leigh et al., 1988, Lowe et al., 1988) contained TDP-43 (Arai et al., 2006, Neumann et al., 2006). The advent of genetic sequencing and analysis provided further understanding of underlying molecular mechanisms involved in ALS using genes identified from families with multiple affected individuals carrying the same genetic mutations.

1.2.2 Pathophysiology

Symptoms of ALS include progressive motor impairment with lower and/or upper motor neuron signs with a focal onset, and with little sign of neuropathic pain or sensory loss (Brooks et al., 2000, Shefner et al., 2020). Some patients with lower motor neuron signs have bulbar- rather than limb-onset and display symptoms such as dysarthria and dysphagia. All of this gives ALS a heterogenic nature in the clinical presentation of the disease, which increases the risk of misdiagnosis due to some symptoms being attributed to mimic diseases such as Primary Lateral Sclerosis and Myasthenia gravis (Singer et al., 2007, Singh et al., 2018). Guidelines such as the El Escorial Criteria (Brooks, 1994), the Revised El Escorial Criteria (Brooks et al., 2000), the Awaji Criteria (de Carvalho et al., 2008), and the Gold Coast Criteria (Shefner et al., 2020) all outline clinical assessments and criteria which help clinicians to pinpoint diagnosis. The most recent takes into account ECG assessment, rigorous testing for disease mimics, and takes bulbar-onset cases into account.

Weight loss is also a key symptom as patients lose fat and muscle tissue during disease progression. Hypermetabolism alongside loss of fat and muscle tissue have also been seen as an indicator of poor clinical prognosis and survival from altered metabolism in patients (Steyn et al., 2018, Guillot et al., 2021, D'Amico et al., 2021, Lee et al., 2021, Moglia et al., 2019), perhaps exacerbated by loss of appetite reported by patients in a small study (Holm et al., 2013). Whilst loss of appetite and dysphagia amongst patients were key factors for weight loss, a subset of spinal onset of patients without dysphagia lost weight regardless of loss of appetite, disease severity, depression, or FTLD (Körner et al., 2013, Moglia et al., 2019). Hypometabolism was associated with delayed need for percutaneous endoscopic gastrostomy and ventilation alongside better survival in comparison with hypermetabolic patients (Cattaneo et al., 2021), and managed dietary intake helped to slow rapid weight loss (López-Gómez et al., 2021).

Environmental risk factors were previously considered, with the only accepted one being smoking. However, non-environmental risk factors reported in literature included genetic variants, being male, and advanced age (Oskarsson et al., 2015). A recent analysis of whole genome of SALS patients found that most carried one or more of 22 newly-identified mutations with a subset of individuals carrying 17 or more of the novel mutations (Logan et al., 2022), leading to the theory that SALS cases arise from interactions between multiple

genetic factors (Luigetti et al., 2011, Chiò et al., 2012, van Blitterswijk et al., 2012a, Pottier et al., 2015).

Whilst astrogliosis has been shown to dampen initial CNS damage and induce repair after spinal cord injury (Wanner et al., 2013), increasing evidence shows a role for astrogliosis in MN loss in models of ALS such as SOD1 (Wong et al., 1995, Bi et al., 2013, Nagai et al., 2007), FUS (Sharma et al., 2016), and TARDBP (Tong et al., 2013, Yang et al., 2014), and in samples from ALS patients (Haidet-Phillips et al., 2011). Evidence suggests astrocyte-induced upregulation of the glutamate receptor subunit GluR2 in neighbouring MNs, giving rise to MN excitotoxicity and progressing neurodegeneration (Van Damme et al., 2007, Haidet-Phillips et al., 2011, Meyer et al., 2014). Microglia act as the innate immune cells of the nervous system, scanning their surroundings for signs of injury or infection and responding to them (Nimmerjahn et al., 2005, Davalos et al., 2005b). Microglial activation been implicated in models of ALS such as SOD1 (Almer et al., 1999), TDP-43 (Zhao et al., 2015), FUS (Ajmone-Cat et al., 2019), and C9orf72 (O'Rourke et al., 2016), as well as in patient post-mortem samples (Brettschneider et al., 2012, Dols-Icardo et al., 2020). However, this has been controversial as microgliosis may be linked to normal brain ageing, which needs to be taken into account as ALS is a late-onset disease (Soreq et al., 2017).

There are only 2 drugs that have been clinically shown to delay the need for invasive ventilation by a number of months – Riluzole and Edaravone (Bensimon et al., 1994, Abe et al., 2014).

1.2.3 Disease causing genes of familial ALS

Of all ALS cases, 90% are sporadic (SALS) and 10% are inherited familial cases (FALS) (Turner et al., 2013). These familial cases provide a foothold for investigating underlying mechanisms of ALS through genetic components passed between generations.

The most commonly occurring genes in FALS cases are in copper/zinc Superoxide Dismutase (SOD1) (Rosen et al., 1993a), the nuclear protein fused in sarcoma (FUS) (Vance et al., 2009b), TAR DNA-binding protein 43 (TARDBP) (Sreedharan et al., 2008), and chromosome 9 open reading frame 72 (C9orf72) (DeJesus-Hernandez et al., 2011, Brown and Al-Chalabi, 2017). Most lead to protein misfolding, which is a hallmark of neurodegenerative diseases, and has been partially ameliorated in disease models by the introduction of cytosolic and ER

chaperone proteins which help with protein folding, including heat shock proteins (Malik et al., 2013, Lin et al., 2013, Crippa et al., 2016). However, motor neurons appear particularly susceptible due to their large size, vital need for efficient axonal transport of resources to and from the soma, and reliance on good protein quality control to prevent accumulation of misfolded proteins (Puga et al., 2015).

1.2.3.1 SOD1

SOD1 was the first gene to be identified and linked to FALS (Rosen et al., 1993a), with the same molecular signature of aberrant 32kDa SOD1 protein in spinal cord samples from FALS and SALS patients (Gruzman et al., 2007). SOD1 encodes the homodimeric copper/zinc superoxide dismutase protein which protects the cell from damage by reactive oxygen species by converting superoxide anion to hydrogen peroxide, which is further reduced to water by glutathione peroxidase (Fridovich, 1986).

Many mutations within the gene have been identified that link SOD1 to ALS, with the most common in Europe, North America, and Russia being D90A, which is mostly inherited recessively (Andersen et al., 1996), and the most studied being G93A, due to the successful development of a mouse model with a well-characterised phenotype (Gurney et al., 1994b). Most SOD1 mutations are inherited in an autosomal dominant manner (Rosen et al., 1993b), and lead to toxic gain of function from misfolded SOD1 creating insoluble aggregates, disrupting cellular homeostasis by as yet unknown mechanisms (McAlary et al., 2016).

1.2.3.2 TARDBP

TAR DNA-binding protein 43 (TARDBP), the gene that encodes TDP-43, was initially identified as suppressor of HIV1-1 gene expression (Ou et al., 1995), but was subsequently identified in ubiquitin-positive tau-negative aggregates in cortical samples from ALS and FTLD patients (Arai et al., 2006, Neumann et al., 2006). TDP-43 is a nuclear RNA-binding protein involved in RNA processing, including splicing and transport (Sreedharan et al., 2008, Rutherford et al., 2008). Although it is primarily located in the nucleus, it shuttles between the nucleus and cytoplasm (Tziortzouda et al., 2021). Under pathological conditions, abnormal truncated forms of the TDP-43 protein mislocalizes to cytoplasmic inclusions (Neumann et al., 2006, Chen et al., 2004), a pathology seen in the post-mortem tissue in the majority of ALS patients not carrying ALS-linked mutations in SOD1 or fused in sarcoma (FUS) (Mackenzie et al., 2007a,

Kwiatkowski et al., 2009). This is also replicated in models of the disease amongst a number of ALS-linked mutations of TDP-43 (Barmada et al., 2010, Mutihac et al., 2015, Chen et al., 2010a) and has become a key histological marker of ALS in both FALS and SALS cases (Sreedharan et al., 2008). Mechanisms explaining the link to TDP-43 mislocalisation to neurodegeneration is unclear, but its depletion or overexpression leads to neurotoxicity (Iguchi et al., 2013, Wu et al., 2012, Kabashi et al., 2010), and its deletion is embryonically lethal in mice (Kraemer et al., 2010).

1.2.3.3 FUS

Fused in Sarcoma (FUS) is an RNA binding protein localised to the nucleus, but, like TDP-43, shuttles between the nucleus and cytoplasm (Zinszner et al., 1997). ALS-linked FUS mutations, especially those located in its nuclear localisation signal domain (NLS), lead to mislocalisation and aggregate formation in the cytoplasm (Niu et al., 2012). Mutations account for 4% of SALS cases, and FUS pathology appears in cases of ALS where there is no TDP-43 pathology for, as yet, unknown reasons (Vance et al., 2009a). FUS is involved in messenger RNA (mRNA) transport and translocation (Fujii and Takumi, 2005, Yasuda et al., 2013), mediates mRNA splicing and silencing (Lagier-Tourenne et al., 2012, Zhang et al., 2013), is recruited into stress granules under stress conditions (Lenzi et al., 2015), and promoted DNA repair under stress (Wang et al., 2013a). ALS-linked mutations affect the ability of FUS to properly mediate RNA metabolism (Lagier-Tourenne et al., 2012), stress response (Lenzi et al., 2015, Dormann et al., 2010), or DNA repair (Deng et al., 2015).

1.2.3.4 C9orf72

The hexanucleotide GGGGCC repeat expansion in the non-coding region of the C9orf72 gene was identified in 2011 (DeJesus-Hernandez et al., 2011, Renton et al., 2011, Gijselinck et al., 2012), and has been shown to be the most common genetic cause of ALs and FLTD in Europe and North America (DeJesus-Hernandez et al., 2011). Whist the true threshold of hexanucleotide repeats is unclear, most healthy individuals carry less than 11 repeats whilst ALs patients are heterozygous for hundreds or thousands of repeats (DeJesus-Hernandez et al., 2011, van Blitterswijk et al., 2013). Theories underlying disease mechanisms include the repeats leading to loss of function through haploinsufficiency (Shao et al., 2019), the repeats being translated to expanded RNAs that accumulate into foci (Lee et al., 2013, Mori et al.,

2013), or the expanded RNAs being transcribed into dipeptide repeat proteins which also accumulate into foci . TDP-43 inclusions were also identified in neurons of patients carrying the repeat expansions (Cook et al., 2020). Mounting evidence suggests a combination of the described mechanisms leading to ALS pathology (Shao et al., 2019, Zhu et al., 2020)

1.2.4 ALS Disease Models

In order to study cellular roles and possible disease mechanisms, transgenic techniques allowed the development of disease models. A motor neuron cell line, NSC34, transfected to express $SOD1^{G93A}$ demonstrated morphological changes to mitochondria accompanied by decreases in electron transport chain activity, and increased cell death in an oxidative environment compared to controls (Menzies et al., 2002). *C.elegans* expressing human $vapB^{P56S}$ presented with adverse locomotion and axonal misguidance, whilst knocking out the homologue *vpr-1* induced age-progressive motor neuron death (Zhang et al., 2017). Induced pluripotent stem cells (iPSCs) from ALS patients revealed transcriptomic commonalities, with potential for use as predictive markers of ALS (Ho et al., 2021). Recently, organoids developed from iPSCs from ALS patients demonstrated altered transcriptomic and DNA repair in astrocytes and neurons in one system (Szebényi et al., 2021).

1.2.4.1 Rodent Models

Rodent models have been a key step in translational neuroscience as system effects of a genetic component observed in a mammal system, or treatments successful in cell lines and non-mammalian organisms could be tested for effectiveness and potential side effects in a more complex biological system. Whilst some rat models of ALS do exist, most have been developed in the mouse.

1.2.4.1.a SOD1 Mice

The most commonly used animal model is the $SOD1^{G93A}$ mouse, which has a well-characterised disease phenotype with consistent progressive loss of spinal motor neurons and muscle atrophy (Gurney et al., 1994a). The SOD1 model helped determine the non-cell autonomous nature of ALS where glial cells were revealed to have roles in the disease, such as the reduction of astrocyte glutamate GLT-1 receptors leading to increased levels of glutamate at synaptic clefts and opening motor neurons to excitotoxicity (Rothstein et al.,

1992). The degeneration of cortical MNs has been reported inconsistently, but is key in the diagnosis of ALS1 (Thomsen et al., 2014, Ozdinler et al.)

1.2.4.1.b TDP-43 Mice

Knocking out TDP-43 in mice was embryonically lethal, but heterozygous mice lived long enough to develop late-onset motor deficits (Kraemer et al., 2010). Reducing expression through the use of conditional floxed TDP-43 resulted in rapid loss of fat and death 9 days after expression was halted (Chiang et al., 2010). Over-expression of TDP-43 led to changes in gait and weight loss coinciding with the loss of corticospinal axons, and TDP-43 proteinopathy in cortical motor neurons (Wegorzewska et al., 2009b, Hatzipetros et al., 2014). Recently, a promising TDP-43 knock-in model in the mouse presented with all of the hallmarks of ALS-TDP pathology from motor deficit down to cellular process, such as abnormal RNA splicing of spinal Bcl-2 pre-mRNA leading to the increase of the negative regulator of autophagy (Huang et al., 2020). A commercial model over-expressing human TDP-43^{Q331K} was recently characterised and found to have significantly reduce muscle mass and function in the hind limbs, increased weight gain, and a lack of classical TDP-43 proteinopathy but an increase in TDP-43 expression in motor neuron nuclei compared to control (Watkins et al., 2021).

1.2.4.1.c FUS Mice

Ubiquitous overexpression of FUS/TLS-R521C led to damage of the BDNF gene, leading to downstream defects in dendritic growth and synapse formation. Splicing defects of other genes involved in those roles was also observed, potentially further exacerbating the presenting symptoms (Qiu et al., 2014). Expression of ΔFUS(1-359) in mice led to late-onset pathology where large cytoplasmic inclusions develop, pro-inflammatory microglia become active, and acetylcholine neurotransmission failed in motor neurons (Funikov et al., 2018). Another model demonstrated how the over expression of human FUS increases downregulation of endogenous FUS, leading to a rapid progressive phenotype and dysregulation of gene expression from defective RNA metabolism (Ling et al., 2019). Mice over-expressing wild type FUS had reduced histone acetylation, which was ameliorated by treatment with a potent histone deacetylase inhibitor and improving survival (Rossaert et al., 2019). A FUS knock-in model demonstrated dysfunction in stress granule processing (Zhang et al., 2020), whilst an over-expression model had accumulation of FUS at synapses, and

evidence of synaptic RNA dysregulation (Sahadevan et al., 2021). Knock-in mice (FUSP525L) were shown to have reduced expression of FUS in the brain and spinal cord and delaying motor neuron degeneration when FUS antisense oligonucleotide was used to silence FUS (Korobeynikov et al., 2022).

1.2.4.1.d C9orf72 Mice

Nuclear foci, dipeptide repeat proteins, TDP-43 pathology, motor deficits, behavioural changes, weight loss, and cortical neuron loss were all observed in the cortices of mice expressing $(G_4C_2)_{66}$ repeats (Chew et al., 2015). Bacterial artificial chromosome (BAC) was used to generate models of ALS from DNA of an ALS/FTLD patient, but only one of the four models developed motor deficits (Liu et al., 2016, Jiang et al., 2016, O'Rourke et al., 2016, Peters et al., 2015). Crossing the model with the motor deficit with a knockdown model showed that motor deficits were exacerbated by reduced C9orf72 protein availability, indicating a protective role for endogenous C9orf72 in the BAC model (Shao et al., 2019). Short GA repeats still produced non-lethal sex-specific ALS/FTLD-like symptoms in mice (Verdone et al., 2022). Treatment with rifampicin ameliorated RNA foci formation, dipeptide repeat cytoplasmic inclusions, synapse and neuronal loss, and mouse memory changes when administered nasally (Hatanaka et al., 2022)

1.2.4.1.e ALS in the Rat

Rat models have been used over mouse models due to their larger size, and ease of direct therapeutic administration through the use of, for example, osmotic pumps to deliver vascular endothelial growth factor (VEGF) in $SOD1^{G93A}$ rats which prolonged their survival (Storkebaum et al., 2005).

Rats expressing human $SOD1^{G93A}$ developed slight motor deficits during early disease progression (Thonhoff et al., 2007). However, overexpression of $SOD1^{G93A}$ in rats led to ALS-like MND with rapid progression, focal loss of EAAT2 glutamate transporter in the ventral horn of lumbar spinal cord, SOD1 inclusions that were ubiquitin-positive, and evidence of gliosis (Howland et al., 2002). This has been shown to be more aggressive in rats than mice (Nagai et al., 2001). Mitochondrial protein import was observed to be inhibited in rats expressing $SOD1^{G93A}$, and proteins key to mitochondrial protein import were upregulated as a possible response (Li et al., 2010).

TDP-43 over-expression also led to ALS-like symptoms including progressive widespread neurodegeneration specific to motor neurons, denervation and atrophy of skeletal muscle, and classic TDP-43 mislocalisation to the cytoplasm (Zhou et al., 2010).

1.3 vapB and ALS8

1.3.1 vapB Discovery, Function, and P56S Mutation

VAMP-associated protein of 33 kilo Daltons (VAP-33) was identified in *Aplaysia Californica*, using yeast two-hybrid system, as a protein that interacted directly with the vesicle associated membrane protein (VAMP) (Skehel et al., 1995). Cell fractionation localised the protein to cell membranes, and *in vitro* intracellular injections of antibodies raised against a recombinant form of the protein inhibited evoked excitatory synaptic potentials, demonstrating the requirement of VAP-33 the release of synaptic vesicles. VAP-33 was also identified in the mouse (mVAP-33), and observed to localise to the cytoplasmic face of the endoplasmic reticulum (ER) to interact with microtubules via ultrastructural analysis (Skehel et al., 2000). Human (hVAP-33) and rat homologues of VAP-33 were also identified and were named vapB, its paralogue vapA, and the vapB splice variant vapC (Nishimura et al., 1999). vapB and vapA were found to form homo- and heterodimers through a dimerization motif (GXXXG) in the transmembrane domains (Kim et al., 2010, Russ and Engelman, 2000), and hVAP-33 had greater distribution amongst tissues than VAP-33 in *A.Californica*, with similar structure and ability to bind VAMP (Weir et al., 1998). The VAPs were composed of an N-terminal major sperm protein domain (MSP), coiled coil domain (CCD), and the C-terminal transmembrane domain (TMD) (), apart from vapC which lacked the CCD and TMD.

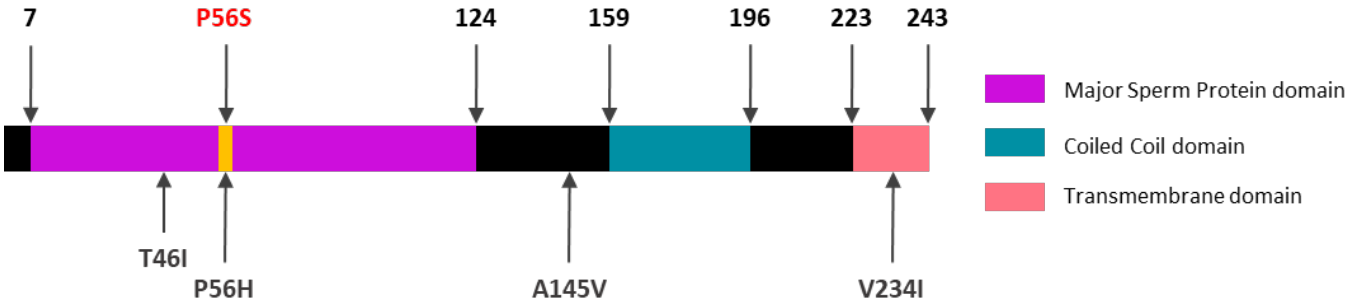

Figure 1.1: Schematic of VAPB with domains and P56S mutation annotated IN RED. Other mutations, described in 1.3.1.2, are marked out in grey below the schematic.

The VAP family of proteins was later expanded with discovery of motile sperm domain-containing proteins MOSPD1, MOSPD2, and MOSPD3, all of which are localised to the ER, and form homo-and heterodimers with other VAP proteins such as vapB and vapA (Cabukusta et al., 2020, Di Mattia et al., 2018, James and Kehlenbach, 2021, Neefjes and Cabukusta, 2021).

The highly conserved N-terminal MSP domain was so named due to its homology to the major sperm protein found in the *C.elegans*, where it acts as a hormone and binds to ephrin (Eph) receptors to activate oocyte maturation (Corrigan et al., 2005). It is also a key component in Ascaris sperm cytosolic filamentous motility system, which utilises MSP rather than an actin-based system for motility (Italiano et al., 1996). There is evidence of an N-terminal cleavage product of vapB in whole brain and spinal cord lysates (Gkogkas et al., 2008). The specific site of cleavage has not yet been described but the cleavage product size indicates a site between the MSP and CCD, indicating that the MSP domain is released as a cleavage product. MSP is noted to have inter- and extracellular presence in *D.melanogaster* wing discs, and is key for alpha lobe formation (Tsuda et al., 2008). MSP has a two phenylalanines in an acidic tract (FFAT) motif-binding site which allows interaction of VAPs with other proteins (Loewen and Levine, 2005). The FFAT binding site in MSP is widely agreed to be EFFDAxE and downstream of an acidic tract (Loewen et al., 2003), and thought to interact as a pair within a VAP dimer when interacting with a pair of FFAT motifs (Kaiser et al., 2005).

1.3.1.1 Cellular roles and interactors of vapB

Proteins containing a FFAT-like motif interact with vapB to enable cellular mechanisms to occur. If the protein binding vapB is resident on the membrane of another organelle, the binding proteins form a tether to anchor the organelle to the ER and allow, for example, the transfer of materials between them. Oxysterol binding protein (OSBP) on the Golgi apparatus binds to vapB, facilitating the formation of a membrane contact site between the Golgi and the ER, and enabling the transfer of lipids (Wyles et al., 2002), ER to Golgi protein trafficking (Kuijpers et al., 2013b, Peretti et al., 2008), and calcium and lipid homeostasis (De Vos et al., 2012, Costello et al., 2017a). Phosphatidylinositol-transfer proteins (Nir1, Nir2, and Nir3) help to maintain the characteristic tubular structure of the ER by creating an interaction between the ER membrane and microtubules (Amarilio et al., 2005).

Other examples of vapB interacting with other proteins to tether the ER to organelles includes the protein tyrosine phosphatase interacting protein 51 (PTPIP51) on mitochondria which is key for normal calcium homeostasis and autophagy (De Vos et al., 2012, Gómez-Suaga et al., 2019), the ceramide transfer protein located on Golgi allowing the transfer of ceramide from the ER which is key in sphingomyelin synthesis (Kawano et al., 2006), acyl-coenzyme A-binding domain protein 5 (ACBD5) allowing the interaction between the ER and peroxisomes (Costello et al., 2017a, Costello et al., 2017b).

In autophagosome formation, vapB interacts with autophagosome proteins such as FIP200 and ULK1 to stabilize their complex to autophagosome formation sites on the ER (Zhao et al., 2018). Regulation of autophagy also involves vapB through its interaction with PTPIP51 to form ER-mitochondrial tethers, which hen loosened, stimulated autophagosome formation (Gomez-Suaga et al., 2017b, Gomez-Suaga et al., 2017a).

The cleavage of the MSP domain of vapB allows for signalling away from the ER. The MSP domain of the *C.elegans* homolog of vapB is secreted and interacts with Roundabout and leukocyte common antigen-related (LAR)-like receptors in striated muscle, helping to localise mitochondria to myofilaments and promote energy production (Han et al., 2013, Han et al., 2012).

Given the vast range of cellular processes vapB is involved in, any change to its normal behaviour could result in changes to any or all of these roles that could lead to neurodegeneration and disease. For example, its interaction with aberrant α-synuclein disrupts vapB-PTPIP51 interactions and affects ER-mitochondrial tethering, and interrupts calcium homeostasis (Paillusson et al., 2017). Such disruptions makes vapB a key protein for ALS modelling.

1.3.1.2 Mutations in vapB

Different point mutations in the gene encoding vapB have been reported. The P56H mutation was discovered in a Chinese Han kindred with a case of FALS with slow progression, muscular cramps and fasciculations (Sun et al., 2017). The T46I mutation was detected in a FALS case and characterised in a *D.melanogaster* model where ubiquitin aggregate formation and neuron cell death were observed (Chen et al., 2010b). The V234I mutation, located in the transmembrane domain, was identified in a case of rapid progression FALS from a Dutch

kindred who also carried C9orf72 repeat expansions (van Blitterswijk et al., 2012b). The A145V mutation, located between the MSP and coiled coil domains, was discovered in a SALS case of rapid progression late-inset ALS (Kabashi et al., 2013).

The most common mutation linked with ALS P56S to ALS8, especially given its prevalence in ALS cases in Brazil. P56S is located in the region encoding the MSP domain, next to the FFAT binding region (Furuita et al., 2010), and inhibits MSP cleavage from the main vapB protein (Tsuda et al., 2008, Gkogkas et al., 2011). Interactions between vapB and target proteins are also affected, such as the vapB-PTPIP51 ER-mitochondrial interaction which is also indirectly affected by TDP-43 (Stoica et al., 2014b), implicating vapB in mechanisms affected by another ALS-related protein. This interaction could have downstream implications for ER and mitochondrial calcium homeostasis as well as mitochondrial function. The tethering of organelles to the ER via vapB was also affected by the mutation, possibly due to delocalisation from the ER to the autophagosome (Yamanaka et al., 2020, Larroquette et al., 2015). The interaction between vapB and autophagosome proteins was also affected by the P56S mutation and impaired autophagy at an early step (Zhao et al., 2018).

1.3.2 Amyotrophic Lateral Sclerosis 8

ALS8 (OMIM [#608627]) is a late-onset subset of ALS first identified in a large Caucasian Brazilian family with 28 affected members over 4 generations (Nishimura et al., 2004a). The initial paper featuring this family did not name the disease but outlined clinical symptoms which included lower motor neuron symptoms confirmed by electrophysiological studies, early postural tremor, fasciculation in limbs and tongue confirmed with needle electromyography, large motor unit activation with reduced recruitment of other units on effort, and normal sensory function and motor nerve conduction. Phenotypic clinical presentation amongst affected members was organised into three diseases: late-onset spinal muscular atrophy, typical ALS with rapid progression, and atypical ALS with slow progression and postural tremor. The proportion of affected members in each family presenting with one of the three phenotypes was not equal, and there appeared to be no sex differences.

Linkage analysis helped to show that all affected members of the family were found to inherit genes in a locus identified in the paper as 20q13.33. In a later paper (Nishimura et al., 2004b), the authors used microsatellite markers, mutation screening, and recombination events in

marker *D20S430* and the *TUBB1* gene to identify a gene with a missense mutation present in all affected members of this family, which was dominantly inherited, and affected members of 6 other families in the study who presented with similar symptoms. The gene encoded the vesicle-associated membrane protein-associated protein B (vapB). The missense mutation in exon 2 replaced nucleotide base cytosine (C) with thymine (T), and changed codon 56 from proline to serine (P56S).

More families with individuals carrying this mutation were found in Brazil (Marques and Marques, 2008, Trilico et al., 2020), which indicated that ALS8 as the most common form of ALS in Brazil (Chadi et al., 2017). Haplotype analysis even established a common founder between the Brazilian families in that paper (Nishimura et al., 2005). However, the disease was not limited to Brazil as other cases have also been reported globally in familial and sporadic cases (Funke et al., 2010, Millecamps et al., 2010, Guber et al., 2018, Di et al., 2016), with evidence that it is not a purely motor disease due to cognitive and behavioural impairments such as apathy and executive dysfunction (de Alcântara et al., 2019).

1.4 vapB *in vivo*

The limited treatment options for ALS speaks to the difficulty in translating findings from current models to the human. Models in *D.melanogaster*, *D.rerio*, and *M.musculus* have all been used to study how the P56S mutation or knocking out VAPB affects biology on cellular, tissue, and whole organism levels. Table 1.1 outlines phenotypes of vapB mutant and knockout models to date. The use of *D.melanogaster*, *D.rerio*, and *M.musculus* provided key insight into the mechanisms affected by disease-causing mutations, and how they affect complex biological environments.

Most models develop cytoplasmic aggregates which appear to sequester wild type vapB and proteins involved in lipid trafficking, ER stress, and ubiquitin pathway for protein degradation. Loss of function cannot be completely decided upon as knocking out vapB in the mouse did not completely replicate outcomes from the knock-in model that expressed vapB and vapB^{P56S} at endogenous levels.

There is a substantial genetic distance between rats and mice on an evolutionary scale (Steppan et al., 2004), an example being that roughly 40% of genes in hippocampal neurons are differentially expressed between rats and mice (Francis et al., 2014), but the gene

encoding vapB in mice and rats is fully homologous. Rats provide an enhanced biological disease model compared to the mouse given their social nature, and similar pathology to humans in instances, such as inflammation after spinal cord injury (Fleming et al., 2006, Norenberg et al., 2004, Metz et al., 2000). They also offer options for developing treatments through applications that are difficult to implement in mice, such as continuous direct spinal delivery of therapeutic agents through an osmotic pump, which are too large to be implemented in mice (Howland et al., 2002).

There is a need to verify the nature of the vapB^{P56S} mutation by replicating endogenous expression in the rat.

Species	Generation	Phenotype	Ref.
Mouse	HR knock-in VAPB$^{Exon\ 2}$	• Reduction in soluble full length vapB and increase in insoluble vapB fragments in het and hom mutants. • Mild motor deficits. • Increase in atypical muscle fibres (nuclear inclusion or atrophy). • Mild partial denervation and synaptic bouton morphology changes. • No change in MN number. • vapB mislocalisation to autophagosome in MNs.	(Larroquette et al., 2015)
	OE hvapB	• Punctate cytoplasmic accumulations of vapB^{P56S} in SMN and CSMN. • Markers of autophagy (ubi and p62) upregulated in mutants. • Reduced weight gain and abnormal motor phenotype in mutants. • UPR activated and degeneration of CSMN, not SMN. • Abnormal translocation of vapB to postsynaptic C-boutons of SMNs, and changed morphology and muscarinic activation.	(Aliaga et al., 2013)
	OE hvapB	• Punctate cytoplasmic accumulations of vapBP56S throughout SC. • No change in motor behaviour. • No signs of MN degeneration or muscle fibre morphology. • No TDP-43 pathology or ubiquitin activity. • ER and mitochondria structurally unchanged • No sign of vapA co-aggregation. • Over-expression of vapBP56S in SOD1^{G93A} mice did not affect disease progression.	(Qiu et al., 2013)
	OE Cloning hvapB	• vapB cytoplasmic inclusions surrounded by ribosome-rich areas • Inclusions include luminal ER proteins and positive for ERAD proteins. • ER morphology changed to tubular structures. • ER cisterns stacked in wild type MN. • Inclusions gradually lost with axotomy.	(Kuijpers et al., 2013)
	OE Cloning hvapB	• Punctate cytoplasmic accumulations of vapB^{P56S} in brain and SC neurons. • No motor deficit or signs of MN degeneration. • Cytoplasmic ubiquitin aggregates and TDP-43 pathology present. • Ubiquitin and TDP43 co-localise. • No TDP-43 cleavage.	(Tudor et al., 2010)
	KO Cre loxP	• Mild late-onset motor deficit • NMJs, muscle innervation, and UPR unaffected	(Kabashi et al., 2013)

Zebrafish	KD antisense Morpholino oligonucleotide	• Developmental/ morphological abnormalities in 20% transgenic fish. • Remaining fish morphologically normal. • Knock down fish have motor deficit not rescued by vapB over-expression. • Mild deficits in axonal projections.	
Fly	p-element excision mutagenesis $DVAP^{\Delta 20}$ $DVAP^{\Delta 448}$ $DVAP^{\Delta 166}$ $DVAP^{\Delta 466}$	• D.melanogaster homologue identified – DVAP-33A. • Severe motor deficit in hemizygous mutant males. • Pre- and post-synaptic localisation at NMJs. • DVAP-33A associated with microtubules. • Fewer larger boutons at NMJs in mutants; overexpression increased number and reduced size. • Mutations affected synaptic microtubule arrangement.	(Pennetta, Hiesinger, Fabian-Fine, Meinertzhagen, & Bellen, 2002)
	Cloning vap^{P58S}	• DVAP localised to ER. • DVAP required for ER protein homeostasis. • DVAP-null mutants have ER stress and accumulation of ubiquitinated proteins. • Oxysterol binding protein mislocalized in DVAP-null flies. • DVAPBP56S caused partial loss of function.	(Moustaqim-Barrette et al., 2014)
		• Fly survival increased and age-dependent motor deterioration delayed when Caspar expressed in glia. • Glial inflammation effected ALS8 progression. • Inclusions in adult brain not affected by Caspar. • *Caspar shown to interact with DVAP as adapter to TER94 (orthologue of p97).* • *DVAP doesn't interact with Caspar in Caspar-mediated glial inflammation.*	(Tendulkar et al., 2022)
	Site-directed Mutagenesis $DVAP^{V260I}$	• Wild type and mutant expression yield similar results: • Reduced survival, altered motor behaviour and neuromuscular deficits. • Neuronal degeneration in adult fly eyes. • Small presynaptic boutons over-produced. • Microtubule cytoskeleton in pre-synaptic boutons affected. • Aggregate formation and altered nuclear morphology. • Over-expression induced heat-shock response.	(Sanhueza, Zechini, Gillespie, & Pennetta, 2014)
	Site-directed Mutagenesis vap^{WT} vap^{P56S}	• Fewer larger boutons at NMJs in mutants; overexpression increased number and reduced size. • Genetic modifiers identified and affected NMJ bouton size, especially TOR pathway components. • Changes to boutons reduced by TOR inhibitor rapamycin.	(Deivasigamani, Verma, Ueda, Ratnaparkhi, & Ratnaparkhi, 2014)
		• Fewer larger boutons at NMJs in mutants; overexpression increased number and reduced size. • VAP-$33A^{P56S}$ ubiquitinated aggregates recruit VAP-$33A^{WT}$. • Microtubule organisation impaired and overexpression of both proteins changes synapses ultrastructurally. • VAP-$33A^{WT}$ overexpression reduced active areas at NMJ.	(Ratnaparkhi, Lawless, Schweizer, Golshani, & Jackson, 2008)
	Homologous Recombination $DVAP^{P58S}$	• DVAP regulated levels of PtdIns4P, necessary for lipid trafficking. Increased levels lead to neurodegeneration and changes to NMJ bouton morphology. • Presynaptic Sac1 necessary for phospholipid transfer, microtubule organisation, axonal transport, and NMJ synapse morphology, and co-localised with DVAP. • Postsynaptic downregulation of Sac affected bouton morphology. Neuron downregulation induced neurodegeneration. • $DVAP^{P58S}$ aggregates bound Sac1.	(Forrest et al., 2013)
	Excision mutagenesis: LoF DVAP-$33A^{\Delta 166}$ Site-directed Mutagenesis: DVAP-$33A^{P58S}$ and	• LoF DVAP-33A expression altered NMJ ultrastructure and neurotransmitter release. • LoF DVAP-33A affects clustering of post-synaptic receptors at NMJs. • $hVAPB^{P56S}$ functionally replaced DVAP-33A, and rescued LoF phenotype.	(Chai et al., 2008)

	hVAPB^{P56S}	• Motor deficit, neurodegeneration, aggregates, and DVAP^{WT} sequestration in DVAP^{P58S} aggregates.	

Table 1.1: Table of *in vivo* ALS8 models.
HR – homologous recombination, OE – overexpression, ERAD – ER-associated protein degradation, UPR – unfolded protein response, LoF – loss of function.

1.5 Project Aims

The late-onset nature of ALS8 would need to be reflected in any animal models to show how the vapB^{P56S} mutation interacts with the natural process of ageing. Past studies have roughly equated 18 month old rats with 45-50 year old humans after taking developmental and ageing landmarks into account, but limitations due to developmental and ageing differences need to be kept in mind (Sengupta, 2011, Sengupta, 2013). Given that most ASL8 patients developed initial symptoms at 46 years of age on average (Nishimura et al., 2004b) and a mouse vapB^{P56S} knock-in model shows a decline in motor function at 11-15 months (Larroquette et al., 2015), monitoring the health and physiology of rats to 18 months would allow for any effects of the VAPB^{P56S} mutation to surface over time.

Sex differences have not been reported in human ALS8 cases (Nishimura et al., 2004b) and none have been reported in murine models. The choice was made to include 3-4 males and 3-4 females of each genotype of interest: vapB as wild type control, vapB$^{P56S/+}$ to represent the disease phenotype, vapB$^{P56S/P56S}$ to determine if the mutation has a dose-dependent effect as seen in one mouse model (Larroquette et al., 2015), and vapB$^{-/-}$ as a negative control and to provide insight to whether the P56S mutation resulted from gain or loss of function.

In Chapter 3, an initial characterisation will be described to determine if vapBP56S leads to weight loss or gain, if the mutation affects the distribution of genotypes amongst pups, if any potential biomarkers of ALS8 can be identified in blood samples, and the mitochondrial capacity to cope with stress conditions.

In Chapter 4, data on motor behaviour from rota rod and CatWalk gait analysis will be described to determine if any motor deficits emerge over the course of 18 months, as other rodent models with changes to their gait have shown progressive and/or late-onset symptoms.

Chapter 5 will outline vapB and vapA expression in lumbar spinal cord, alongside the expression of proteins known to interact with vapB. This will help to determine how the mutation affects vapB localisation, whether vapA might compensate for vapB^{P56S}, and if interacting proteins are affected by the vapB^{P56S} mutation.

(Gomez-Suaga et al., 2017b, Baron et al., 2014, Pennetta et al., 2002, Skehel et al., 1995)

Chapter 6 will cover the number and morphology if spinal motor neurons, TDP-43 proteinopathy, and signs of gliosis as all are major histological signs of ALS in animal models and in some patient tissue.

Knockout animals that were generated collaterally were also used to help determine if the P56S mutation was similar to knocking out the MSP domain, and hence would be a loss-of-function mutation. Any changes observed as a result of the mutation would open avenues to elucidate cellular mechanisms affected and how they relate to disease instigation and progression.

2 Materials and Methods

2.1 Colony Generation

The CLICK (CRISPR with lssDNA inducing conditional knockout alleles) protocol (Miyasaka et al., 2018) enabled the generation of conditional knock outs using Fisher F344 rats. A simplified overview of the protocol can be found in . This allowed for mutant vapB to be expressed at endogenous levels, which were only affected by the mutation, rather than purposeful over-expression as depended upon in other rodent models. Rats with exon 2 of vapB knocked out were also generated as a result of the process.

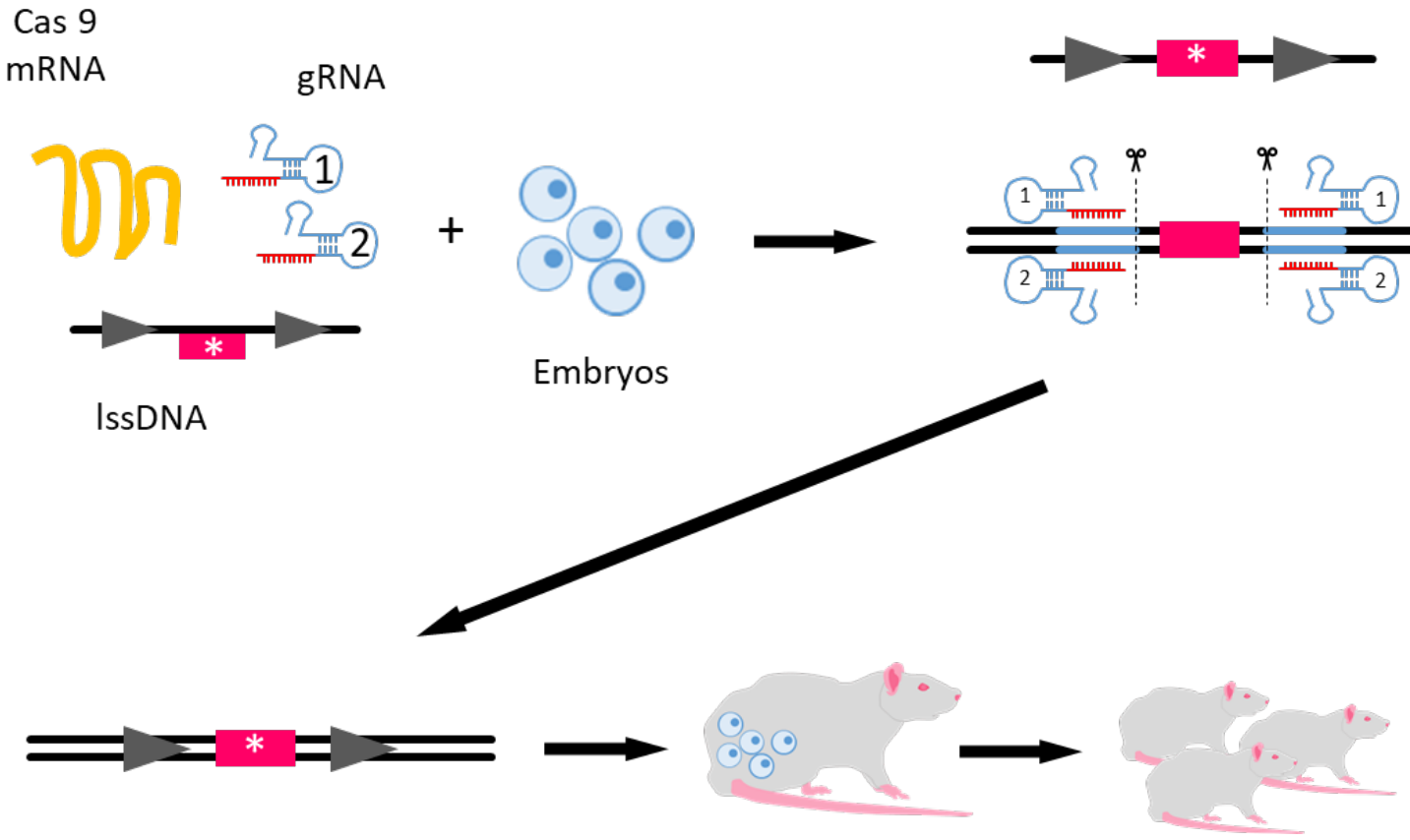

Figure 2.1: CLICK generation of conditional knockouts.
Adapted from (Miyasaka et al., 2018). Long single stranded DNA (lssDNA) fragment containing floxed exon2 with P56S mutation (magenta), 2 guide RNAs (gRNA), and Cas9 messenger RNA (mRNA) were introduced into single-celled rat embryos via electroporation and implanted into foster dams. Cas9 located regions homologous to the gRNAs and induced double stranded breaks around exon 2 of endogenous vapB. The lssDNA was used as a template to incorporate floxed exon 2 carrying the P56S mutation. Electroporated embryos were implanted into foster dams and chimeric offspring were produced (F0). Half of F0 carried the floxed P56S exon 2 of vapB indicating success in generating conditional knockout rats carrying the mutation. Germline transmission of the mutation was successful, and crossbreeding with Cre-expressing F344 rats induced a knockout of exon 2 to create knockout animals.

2.2 Colony Husbandry

All procedures were carried out in alignment with the UK Animals (Scientific Procedures) Act 1986, and in accordance to personal and project licences issued by the UK Home Office. All experiments were reviewed and approved by a University of Edinburgh Named Veterinary Surgeon and Named Animal Care and Welfare Officer. Full training was administered to ensure competency and limit animal suffering. Animals in the ageing cohort had their weight and body condition monitored within the confines of the project licence, and severity at end points was recorded in accordance with UK Home Office requirements. Animals were kept on a 12 hour dark-light cycle with food and water available ad libitum.

Individuals were monitored and genotypes were identified. The advent of splenomegaly and anaemia in 3 males at 17.5 months led to reducing the maximum ageing end point to 17 months instead of 18 months to prevent further adverse cases from occurring. Some female rats also developed over-production of porphyrin in one of either eyes from 12 months onwards which was not genotype-specific. This was managed with attentive husbandry and saline eye washes by animal technicians to reduce irritation and chance of infection.

2.3 Genotyping

Ear clips taken to identify individual pups at weaning were stored at -20ºC. DNA was extracted using the ChargeSwitch^{TM} gDNA Micro Tissue Kit (Thermo Fisher). To amplify exon 2 of vapB, PCR reagents (1 unit/µl Taq DNA Polymerase, 1X PCR buffer, dNTPs. #201205, QIAGEN) were added to 0.2µl of extracted DNA along with primers for vapB-exon 2 (forward: 5'-TGTGGTTCTGTGGAAGCAAG-3'; reverse: 5'-AGTGTGGTACCCGAGGTGAG-3'). A programme of 35 cycles was set up – hot start at 85ºC, denature 3 minutes 94ºC, 30 seconds 94ºC, anneal 1 minute 60ºC, extend 45 seconds 72ºC, 3 minutes 72ºC. When the cycles had ended, products were stored at 4ºC short-term, or -20ºC for long-term storage.

PCR products were visualised on 1% agarose gel (2% 50 X TAE buffer and 0.1% SYBRsafe Dye) with DNA ladder (1kb DNA Ladder, N3232, New England BioLabs) and run at 65V for 30 minutes. Records of individual animals were updated accordingly.

2.4 Behaviour – Rotarod

Figure 2.2 shows a schematic of the rota rod apparatus. Data was collected every 2 weeks from 1 month to 6 months of age between 08:00 and 12:00. As there was not the option to automatically accelerate rotating speed from 4 to 44rpm for 300 seconds as seen elsewhere in literature (Steventon et al., 2016), latency to fall was recorded at 5rpm and 12rpm. These speeds, in addition to 20rpm, were chosen to represent the range of speeds available on the rota rod that rats had proved they could stay on the rod during training sessions. However, 20 rpm was removed as the rats fell from the rod too quickly to gain meaningful data during practice trials. It has been shown that speeds above 20 rpm have little to no effect on latency to fall (Rustay et al., 2003).

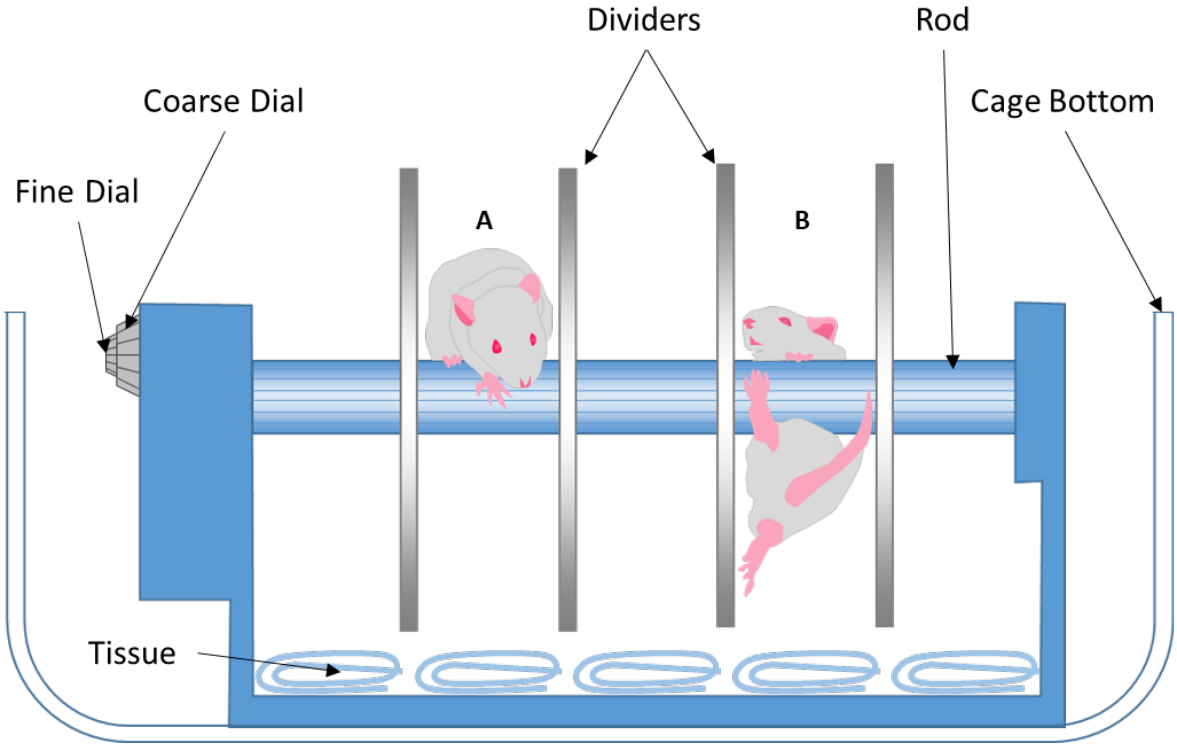

Figure 2.2: Rotarod Schematic.
The apparatus was placed into an empty cage bottom to prevent rats from escaping when they fell from the rod. Paper towels are placed on the rotarod base to reduce risk of injury **A**: Rat balancing on rod during rotation **B**: Rat falling off of the rod. Adapted from (Bryan, 2013, 0:54).

Rats were trained for 3 consecutive days prior to the first test. Training consisted of 20 minute habituation and 3 trials each lasting 30 seconds at the slowest speed (5.72rpm) with a 5 minute inter-trial break in their home cage. On the days of data collection, animals were habituated for 20 minutes in their home cage. The rod was started up, and the animals were

placed onto the rod. Latency to fall was recorded using a stopwatch. The maximum end point to avoid fatigue was 5 minutes (300 seconds), after which rats were removed from the rod and 300 seconds was recorded. If the rat clung onto the rod and completed a rotation, or if they fell off before the first 5 seconds, the trial was stopped and the rat was returned to its home cage for 10 minutes before repeating the trial. To avoid fatigue, animals were not subjected to more than 4 trials per session. In total, data from 3 trials at 5rpm and 12rpm were collected. Animals were weighed at the end of each session.

2.5 Behaviour – CatWalk

A schematic of the CatWalk apparatus (Hamers et al., 2006, Hamers et al., 2001) and a description of its mechanism for recording paw prints is shown in Figure 2.3. As light intensity was the key measurement, experiments were carried out in a dimly-lit room. Thresholds to identify individual paw prints were set by allowing a non-experimental animal walk up and down the walkway whilst adjusting settings on the software (minimum run duration 0.5 seconds, maximum run duration 10 seconds, maximum allowed speed variation 60%, camera gain 28.2, intensity threshold 0.23, abort runs after 10 seconds, label assigned to paw when max intensity is greater than 100). As the dim light source remained constant throughout all CatWalk data collection, the threshold settings also remained consistent.

The day before data collection, animals were allowed to have 3 practice runs and were habituated in their home cage in the behaviour room for 30 minutes. An animal was removed from its home cage and placed on the end of the walkway furthest from the home cage. Software automatically started capturing data once the rat was visible in the pre-defined run capture area. Recording was aborted if the animal did not run to the end of the capture area within the maximum run time set at 10 seconds. The practice runs were completed with 5 minute breaks in the home cage between runs.

On test day, rats were habituated in the dark for 30 minutes. Data for 10 runs were collected with a 5 minute break between runs. After collecting all runs, body weight was recorded and animals were returned to their housing units. Data collected by the software was exported for analysis. Parameters and their definitions can be found in Table 2.1.

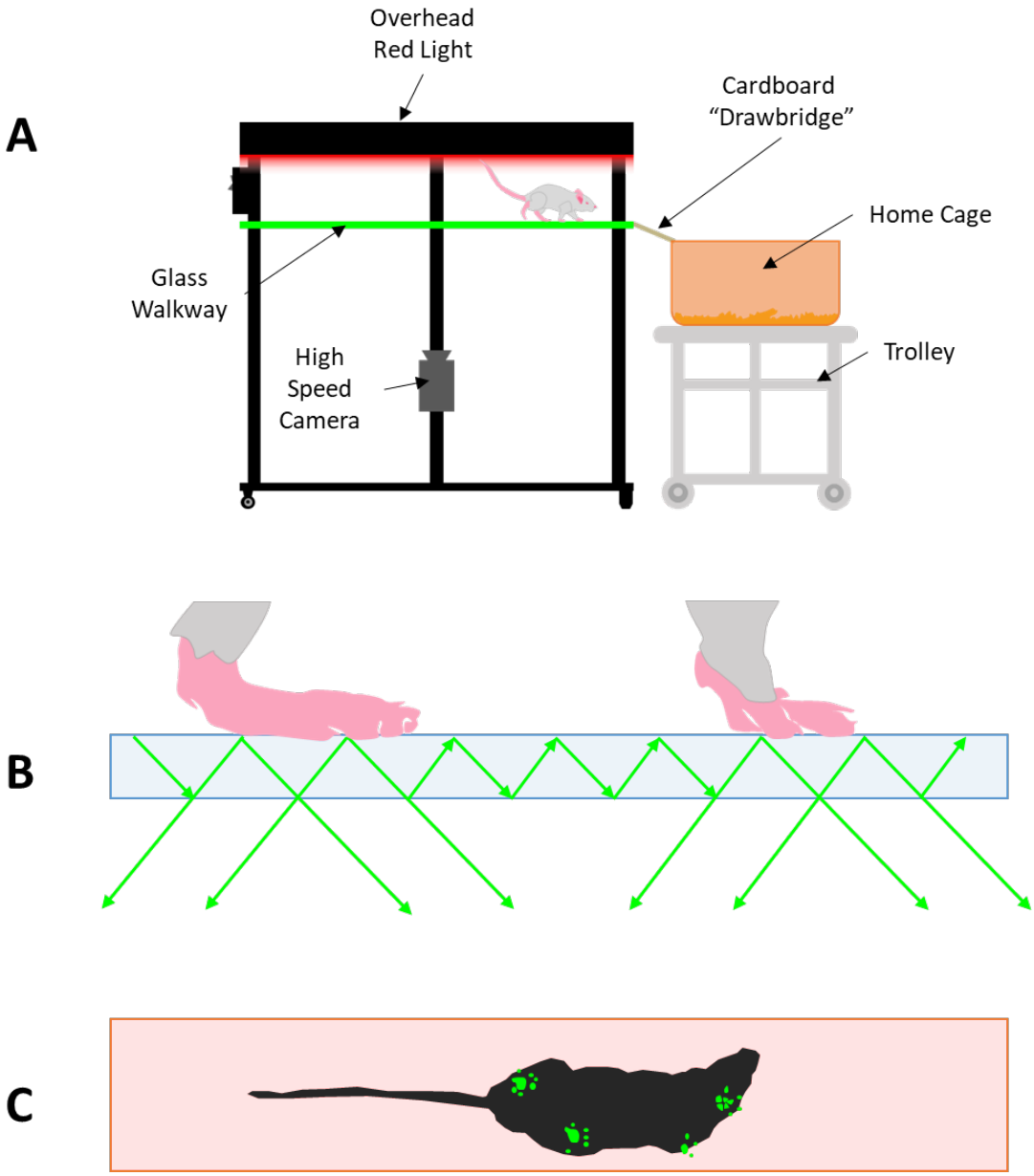

Figure 2.3: Schematic of CatWalk apparatus.
A: Animals were placed at one end of the glass walkway and their cage was made accessible on the other end by elevating it on a trolley and bridging the gap between the walkway and cage using a cardboard bridge. The smell of their home cage was the best incentive to walk across the walkway. **B**: The glass walkway was illuminated from the side. The green light refracted between the outer surfaces of the glass and appeared clear in images captured by the high speed camera. When a paw was placed on the top glass surface, it disrupted the refraction and green light was reflected down into the high speed camera. Paw pressure affected signal intensity captured. **C**: View of animal on glass walkway. The overhead red light captured the outline of the rat as it ran along the walkway, allowing the software to label each paw in relation to body position. To minimise the likelihood of animals stopping in the middle of runs to inspect odours, the glass walkway and walls were cleaned with 70% ethanol and Distel ™ cleaning solution.

	Parameters	Units	Definition
Paw Size	Base of Support (BOS)	Mm	Average width between girdle paw pairs (front pair, hind pair)
	Duty Cycle	Stand as % of Step Cycle	Average proportion of Step Cycle for specific paw spent supporting weight.
	Number of Steps	Number	Number of steps within one run
	Print Positions	Mm	Average distance between lateral paws (left pair, right pair)
	Stand	S	Average time paw is in contact with glass
	Stride Length	mm	Average distance between sequential paw placements
	Support	%	Proportion of run that rat is not in contact, or is in contact with runway on 1 paw, a diagonal pair of paws, a lateral pair of paws, a girdle pair of paws, 3 paws, or all 4 paws.
Pressure	Maximum Contact Maximum Intensity	AU	Average maximum intensity at maximum contact (from 0 to 255). Intensity increases with pressure
	Maximum Contact Mean Intensity	AU	Average mean intensity at maximum contact (from 0 to 255). Intensity increases with pressure
	Maximum Intensity	AU	Average maximum intensity of complete paw
	Maximum Contact At	S	Average time since start of run that largest part of paw makes contact with glass
	Minimum Intensity	AU	Average minimum intensity of complete paw
	Mean Intensity	AU	Average mean intensity of complete paw

Speed	Average Speed	frames/s	Average speed across one run
	Maximum Variation	%	Maximum variation of running speed within one run
	Run Duration	s	Total time taken to traverse the runway on one run
	Step Cycle	s	Average time between two consecutive initial contacts of the same paw.
	Swing Speed	frames/s	Average speed between sequential paw placements
Coordination	Body Contacts	% of run	Proportion of run the other body parts (right or left hip, right or left knee, nose, tail, abdomen, gonads, or tail) contacted the walkway
	Cadence	steps/s	Average number of steps taken per second during a run
	Number of Patterns	Number	Number of recognised step sequences within a single run
	Phase Dispersions	% of Anchor Step Cycle	Mean delay between the placement of two paws
	Regularity Index	% in pattern	Proportion of steps included in recognised step patterns
	Stand Index	frames/mm^2	"Speed paw loses contact with glass (indicates paw dragging)stand index= (a/0x)*frame rates from y=ax+b describing line of best fit of t(Max Area) in 90% percentile, 0x is max contact area“
	Step Sequence	%	Proportion of runs in cruciate, alternate, or rotate sequences
	Swing	s	Average time paw is not in contact with walkway
Paw Shape	Maximum Contact Area	mm^2	Average maximum area of paw that comes in contact with glass
	Maximum Contact At	% of stand	Percentage of stand time transitioning from braking to propulsion during Stand
	Print Area	mm^2	Average area pf paw print
	Print Length	Mm	Average length of paw print
	Print Width	mm	Average width of paw print

Table 2.1: Table of CatWalk parameters.

2.6 Blood Collection and Analysis

Blood samples were collected from 3 – 5 month old male and female rats. To assist vasodilation before collecting samples, individual animals were placed into a heating chamber (35 ºC for no longer than 10 minutes), and peripheral blood was collected from the lateral tail vein of 3 – 5 month old rats using a 25G butterfly needle. Samples were stored in lithium heparin or K2EDTA tubes for haematology and biochemistry analyses respectively. The samples were stored at room temperature for less than 12 hours, or at 4ºC for 24-48 hours, before being sent to Easter Bush Clinical Pathology lab for analysis of erythrocytes, leukocytes, and blood chemistry.

2.7 Cerebrospinal Fluid Collection

A method of extracting cerebrospinal fluid (CSF) from adult rats was developed with ML, and adapted from (Nirogi et al., 2009). For the syringe, a 2.5ml syringe was fitted with a 19 gauge needle. Liquid superglue was used to attach 12 inches of PE-50 tubing, and sealed with gel superglue. A pulled pipette shortened to roughly 1cm long was glued to the other end of the tubing using the same types of superglue. Syringes were left to dry for a minimum of 20 minutes before use, and syringe plungers were pulled to release the air seal. Pulling and pushing the plunger helped to look out for air leaks. Figure 2.4 demonstrates syringe assembly. At least 2 syringes were assembled per animal before the procedure.

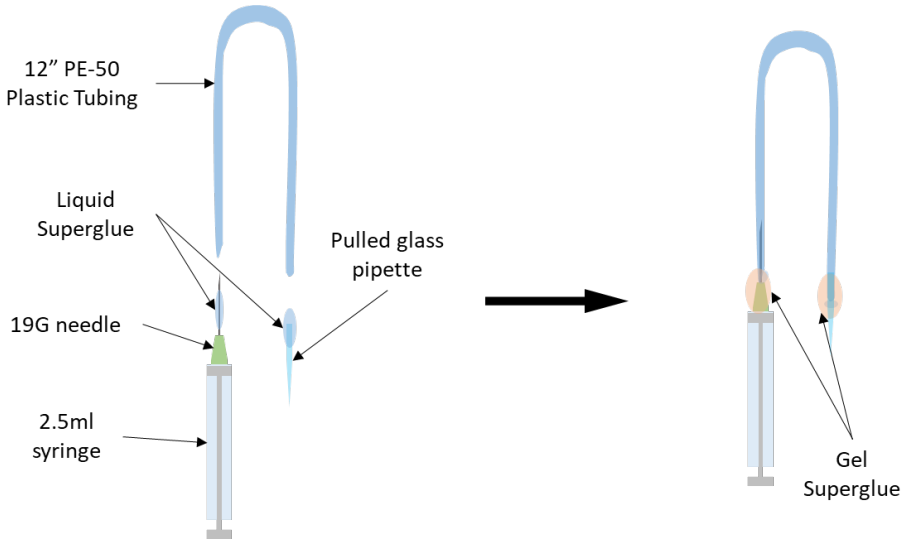

Figure 2.4: Assembly of syringe for CSF Extraction.
Average liquid superglue was too thin to create an airtight seal around the points where the plastic tubing met the 19G needle and pulled glass pipette, so thicker gel superglue was used to do this.

After inducing anaesthesia with isoflurane, the rat was placed into a stereotaxic rig taking care to angle the head downward by about 30º. The procedure to extract CSF from rats is outlined in Figure 2.5. CSF was deposited into a pre-cooled Eppendorf and placed on dry ice before being transferred to storage at -80^{o}C. If the sample started to appear pink with blood, the PE-50 tubing containing contaminated sample was pinched and cut off, leaving clean sample to deposit into an Eppendorf. Immediately after CSF collection, an overdose of sodium pentobarbital was administered intraperitoneally to end the surgery.

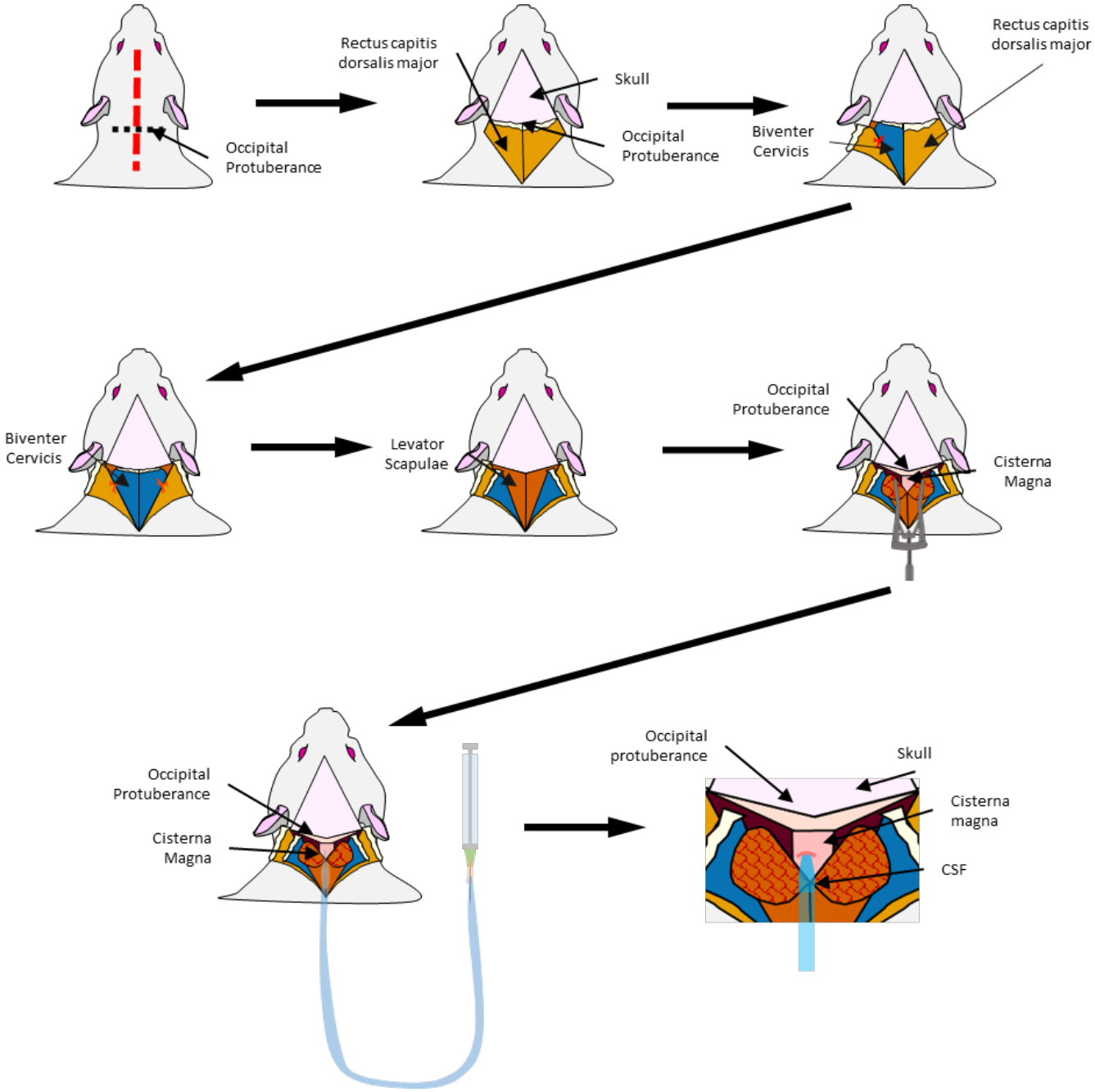

Figure 2.5: CSF extraction through cisterna magna.
Terminal procedure to extract CSF from rats under anaesthesia induced by isoflurane.

2.8 Mitochondrial Stress Test

Mitochondrial performance under stress conditions was measured using the Agilent Seahorse XFe24 Analyzer. Hippocampal cultures were prepared by PS in the day prior to experimentation. Briefly, hippocampi from P0 – P1 pups were dissected out and washed with Leibocitz's L-15 medium, and tail tissue was excised and stored at -20^{o}C for later genotyping. Individual hippocampi were transferred to individual Eppendorf tubes and incubated in Hank's/Hepes solution, Trypsin, and DNAse for 20 minutes at 37ºC. Wells were washed with growth medium (Basal Medium Eagle, Horse Serum, Penicillin-Streptomycin, 32.5% glucose solution, 100mM Sodium Pyruvate, N2 supplement) which was decanted, and hippocampi triturated with a fire-polished glass Pasture pipette in DNAse-growth medium solution. Cells were counted, and wells of a Seahorse XFe24-well plate were seeded with 100,000 to 800,000 cells each. Cells were incubated at 37ºC overnight for single-cell layer proliferation.

Cultures were incubated in Seahorse medium (Seahorse Base Medium, 1mM pyruvate, 2mM glutamine, 10mM glucose, pH 7.4) in a non-CO_2 incubator at 37ºC for at least 1 hour as CO_2 affected the pH of the cell media. The lid of the plate contained chambers for reagents to be added into as shown in Figure 2.6 and was prepared whilst cells incubated. The plate and its chambered lid was inserted into the Agilent Seahorse XFe24 Analyzer where fibre optic probes measured extracellular flux and helped to mix reagents after injection. The experiment mixed the medium for 3 minutes, waited for 2 minutes, and measured for 2 minutes for 4 cycles when taking baseline measurements and measurements after the injection of each drug. Data was exported for analysis. When the plate was ejected, cells were homogenised and had their protein concentration measured using Coomassie Plus (Pierce^{TM} Thermo Fisher), reading absorbance at 595nm. Mitochondrial stress test data was normalised to protein concentration before analysis.

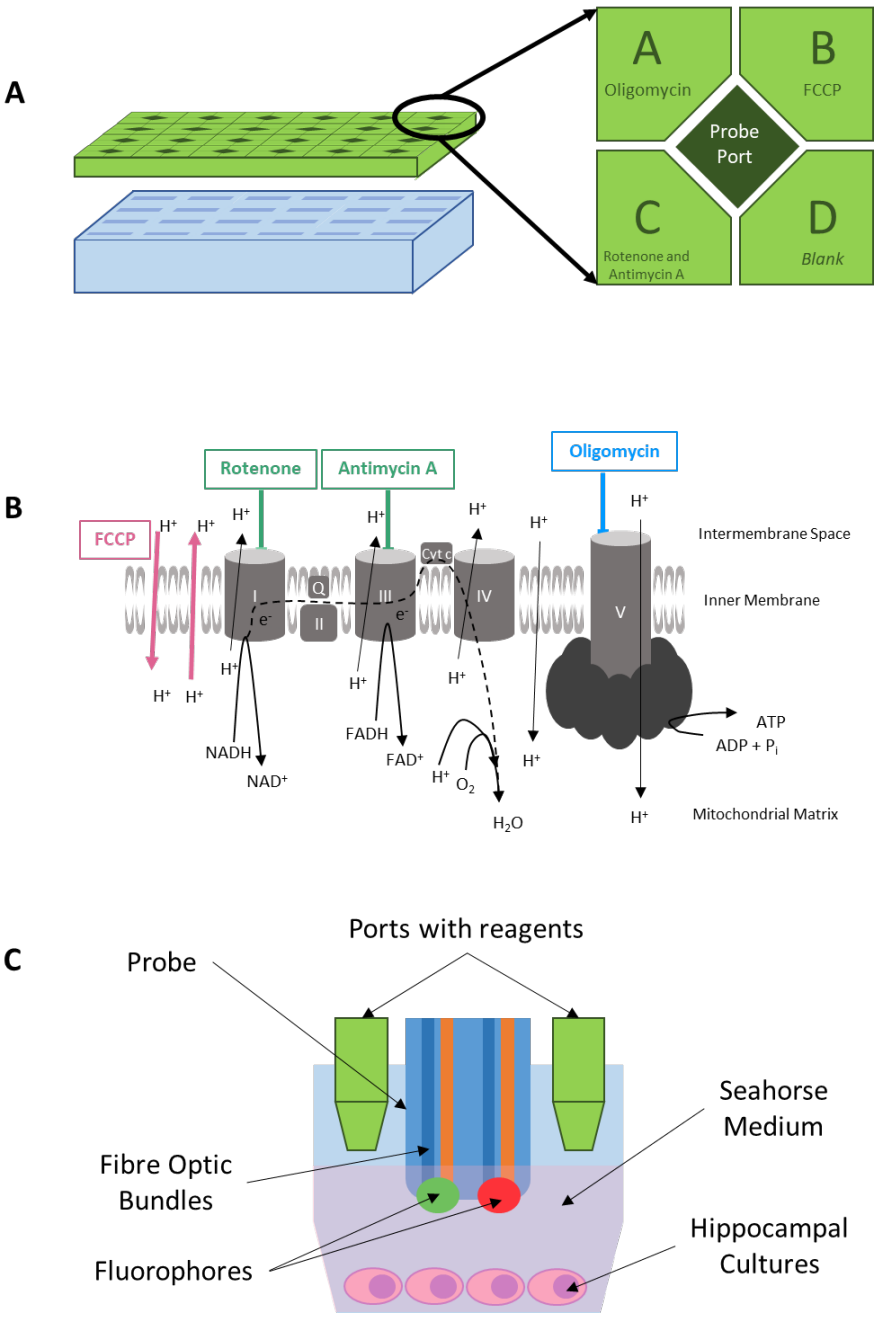

Figure 2.6: Schematic of 24-well plate lid, Seahorse drug targets, and microfluidic chamber.
A: 1µM of each reagent was placed into ports and were kept in place by capillary action. Once in the Analyzer, a blast or air injected the drug into cell media at the assigned time point, and probes were raised and lowered to help mix the reagent into the media **B**: Electron transport chain components affected by reagents. Oligomycin inhibited ASP synthase, disrupting the flow of protons from the inter-membrane space into the mitochondrial matrix. FCCP permeabilized the membrane to uncouple the electron transport chain from oxidative phosphorylation. Rotenone and Antimycin A inhibited complexes I and III respectively to completely shut down the ETC **C**: During the Mito Stress Test, fluorophores embedded at the end of probes were excited by light emitted by the fibre optic bundles. The fluorophores were quenched by either oxygen or protons generated by hippocampal cultures in cell media. This information was used to record the concentration of both metabolites in real-time and to calculate the oxygen consumption rates (OCR) and extracellular acidification rate (ECAR) in real time, which provided insight into mitochondrial respiration and glycolysis respectively.

2.9 Antibodies

Details of the antibodies used in western blot, immunofluorescence, and immunohistological assays are listed in Table 2.2.

Use	Antibody	Target	Location	Host	Dilution	Incubation	Source
WB	vapB #38	VAMP-Associated Protein B	Endoplasmic Reticulum	Rabbit	1:1000	Overnight 4ºC	Made in-house
WB	vapA	VAMP-Associated Protein A	Endoplasmic Reticulum	Rabbit	1:1000	Overnight 4ºC	Made in-house
WB	Tubulin BIII	Tubulin BIII	Microtubules	Mouse	1:1000	Overnight 4ºC	MAB1637, Sigma-Aldrich/ Chemicon
WB	VAMP2	Vesicle-Associated Membrane Protein 2	Vesicles	Rabbit	1:1000	Overnight 4ºC	AB3347, Abcam
WB	Syntaxin 1	Syntaxin 1	Vesicles	Mouse	1:15,000	Overnight 4ºC	10011, Sysy
WB	GFAP Monoclonal	Glial Fibrillary Acidic Protein	Astrocytes	Rat	1:5000	Overnight 4ºC	13-0300 Thermo Fisher Scientific
WB	Mitofusin2	Mitofusin 2	Mitochondria	Mouse	1:300	Overnight 4ºC	Ab124773, Abcam
WB	BiP/GRP78	Binding Immunoglobulin Protein/ Glucose-Regulated Protein 78	ER Stress Marker	Rabbit	1:200	Overnight 4ºC	SC-13539, Santa Cruz

IF	vapB #6	VAMP-Associated Protein B	Endoplasmic Reticulum	Rabbit	1:100	48 hrs 4ºC	Made in-house
IF	vapA	VAMP-Associated Protein A	Endoplasmic Reticulum	Rabbit	1:200	48 hrs 4ºC	Made in-house
DAB	ChAT144P Polyclonal	Choline Acetyltransferase	Cholinergic Neurons	Goat	1:100	Overnight 4ºC	AB144P Merck/ Sigma-Aldrich
DAB	TDP-43 Polyclonal	TAR DNA Binding Protein 43	Cell Nucleus	Rabbit	1:2000	Overnight 4ºC	10782-2-AP ProteinTech
IF	AIF-1/ Iba1 Polyclonal	Ionized Calcium-Binding Adapter Molecule 1	Microglia	Goat	1:500	Overnight 4ºC	NB100-1028 Novus Biologicals
IF	GFAP Monoclonal	Glial Fibrillary Acidic Protein	Astrocytes	Rat	1:200	Overnight 4ºC	13-0300 Thermo Fisher Scientific

Table 2.2: Table of primary antibodies used in this project.
WB – Western Blots. IF – Immunofluorescence. DAB – 3, 3'-Diaminobenzidine used for immunohistology.

2.10 Western Blotting

Lumbar spinal cord was excised and stored at -80ºC. Frozen lumbar spinal cord was manually homogenised in HEPES buffer (20mM, cOmplete protease inhibitor, Roche) on ice. Coomassie Plus (Pierce™ Thermo Fisher) and spectrophotometer were used to determine protein concentration and dilute homogenates to 2mg/ml with 1x SDS running buffer.

Samples were heated at 90ºC for 15 minutes before being run on 10% or 7.5% acrylamide gels in Novex™ Tris-Gycine SDS running buffer (Thermo Fisher) at 100V for 50 minutes or until the dye front reached the bottom of the cassette. Proteins were transferred to 0.75µm PVDF membrane at 100V in cold NuPAGE™ transfer buffer (Thermo Fisher) for 1 hour. Membranes were blocked in 5% milk TBST for 1 hour and left to incubate in primary antibody overnight in 5% milk TBST at 4ºC. Membranes were washed in TBST 3 times for 5 minutes, and incubated in HRP- (Goat F(ab) Anti-Rabbit IgG H&L (HRP) ab7171 for vapB #6 and vapA) or IRDye®-conjugated secondary antibodies (IRDye® 800CW Donkey anti-Rabbit IgG 926-32213 for VAMP2, BiP/GRP78, PTPIP51, and Histone H3; IRDye® 800CW Donkey anti-Mouse IgG 926-32212 for Syntaxin; IRDye® 800CW Goat anti-Rat IgG 926-32219 for GFAP) for 1 hour or 30 minutes respectively. Membranes were washed in blocking solution before developing images of membranes on X-ray film or imaging on LI-COR Odyssey 9120 Infrared Imaging System.

2.11 Histology of Lumbar Spinal Cord

Tissue was dissected from animals following transcardial perfusion with cold PBS followed by 4% paraformaldehyde, and post-fixed in 4% paraformaldehyde for 12 hours. Tissue was processed in a Sakura Tissue-Tek TEC 6 processor, embedded in paraffin, and stored at room temperature. Sections of L3 – L5 spinal cord were cut at 10µm thickness on a Leica-RM2245 microtome, mounted onto SuperFrost Plus™ slides using a 40^{o}C hot water bath, dried for 12 hours at 60ºC, and stored at room temperature. At the start of each procedure below, slides were de-waxed by immersion in xylene and decreasing concentrations of ethanol, and re-hydrated in running water for 5 minutes.

For Haematoxylin and Eosin (H&E) staining of tissue, slides were incubated in haematoxylin for 3 minutes, washed for 2 minutes in running water, and placed into Scott's Tap Water Substitute (STWS) for 5 minutes. Slides were washed for 3 minutes in running water,

incubated in eosin for 2 minutes, dipped in running water, and incubated in potassium alum for 2 minutes. They were washed again in running water for 5 minutes before being immersed in increasing concentrations of ethanol for 2 minutes each, and cleared in xylene for 5 minutes. Slides were mounted with DPX (Dibutylphthalate Polystyrene Xylene) and left in a fume cupboard for 48 hours to harden.

For immunohistochemical and immunofluorescent staining, slides were incubated in 10mM sodium citrate buffer (pH6.0) whilst being microwaved at 400V for 4 times 5 minute cycles. After cooling and washing in tap water, slides were incubated with 3% H_2O_2 (in TBS) for 10 minutes and followed by 2x10 minute TBST washes. Slides were then blocked for 1 hour at room temperature with 4% Normal Goat Serum in TBST (or Bovine Serum Albumin for primary antibodies raised in goats), and incubated with the primary antibody. After 3x10 minute TBST washes, tissues were incubated for 1 hour at room temperature with either biotinylated secondary antibodies and signal developed (VECTASTAIN ® ABC-HRP Kit, Rabbit IgG, PK-4001 for TDP-43; Polyclonal Rabbit Anti-Goat #E0466 Dako for ChAT144P), or fluorescent secondary antibodies in 4% NGS or BSA TBST block (Cy™3 AffiniPure Donkey Anti-Rabbit IgG (H+L) for vapB #6 and vapA; Cy™3 AffiniPure Donkey Anti-Goat IgG (H+L) for Iba1; Cy™3 AffiniPure Donkey Anti-Rat IgG (H+L) for GFAP). Sections were washed again in TBST. For all sections, coverslips were mounted using VECTASHIELD® HardSet™ Antifade Mounting Medium (H-1400-10, Vector Laboratories) and stored in the dark at 4ºC.

2.12 Image Capture

Images were captured on an Axio Scan.Z1 slide scanner at 40x magnification (Plan-Apochromat 40x/0.95 Korr M27 objective), and was set up to capture a whole section of lumbar spinal cord in one stitched image. Brightfield images were captured with a Hitachi HV-F202SCL camera, and fluorescence images with a Hamamatsu Arca Flash camera. During analysis, images were opened using QuPath (Bankhead, 2017) and processed in FIJI/ImageJ (Schindelin et al., 2012).

2.13 Statistical Analysis

Comparison of vapB$^{P56S/+}$, vapB$^{P56S/P56S}$, and vapB$^{-/-}$ back to vapB was carried out using one- or two-way ANOVA with Dunnett's post-hoc test in GraphPad Prism 7.0. For CatWalk data, genotypes were compared back to vapB using two-way ANOVA with Tukey's post-hoc test in GraphPad 9.3 for consistency, with analysis aided by HT.

3 Primary Characterisation

3.1 P56S mutation and knock out inherited in Mendelian proportions

The colony was maintained through breeding vapB$^{P56S/+}$ or vapB$^{+/-}$ pairs. As far as possible, male and female rats were replaced after 6 months, but during rationalisation of the colony, some breeding pairs were maintained for longer. This was based on reports stating a better success rate when female rats remain with their initial mating partner (Peng and Huang, 1972, Acuña et al., 2009, Goltzsch and Clauss, 1990, Ferreira-Nuño et al., 2005, Lovell et al., 2007). Data on the number of pups per litter and the age of dams in vapB, vapB$^{P56S/+}$, and vapB$^{+/-}$ pairs can be seen in Figure 3.1.

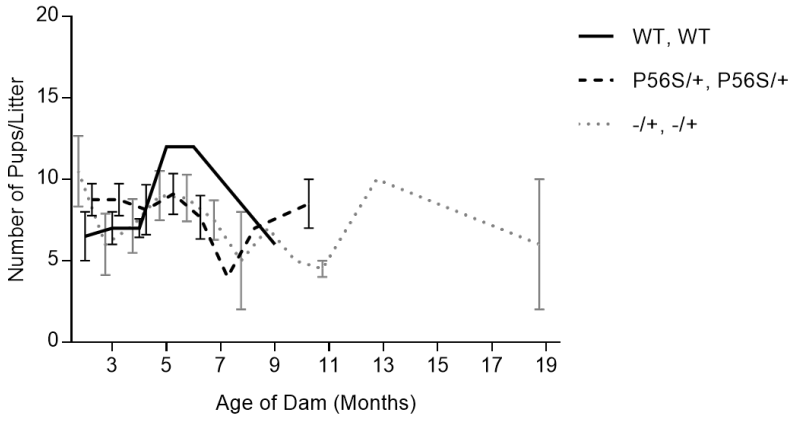

Figure 3.1: Average number of pups per litter born to vapB, vapB$^{P56S/+}$ and vapB$^{-/+}$ pairs over time. Two-way ANOVA determined no statistically significant differences between genotypes at each age. Data based on live births. n=37 litters from vapB$^{-/+}$ pairs, and n=22 litters from vapB$^{P56S/+}$ pairs.

Whilst there were no statistical differences in the number of pups/litter for each genotype pair, there was a notable decline in number at 6 months for all three genotypes. As the data for dams older than 6 months was limited, it was not possible to determine whether the declining trend carried on and if it became statistically significantly decreased between 2 and 6 months. If so, it would support evidence in literature for the general decline in numbers after the age of 6 months.

To see if genetic modification affected the proportion of genotypes carried by pups in each litter, the number of pups that were wild type, and either heterozygous or homozygous for

the modification was recorded and analysed. Both vapB$^{P56S/+}$ pairs and vapB$^{-/+}$ pairs produce offspring in roughly Mendelian proportions (C) which were not significantly different (A). There was also a rough 50/50 split of male and female pups in all litters (D) which was not significantly different between the genotypes (B).

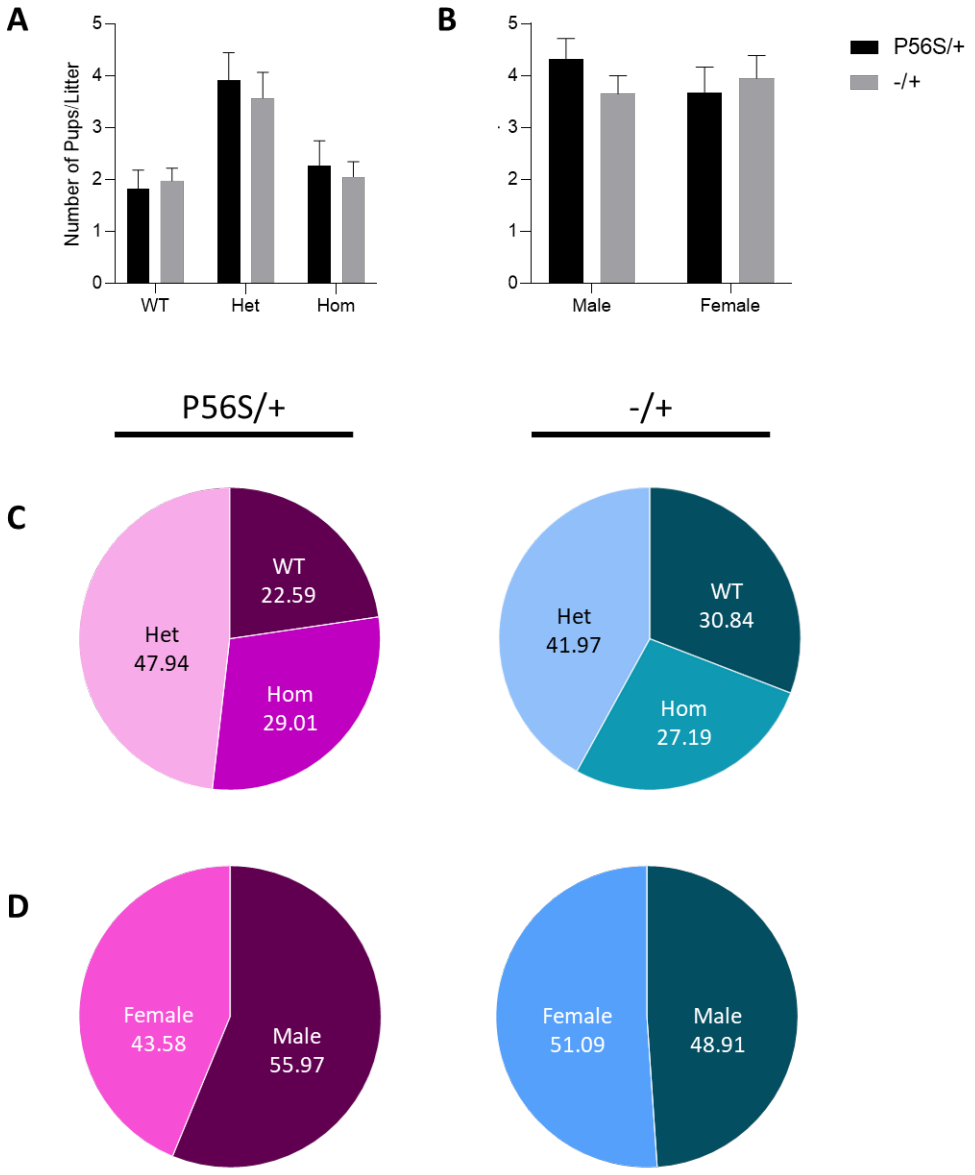

Figure 3.2: Inheritance of P56S mutation and knock out.
A: The number of vapB, homozygous, and heterozygous pups per litter from vapB$^{P56S/+}$ pairs. **B**: The number of vapB, homozygous, and heterozygous pups per litter from vapB$^{-/+}$ pairs. **C**: Pie charts depicting proportions of genotypes carried by pups born in each litter. **D**: Pie charts depicting proportions of pups belonging to either sex in each litter. Two-way ANOVA with Sidak's post-hoc test applied. Data based on live births. n=37 litters from vapB$^{-/+}$ pairs, and n= 22 litters from vapB$^{P56S/+}$ pairs.

3.2 Male vapB$^{P56S/P56S}$ and vapB$^{-/-}$ gain more weight than wild type after 7 months

The majority of individuals were kept to maintain the colony or to produce tissue for pilot studies, so most rats were not kept beyond 6-7 months of age. Up to the age of 17 months, there were records for at least 4 animals per genotype per sex (apart from 6 month old vapB males, where there was only 1 record available). shows average weight according to sex and genotype.

There was a significant increase in weight gained in male vapB$^{P56S/P56S}$ and vapB$^{-/-}$ compared to vapB between 7 and 17 months (B – C). There was also an increase in weight gained in male vapB$^{P56S/+}$ compared to vapB between 8 and 12 months but this was not statistically significant (A). Female rats had very similar rates of weight gain over time, but vapB$^{P56S/P56S}$ females gained more weight from 10 to 17 months compared to vapB which was not statistically significant (E).

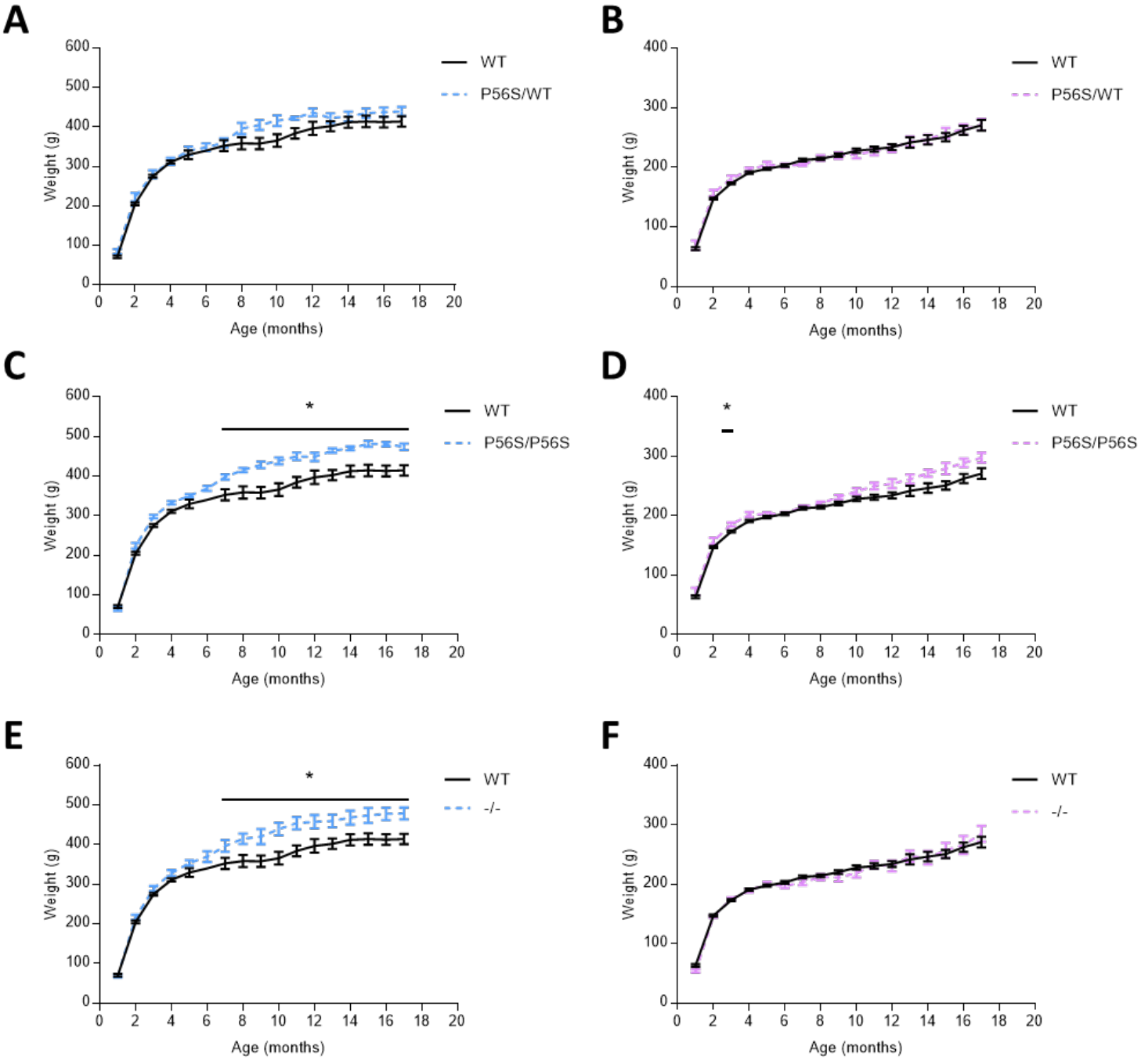

Figure 3.3: Weight of male and female rats over 18 months.
Wild type vapB was compared to vapB$^{P56S/+}$ (**A** and **D**), vapB$^{P56S/P56S}$ (**B** and **E**) and vapB$^{-/-}$ (**C** and **F**). One way ANOVA carried out at each age point comparing back to vapB animals. * p <0.0500. Additional analysis comparing vapB$^{P56S/+}$ to vap$^{BP56S/P56S}$ and vapB$^{-/-}$ revealed no significant differences between the genotypes. At least 4 animals per sex and genotype were weighed, apart from 6 month vapB males where only one data point was available. * p<0.0500; **p<0.0100.

3.3 Pilot blood analysis suggest changes to male vapB$^{-/-}$ erythrocyte morphology

Blood was obtained and analysed as described in Chapter 2. Cell populations and biochemical markers in the samples were analysed, and results for red blood cell (RBC) analysis were shown in . Male vapB$^{P56S/P56S}$ blood chemistry data was not obtained due to insufficient sample volume for analysis.

Male vapB$^{-/-}$ rats had a lower concentration of RBCs, reduced proportion of total cell population, and reduced haemoglobin concentration than vapB (A-C). However, there were no changes in RBC volume, average haemoglobin concentration per RBC, or in platelet concentration (D – F). Male vapB$^{-/-}$ also have an altered variation in RBC sizes (aniocytosis) as indicated in the reduction of cell distribution width (G). These differences were not reflected in the females (H – N).

Parameters of white blood cell (WBC) analysis were shown in . Segmented neutrophilia was detected in vapB$^{P56S/P56S}$ (G), and lymphocytosis in vapB$^{-/-}$ female rats (I). There were no statistically significant differences in WBC parameters for male animals.

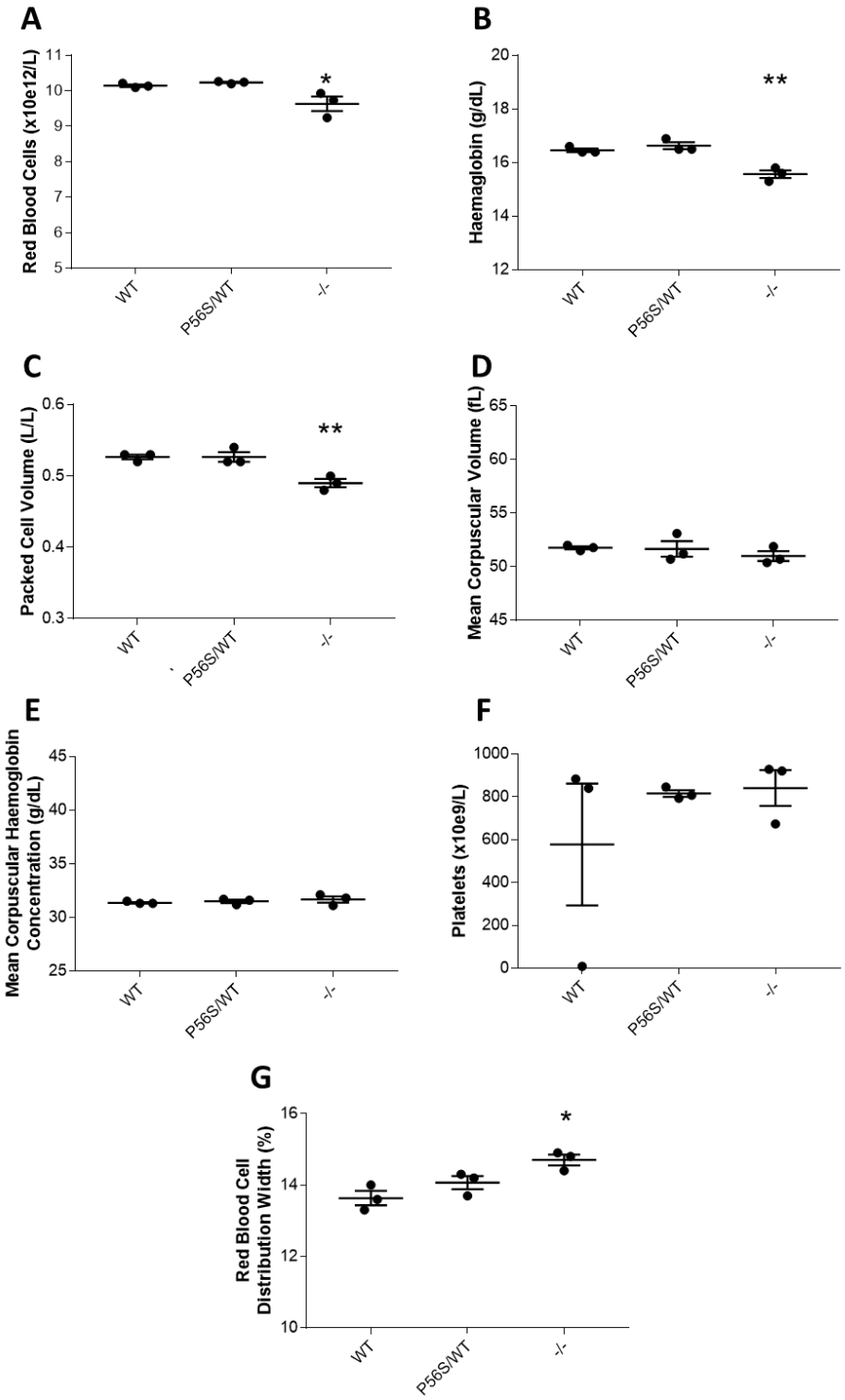

Figure 3.4: Red blood cell analysis from male rats.
A: Red Blood Cells – number of red blood cells (x10e12) per litre (p=0.0424). **B**: Haemoglobin – concentration of haemoglobin (p=0.0033) **C**: Packed Cell Volume – proportion of sample consisting of cells (p=0.0056). **D**: Mean Corpuscular Volume – average volume of RBC. **E**: Mean Corpuscular Haemoglobin Concentration – average haemoglobin concentration per RBC. **F**: Platelets – concentration of platelets. **G**: Red Blood Cell Distribution Width – amount of variation in RBC size and volume. One way ANOVA with Dunnett's post-hoc analysis compared each genotype back to wild type. n=3 for all genotypes.

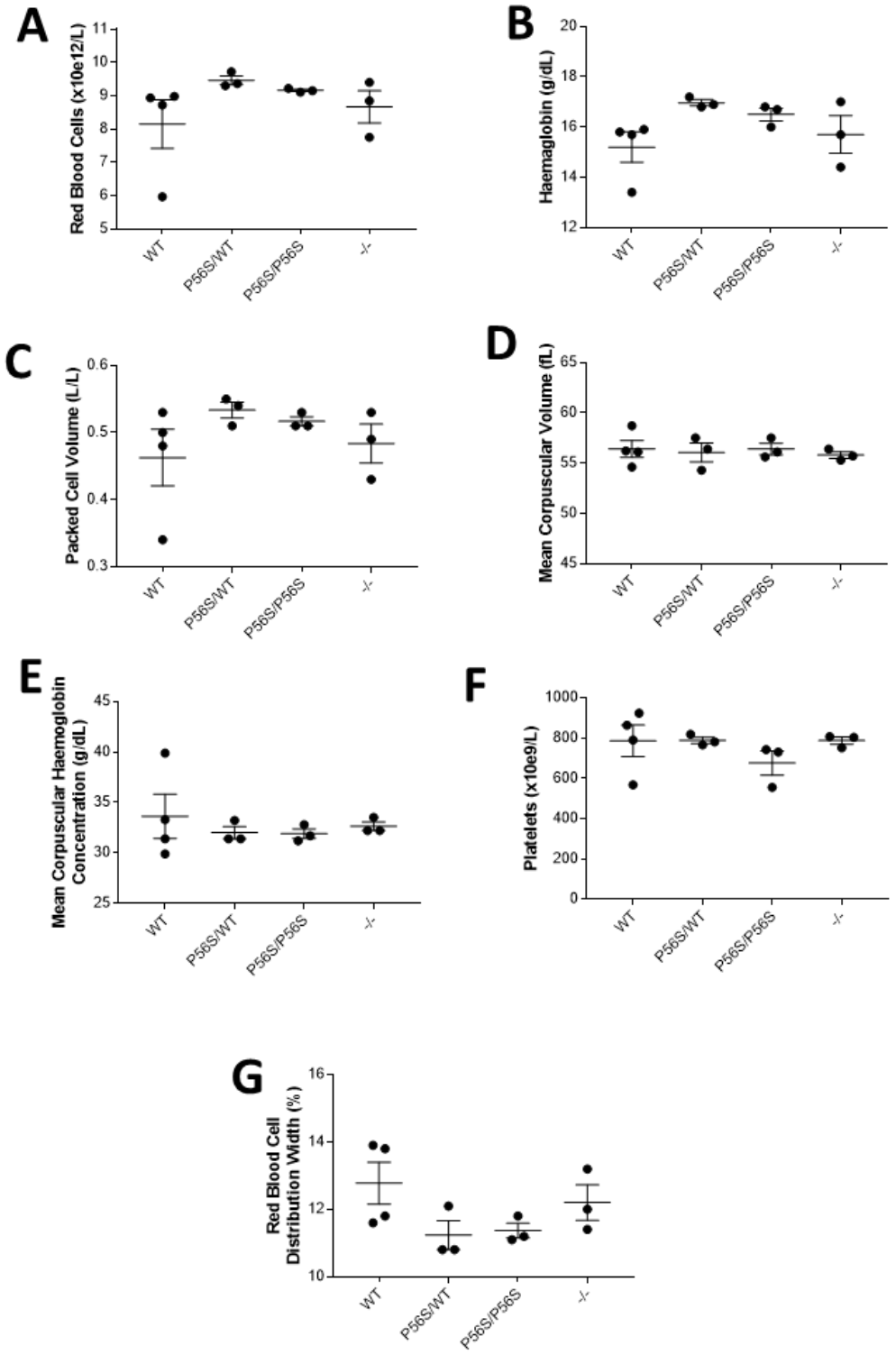

Figure 3.5: Red blood cell analysis from female rats.
A: Red Blood Cells – number of red blood cells (x10e12) per litre (p=0.0424). **B**: Haemoglobin – concentration of haemoglobin (p=0.0033) **C**: Packed Cell Volume – proportion of sample consisting of cells (p=0.0056). **D**: Mean Corpuscular Volume – average volume of RBC. **E**: Mean Corpuscular Haemoglobin Concentration – average haemoglobin concentration per RBC. **F**: Platelets – concentration of platelets. **G**: Red Blood Cell Distribution Width – amount of variation in RBC size and volume. One way ANOVA with Dunnett's post-hoc analysis compared each genotype back to wild type. n=4 for female VAPB^{WT}, and n=3 for remaining female genotypes.

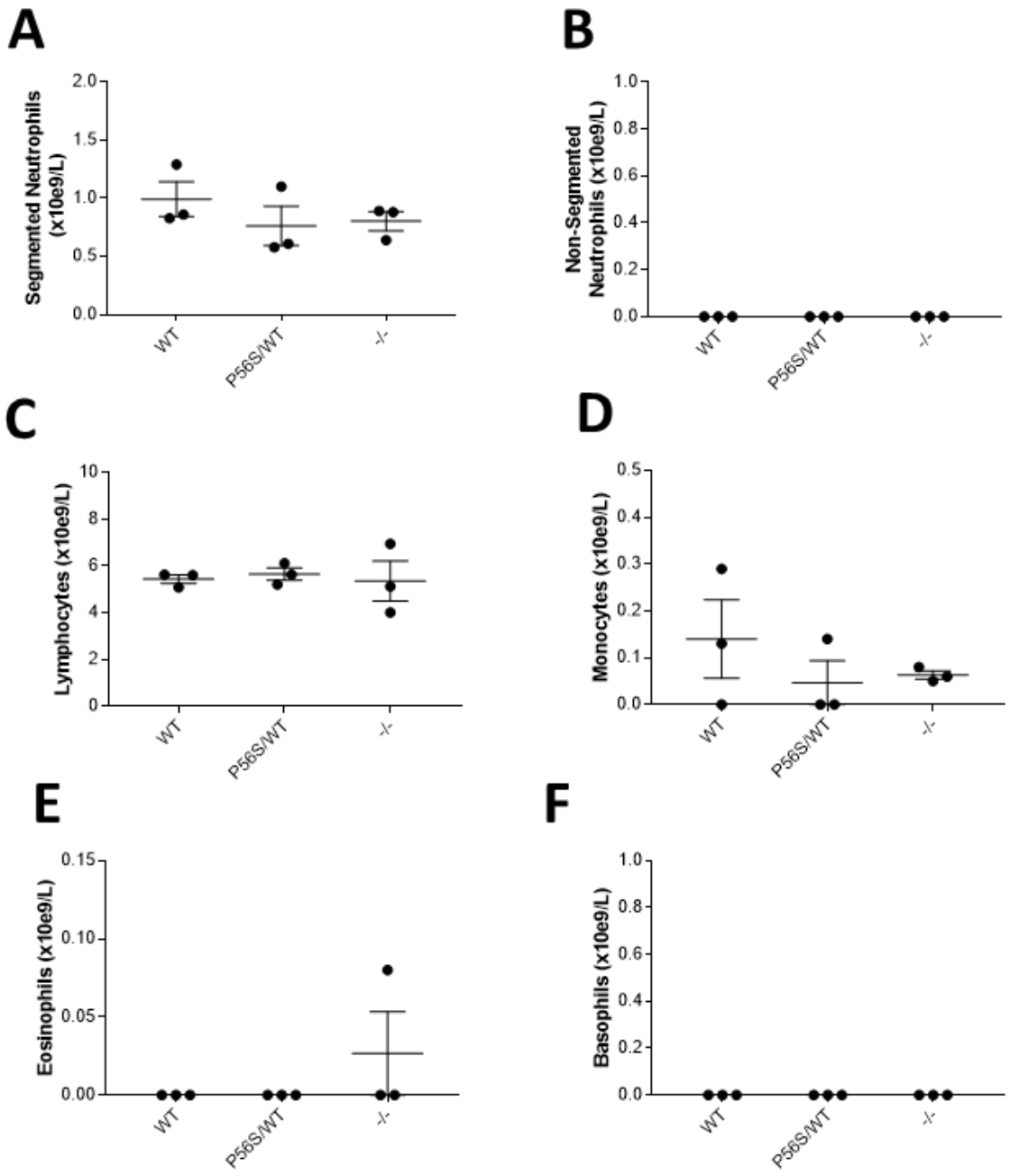

Figure 3.6: White blood cell analysis for male rats.
A: Segmented Neutrophils – Mature first responder and most abundant. Apoptotic, cytotoxic, phagocytic, and induces immune response p=0.0043). **B:** Non-Segmented Neutrophils – First responder and most abundant. Apoptotic, cytotoxic, phagocytic, and induces immune response. **C**: Lymphocytes – Include antibody-producing B and cytotoxic T cells (p=0.0089). **D**: Monocytes precursor to macrophages that attack and devour labelled targets. **E**: Eosinophils – phagocytose antibody-antigen complexes and produce histamines. **F**: Basophils – mainly involved in allergic reactions by releasing granules of histamine, and recruits other cells to sites of infection. One way ANOVA with Dunnett's post-hoc analysis compared each genotype back to wild type. n = 3 for all genotypes.

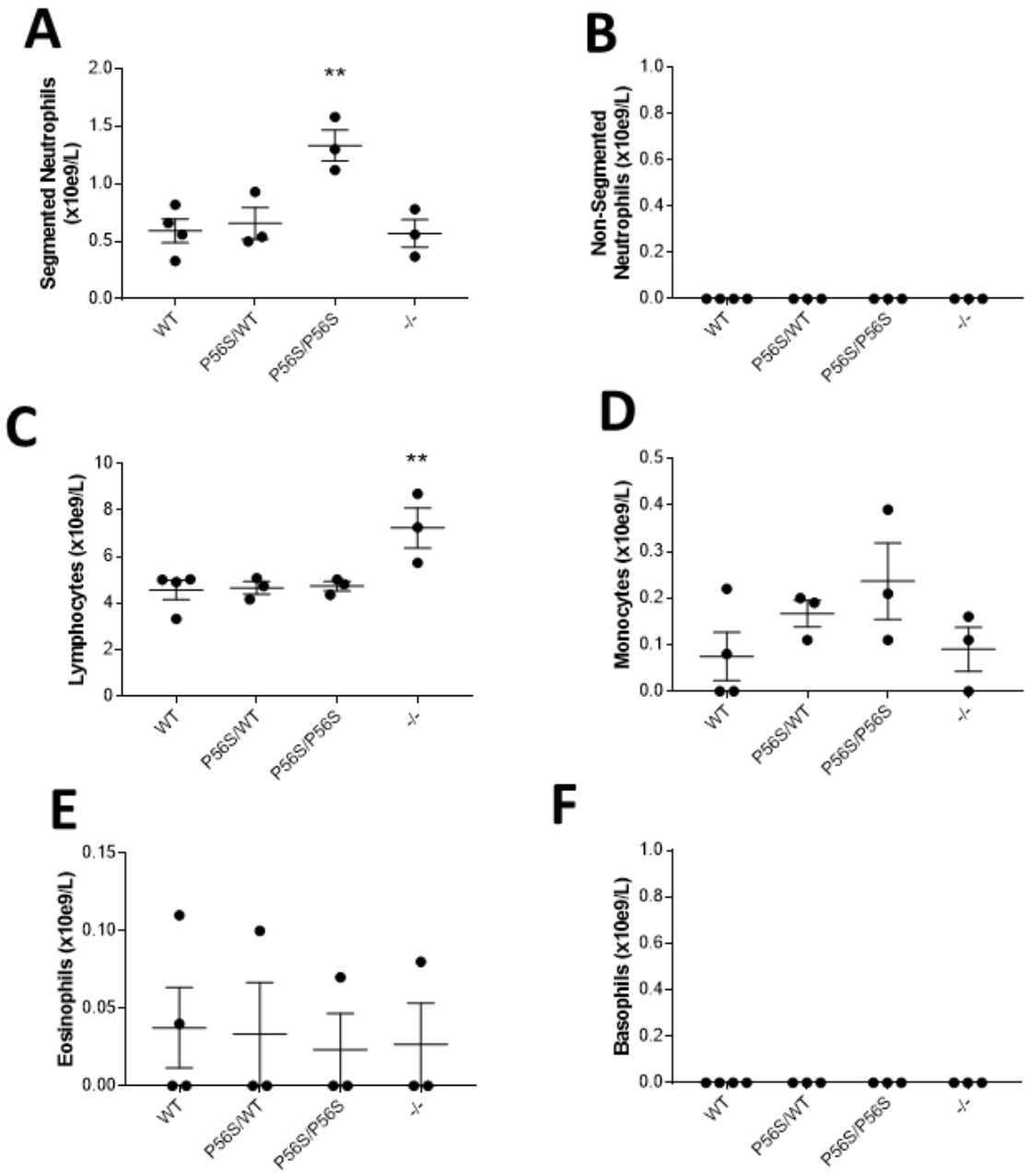

Figure 3.7: White blood cell analysis for female rats.
A: Segmented Neutrophils – Mature first responder and most abundant. Apoptotic, cytotoxic, phagocytic, and induces immune response p=0.0043). **B:** Non-Segmented Neutrophils – First responder and most abundant. Apoptotic, cytotoxic, phagocytic, and induces immune response. **C**: Lymphocytes – Include antibody-producing B and cytotoxic T cells (p=0.0089). **D**: Monocytes precursor to macrophages that attack and devour labelled targets. **E**: Eosinophils – phagocytose antibody-antigen complexes and produce histamines. **F**: Basophils – mainly involved in allergic reactions by releasing granules of histamine, and recruits other cells to sites of infection. One way ANOVA with Dunnett's post-hoc analysis compared each genotype back to wild type. n = 3 for all male genotypes, n = 4 for female $VAPB^{WT}$, and n = 3 for remaining female genotypes.

Blood biochemistry was not available for male rats due to difficulty in obtaining sufficient volumes of blood for analysis. shows blood chemistry analysis from female rats. No statistically significant changes were detected.

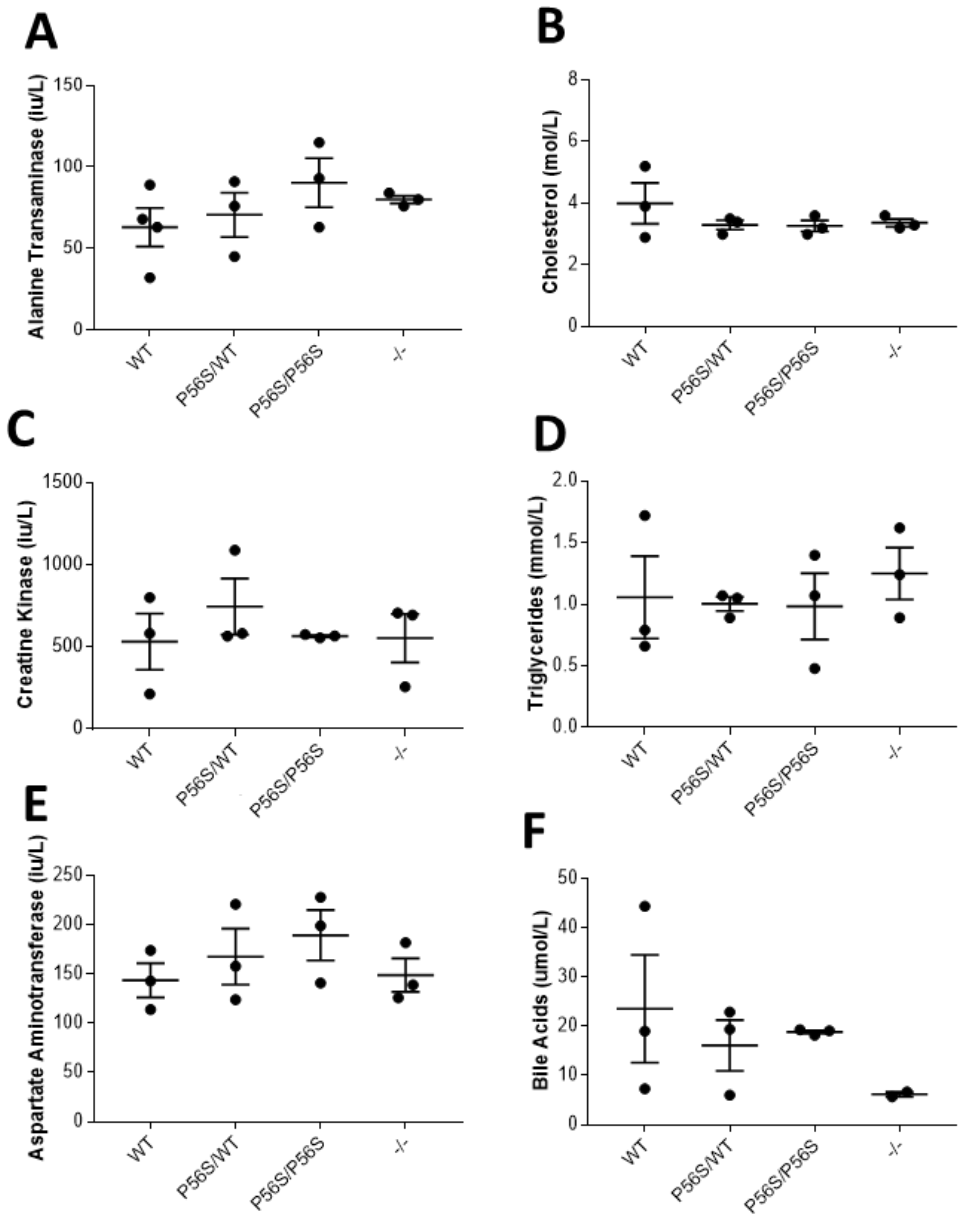

Figure 3.8: Figure 8: Blood chemistry from female rats.
A: Alanine Transaminase (AST) – released from liver into blood stream due to damaged. **B**: Cholesterol – vital role in composition of cell membrane. **C**: Creatine Kinase (CK) – released into blood stream from skeletal or cardiac muscle due to damage Creatine ensures constant supply of energy to working muscles. **D**: Triglycerides – main component of dietary fat and used to store energy. **E**: Aspartate Aminotransferase (AST) – released into bloodstream from liver or heart due to damage. **F**: Bile Acids – transports fat-soluble waste and helps absorption of fat-soluble compounds through intestine. One way ANOVA with Dunnett's post-hoc analysis compared each genotype back to wild type. n = 4 for female WT, and n = 3 for remaining female genotypes.

3.4 Pilot mitochondrial metabolism analysis suggests reduced vapB$^{P56S/+}$ capability in stress environment

The Seahorse XFe24 analyser measures the oxygen consumption rate (OCR) and the extracellular acidification rate (ECAR). OCR (A) was used as a measure of mitochondrial function due to O_2 being used to store free electrons from the electron transport chain (ETC). ECAR (B) was used to measure glycolysis due to protons being released into cell medium by lactic acid, which was the primary source of extracellular protons and the product of generating ATP from glucose. Oligomycin, FCCP, and Rotenone and Antimycin A were reagents used to sequentially induce mitochondrial stress by inhibiting ATP synthase, increasing the porosity of the mitochondrial membrane and inhibiting the ETC respectively (C). Parameters recorded during the Mito Stress Test and their definitions were shown in Table 3.1.

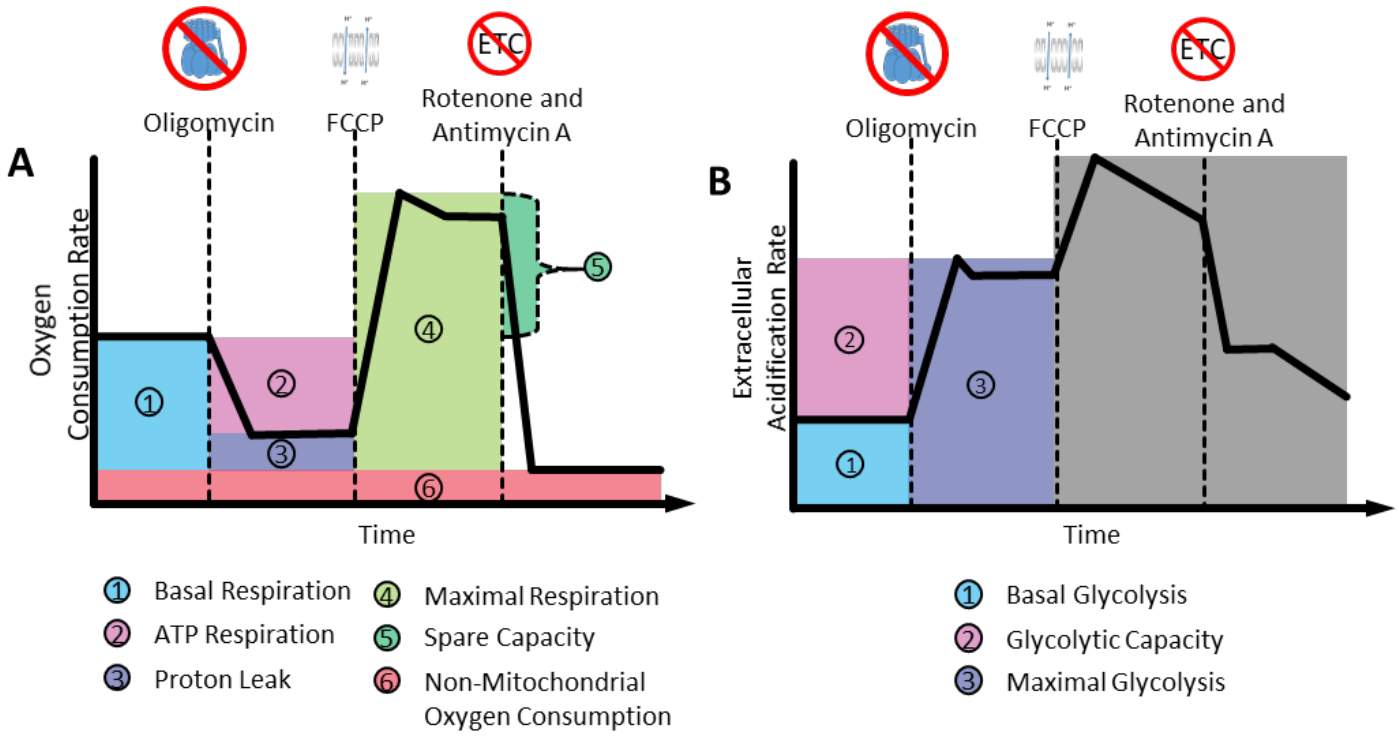

Figure 3.9: Outline of the plots of OCR and ECAR from cell medium.
A: oxygen consumption rate (OCR) over the course of the Mito Stress Test. **B**: extracellular acidification rate (ECAR) over the course of the Mito Stress Test.

Parameter	Definition
Basal Respiration	Baseline consumption of oxygen from cell media before the addition of reagents
ATP Respiration	Calculated as reduction in O_2 consumption after inhibiting ATP synthase with oligomycin.
Proton Leak	Residual passing of protons from inter-membrane space back into mitochondrial matrix without ATP synthase. Could indicate mitochondrial damage.
Maximal Respiration	Induced by FCCP increasing inner mitochondrial membrane permeability, allowing protons to flow freely between mitochondrial matrix and inter-membrane space. This forces ETC complexes to work harder to restore concentration gradient across membrane, consequently transporting more electrons across ETC, and driving up O_2 consumption to store electrons.
Spare Capacity	Additional facility of mitochondria to deal with stress from increased membrane permeability.
Non-Mitochondrial Oxygen Consumption	Use of O_2 in other cellular processes measured when ATP synthase and ETC were both inhibited.
Basal Glycolysis	Measured before addition of any reagents.
Maximal Glycolysis	Triggered by inhibition of ATP synthase, and alternative method of producing ATP (glycolysis) moves to compensate for this loss.
Glycolytic Capacity	Additional facility available in cells to produce ATP when ATP synthase was dysfunctional.

Table 3.1: Parameters recorded and calculated by Seahorse XFe24 analyser during Mito Stress test.

B shows that vapB$^{P56S/+}$ hippocampal cultures have reduced maximal respiration, and reduced non-mitochondrial respiration compared to vapB. The ETC of vapB$^{P56S/+}$ was less able to compensate for additional mitochondrial porosity than vapB, and other cell processes involving the consumption of O_2 were reduced compared to vapB. There were no significant differences in measures of glycolysis (C). There were insufficient samples for vapB$^{P56S/P56S}$.

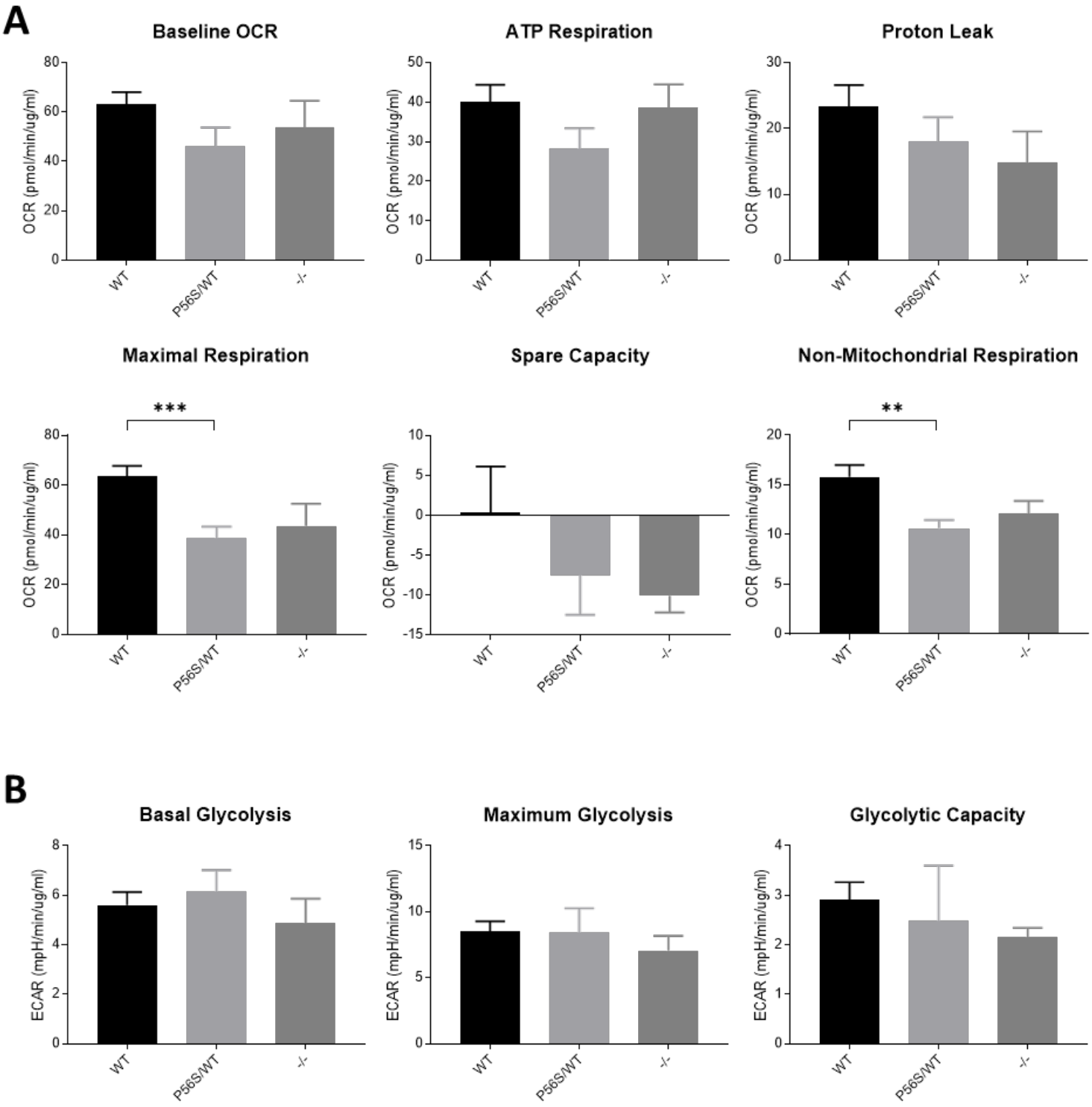

Figure 3.10: Measures of mitochondrial stress test from Seahorse XFe24 analyser.
A: Measures of mitochondrial respiration of hippocampal cultures and **B**: Measures of glycolysis of hippocampal cultures from vapB, vapB$^{P56S/+}$, and vapB$^{-/-}$. vapB n=14, vapB$^{P56S/+}$ n=11, vapB$^{-/-}$ n= 4 animals. One way ANOVA with Dunnett's post-hoc test applied. *** p<0.0010, ** p<0.0100. There appears to be a consistent reduction in Maximal Respiration and Non-Mitochondrial Respiration for vapB$^{-/-}$ but neither were significantly reduced from vapB wild type (p=0.0597 and 0.1391 respectively). Male and female samples pooled as individuals were not genotyped for sex.

3.5 Discussion and Future Work

3.5.1 Litter Proportions

Whilst data on the number of pups per litter from vapB^{P56S} rodent models was not available in literature, general consensus holds on not keeping breeding animals beyond 6 months to reduce possible pup mortality (Niggeschulze and Kast, 1994), and reduce the likelihood of adverse effects as a result of ageing such as vaginal prolapse, the risk of which increases with repeated mating (Couri et al., 2012).

Evidence from literature, based mainly around Sprague Dawley rats, indicated the first signs of reproductive senescence in female rats appeared from 8-10 months and most females had a reduced number of pups/litter from 6 months onward (Peng and Huang, 1972, Acuña et al., 2009). It was long believed that male ageing did not have an effect on offspring outcomes (Goltzsch and Clauss, 1990), but other evidence pointed to male fertility starting to decline at 12 months which was reported in Wistar rats (Rodríguez-González et al., 2014) and Long-Evans Rats (Smith et al., 1992). Further study would be needed to see how advanced age of male and female rats in conjunction affect the overall outcomes of offspring from this colony. It was decided that male and female rats would be replaced at 6 months of age as there was a better rate of mating success with virgin rats staying with their initial mating partner than in replacing partners after 6 months. Whilst the data for this phenomenon was not available for this colony, evidence in literature indicates female rats had a consistent preference for the same male partner (Ferreira-Nuño et al., 2005, Lovell et al., 2007).

The distribution of pups born to mating pairs shows a Mendelian distribution, which reflects the autosomal dominant nature of the vapB$^{P56S/+}$ mutation in human patients (Nishimura et al., 2004b, Harel et al., 2015). It has been found that there were no negative selective pressures on fertility related to ALS, mostly due to the fact that the great majority of patients develop symptoms in later stages of life (Uysal et al., 2021). Further research could investigate the incidence of pregnancies not carried to full term, but this would raise major ethical concerns.

Other rodent models of ALS report similar findings of genetic expression in litters. For example, overexpression of human FUS in mice resulted in Mendelian expression of non-transgenic, hemizygous, and heterozygous offspring (Mitchell et al., 2013). The knock-in

murine model of ALS8 generated mice heterozygous and homozygous for the vapB^{P56S} mutation, but the proportion of knock-out mice to wild type was not specified (Larroquette et al., 2015).

3.5.2 Weight

The weight gain seen in vapB$^{P56S/P56S}$ and vapB$^{-/-}$ was contrary to findings in ALS patients and in other rodent models of ALS8. Of the three mouse models that over-expressed vapB^{P56S} and were monitored between 18-24 months, only 1 displayed significant weight loss compared to wild type littermates (Aliaga et al., 2013). The other two models (Qiu et al., 2013, Tudor et al., 2010) had no significant change in body weight. The SOD1/vapB mouse model had similar significant weight loss to the SOD1 mouse, but it was delayed by 2 weeks (Kim et al., 2016). There were no significant changes in body weight of vapB^{P56S} knock-in mice (Larroquette et al., 2015), and no data was reported on weight for the vapB$^{-/-}$ mouse model (Kabashi et al., 2013).

In other rodent models of ALS, most models reporting weight loss involved expression of TDP-43. However, some SOD1 mice and a model overexpressing human FUS in the mouse also reported weight loss (Stribl et al., 2014, Mitchell et al., 2013, Chiang et al., 2010, Graffmo et al., 2012, Wu et al., 2012, Shan et al., 2010, Wegorzewska et al., 2009a). One mouse model of ALS, which expressed TDP-43^{Q331K}, experienced weight gain compared to wild type and non-transgenic littermates (Watkins et al., 2021, White et al., 2019). It was suggested that hyperphagia, associated with FTLD, may have been the root cause given the link of TDP-43 mislocalisation from the nucleus in both ALS and FTLD (White et al., 2018). However, overexpression of TDP-43 has also been found to affect Glucose-4-transporter (Glut4) translocation in skeletal muscle, leading to an increase in fat deposits in mice (Stallings et al., 2013). Further assessment on food intake and lipid metabolism in vapB rats would be needed to find the root cause of weight gain seen in male vapB$^{P56S/P56S}$ and vapB$^{-/-}$. Such weight gain may have affected data collected on gait (Pitzer et al., 2021), but this will be discussed in more detail in Chapter 4. ALS in rodents has been linked to altered lipid metabolism in the past (Kim et al., 2011, Vejux et al., 2018), so it would be worth trying to get blood biochemistry analysis from male rats in the future.

Body weight has been a standard marker of overall health of patients and rodents, usually in diseases such as cancer (Reuben et al., 1988, Redgate et al., 1991), but weight loss, gain, or maintenance, effects ALS patient prognosis and survival (Shimizu et al., 2019). A combination in the loss of muscle mass, fat loss, and increased resting metabolism contributes to a significant proportion of ALS patients suffering from overall weight loss during disease progression (Desport et al., 1999). However, it has not been considered a factor in diagnostic criteria as it was not a defining feature of the disease (Brooks et al., 2000, de Carvalho et al., 2008, Hannaford et al., 2021). Weight loss has been linked to increased chance of developing complications and fatigue (Heffernan et al., 2004). Studies have also linked factors such as the development of hypermetabolism (Ioannides et al., 2017), loss of appetite (Ngo et al., 2019), hypothalamic atrophy (Ahmed et al., 2021), and declining mental health (Wang et al., 2021) as contributing factors for weight loss in ALS patients. Dysphagia was mentioned in many studies but was not directly linked with weight loss. Hypermetabolism alongside weight loss has also been seen as an indicator of poor clinical prognosis and survival (Steyn et al., 2018, Nakayama et al., 2019), whereas hypometabolism was associated with delayed need for PEG and ventilation alongside better survival in comparison with hypermetabolic patients (Cattaneo et al., 2021). Clinical guidelines advise the use of percutaneous endoscopic gastrostomy tube (PEG) for feeding after specific criteria were met (Andersen et al., 2005), although stress from installing PEGs might increase disease progression in some patients (Körner et al., 2013).

3.5.3 Pilot Blood Analysis

ALS has been a difficult disease to diagnose and treat due to its heterogeneity (Sabatelli et al., 2013, Ghasemi and Brown, 2018) and the potential to misdiagnose mimic diseases such as primary lateral sclerosis (Tartaglia et al., 2007, Kuipers-Upmeijer et al., 2001) and spinal and bulbar muscular atrophy (Grunseich and Fischbeck, 2015). In the search for potential biomarkers or biochemical changes linked to ALS, various differences in blood components and biochemistry have been found in ALS patients when compared to healthy controls. Multiple studies have shown changes in peripheral myeloid cell populations in ALS patients, which were outlined in Table 3.2, and have the potential to be biomarkers for ALS. These results opened a new line of enquiry regarding the colony: could there be any changes to blood composition or biochemistry linked to genetic modification?

Cell Type	Changes Seen	Reference(s)
RBC	Increased RBC deformation; decreased nitrous oxide efflux	(Lima et al., 2016)
RBC Biochemistry	Increased RBC polyamines	(Gomes-Trolin et al., 2002)
	Increased HGBA1c in SALS led to worse survival	(Wei et al., 2017)
Neutrophils	Increased percentage of circulating neutrophils	(Murdock et al., 2016) (Swindell et al., 2019)
Lymphocytes	Tregs reduced and less effective in immune suppression	(Jin et al., 2020) (Mantovani et al., 2009) (Henkel et al., 2013) (Beers et al., 2017)
	Cytotoxic T cells increased	(Rentzos et al., 2012) (Jin et al., 2020)
Monocytes	Increase in activated monocytes and macrophages in spinal cord	(Henkel et al., 2004) (Butovsky et al., 2012) (Zondler et al., 2016) (Zhao et al., 2017) (Zhang et al., 2005)
	Fewer monocytes in ALS with bulbar involvement	(McGill et al., 2020)
Eosinophils	Eosinophil-derived neurotoxin increased in patient serum	(Liu et al., 2013)
Basophils	More found in slow-progression cases of ALS	(Greco et al., 2021)

Table 3.2: Changes in blood cell populations from ALS patients reported in literature.
RBC – red blood cells; HGBAc1 – haemoglobin Ac1; SALS – sporadic ALS; Tregs – regulatory T cells. Sex-specific changes were not outlined as patient data was pooled for all studies mentioned.

Pilot blood analysis suggests major sex-specific differences. The reduction in the concentration of erythrocytes, haemoglobin concentration, and the increased variability of the width of erythrocytes from vapB$^{-/-}$ male rats would indicate morphological changes in erythrocytes in the absence of functional vapB. Mature erythrocytes do not contain an endoplasmic reticulum, but this, along with other organelles such as the nucleus and mitochondria, were expelled from immature erythroblasts as a necessary step in maturation (Skutelsky and Danon, 1970, Simpson and Kling, 1967, Skutelsky and Danon, 1967, Awai et al., 1968, Campbell, 1968). Autophagy has been shown to be a key step in the elimination process of mitochondria from erythroblasts which leads to severe anaemia when defective

(Mortensen et al., 2010), and vapB has key roles in regulating autophagy, including ER-orchestrated autophagosome biogenesis through interaction with ULK1 and WIPI2 (Zhao et al., 2018), interactions with PTPIP51 to form an ER-mitochondria tethering complex (Gomez-Suaga et al., 2017b, Stoica et al., 2014b), and interaction with autophagosome adapter sequestosome 1 (James et al., 2021, Cha-Molstad et al., 2017). The vapB^{P56S} mutation has been shown to alter early and late stages of autophagy in muscle and skin fibroblast samples from ALS patients (Tripathi et al., 2021a), and cause mislocalisation of vapB^{P56S} from the ER to the autophagosome in the motor neurons of a knock-in murine model (Larroquette et al., 2015). The reduction of functional vapB could have a detrimental effect on the maturation process of erythrocytes through altered interaction with proteins such at PTPIP51, leading to the changes seen in this study.

Female rats do not have any significant changes in erythrocyte parameters, but vapB$^{P56S/P56S}$ have an elevated concentration of segmented neutrophils, and vapB$^{-/-}$ have a high concentration of lymphocytes. Continuous screening for infections in the rodent housing units detected Kilham Rat Virus (KRV) and Rat Parvovirus (RPV) were around the same time as blood sample collection. KRV induces autoimmune diabetes in rats mediated by T lymphocytes and involving lymphocyte infiltration of the pancreas (Chung et al., 2000, Ellerman et al., 1996, Guberski et al., 1991), whereas RPV decreases lymphocyte viability and suppresses T lymphocyte function and proliferation (McKisic et al., 1995) However, there were no significant changes in male rat leukocytes. Studies of sex differences in susceptibility to viral infection indicate male rats were more likely to be infected than females (Kosyreva et al., 2020, Klein et al., 2001, Hannah et al., 2008), likely to be linked to progesterone which has been shown to suppress dendritic cell-stimulated activation of T lymphocytes and suppress pro-inflammatory cytokine production (Butts et al., 2007). There was no literature on the effect of these infectious agents on erythrocytes, so changes seen in male vapB$^{-/-}$ cannot be linked to viral infection without further study. The presence of infectious agents at the time of blood sampling was an important factor that should be taken into account when interpreting such results in any future work of the colony.

Activated monocytes were recruited to the spinal cord of an ALS mouse model, and the microRNA inflammatory signature was similar to that found in ALS patients (Butovsky et al., 2012) but monocytes remained unchanged in the blood samples of 3 – 5 month old rats in

this study. However, lymphocytosis in female vapB$^{P56S/P56S}$ may indicate similar changes in ALS patients where cytotoxic T lymphocytes (CD8^{+}) were recruited and had a detrimental effect on disease progression (Rentzos et al., 2012, Jin et al., 2020). Given the relatively young age point at which blood samples were obtained in this study, future work should involve taking samples at a later age to detect potential elevations in monocytes and lymphocytes, and mild anaemia coupled with increased variability in erythrocytes. However, limitations in lateral vein blood collection from older rats should be taken into account.

Further blood chemistry analysis would be beneficial from male rats given the excess weight gain in vapB$^{P56S/P56S}$ and vapB$^{-/-}$ males compared to vapB. Cholesterol, triglycerides, and AST in those genotype might be elevated compared to vapB, indicating weight gain from aberrant lipid metabolism. This, in conjunction with measuring food intake, could help to determine if changes in lipid metabolism or hyperphagia may have roles in increased weight gain seen here.

There was no literature specifically investigating the role of vapB in erythropoiesis, and data on blood analysis in rodents was not split by sex. However, the MSP domain was studied as a potential biomarker of ALS from peripheral blood leukocytes (Deidda et al., 2014), and vapB was misfolded in the peripheral mononuclear cells of ALS patients (Cadoni et al., 2020). As the region coding the MSP domain of vapB was knocked out in vapB$^{-/-}$ rats, this might indicate a role in the domain in oxygen dynamics in the blood.

3.5.4 Pilot Mitochondrial Metabolism Analysis

Maximum capacity for mitochondria to endure a stressed environment was induced by increasing the porosity of mitochondrial membrane, and forcing complexes of the ETC to work hard to restore the mitochondrial membrane potential needed to generate ATP by ATP synthase. The ability to cope with this kind of stress was reduced in vapB$^{P56S/+}$ compared to vapB hippocampal cells, indicating altered capability of the ETC of vapB$^{P56S/+}$ in stressful conditions. This was reflected in the reduced activity of ETC complexes in SOD1 mouse models (Clark-type electrode oxygraph showed reduced ETC complex activity and oxidative phosphorylation (Mattiazzi et al., 2002), spectrophotometric enzyme assay found reduction in activity in lumbar spinal cord from SOD1 G93A mice (Jung et al., 2002) and loss of cytochrome C from ETC of mitochondria (Kirkinezos et al., 2005), Seahorse assay revealed

shift from oxidative phosphorylation to glycolysis in fibroblasts cultured from SOD1^{I113T} patients (Allen et al., 2014)). There was also proof of impaired mitochondrial respiration in TDP-43 (Hong et al., 2012, Wang et al., 2013b, Duan et al., 2010, Lu et al., 2012), FUS over-expression (Deng et al., 2015, Stoica et al., 2016), SIGMAR1 mutation related to ALS (Tagashira et al., 2014), and SQSTM1 knockout and fibroblasts from patients with VCP/p97 (Bartolome et al., 2013). Changes in mitochondrial respiration could have been affected by impaired calcium homeostasis (Glancy et al., 2013, McCormack and Denton, 1989), decreased anterograde axonal transport (Fang et al., 2012), or disrupted ER-mitochondria contacts (Stoica et al., 2016) all implicated in the presence of vapB^{P56S} (De Vos et al., 2012, Mórotz et al., 2012).

There was also a reduction in non-mitochondrial O_2 consumption by vapB$^{P56S/+}$ hippocampal cultures compared to vapB. Whilst the role of non-mitochondrial oxygen consumption has not been specifically defined, potential contributors include enzymatic reactive oxygen species (ROS) generation (Manes and Lai, 1995, Boveris et al., 1972, Boveris and Chance, 1973, Turrens, 2003, Johnson et al., 2007b, Johnson et al., 2007a, Piccoli et al., 2005). There was also evidence of O_2 consumption at cell surface level (Herst and Berridge, 2007) to support rapidly proliferating cells producing ATP through glycolysis (Krisher and Prather, 2012). The reduction in non-mitochondrial oxygen consumption being linked to ROS production could be supported by evidence of iPSC-derived MNs from ALS8 patients having lower levels of ROS compared to healthy controls (Oliveira et al., 2020).

ER calcium regulation and ROS production were closely linked (Grupe et al., 2010, Florea and Blatter, 2008, Redondo et al., 2004), and vapB interaction with PTPIP51 in calcium regulation was altered by the P56S mutation (De Vos et al., 2012), but ROS have also been shown to have important signalling properties in the innate and adaptive immunity (Chandel et al., 2000, West et al., 2011, Heid et al., 2013) and induce reversible post-translational modification (Paulsen et al., 2011, Krishnan et al., 2011). The reduction in non-mitochondrial oxygen consumption could point to a reduction in cellular oxygenase activity, altered calcium regulation, altered ER-mitochondria contacts, or modified redox signalling.

There was evidence of reduced ROS in the muscle of *C.elegans* carrying the vpr-1 (homolog of vapB) null mutation (Han et al., 2012).post m However, most literature regarding ROS and ALS indicate increased oxidative damage in the spinal cord and motor cortex (Ferrante et al.,

1997, Abe et al., 1995, Beal et al., 1997, Shaw et al., 1995), and reduced glutamate binding in synapses when exposed to ROS (Volterra et al., 1994, Trotti et al., 1996, Rao et al., 2003). Whether reduced non-mitochondrial oxygen consumption in vapB$^{P56S/+}$ was linked to changes in ROS production or oxidative damage would need to be investigated by comparing ROS production in vapB tissue.

Data from this study was not separated by sex, but this is an avenue to explore in future work by genotyping for sex as well as vapB mutation, especially given the differences in weight gain in males.

3.5.5 Major Sperm Protein in Cerebrospinal Fluid

A method was adapted from (Nirogi et al., 2009) with great help from ML to obtain CSF from adult rats in a terminal procedure, the details of which can be found in Chapter 2. However, initial western blots of samples were carried out but failed to detect a vapB-MSP signal.

Deidda and colleagues used 100µg of total protein from human CSF samples to detect MSP by immunoblotting, whilst 4-5µg of total protein was obtained per rat CSF sample. Given the faint signal detected by #6 antiserum against vapB-MSP (see Chapter 5), with homogenates having a total protein concentration of 20-25µg (see Chapter 2), this was not enough to obtain a detectable signal from immunoblotting. There was insufficient time to find alternative methods to detect and quantify MSP from individual or pooled rat CSF samples.

A study set out to identify biomarkers in CSF of neurotoxicity in 8-9 month old male F344 rats exposed to carbonyl sulphide (Lardinois et al., 2014). Samples were collected via lumbar puncture for analysis. Two main methods were utilised to detect and quantify low concentrations of proteins: Enzyme-Linked Immunosorbent Assay (ELISA) and Mass Spectroscopy (MS). ELISA was utilised to determine the amount of blood that contaminated CSF samples. In the indirect ELISA protocol followed in the study, samples coated the wells and were probed with rabbit anti-rat haemoglobin antibody and detected using a secondary antibody tagged for chemiluminescence, the emission of which was recorded by a microplate reader. Contamination was defined as 1/500,000 dilution of whole blood sample, roughly equivalent to 10 RBC/µl (Zhang, 2007) due to the high protein content of blood compared to CSF (You et al., 2005). Of their samples, 86% were deemed to be contaminated. This included samples visually deemed to be clear compared to red samples with evident blood

contamination. Other proteins present in blood but not present in CSF could be measured such as apolipoprotein B (apoB), which in humans was a contaminant at 1:6000 in concentration in CSF (Zhang, 2007). Control concentrations of haemoglobin or apoB in wild type rats should be established as a baseline to compare experimental samples as concentrations of various proteins differs between species (Martens, 2015). Low speed centrifugation could pellet myeloid cells, but dissolved proteins may still artificially drive up the total protein concentration of samples. Analysing MSP in rat serum and using data to "normalise" data obtained from contaminated samples could be an option, but would involve determining the degree of contamination in each sample as well as a baseline of MSP in blood for each genotype.

ELISA could be utilised to detect MSP in pooled CSF samples, but detection using #6 rabbit anti-MSP serum would likely yield a very faint signal given results from this project. Biotin amplification may help to boost the signal by applying a biotinylated secondary anti-rabbit antibody and incubating with HRP-conjugated avidin or streptavidin. This could be further assisted by protein enrichment techniques prior to ELISA detection, such as precipitation and fractionation. These techniques were utilised in a proteomic study of human CSF to find age-related changes (Zhang, 2007). Fractionation was also utilised in the neurotoxicity study by Lardinois and colleagues to enrich low abundance proteins and deplete high abundance proteins fraction by fraction. Fractions were subjected to matrix assisted laser desorption/absorption mass spectrometry (MALDI-MS) which utilises "soft ionisation" to apply a charge to large molecules. This confirmed that fractionation depleted abundant proteins such as albumin and haemoglobin, and low abundance proteins were enriched in later fractions.

In a pilot study, Lardonis and colleagues pooled 10 CSF samples and put them through MALDI-MS. The presence of haemoglobin indicated contamination and implied other protein concentrations may have been compromised. CSF samples deemed to not be contaminated (via ELISA) were put through liquid chromatography electrospray ionisation tandem mass spectroscopy (LC-ESI-MS-MS). This would have provided the best chance to detect proteins a low concentrations, but detection failed in these samples due to the extremely low concentration of protein available in the non-contaminated samples. The group concluded that alternative methods for obtaining CSF that limited blood contamination and obtaining

samples when neurotoxicity would have been more extensive might have resulted in a greater concentration of proteins that would have been detectible. Even if no blood contamination occurred, protein concentration would still be below detection unless samples were pooled and low abundance proteins enriched.

It was also key to keep in mind the rostrocaudal gradient effect in CSF as some analytes were more abundant in some regions of CNS than others (Tarnaris et al., 2011), so sampling CSF from the cisterna magna at the base of the skull rather than close to the lumbar region of the spinal cord may have an effect on CSF protein composition.

3.5.6 Ageing Fischer Rats and Splenomegaly

There appeared to be an issue with the health of the spleen in male Fischer F344 rats in the ageing cohort. Within weeks of each other, 2 male rats (1 x vapB and 1 x vapB$^{P56S/+}$) at 17.5 months became lethargic, and appeared to have pale eyes, nose, ears, and paws. When handled, a large, long, rigid mass could be felt in the abdomen. During post-mortem, this transpired to be an enlarged spleen. Rats in the ageing cohort were limited to age up to 17 months instead of the intended 18 to prevent the development of further cases.

The University of Edinburgh Bioresearch and Veterinary Services Named Veterinary Surgeon clarified that Kilham Rat Virus (KRV) infection was detected in the housing unit around the same time that symptoms developed. KRV has been linked to the development of T cell-dependent autoimmune diabetes in rats (Ellerman et al., 1996), and diabetes has been linked to spontaneous splenomegaly in mice fed a high-fat high- sugar diet (Buchan et al., 2018). A high fat diet alone in rats did not change splenic morphology in rats (Jakobsdottir et al., 2013) so the addition of sugar or the larger amount of fat included in the mouse study may have helped to induce splenomegaly as already noted (Buchan et al., 2018). The vapB$^{P56S/+}$ and vapB$^{-/-}$ male rats in this study gained more weight than vapB between 10 and 17 – 18 months, so this in conjunction with KRV infection might have induced splenomegaly, especially if lipid metabolism was altered.

Another potential culprit was mononuclear cell leukaemia (MCL) as symptoms match observations in these rats. This was a condition that F344 rats are susceptible to when ageing, with 22.2% of males developing the condition and the risk of developing the condition increasing from 20 months old (Stromberg and Vogtsberger, 1983). Incidence in this colony

was 2 out of the 14 males (14.3%) ageing to 18 months with each case happening around 17.5 months of age. Implanting tumorous cells into healthy recipient rats resulted in haemolytic anaemia, presence of tumorous cells in peripheral blood and spleen, dispersion of splenic lymphoid tissue (Stromberg et al., 1990). Regarding haematology, an increase in the number of immature red blood cells (reticulocytosis), severe haemolytic anaemia, neutrophilia, reduction in lymphocytes (lymphocytopenia), marked reduction in platelets (thrombocytopenia), and aniocytosis (Stromberg et al., 1983) are also hallmarks of MCL.

Official diagnosis would need to be made by histological processing of spleens and livers collected and embedded in paraffin wax to find signs of abnormal or tumorous cells infiltrating the spleen and liver. Aniocytosis was identified in the 3 – 5 month old $vapB^{-/-}$ male rats, and neutrophilia was identified in female $vapB^{P56S/P56S}$ rats. A survival study where blood samples were monitored for monocyte proliferation, erythrocyte depletion, and analysis to see if genotype affects either parameter would help to maintain any future ageing colonies. As shown in this project, blood collected from 3 – 5 month old animals had unchanged monocyte concentrations in male and female rats which were relatively normal compared to data collected elsewhere (Stromberg et al., 1983), so samples would also have to be taken at later age points for monitoring if a longer study was carried out.

4 Motor Behaviour

4.1 RotaRod

The rotarod was a widely used piece of equipment used as an assay for the motor behaviour of rodents, so a pilot longitudinal study of vapB and vapB$^{P56S/+}$ female rats over the course of 6 months was carried out. Data was collected every 2 weeks and Figure 4.1 shows the results. Performance was measured at slow (5rpm) and medium (12rpm) speeds, and weight data was also collected from each animal throughout the study.

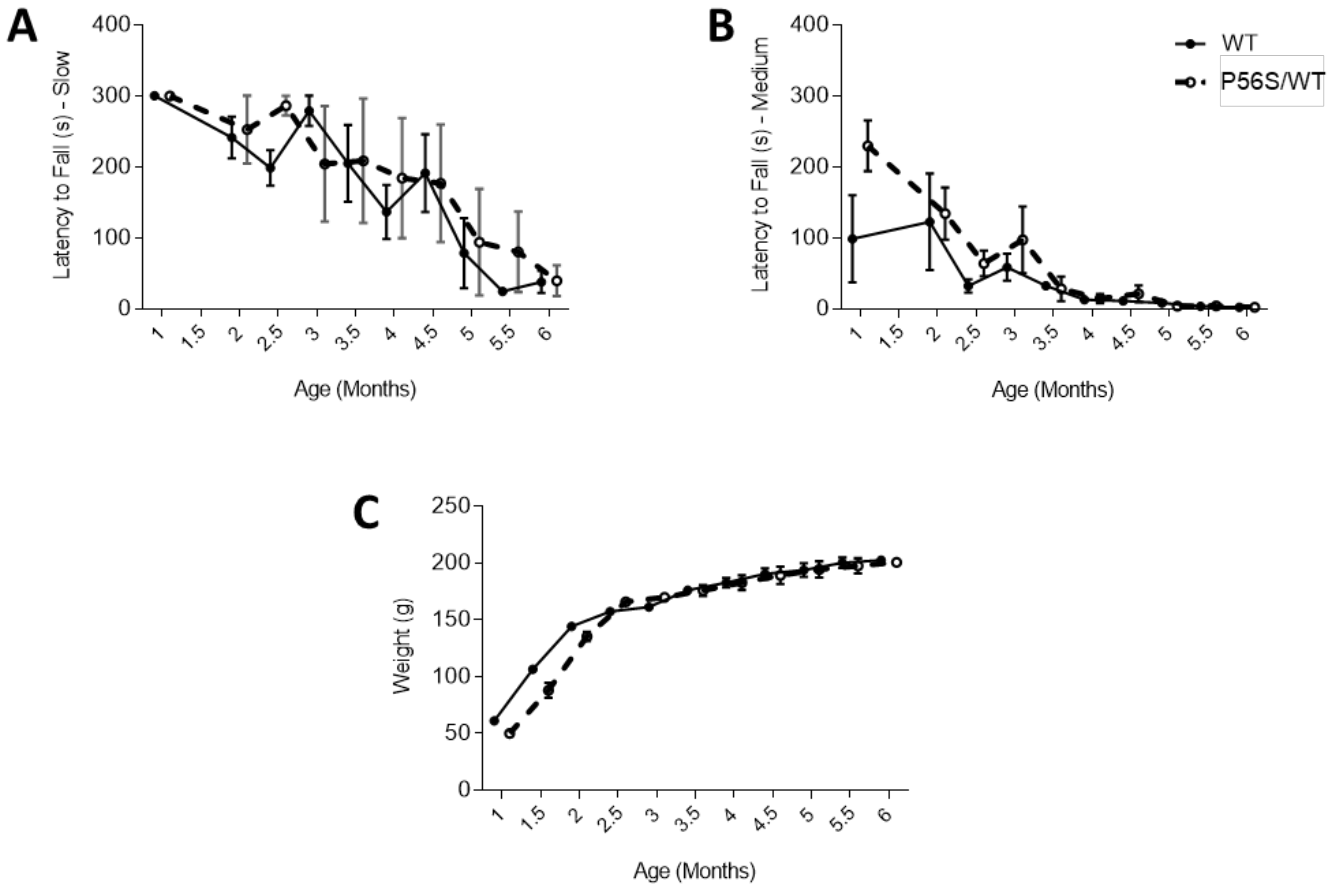

Figure 4.1: Rotarod motor assessment and weight gain over 6 months for vapB and vapB$^{P56S/+}$ female rats.
A: Latency to fall at slow speed (5rpm). **B**: Latency to fall at medium speed (12rpm). **C**: Weight measured over course of rotarod assessment. Mean and S.E.M displayed. Bonferroni-Dunn t-tests applied for rotarod performance and weight gain. n=3 for both groups.

Performance of both groups did not differ significantly from each other, but there was an average reduction in latency to fall over the course of 6 months for both groups. Data for

these female rats was not collected beyond 6 months/200g due to the rota rod motor being unable to cope with heavier rats “dragging” the rod as they fell, suddenly accelerating the speed of the rod and causing other rats on the rod to fall prematurely. Male rats reached 200g at 2 months old on average. The limitations of the rod motor being able to withstand the weight of animals over 200g and the excessive time it would have taken to record individual performances over the course of 18 months made the rota rod an inefficient method of gaining mobility data from the ageing cohort. That, in combination with the level of handling and researcher involvement in data collection, had the potential to influence or mask subtle changes in mobility over time. An alternative method for recording motor behaviour needed to be sought out.

4.2 CatWalk Gait Analysis

The CatWalk Gait Analysis system uses light intensity and images captured by a high-speed camera to capture the gait of individual animals as they run across a walkway, and compute subtle changes in gait from paw prints (Hamers et al., 2006, Hamers et al., 2001) as shown in Figure 4.2.

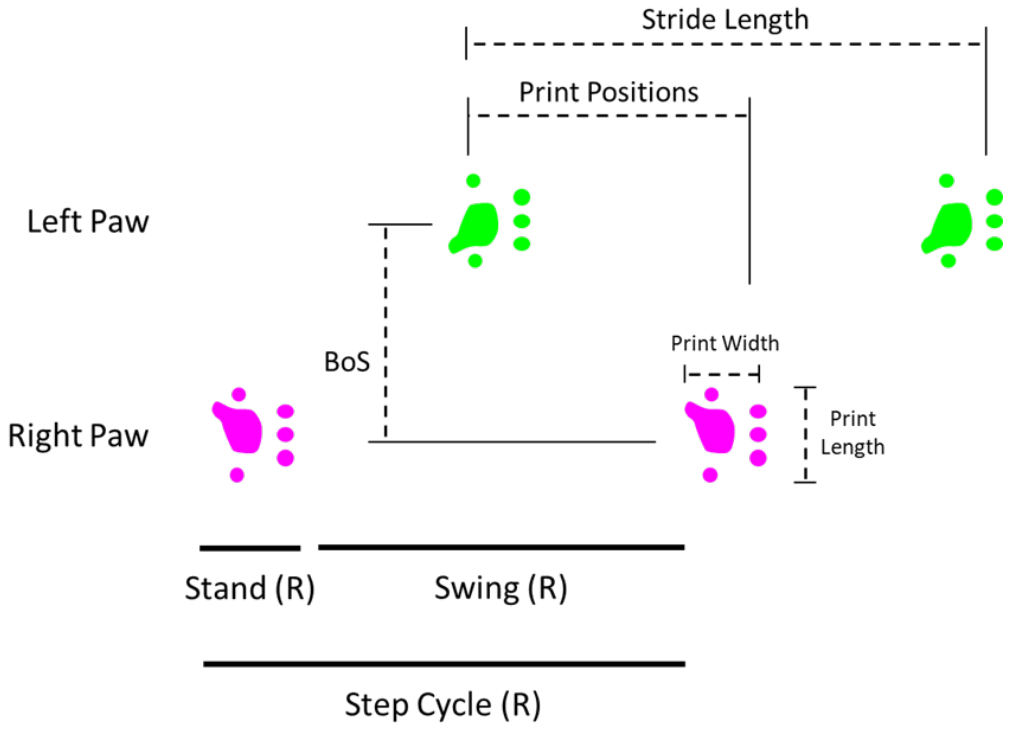

Figure 4.2: Key parameters recorded by CatWalk XT 8.1 software.
Spatial and temporal parameters calculated from information gained from paw prints generated by frustrated total internal reflection (fTIR). BoS – Base of Support.

Data was separated by sex due to significant weight differences between male and female rats. Multiple spatial and temporal parameters were imputed from information captured about signal intensity, paw placements, paw print area, and temporal relationships between paws that represent aspects of coordination. Table 4.1 shows how each parameter captured by the software was grouped in this study.

The p-values from statistical analysis on all parameters can be found in Appendix 1, but there were a number of key findings. In the male rats, the greatest changes were in parameters relating to paw pressure, namely the signal intensity of paws against the glass walkway that was recorded. Male vapB$^{P56S/P56S}$ exerted less pressure through their paws at 12 and 17 – 18 months than vapB (A – C), indicating a lighter paw tread. The minimum intensity of vapB$^{P56S/+}$ at 6 months was greater than vapB (D), implying that their lighter paw treads at that age were not as light as vapB.

There was also a change in paw intensity in female rats that was most prominent at 17 – 18 months where vapB$^{P56S/P56S}$ and vapB$^{-/-}$ both exerted less pressure on their paws than vapB (A – C), but their minimum intensity was greater at this age (D). This indicates a reduced range of paw pressure at 17 – 18 months.

The female vapB$^{P56S/P56S}$ and vapB$^{-/-}$ rats also had reduced paw size parameters at 17 – 18 months compared to vapB (A – E). This, in conjunction with the reduction in paw pressure exerted by paws, depicts a “tip-toe” like gait acquired by these rats by the time they reach 17 – 18 months.

	Parameter	Paw Statistic	Units	Definition
Support	Base of Support (BOS)	N	mm	Average width between girdle paw pairs (front pair, hind pair)
	Duty Cycle	Y	Stand as % of Step Cycle	Average proportion of Step Cycle for specific paw spent supporting weight.
	Number of Steps	N	#	Number of steps within one run
	Print Positions	N	mm	Average distance between lateral paws (left pair, right pair)
	Stand	Y	s	Average time paw was in contact with glass
	Stride Length	Y	mm	Average distance between sequential paw placements
	Support	Y	%	Proportion of run that rat was not in contact, or was in contact with runway on 1 paw, a diagonal pair of paws, a lateral pair of paws, a girdle pair of paws, 3 paws, or all 4 paws.
Pressure	Maximum Contact Maximum Intensity	Y	AU	Average maximum intensity at maximum contact (from 0 to 255). Intensity increases with pressure
	Maximum Contact Mean Intensity	Y	AU	Average mean intensity at maximum contact (from 0 to 255). Intensity increases with pressure
	Maximum Intensity	Y	AU	Average maximum intensity of complete paw
	Maximum Contact At	Y	s	Average time since start of run that largest part of paw makes contact with glass
	Minimum Intensity	Y	AU	Average minimum intensity of complete paw
	Mean Intensity	Y	AU	Average mean intensity of complete paw
Speed	Average Speed	N	frames/s	Average speed across one run
	Maximum Variation	N	%	Maximum variation of running speed within one run
	Run Duration	N	s	Total time taken to traverse the runway on one run
	Step Cycle	Y	s	Average time between two consecutive initial contacts of the same paw.
	Swing Speed	Y	frames/s	Average speed between sequential paw placements

Coordination	Body Contacts	N	% of run	Proportion of run the other body parts (right or left hip, right or left knee, nose, tail, abdomen, gonads, or tail) contacted the walkway
	Cadence	N	steps/s	Average number of steps taken per second during a run
	Number of Patterns	N	#	Number of recognised step sequences within a single run
	Phase Dispersions	N	% of Anchor Step Cycle	Mean delay between the placement of two paws
	Regularity Index	N	% in pattern	Proportion of steps included in recognised step patterns
	Stand Index	Y	frames/mm^2	"Speed paw loses contact with glass (indicates paw dragging)stand index= (a/0x)*frame rates from y=ax+b describing line of best fit of t(Max Area) in 90% percentile, 0x was max contact area“
	Step Sequence	N	%	Proportion of runs in cruciate, alternate, or rotate sequences
	Swing	Y	s	Average time paw was not in contact with walkway
Paw Shape	Maximum Contact Area	Y	mm^2	Average maximum area of paw that comes in contact with glass
	Maximum Contact At	Y	% of stand	Percentage of stand time transitioning from braking to propulsion during Stand
	Print Area	Y	mm^2	Average area of paw print
	Print Length	Y	mm	Average length of paw print
	Print Width	Y	mm	Average width of paw print

Table 4.1: Parameters generated by CatWalk XT8.1 software.
Parameters grouped by Support, Pressure, Speed, Coordination, and Paw Size. Parameters relating to specific paws (right front, left front, right hind, and left hind) were marked out in the Paw Statistic column marked by “Y” (yes), and others marked with “N” (no).

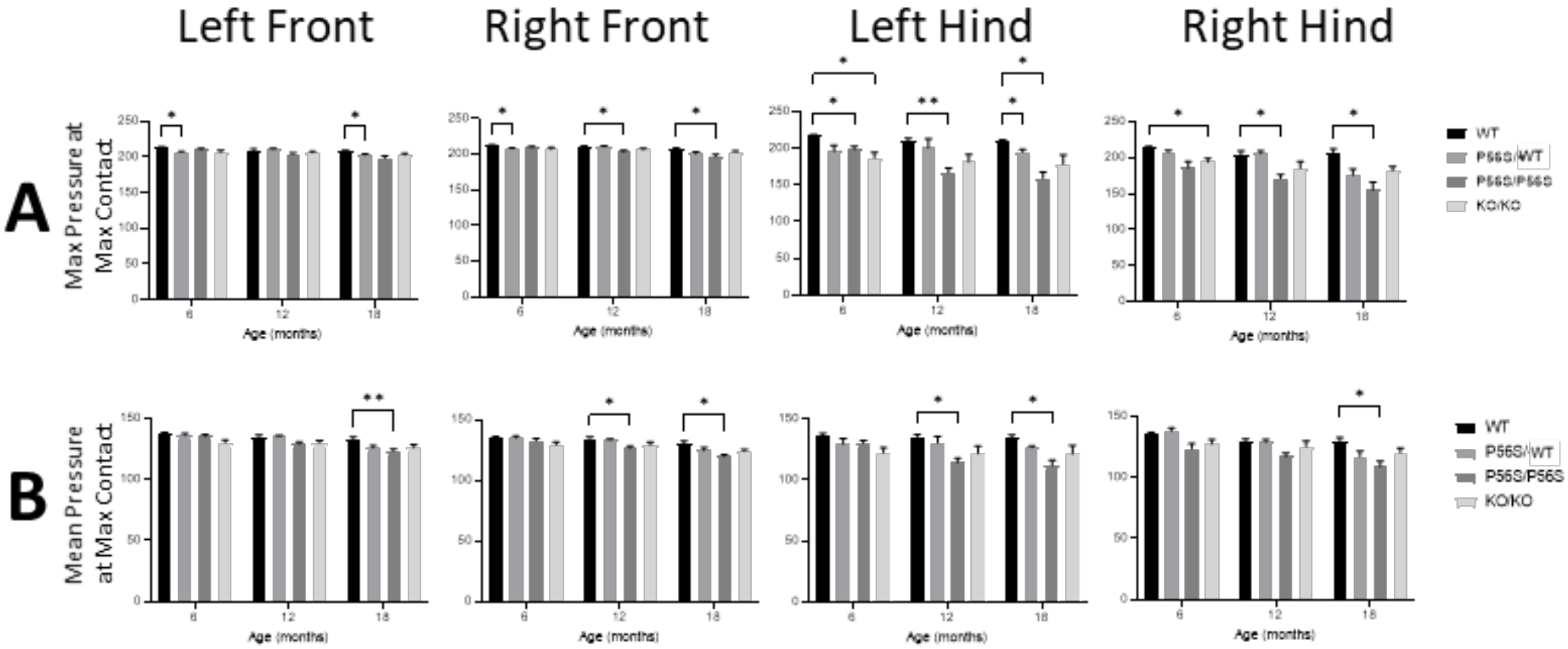
Left Front
Right Front
Left Hind
Right Hind
A
Max Pressure at Max Contact
B
Mean Pressure at Max Contact
Age (months)
WT
P56S/WT
P56S/P56S
KO/KO

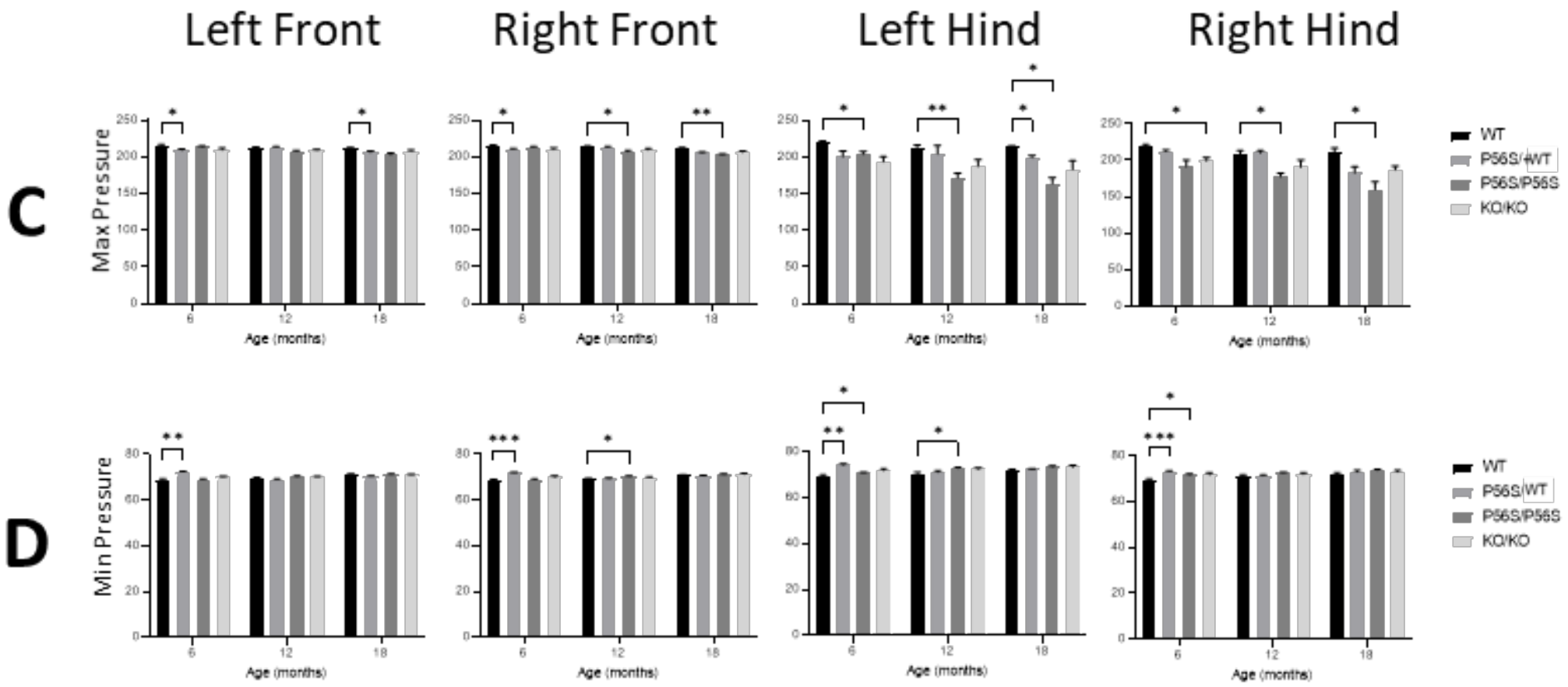

Figure 4.3: Parameters related to Print Intensity of male rats at 6, 12, and 17 – 18 months.
A: Max Pressure at Max Contact – Maximum pressure exerted by paw when maximal contact area was generated by the paw. **B**: Mean Pressure at Max Contact – Average pressure exerted by paw when maximal contact area was generated by the paw. **C**: Max Pressure – Maximal pressure exerted by the paw. **D**: Min Pressure – Minimal pressure exerted by the paw. Two-way ANOVA with Tukey's post-hoc test applied to each parameter. n=3-5 animals per sex per genotype. * p<0.0500, ** p, 0.0100, *** p<0.0010, **** p<0.0001.

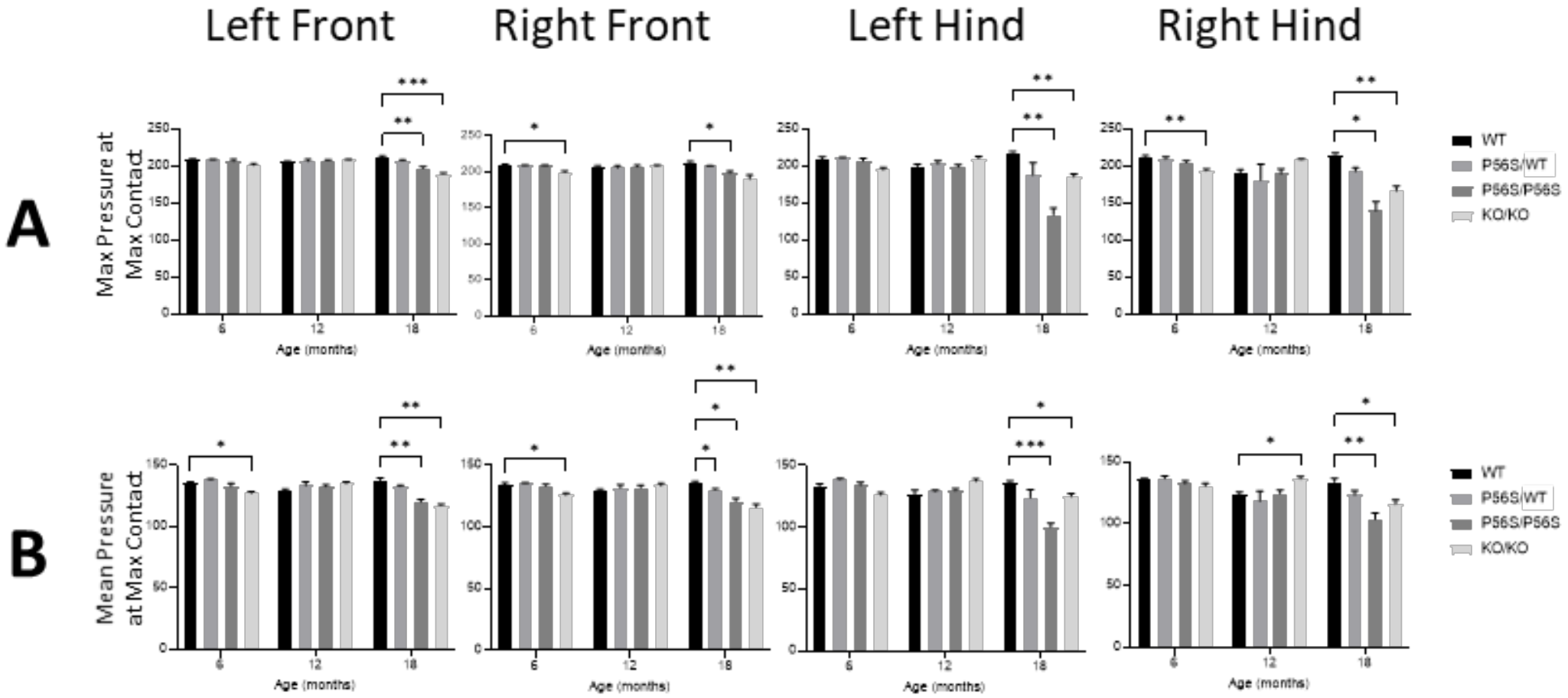
Left Front
Right Front
Left Hind
Right Hind
A
Max Pressure at Max Contact
B
Mean Pressure at Max Contact
Age (months)
WT
P56S/WT
P56S/P56S
KO/KO

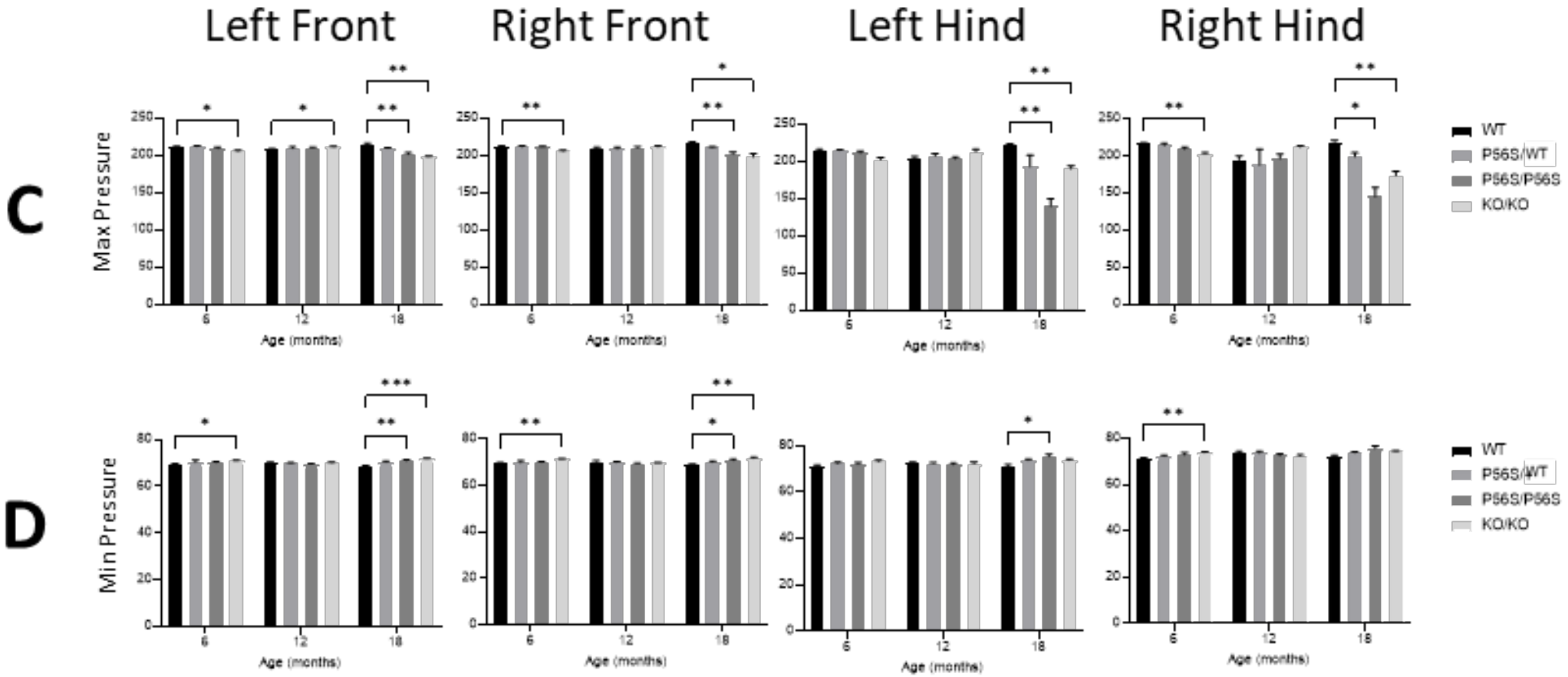

Figure 4.4: Parameters related to Print Intensity of female rats at 6, 12, and 17 – 18 months.
A: Max Pressure at Max Contact – Maximum pressure exerted by paw when maximal contact area was generated by the paw. **B**: Mean Pressure at Max Contact – Average pressure exerted by paw when maximal contact area was generated by the paw. **C**: Max Pressure – Maximal pressure exerted by the paw. **D**: Min Pressure – Minimal pressure exerted by the paw. Two-way ANOVA with Tukey's post-hoc test applied to each parameter. n=3-5 animals per sex per genotype. * p<0.0500, ** p, 0.0100, *** p<0.0010, **** p<0.0001.

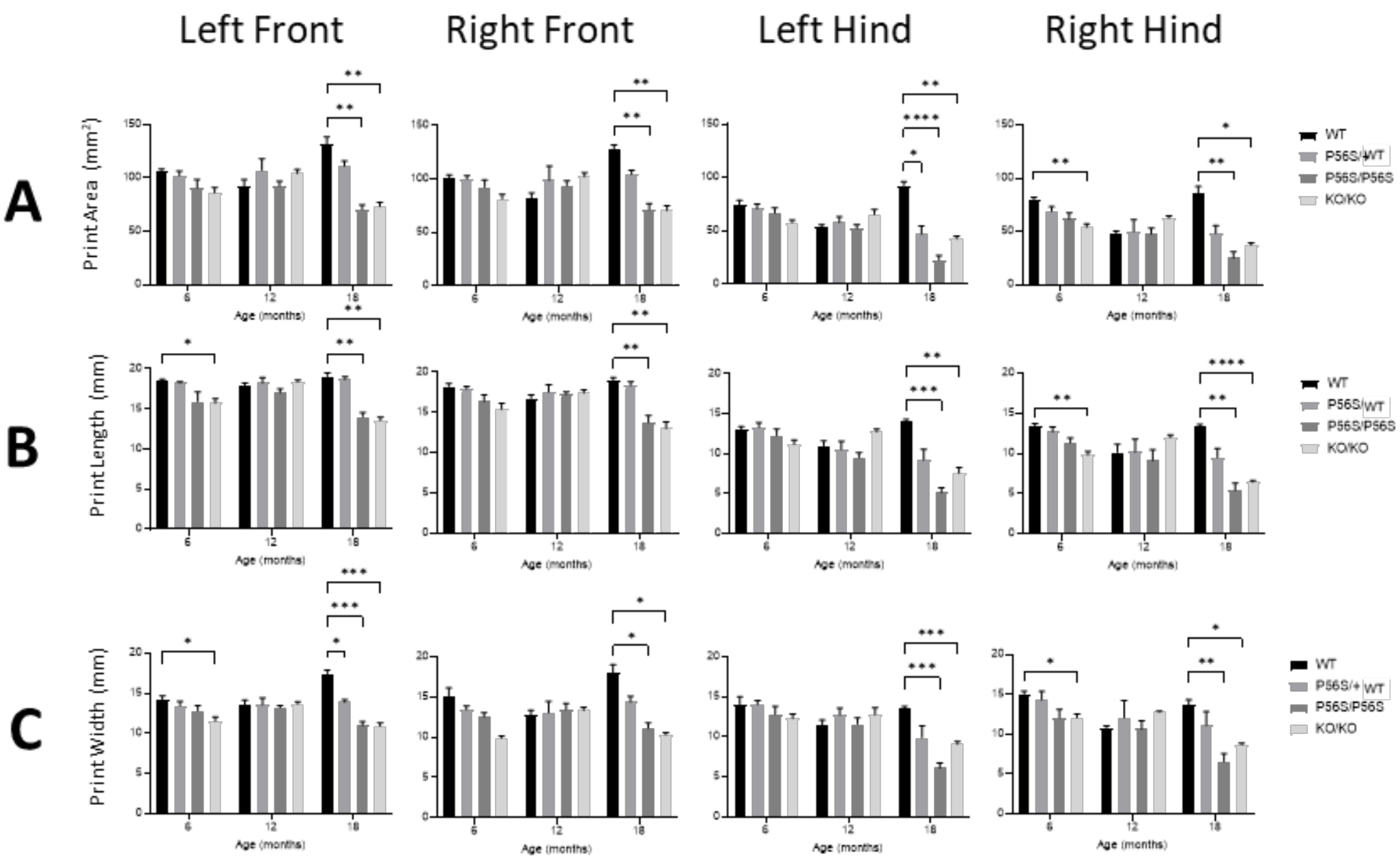
Left Front
Right Front
Left Hind
Right Hind
A
B
C
Print Area (mm²)
Print Length (mm)
Print Width (mm)
Age (months)
WT
P56S/+WT
P56S/P56S
KO/KO

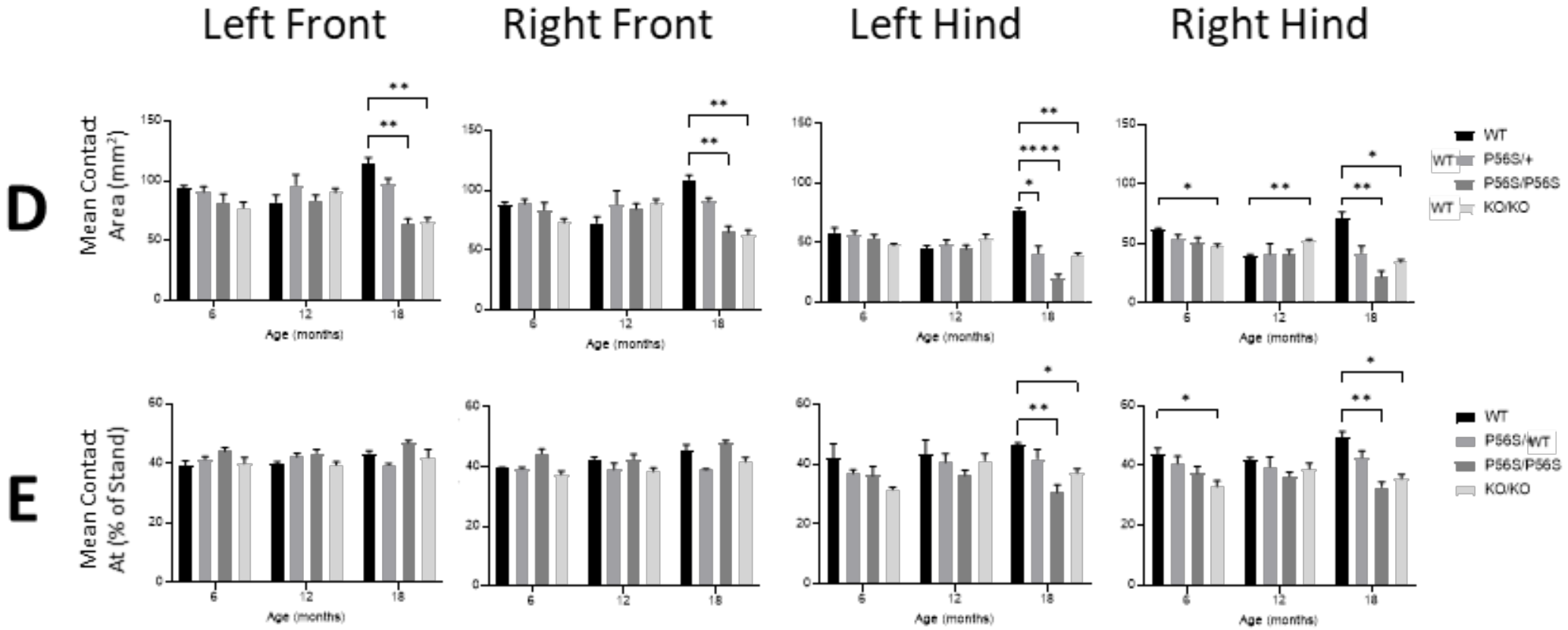

Figure 4.5: Parameters related to Paw Size of female rats at 6, 12, and 17 – 18 months.
A: Print Area – Average area of paw print recorded. **B**: Print Length – average length of paw print recorded. **C**: Print Width – Average width of paw print recorded. **D**: Max Contact Area – Maximum contact area generated by the paw. **E**: Max Contact At – The point during Stand where maximum contact was generated by the paw. Two-way ANOVA with Tukey's post-hoc test applied to each parameter. n=3-5 animals per sex per genotype. * p<0.0500, ** p, 0.0100, *** p<0.0010, **** p<0.00.

There has been data to suggest that speed has a large effect on the acquisition and calculation of many CatWalk parameters (Batka et al., 2014), so normalisation of parameters to speed would have mitigated this. However, only vapB$^{-/-}$ females at 12 months were significantly faster than vapB whilst all other groups had no significant changes in their average speed (C – D). This was reflected in vapB$^{-/-}$ having a faster Swing Speed (A) and longer Stride Length (B) compared to vapB, which was not the case with all other groups.

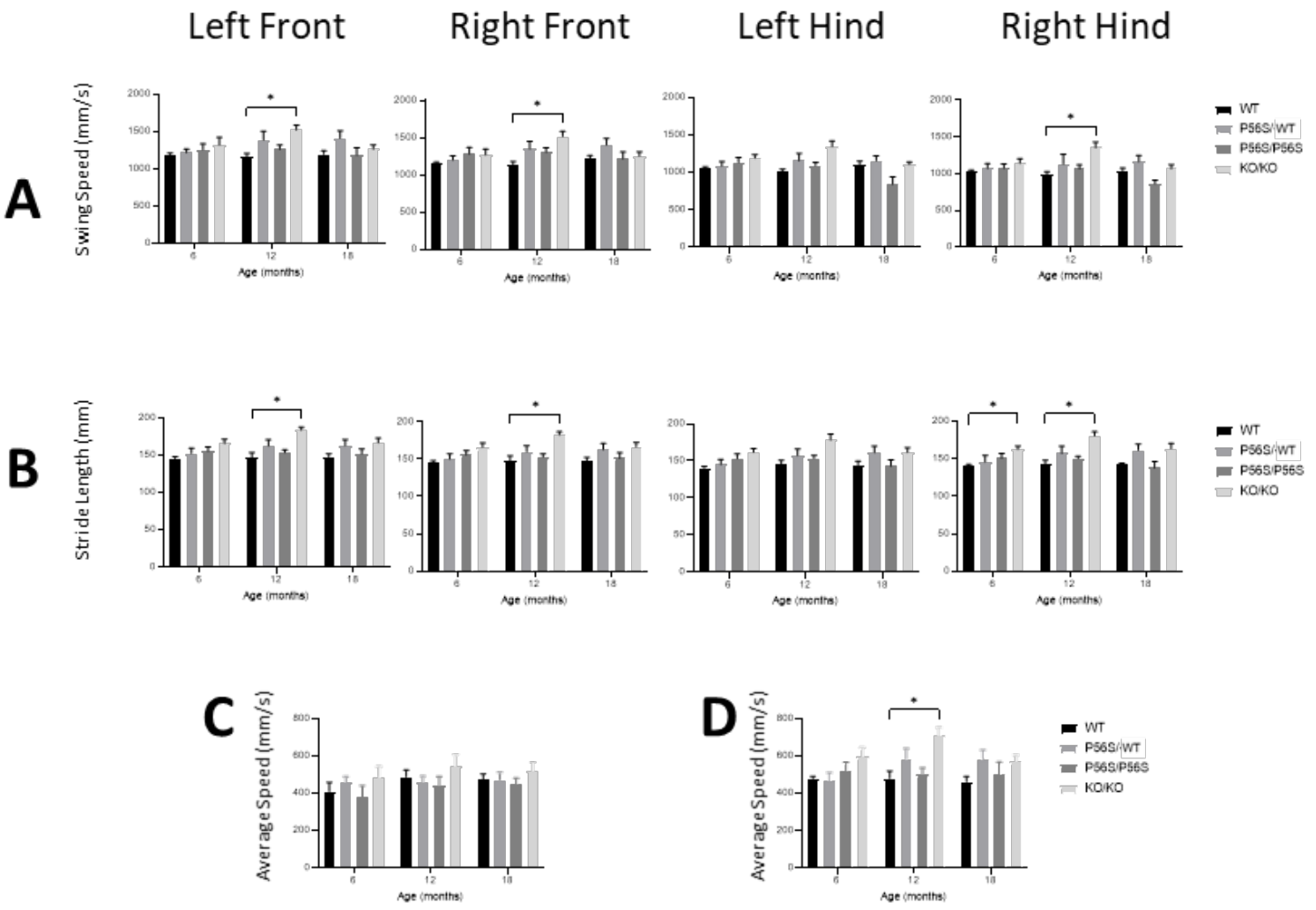

Figure 4.6: Swing Speed, Stride length, and Average Speed in female rats.
A: Swing Speed – Average speed in mm/s of the limb swinging from one placement onto the glass and the next. **B**: Stride Length – Average distance in mm of the limb swinging from one placement onto the glass and the next. Average Speed – How quickly an animal moved from one end of the CatWalk walkway to the other averaged across a run for male (**C**) and female (**D**) rats. Two-way ANOVA with Tukey's post-hoc test applied to each parameter. * p<0.0500, ** p, 0.0100, *** p<0.0010, **** p<0.0001.

The hind limb Base of Support (BoS) for 12 month old vapB$^{P56S/+}$, and 12 and 18 month old vapB$^{P56S/P56S}$ males was wider compared to vapB. However, front limb base of support for 18 month old vapB$^{P56S/P56S}$ was wider than vapB. Female vapB$^{-/-}$ also had wider front BoS across the age groups, but significantly so at 6 and 18 months ().

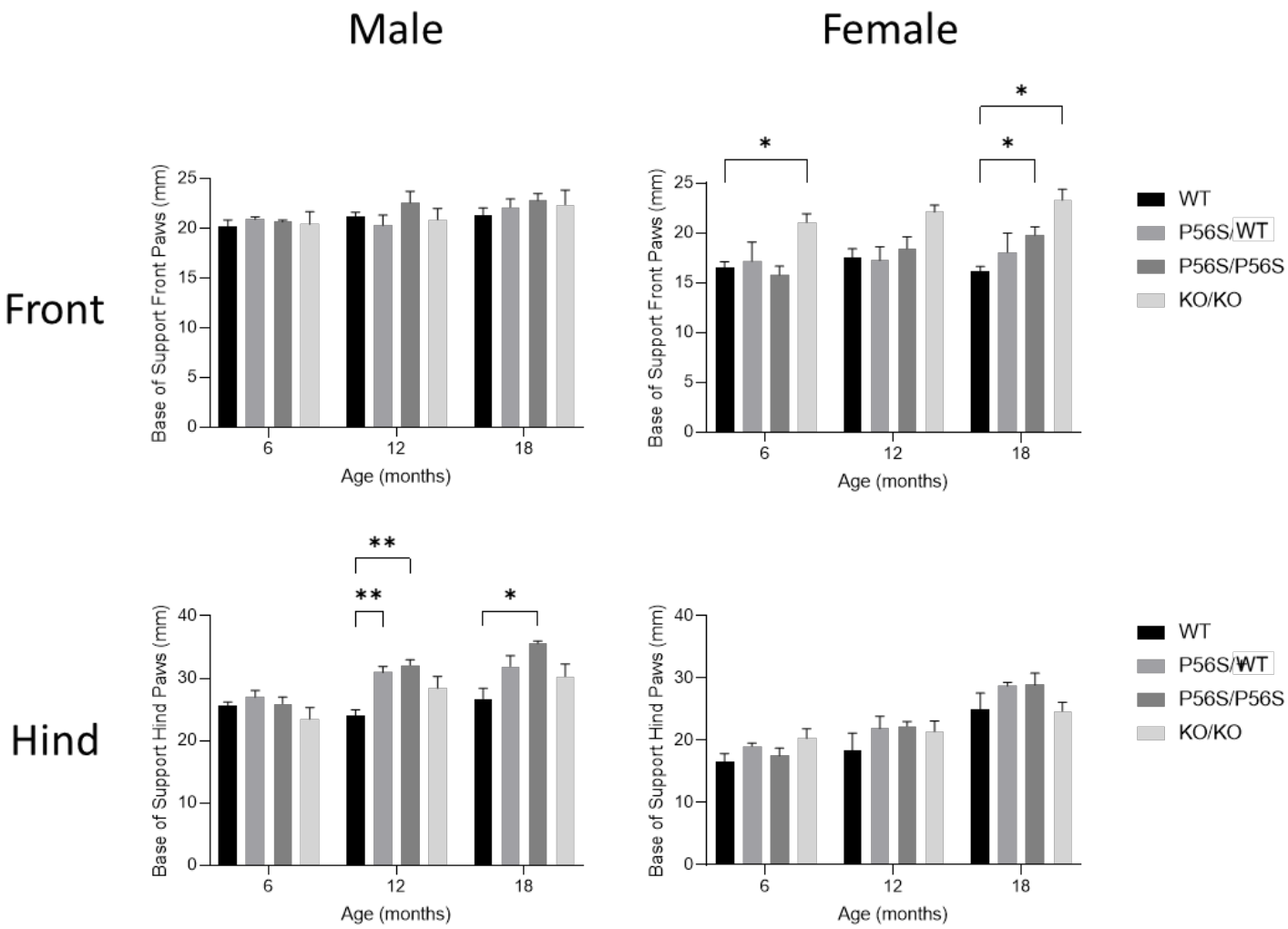

Figure 4.7: Base of Support (BoS) in male and female rats.
Two-way ANOVA with Tukey's post-hoc test applied to each parameter. n=3-5 animals per sex per genotype. * p<0.0500, ** p, 0.0100, *** p<0.0010, **** p<0.0001.

Overall, male vapB$^{P56S/P56S}$ had reduced paw pressure at 12 and 17 – 18 months compared to vapB, but this would need to be corroborated by correcting for weight gain. This does not appear to be connected increased weight gain at these ages (see Chapter 3) as vapB$^{-/-}$ also gain weight at the same rate and do not have similar changes in paw pressure. As previously mentioned, there were no significant differences in average speed so it was unlikely to be a factor.

For female rats, the greatest changes can be seen in paw print area and paw pressure, where both sets of parameters decrease at 17 – 18 months for vapB$^{P56S/P56S}$ and vapB$^{-/-}$. This does not appear to be connected to speed as there were no significant changes in average speed, and weight gain does not change over the course of 18 months (see Chapter 3).

4.3 Discussion and Future Work

The main motor changes in this model indicate a lighter tread during ambulation in male vapB$^{P56S/P56S}$ and female vapB$^{P56S/P56S}$ and vapB$^{-/-}$ at 18 months. This is in agreement with studies carried out in ALS patients who exerted less force in their footsteps (Fraiwan and Hassanin, 2021, Akgun et al., 2018). Patients also tended to have a greater variability in the time taken to complete step cycles, longer swing phase, longer step cycle (Hausdorff et al., 2000, Wu and Krishnan, 2009) shorter stride length, more time supported on two legs than one leg (Radovanović et al., 2014) and reductions in cadence and speed (Goldfarb and Simon, 1984). Changes in gait have been investigated as markers of ALS (Sanjak et al., 2017), and have opened up the possibility of classifying gait abnormalities in neurological disorders to assist in diagnosis (Fraiwan and Hassanin, 2021, Felix et al., 2021, Prabhu et al., 2020, Akgun et al., 2018). However, translating such findings from bipedal to quadrupedal organisms is not straightforward.

Studies into the gait of animal models of ALS have provided information on temporal and inter-paw relationships. Table 4.2 summarises changes in rodent models of ALS. Most data available for gait of rodent models of ALS have been generated with the SOD1^{G93A} mouse. Whilst there was no gait data for transgenic rats, SOD1^{G93A} rats had reduced spontaneous walking activity at 120 and 160 days (Nagai et al., 2001), and TDP-43 rats tended to cover less ground in open-field assays (Tong et al., 2013, Huang et al., 2012).

There are some conflicts regarding gait changes in existing rodent models of ALS. Swing speed of SOD1^{G93A} is faster than WT, but AMPKα2$^{-/-}$ is slower compared to WT. Stride length is longer for both FUF models, but shorter for SOD1, TDP-43, and AMPKα2$^{-/-}$. AMPKα2$^{-/-}$ rely more on diagonal support whilst SOD1 and TDP-43 have less reliance. Two different mouse models of SOD1^{G93A} have increased or decreased propulsion from stance phase, but both were analysed using treadmill gait analysis. It is inaccurate to put these differences down to the method of acquisition of data as treadmill and CatWalk data have provided the same outcomes for

SOD1^{G93A} models (longer stand duration, shorter stride length), and differing outcomes for the same method (propulsion). Data analysis and whether speed and weight were accounted for might have affected final conclusions, but replication of gait analysis in these models would offer better comparison of gait changes according to mutation. Applying false discovery rate to the vast array of data might also reduce the number of type 1 errors in the data, but time constraints limited the analysis.

	Mouse						Rat		
	SOD1^{G93A}	TDP-43	C9orrrf72 BAC	FUS ^{R514G}	FUS ^{R521C}	AMPKα2$^{-/-}$	vapB$^{P56S/P56S}$	vapB$^{-/-}$	Female vapB$^{P56S/P56S}$ and vapB$^{-/-}$
Stand Duration	↑ *(Haulcomb et al., 2017) +(Mancuso et al., 2011) *(Mead et al., 2011)					↑ *(Vergouts et al., 2015)			
Swing Duration			↑ +(Liu et al., 2016)			↑ *(Vergouts et al., 2015)			
Swing Speed	↑ *(Haulcomb et al., 2017)					↓ *(Vergouts et al., 2015)			

Stride Duration		↓ +(Chan et al., 2020)							
Stride Length	↓ +(Allodi et al., 2021) *(Mead et al., 2011) +(Hampton and Amende, 2009)	↓ +(Chan et al., 2020)		↑ **(Ling et al., 2019)	↑ **(Ling et al., 2019)	↓ *(Vergouts et al., 2015)			
Paw Pressure	↓ *(Haulcomb et al., 2017) *(Mead et al., 2011)						↓	↓	
Paw Area									↓
Base of Support		↑ *(Watkins et al., 2021)							

Diagonal Support	↓ *(Mead et al., 2011)	↓ *(Watkins et al., 2021)				↑ *(Vergouts et al., 2015)			
Propulsion	↑ +(Mancuso et al., 2011) ↓ +(Hampton and Amende, 2009)								
Paw Dragging	↑ +(Allodi et al., 2021)								
Relative Paw Position	↑ *(Haulcomb et al., 2017) *(Gerber et al., 2012)								

Table 4.2: Changes in gait of rodent models of ALS.
Unless specified, the vapB results combine changes in male and female animals. References included for other rodent models of ALS where gait is analysed.
* refers to gait analysis by CatWalk apparatus. + indicates gait analysis by treadmill. ** indicates gait analysis from paw prints taken using non-toxic paint.

Reduced paw pressure of male vapB$^{P56S/P56S}$ at 17-18 months was surprising given the increased weight gain compared to wild type (see Chapter 3), and that weight gain may have affected the gait of male rats rather than genotype (Pitzer et al., 2021). However, changes in gait seen in male vapB$^{P56S/P56S}$ at 12 and 17 – 18 months old were not reflected in vapB$^{-/-}$, suggesting a change not relating to weight gain.

Only 12 month old female vapB$^{-/-}$ rats were significantly slower than vapB, but this was the only statistically significant finding regarding average speed. It would be worth normalising data to speed and weight using a linear mixed model statistical method or regression analysis as used elsewhere (Haulcomb et al., 2017) which might have given more clear changes as speed especially affects CatWalk parameters (Batka et al., 2014). Regression analysis would allow for weight to also be factored in as this could affect data variability (Machado et al., 2015). Regression analysis was not completed on this data due to time constraints.

5 VAP Expression and Interactions

5.1 Size of vapB exon 2 affected by loxP sites or collateral knockout from CLICK knock-in generation

The distinct bands identifying each genotype were shown in Figure 5.1. The floxed sites around P56S-exon 2 increased the size of the gene, whilst knocking out exon 2 reduced the size of the gene.

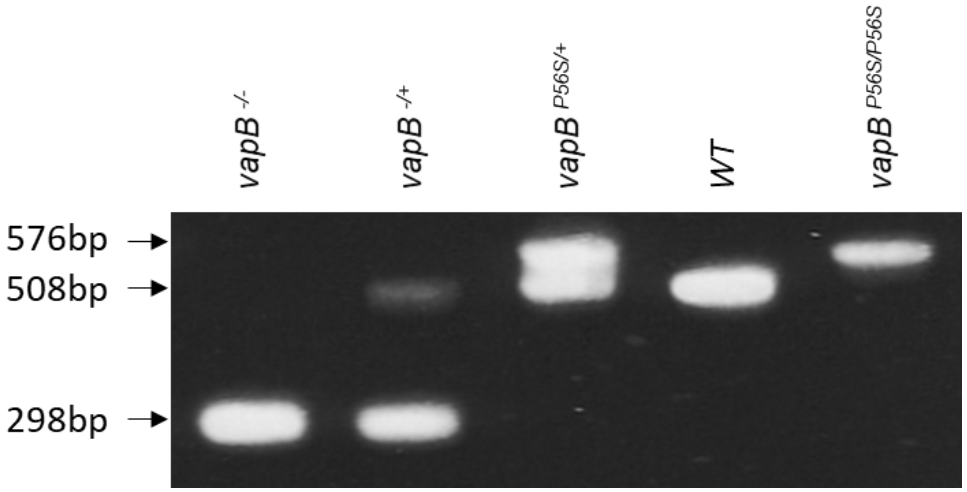

Figure 5.1: DNA bands for exon 2 of vapB.
PCR primers used here flanked exon 2 of vapB. Wild type vapB was 508 base pairs (bp) long, and CLICK generation of conditional knockout rats inserted floxed exon 2 carrying the P56S mutation increasing the size of the mutated version of vapB ($vapB^{P56S}$) to 576bp. Knocking out exon 2 as collateral from CLICK reduced the size of vapB ($vapB^{-}$) to 298bp.

5.2 Specificity of antisera against vapB

Whilst inoculation and extraction of serum from animals was a practical and cost-effective method of generating antibodies through the use of commercial services, targets for inoculation still needed to be constructed and provided in enough volume and of good enough quality to reduce the likelihood of non-specificity (Maurer and Callahan, 1980, Harlow and Lane, 1988). Protein constructs of vapB and methods used to produce antisera against them were outlined in Table 5.1.

Antiserum ID	Animal	Construct	Construct method of production
#6	Rabbit	vapB-MSP	Glutathione-S-Transferase (GST) (Smith and Johnson, 1988) transfusion with thrombin cleavage site (Guan and Dixon, 1991). Affinity-purification, and GST cleaved before inoculation
#38	Rabbit	vapB	Histidine-tagged construct. Chromatography purification.
#84	Sheep	vapB (174-189)	Multi-antigenic peptide (MAP) form of 174-189. Affinity-purified against immunizing peptide (Gkogkas et al., 2008)
vapA	Rabbit	vapA	Histidine-tagged construct. Protein purified by chromatography (Skehel et al., 2000)

Table 5.1: Table of antisera, animals, and protein constructs involved in antiserum production.

Specificity of each serum was examined by probing constructs used in their generation with each antiserum on western blots, as shown in Figure 5.2. Regions of vapB targeted by each antiserum were outlined in Figure 5.3.

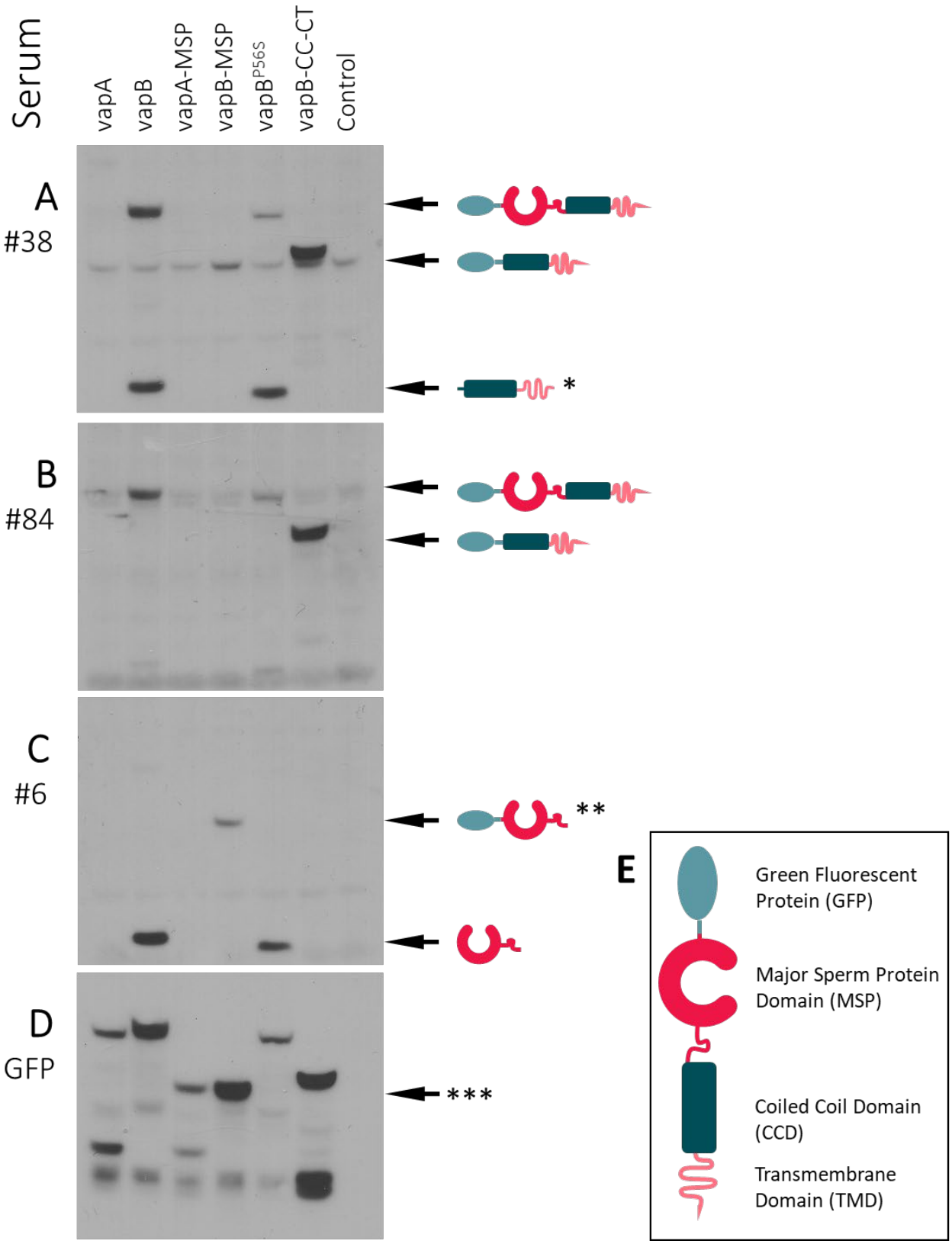

Figure 5.2: Western blots demonstrating specificity of antisera raised against vapB.
A: All constructs probed with vapB#38, * CCD and TMD not bound to Green Fluorescent Protein (GFP) used in the generation of constructs. **B**: All constructs probed with vapB#84. **C**: All constructs probed with vapB#6, ** MSP bound to GFP. **D**: All constructs probed with antibody against GFP, *** vapB-MSP band. **E**: Schematic of components of vapB-GFP.

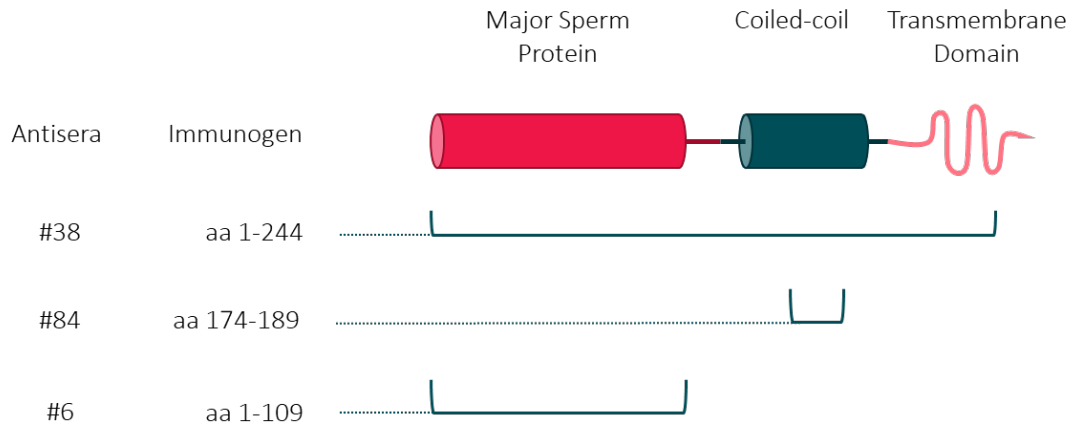

Figure 5.3: Schematic of vapB with regions of specificity of antisera to distinct parts of the protein.

As vapB#38 was raised against the whole protein, the bands at the bottom of Figure 5.2 A (annotated with *) were likely to correspond to the truncated form of vapB seen in the vapB and vapB-MSP homogenates, so vapB#38 could show the full length and truncated forms of vapB. The full-length form of vapB was reduced in the vapB-MSP lane compared to the wild type vapB lane, further supporting the idea that vapB^{P56S} mutation affected the expression of the full-length protein as seen in Figure 5.3. However, there appeared to be no difference in signal corresponding to the truncated form of vapB in the wild type or mutant lanes.

There was also a notable reduction in signal from vapB to vapB^{P56S} in Figure 5.2 C where homogenates were probed with vapB#6 raised against vapB-MSP, further implying the involvement of the mutation in protein expression or detection. It also confirmed that the band at Figure 5.2 A (*) was likely to be truncated vapB rather than the MSP domain. In Figure 5.2 C (**), the vapB-MSP signal was weak when probed with #6. The same position for the same homogenate when probed for GFP was much stronger (Figure 5.2 D***). This suggested GFP bound to MSP may have inhibited vapB#6 antibody from binding to a dominant epitope at MSP N-terminus.

Blots obtained during optimisation of vapB#38 (see Appendix Figure 9.1) produced cross-reacting bands against various tissues, making interpretation of any histological work problematic. However, vapB#6 maintained specificity against the MSP domain and became the key candidate for use in immunofluorescence (see Chapter 6). The comparative signal detection between vapB#38 and vapB#6 in western blots identified vapB#38 as the best candidate for western blots below. The presence of cross-reacting bands in vapB#38 and vapB#84 could be reduced by purifying the antibodies with techniques such as Protein G

purification (Iangone, 1982), gel filtration (Grodzki and Berenstein, 2010), or antigen affinity chromatography (Jack, 1994), but this could affect the titre and subsequent signal when used in experiments. Pre-absorbing antibodies on tissue from vapB$^{-/-}$ animals could be another way to reduce the signals of non-specific bands, but this could also affect the detection of truncated proteins as vapB$^{-/-}$ was only missing exon 2.

5.3 Expression of vapB and vapA in Lumbar Spinal Cord

There was ubiquitous expression of vapB and vapA in all tissues in rats and in humans, however its expression was reduced in the presence of the P56S mutation (Nishimura et al., 1999, Gkogkas et al., 2008, Teuling et al., 2007, Anagnostou et al., 2010). Most mouse models to date do not reflect this as they over-express wild type and mutant vapB (Kim et al., 2016, Kuijpers et al., 2013a, Tudor et al., 2010, Aliaga et al., 2013, Qiu et al., 2013), but it was reflected in the knock-in mouse model where there was a reduction in the expression of full-length vapB in the heterozygous and homozygous mutants, and an increase in truncated forms of vapB detected in insoluble fractions from the spinal cord (Larroquette et al., 2015). The truncated products also appear under normal conditions in CNS tissue as vapB was thought to cleave at an, as yet, unknown point between the MSP and coiled coil domains, and has been shown to have roles in intra- and extracellular signaling (Tsuda et al., 2008, Han et al., 2012, Deidda et al., 2014). Changes in the expression of vapB in the presence of the P56S mutation were also reflected in this project where homogenates of lumbar spinal cord were probed for vapB and vapA using vapB#38 and vapA antisera. In this rat model of ALS8, vapB expression was reduced in LSC homogenates from vapB$^{P56S/+}$, and absent in vapB$^{P56S/P56S}$ and vapB$^{-/-}$ (B). The expression of vapA was not expected to change in tissues from this colony. However, there appears to be a reduction in the level of vapA expressed in lumbar spinal cord in vapB$^{P56S/+}$ and vapB$^{-/-}$ (A). Time constraints limited the number of samples per genotype to only one, so repeat blots with other samples are needed to confirm this change in vapA expression.

Figure 5.4: Immunoblots probing lumbar spinal cord homogenates for vapB and vapA.
vapB (**A**) and vapA (**B**) bands at 33kDa. Samples taken from homogenates of lumbar spinal cord of 17-18 month old animals. Analysis not completed as only one sample per genotype.

5.4 Motor Neurone Expression of vapB and vapA

Evidence in literature points to vapB^{P56S} forming aggregates in fibroblasts from SALS patients and peripheral blood mononuclear cells (Cadoni et al., 2020), which was reflected in mouse models of ALS8, including the knock-in model where cytoplasmic inclusions were present in MN (Larroquette et al., 2015).

To see if such aggregates were present in the rat model, LSC sections of 17 – 18 month old rats were probed for vapB or for vapA using vabP#6 and vapA antisera respectively. Criteria for cell selection for analysis was as follows: thresholding and particle analysis tools from FIJI/ImageJ were used to select and measure cells >700µm^2, and they should have clear nucleolus for true middle cross section. The latter criterion was added as the signal distribution within cells became more striated the further from the nucleolus the cross section became (Figure 5.5 C). The cell area and mean grey values of the cytoplasm were collected and analysed with GraphPad Prism 7. As aggregates were not immediately obvious, the signal distribution within cells was instead categorised as homogenous, granular, striated, or ring-like (Figure 5.5 A and B), and the frequency of each category along with mean grey value (MGV, for signal intensity) were recorded.

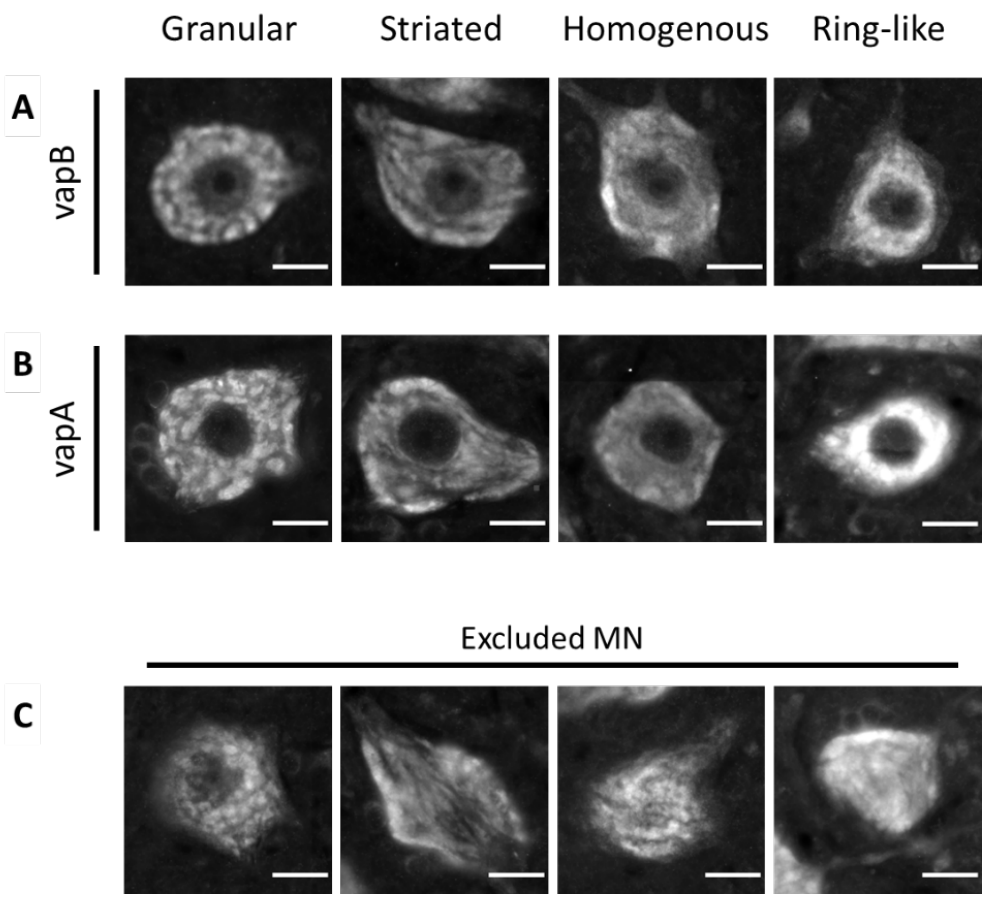

Figure 5.5: Distribution of vapB and vapA signal in MN
A and **B**: MN separated into 4 groups: granular, striated, homogenous, and ring-like. **C**: Signal arrangement around the nucleus was less distinguishable when cross section of MN further away from nucleolus, so cells were excluded from analysis. Scale bars 20µm.

The number of MN positive for vapB#6 or vapA antibody, and their area and signal were all recorded and analysed. As data in Chapter 6 will show, there was a reduction in the number of MN in vapB$^{P56S/+}$ and vapB$^{P56S/P56S}$ lumbar spinal cord, so data here was normalised to average number and area of ChAT-positive cells. For vapB#6-positive MN, there was a marked reduction in the signal of vapB$^{-/-}$ MN with homogenous signal distribution (Figure 5.6 F) which was expected due to exon 2 being knocked out and vapB#6 used here has been shown to identify the MSP domain. Otherwise there were no other statistically significant changes in vapB#6-positive MN (Figure 5.6).

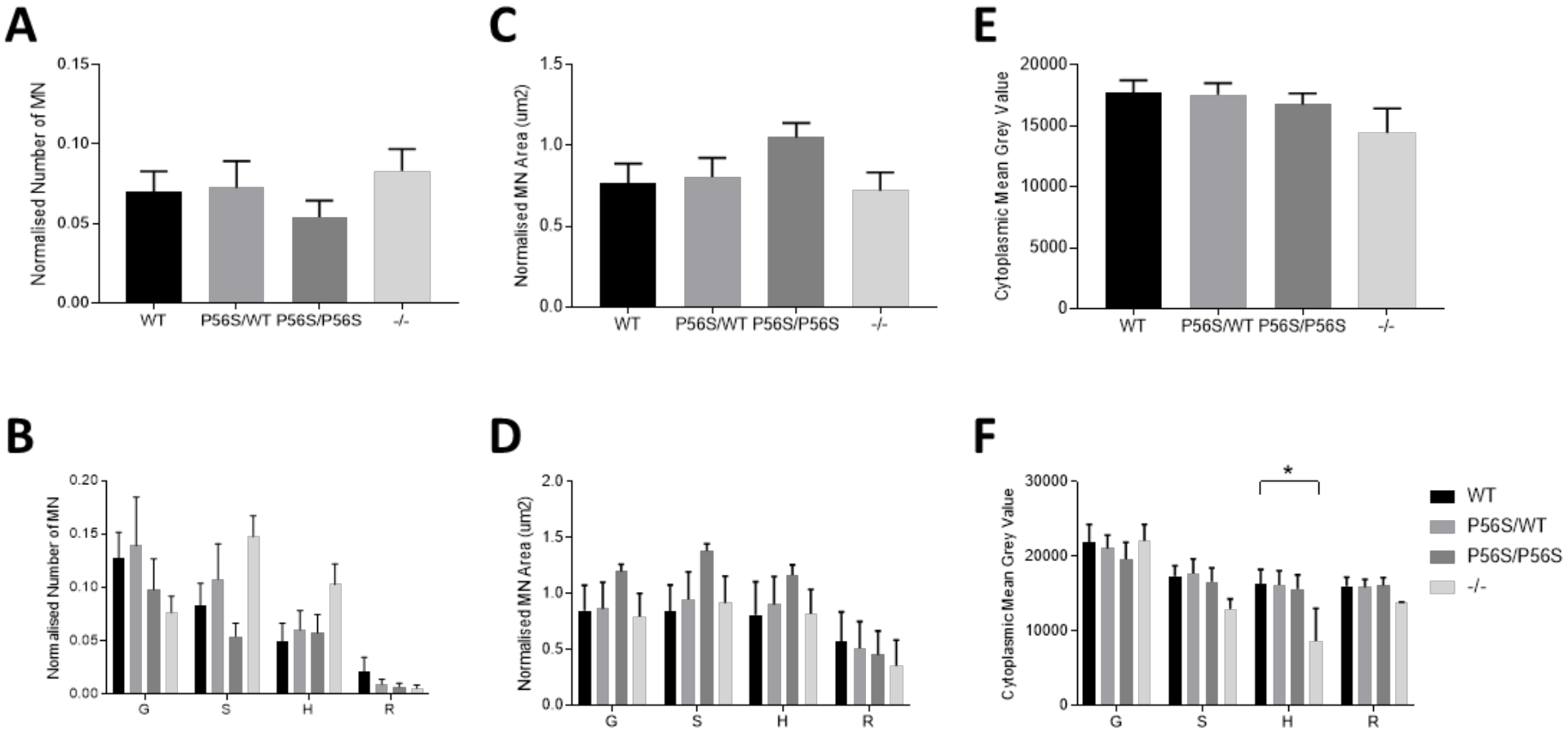

Figure 5.6: Number, area, and signal, or mean grey value (MGV) of vapB #6-positive MNs
MN >700µm^2 in area included in analysis. Data was compared across genotypes (**A**, **C**, and **E**) and then vapB signal distributions were compered within genotypes (**B**, **D**, and **E**) where G = granular, S = striated, H = homogenous, and R = ring-like. Relative frequency and MN area normalised for average values gained from ChAT-positive MN. One-way ANOVA with Dunnett's post-hoc applied to genotype comparisons, and two-way ANOVA with Dunnett's post-hoc comparisons applied to signal distribution analysis. 3 sections per animal and 3 – 4 animals per genotype were included. *p<0.0500.

Images from LSC probed for vapA were also analysed and data was normalised to average MN number and area of ChAT-positive MN. For vapA-positive MN, vapB$^{P56S/P56S}$ neurons were larger than WT, with the significant difference in MN expressing vapA homogenously (Figure 5.7 C and D). Overall, vapB$^{P56S/P56S}$ MN also had a greater signal than WT, but this was not significant to any of the signal distributions (Figure 5.7 E).

The ER marker PDI was not optimised in time to determine if these staining patterns colocalised with the ER, and if they exhibited the morphology of the ER in MN. Whilst there was evidence of vapB colocalising with PDI (Tsuda et al., 2008) and other ER markers such as GRP78 (Cadoni et al., 2020), it only appears to do so in the presence of the P56S mutation. Therefore, the changes in "MN area" could just reflect changes in vapB-MSP and vapA distribution either across the ER or throughout the cell body. However, changes in vapA cell signal suggests some sort of re-distribution which could be compensatory in the presence of the P56S mutation.

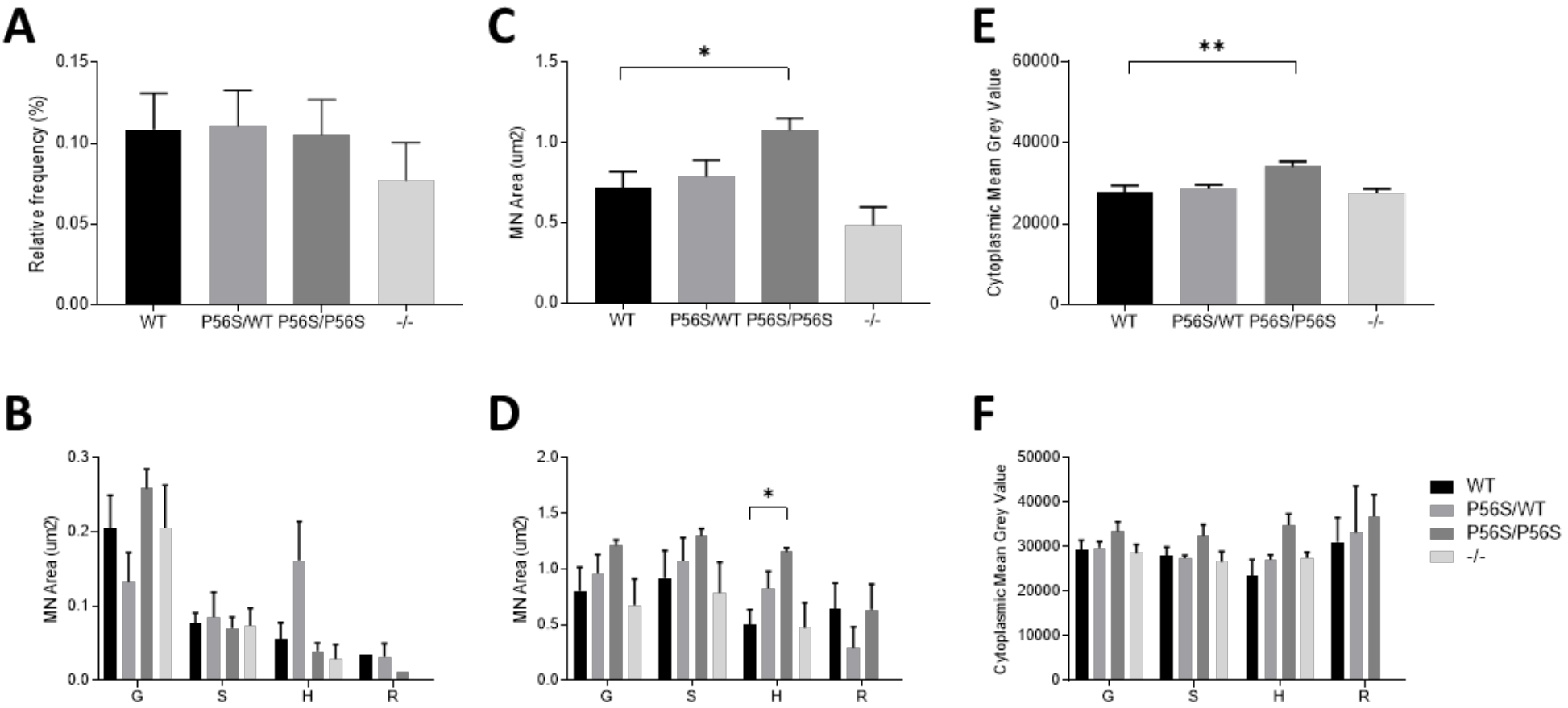

Figure 5.7: Number, area, and mean grey value (MGV) of vapA-positive MNs

MN >700µm^2 in area included in analysis. Data was compared across genotypes (**A**, **C**, and **E**) and then vapB signal distributions were compered within genotypes (**B**, **D**, and **E**) where G = granular, S = striated, H = homogenous, and R = ring-like. Relative frequency and MN area normalised for average values gained from ChAT-positive MN. One-way ANOVA with Dunnett's post-hoc applied to genotype comparisons, and two-way ANOVA with Dunnett's post-hoc comparisons applied to signal distribution analysis. 3 sections per animal and 3 – 4 animals per genotype were included. *p<0.0500, **p<0.0100.

5.5 Reduced expression of Syntaxin in vapB$^{P56S/P56S}$ spinal cord

The VAMP-associated proteins vapA and vapB help to tether organelles to the ER by interacting with proteins containing a two-phenylalanines in an acidic tract (FFAT) motifs found on target organelle membranes (Di Mattia et al., 2018, Cabukusta et al., 2020).

Syntaxin 1A and VAMP2 interact with VAP proteins to allow interaction between vesicles and the ER (Weir et al., 1998, Foster et al., 2000, Kanekura et al., 2006), and α-Tubulin also co-sediments with vapB in the presence of microtubules, and interrupted transport vesicles form ER to Golgi forming when over-expressed or in the presence of the vapB^{P56S} mutation (Pennetta et al., 2002). Antibodies against Syntaxin 1A, VAMP2, and Tubulin BIII were used to probe homogenates of lumbar spinal cord. Tubulin BIII was used rather than α-tubulin due to antibody availability. In this model, syntaxin 1A was significantly reduced in vapB$^{P56S/P56S}$ LSC. There were no changes in VAMP2 or tubulin BIII ().

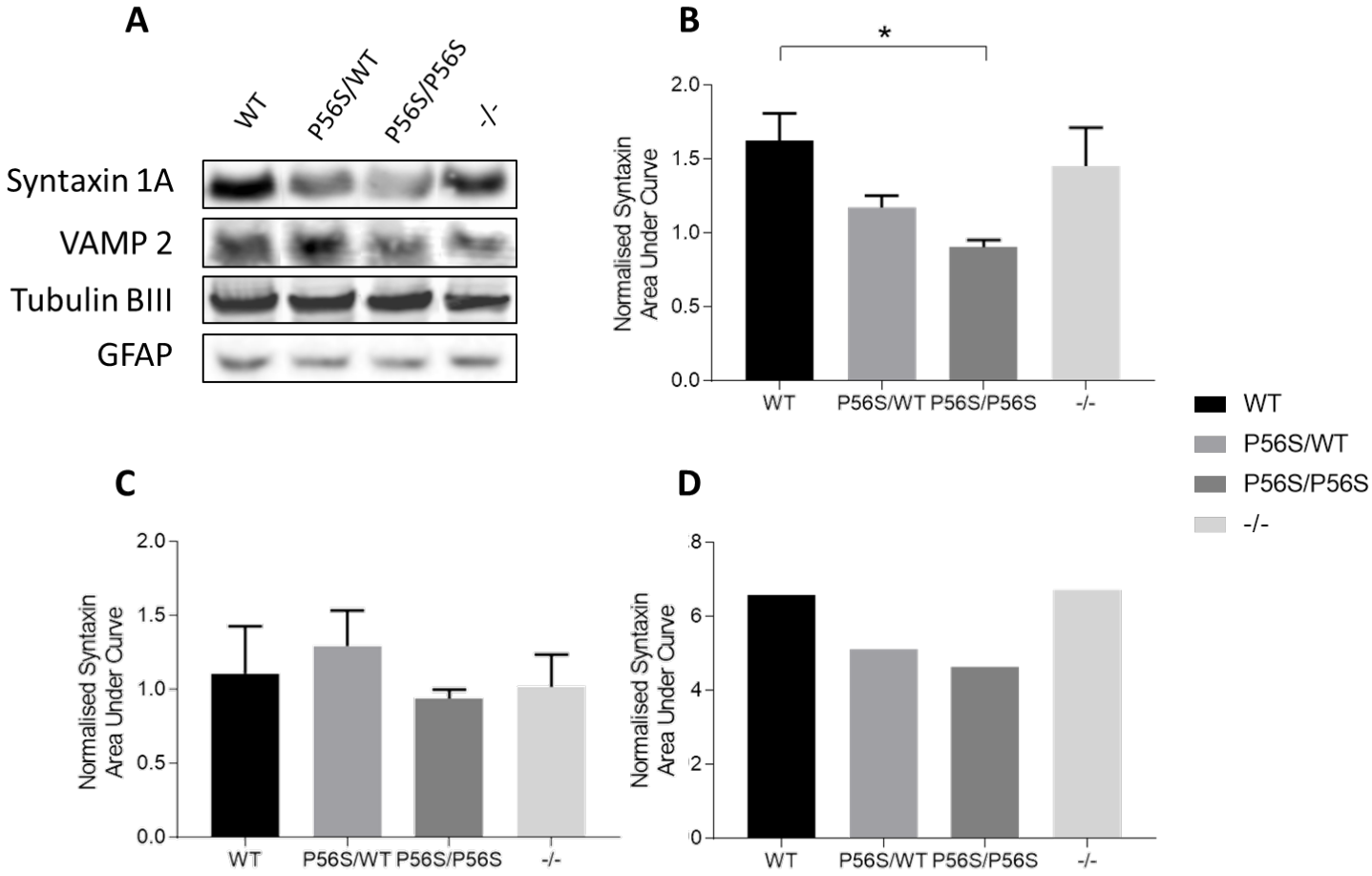

Figure 5.8: Expression of VAP interactors in lumbar spinal cord.

A: Immunoblots of 17 – 18 month old lumbar spinal cord probed for Syntaxin 1A (35kDa), VAMP2 (17kDa), and Tubulin BIII (50kDa). Blots were normalised to GFAP (50kDa). Densitometry analysis was performed using FIJI/ImageJ for syntaxin 1A (**B**), VAMP2 (**C**), and tubulin BIII (**D**). Significant reduction in syntaxin 1A in vapB$^{P56S/P56S}$ compared to vapB. Two-way ANOVA with Dunnett's post-hoc test applied. 2 – 3 animals per genotype.*p<0.0500.

The vapB^{P56S} mutation might have had an impact on ER stress. One marker of this is the glucose regulated protein of 78 kDa (GRP78) which is a key ER protein involved in a range of cellular processes including calcium homeostasis (Ouyang et al., 2011), and sensing ER stress (Lee, 2005). A shows a preliminary blot probing LSC for GRP78, and indicates no change in expression across genotypes.

The vapB^{P56S} mutation might have also affected the behaviour of other tethering proteins interacting with the ER such as the mitochondrial protein mitofusin. Whilst it is involved in many cellular roles including mitochondrial autophagy (Franco et al., 2016) and motility (Rocha et al., 2018), its role as a mitochondrial tether to other organelles including the ER indicates its importance in mitochondria-ER interactions. When mitofusin expression was silenced, ER morphology was disrupted which affecting mitochondrial calcium uptake (de Brito and Scorrano, 2008). Preliminary blot probing LSC for mitofusin shows a reduction in mitofusin in all genotypes compared to vapB, as shown in B.

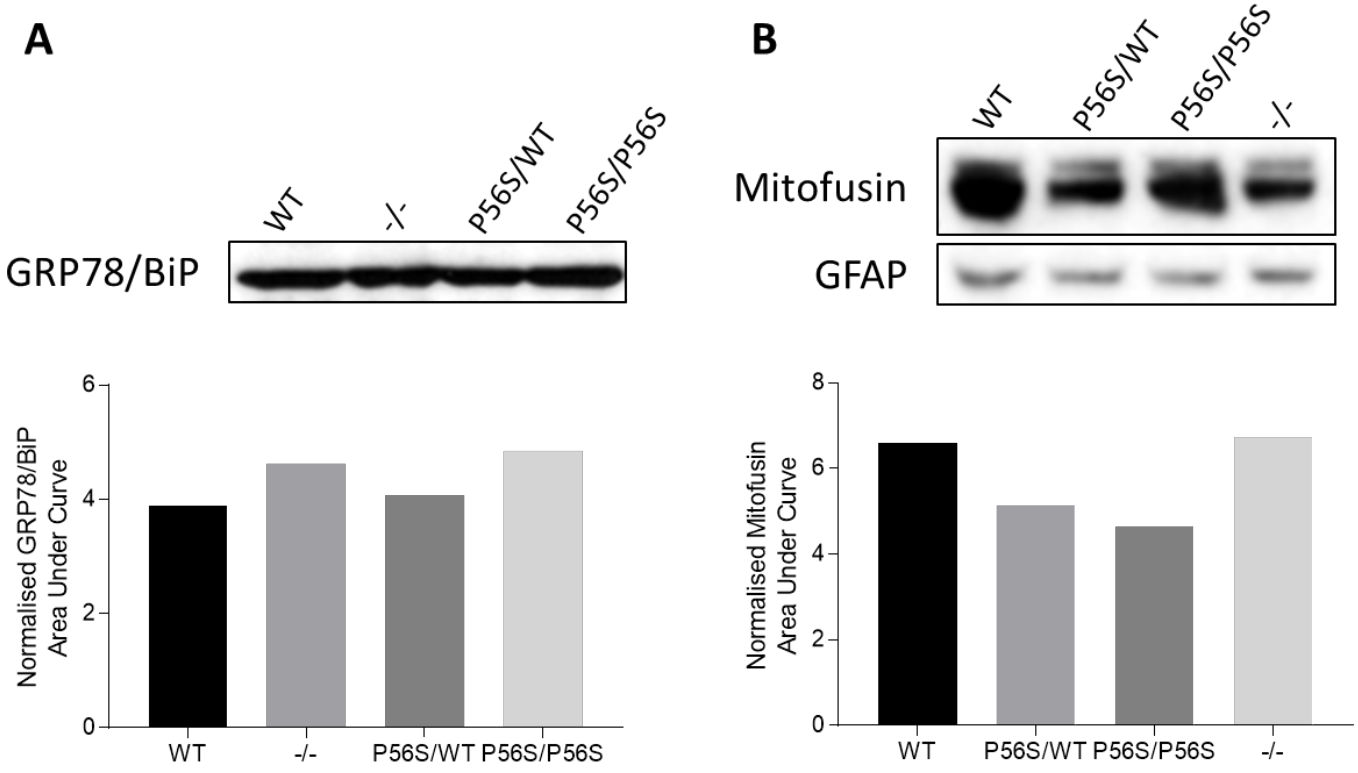

Figure 5.9: Preliminary immunoblots on cortical homogenates.
A: Expression of GRP78/BiP (78kDa). **B**: Expression of mitofusin (84kDa). GFAP (50kDa) as the control for both blots. n=1 for each genotype, hence no analysis.

5.6 Discussion and Future Work

Literature on mouse models of ALS8 carrying the vapB^{P56S} mutation (see Chapter 1) did not provide PCR results for each genotype being studied, and instead provide immunoblots to represent expression differences between genotypes. Although this provides quantitative information on the effect of the mutation on protein expression as shown in **Error! Reference source not found.**, relative expression of proteins would need thresholding to identify specific genotypes. This was the case for vapB$^{P56S/+}$ and vapB$^{P56S/P56S}$ as their expression levels appear very similar and difficult to distinguish through the immunoblot alone.

There was a lower level of vapB expression in vapB$^{P56S/+}$, similar to vapB$^{-/-}$and to what has been reported in other models (Larroquette et al., 2015). However, this was in contrast to other models in transgenic mouse models, likely due to over-expression of vapB and vapB^{P56S} (Tudor et al., 2010, Qiu et al., 2013, Aliaga et al., 2013, Kim et al., 2016) or were generated as knock-in or knock out (Kabashi et al., 2013) mice.

Homogenates of a range of tissues from rats also show that whilst vapA was cleaved in all tissues analyzed, vapB only had detectible cleavage products in CNS tissue (Gkogkas et al., 2008). Antibodies to differing epitopes of vapB may have been used to detect the cleavage products, but this was something worth looking into in the future given the important extracellular signaling functions of the MSP domain, and the mutation affecting cleavage and release of the MSP domain (Gkogkas et al., 2011). There is, however, a clear reduction in vapB expression in vapB$^{P56S/+}$ and vapB$^{-/-}$, with a lesser reduction in vapB$^{P56S/P56S}$ LSC. It was not clear if the vapB^{P56S} mutation contributes to ALS8 by a loss- or gain-of-function. Models over-expressing vapB report cytosolic aggregates forming in MNs, suggesting gain of function toxicity. However, given that vapB expression was reduced in this model and in the spinal cord of SALS patients (Anagnostou et al., 2010), it was likely that ALS results from a lack of functional protein available to complete key cellular tasks (Borgese et al., 2021). This could also be disputed as a vapB$^{-/-}$ mouse model was unable to replicate ALS phenotype (Kabashi et al., 2013), but the mouse vapB knock-in model reported mild motor deficit, cytoplasmic vapB and ubiquitinated inclusions, and ER stress. The motor deficit was more severe in homozygous mutants, but homozygous mutants also expressed vapB to a lesser degree than wild type or the heterozygous mutant (Larroquette et al., 2015). Given the differences seen in this model so far, it was difficult to make the case for vapB^{P56S} being a loss-of-function mutation as vapB$^{P56S/+}$ and vapB$^{-/-}$ would be expected to produce similar outcomes which has not been the case so far.

The cellular distribution of vapB and vapA would need to be investigated further. The relative size of MN expressing both proteins may just reflect changes in morphology of ER, or distribution in MN as vapB and vapA have already been shown to localise to differing parts of HEK293 cells in culture (Gkogkas et al., 2008). The reduction in vapB#6 signal (mean grey value) in vapB$^{-/-}$ and vapB$^{P56S/+}$ was not as dramatic as expected from the immunoblot probing LSC homogenates for vapB. However, vapB#38, which recognises the whole of vapB, was used in the immunoblot whilst vapB#6 only recognised the MSP domain. This may point to why aggregates of the protein were not immediately obvious so vapB#38 could have provided information about how the full length protein was distributed. However, vapB#38 was not suitable for immunofluorescence due to a large cross-reacting band present in blots against tissue homogenates (see Appendix Figure 9.1) which would have interfered with interpreting

images. The vapB#84, which recognises the TMD and CCD, was not optimised for histology in time for this project, but it would offer more information about how this part of the protein was distributed in MN in a co-localisation study. The signal of vapB in vapB$^{-/-}$ was reduced compared to vapB, but only in MN with homogenous signal distribution. This could be explained by the immunoblot probing cortical homogenates with vapB#6 where there was a non-specific band across all samples.

Given the diversity of cellular roles that vapB has been implicated in, a mutation in the MSP domain which inhibits cleavage was likely to affect interactions with proteins and complexes needed to initiate steps for specific cell processes. Syntaxin 1A expression was significantly reduced in vapB$^{P56S/P56S}$ compared to vapB. Syntaxin immunoreactivity in ALS patients was relatively unchanged compared to healthy controls (Ikemoto et al., 2002), but was up-regulated when TDP-43 was silenced in cortical cultures from mouse foetal brains (Honda et al., 2013), giving a mixed profile of syntaxin expression across models of ALS.

The mitochondrial protein mitofusin2 shown to tether mitochondria to ER and disrupts ER morphology if expression was silenced, affecting mitochondrial calcium uptake (de Brito and Scorrano, 2008). If confirmed in multiple samples, this should be followed up with ER stress markers and markers of calcium homeostasis as mitochondrial protein mitofusin was necessary for mitochondrial fusion and building the network of mitochondrial tubules (Chen et al., 2003).

The lack of change in these interactors may signify interaction with other FFAT-recognising proteins such as the recently discovered motile sperm domain-containing proteins (MOSPD1, MOSPD2, and MOSPD3), which were identified as potential compensatory proteins working in the absence of vapB or vapA, and preventing the expected reduction in ER-organelle interactions such as ER-mitochondria (Stoica et al., 2014a), and ER-endosome (Dong et al., 2016, Eden et al., 2016). However, the P56S mutations was found to destabilise vapB interaction with β-tubulin (Mitne-Neto et al., 2007).

The expression of VAMP2 and tubulin BIII were unchanged amongst the genotypes studied here. VAMP2 interacts with VAPs to form close connections between the ER and vesicle membranes. VAMP2 has a role in the SNARE complex that mediates fusion of synaptic vesicles. It was downregulated in a *C. elegans* model of SOD1^{G93A} (Wang et al., 2009) but there was no evidence of changes in expression in rodent or human samples. Studies in *S. cerevisiae*

show that upregulation of α-tubulin made no changes to the expression of β-tubulin, but upregulation of β-tubulin led to widespread microtubule dysfunction (Burke et al., 1989, Weinstein and Solomon, 1990). It was possible that any changes to α-tubulin may not have translated to β-tubulin very well in this model. Future work should investigate α-tubulin given that vapB$^{P56S/P56S}$ MN were smaller than vapB (see Chapter 6), and should also focus on the interaction between vapB and PTPIP51 which helps to tether ER to mitochondria, with special interest in vapB$^{-/-}$ spinal cord due TDP-43 pathology being present (see chapter 6) and the ability for TDP-43 to disrupt vapB-PTPIP51 interaction. Markers for ER stress such as GRP78/BiP (Dudek et al., 2009), and the unfolded protein response (UPR) such as ATF6 (Yoshida et al., 2001, Gkogkas et al., 2008) should also be studied given that ER stress and the UPR were both mechanisms heavily implicated in ALS (Ilieva et al., 2007, Prell et al., 2012). There should also be a focus on the expression of oxysterol binding proteins (ORPs) given their relationship with vapB and lipid homeostasis (Jansen et al., 2011, Darbyson and Ngsee, 2016), and that male vapB$^{P56S/P56S}$ and vapB$^{-/-}$ rats in particular gained weight more rapidly than vapB which could point to changes in lipid metabolism.

6 Markers of ALS

6.1 Fewer motor neurons in vapB$^{P56S/+}$ and vapB$^{P56S/P56S}$, and vapB$^{P56S/P56S}$ motor neurons have reduced size

The loss of upper and/or lower motor neurons (MN) was a classic hallmark characteristic of ALS (Charcot, 1869, Rösler et al., 2000, Brown and Jaatoul, 1974, Dantes and McComas, 1991), making it a marker of ALS to be investigated when developing animal models of ALS. Whilst some targeted methods of quantifying MN number have involved retrogradely labelling MN by injecting dye into the hind limb of rodents (Yu et al., 2015), most groups use antibodies against Choline Acetyltransferase (ChAT) in histology studies due to its reliable extensive labelling of the soma, axons, and terminals of MN (Barber et al., 1984).

To investigate if changes to endogenous vapB led to signs of MN degeneration, the first step was to label MN in the spinal cord using an antibody against ChAT. However, the available antibody (AB143, Merck-Millipore) appeared to target an epitope of the protein not localised to MN (Houser et al., 1984, Phelps et al., 1984, Borges and Iversen, 1986), leading to a non-specific stain of neurons in LSC (Figure 6.1 A). Later troubleshooting and optimisation found that the use of AB144P (Merck Millipore) specifically targeted large multipolar neurons in the ventral horn of the spinal cord as recorded in literature elsewhere (Figure 6.1 B). Evidence of inconsistent localization of the two anti-ChAT antibodies indicates each antibody targets different epitopes of ChAT in rodent neuronal tissue (Bhagwandin et al., 2006).

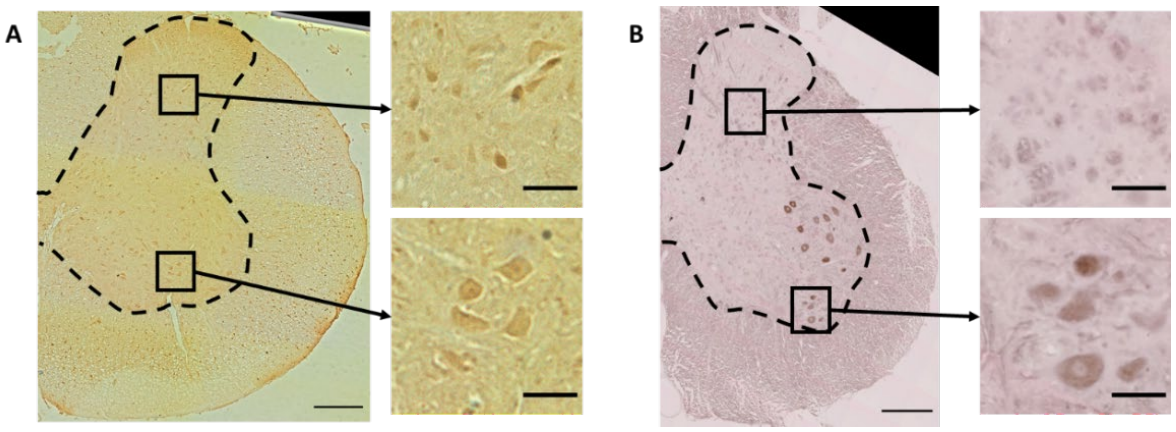

Figure 6.1: Immunoreactivity of cholinergic neurons against ChAT143 and ChAT144P.
A: AB143 stained the soma of cells in both the dorsal (top insert) and ventral (bottom insert) horns of grey matter **B**: AB144P stained the soma of large multipolar cells in the ventral horn of the spinal cord (bottom insert) more strongly than other cells both the dorsal (top insert) and ventral horn. Scale bars at 100um for section images, and 20um for inserts.

Whilst troubleshooting ChAT staining, an alternative method of characterising MN in LSC sections stained with H&E was developed. Criteria from literature defined MN in rat lumbar spinal cord as large multipolar cells located in the ventral horn of grey matter with a diameter ≥30um (Ferrucci et al., 2018). Given that the ageing cohort had not reached 17 – 18 months at this point, images of H&E-stained cervical, thoracic, and lumbar spinal cord from 9 month old vapB rats were thresholded in FIJI/ImageJ (Schindelin et al., 2012) to select cell soma, the number and area of which were recorded using the Analyse Particles function. The average median value between the mean and minimum cell area was rounded to the nearest 100 μm^2, and used as the lower threshold to define motor neurons by area, which could be used to select cells of that size and larger using the Analyse Particles function in FIJI/ImageJ. The lower area threshold for each level of spinal cord was as follows: Cervical and Thoracic were 300μm^2, and Lumbar was 700μm^2.

To analyse MN number and morphology, first in H&E stained sections (A) then in ChAT144P labelled sections once optimisation was complete(C), the ventral horn (grey matter at and below the central canal) was selected using the Free Selection tool on FIJI/ImageJ. The image was thresholded to pick out cell bodies, and particles between 700-2500μm^2 (B and D) and were analysed to obtain data on circularity (1=smooth perimeter, 0=amorphous perimeter), aspect ratio (inverse of round), round (1=perfectly spherical, 0=elongated morphology), solidity (Area of cell/ convex hull area, defined as smallest shape that captures all outer points of an object); inverse of object density), and the number of MN in each section.

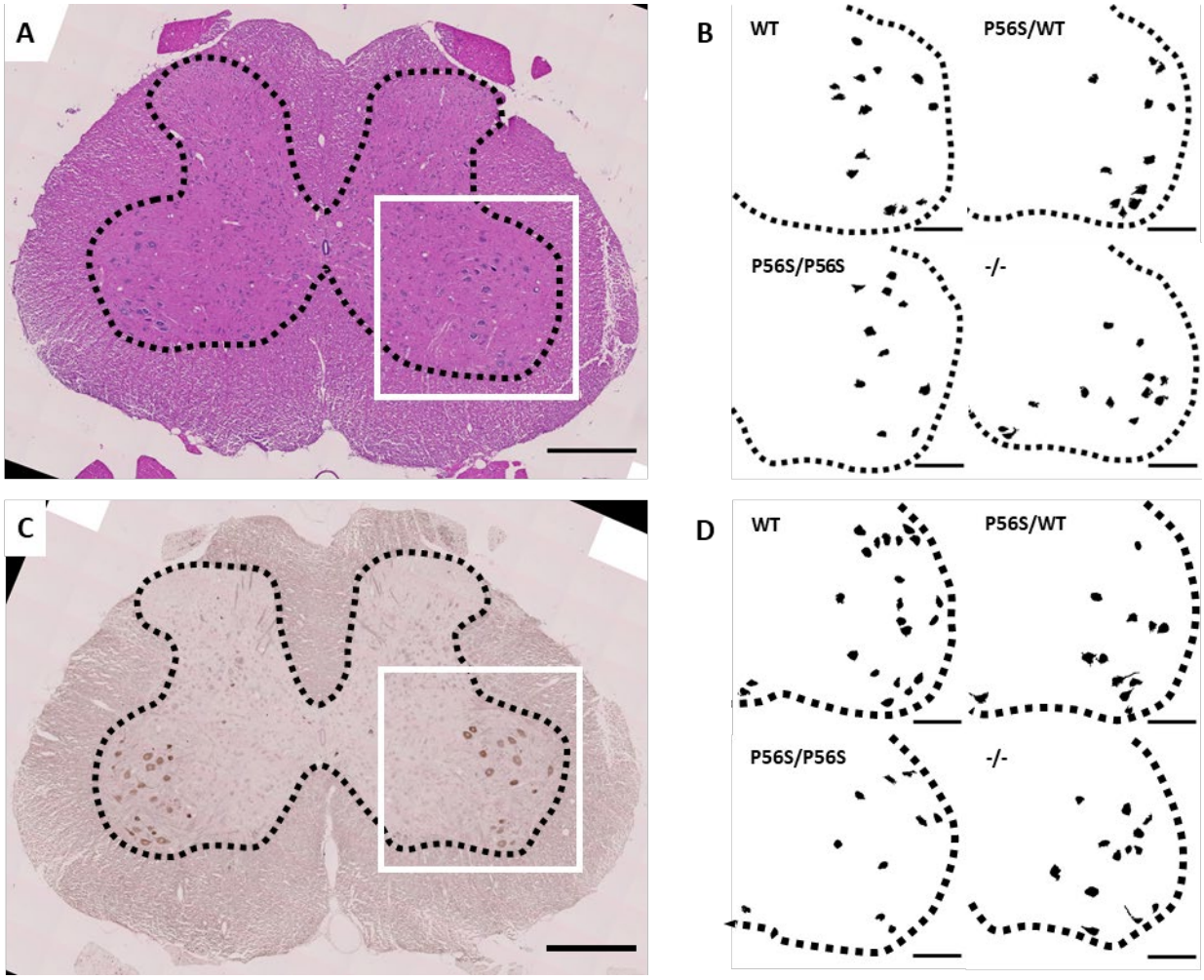

Figure 6.2 H&E and ChAT144P LSC from 18 month old rats.
A: Micrograph of H&E-stained LSC. **B**: Images of H&E-LSC ventral horn thresholded using FIJI/ImageJ. **C**: Micrograph of LSC probed for ChAT144P. **D**: Images of ChAT144P-LSC ventral horns thresholded using FIJI-ImageJ. Micrograph scale bars 500µm. Threshold image scale bars 200µm.

Additional analysis indicated no difference in the number of MN from male or female lumbar spinal cord (), so data was pooled by genotype for subsequent analyses.

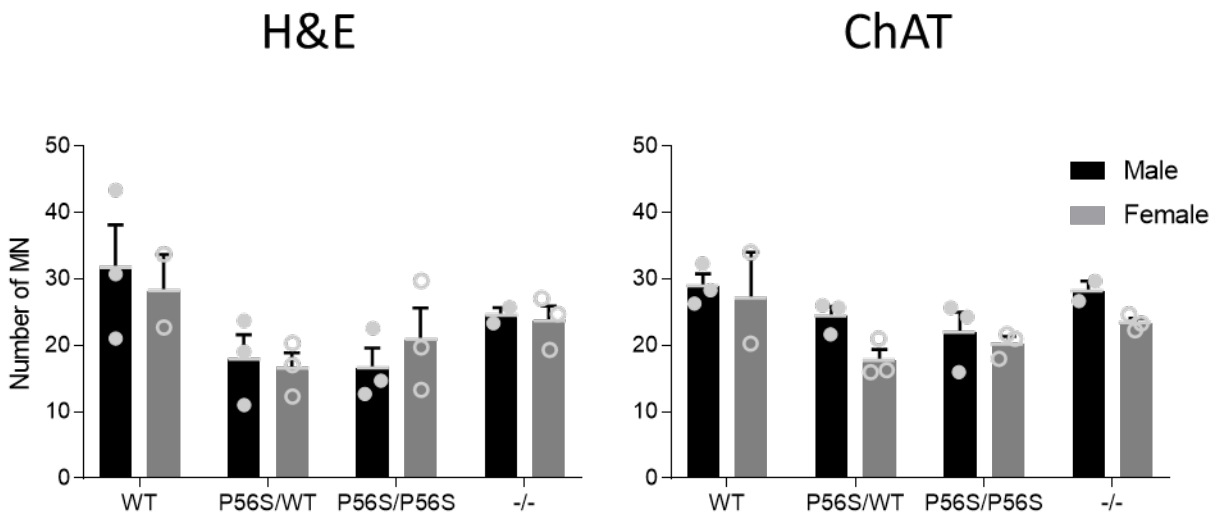

Figure 6.3: Number of MN number in lumbar spinal cord between sexes at 18 months.
Data for individuals shown as closed circles (male) and open circles (females). Two-way ANOVA with Sidak's post-hoc analysis with $p \leq 0.05$ applied. 3 sections per animal, and 2 – 3 animals per genotype included in analysis.

Images taken from H&E and ChAT144P spinal cord both show that there were fewer MN in vapB$^{P56S/+}$ and vapB$^{P56S/P56S}$ LSC compared to vapB. The average vapB$^{P56S/P56S}$ MN was also smaller compared to vapB. There were no changes in morphology of MN relating to genotype at 18 months (E and F).

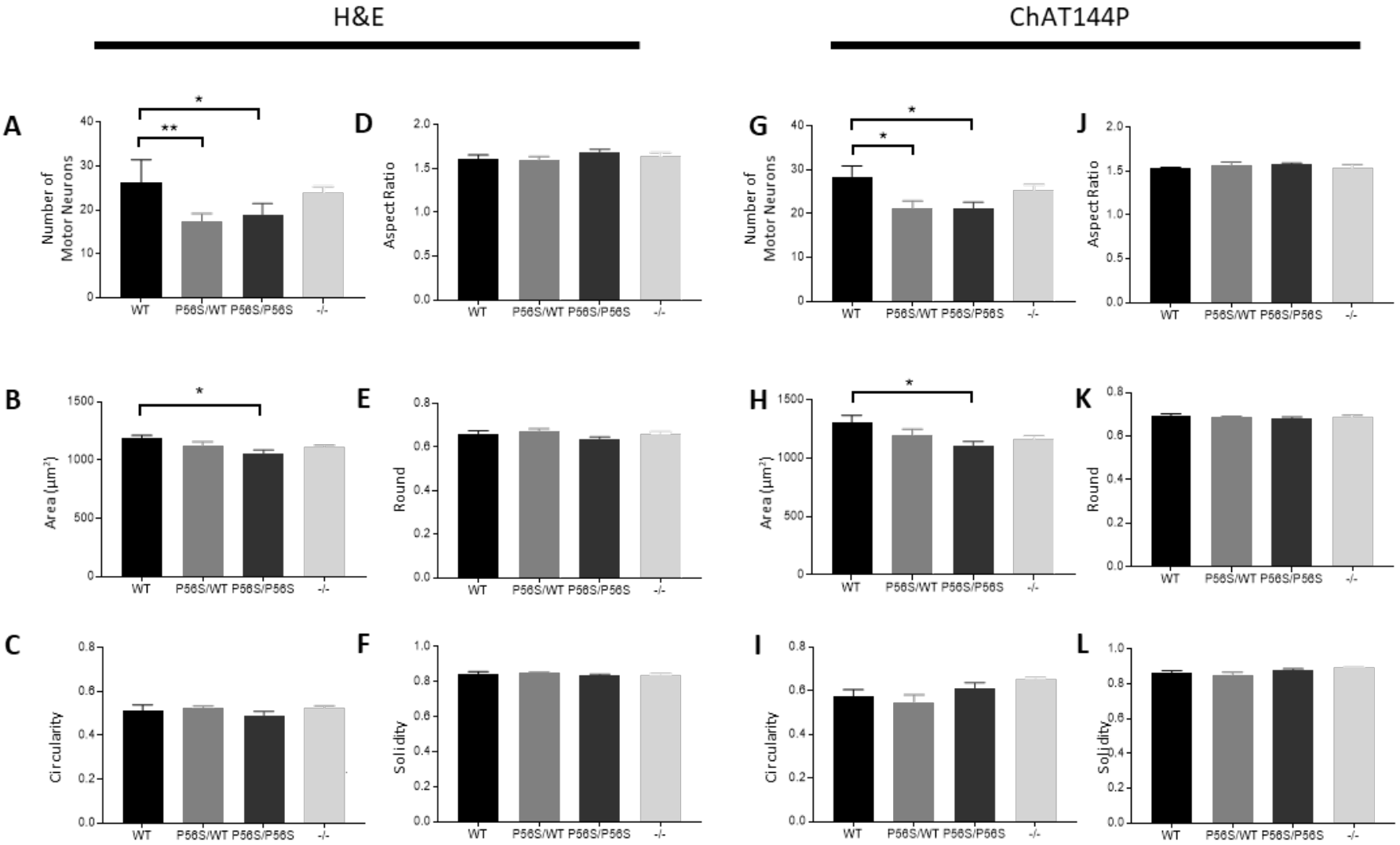

Figure 6.4: Number and morphology parameters of motor neurons from lumbar spinal cord probed for ChAT144P or stained by H&E.
All cells included in analysis ≥700µm2 in area. **A** and **G**: Number of MN per section. **B** and **H**: Area of MN. **C** and **I**: Circularity, 1=smooth perimeter, 0=amorphous perimeter. **D** and **J**: Aspect Ratio, Inverse of Round. **E** and **K**: Round, 1=perfectly spherical, 0=elongated morphology. **F** and **L**: Solidity, Area of cell/ convex hull area (defined as smallest shape that captures all outer points of an object); inverse of object density). Both stains show reduction in the number of MN in vapB$^{P56S/+}$ and vapB$^{P56S/P56S}$ from vapB, and that vapB$^{P56S/P56S}$ MN were smaller in area compared to vapB. One way ANOVA with Dunnett's post-hoc test applied. 3 sections per animal, and 3 – 4 animals per genotype included in analysis. *p<0.0500, **p<0.0100.

6.2 TDP-43 mislocalisation in vapB$^{-/-}$ motor neurons

TDP-43 was a ubiquitously expressed nuclear protein involved in RNA regulation, but mislocalizes to tau-negative ubiquitin-positive cytoplasmic inclusions in pathological conditions (Neumann et al., 2006, Arai et al., 2006). TDP-43 pathology has been implicated in a number of neuropathies, but especially so in ALS (Mackenzie et al., 2007b, Tan et al., 2007) and frontotemporal lobar degeneration (Cairns et al., 2007, Davidson et al., 2007), and has also been implicated in rodent models of ALS (Stribl et al., 2014, Wegorzewska et al., 2009a, Wils et al., 2010, Fratta et al., 2018). During TDP-43 pathology, there was also a lack of normal nuclear TDP-43 in neurons (Neumann et al., 2006), indicating the loss of normal nuclear TDP-43 to be a marker to ALS as well as the cytoplasmic inclusions (Ayala et al., 2008, Johnson et al., 2008, Sreedharan et al., 2008).

To determine the presence of TDP-43 pathology in this model, cells more than 700µm^2 in area were selected by thresholding and particle analysis in FIJI/ImageJ. A spherical region of interest (ROI) with a diameter of 5µm was placed in the nucleus of each cell, with 4 additional ROIs placed in the cytoplasm at 0º, 90º, 180º, and 270º from the horizontal orientation of the image (Figure 6.5). The mean grey value (MGV) of each ROI was measured, and the cytoplasm MGV was taken as the average of the 4 cytoplasmic ROIs.

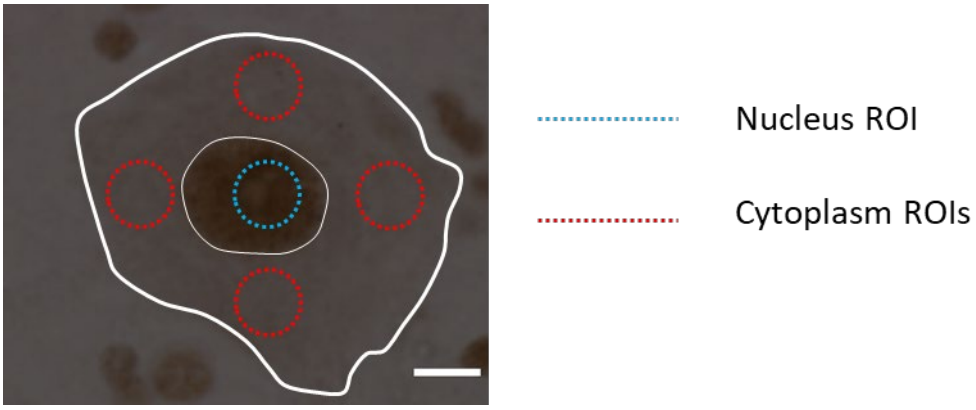

Figure 6.5: Placement of regions of interest (5µm circles) in a TDP-43 stained MN.
Nuclear (blue) and 4 cytoplasmic (red) ROI were used to measure the average signal of TDP-43. Scale bar 5µm.

Whilst the ratio of nuclear to cytoplasmic TDP-43 signal was elevated, albeit to a non-significant degree, in vapB$^{-/-}$ (D), there was a significant increase in TDP-43 signal in the cytoplasm of vapB$^{-/-}$ LSC compared to vapB (B). The nuclear TDP-43 signal was less than vapB, but not to a statistically significant degree (C).

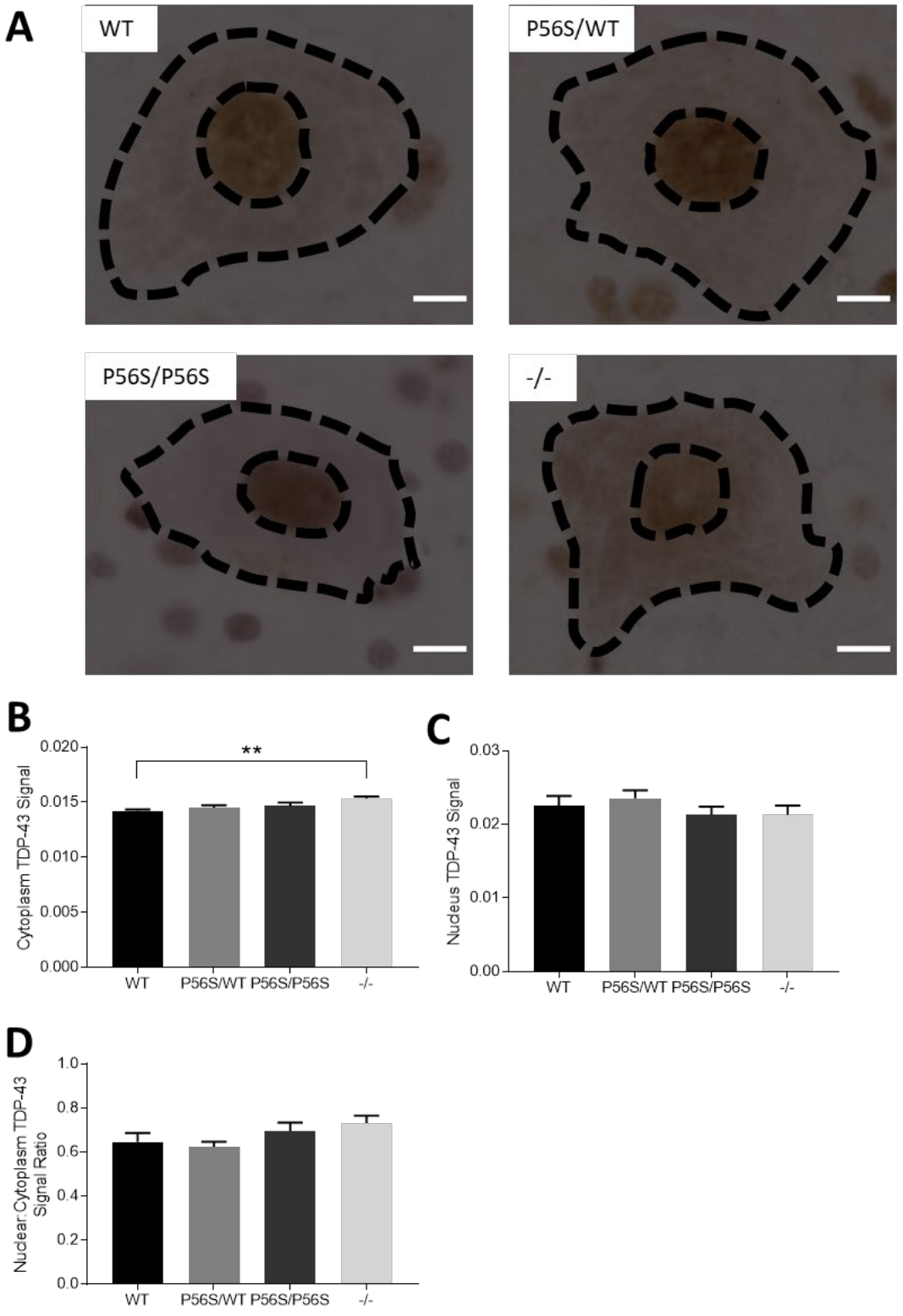

Figure 6.6: Analysis of TDP-43 pathology in MN of lumbar spinal cord.
A: Examples of MN from each genotype with the cell body and nucleus outlined in black dotted lines. **B**: Mean grey value of the cytoplasm. **C**: Mean grey value of the nucleus. **D**: Ratio of mean grey values Nucleus: Cytoplasm. Scale bar was 5µm in all images. 3 sections per animal, and 3 – 4 animals per genotype included in analysis. **p<0.0100.

6.3 No change in astrocyte occupancy or GFAP expresion in lumbar spinal cord

Whilst methods for quantifying astrogliosis have been developed to detect changes in expression of specific markers (Zamanian et al., 2012), commonly-used methods rely on histological techniques and visual assessment of changes in morphology (Anan'ina et al., 2020). In this study, an antibody against glial fibrillary acidic protein (GFAP) was used to mark astrocytes in LSC sections and images captured. Counting individual astrocytes was not possible due to the fine nature of their morphology, and images were captured on a single Z-plane so the full morphologies of sample astrocytes could not be analysed as seen elsewhere (SheikhBahaei et al., 2018, Wilhelmsson et al., 2006). Similar to (Gottipati et al., 2012), percentage occupancy of astrocytes was recorded as a measure of branch extension and invasions into neighbouring astrocyte domains (Wilhelmsson et al., 2006) (Figure 6.7 A – C). There was no change in the occupation of astrocytes in ROIs (Figure 6.7 D).

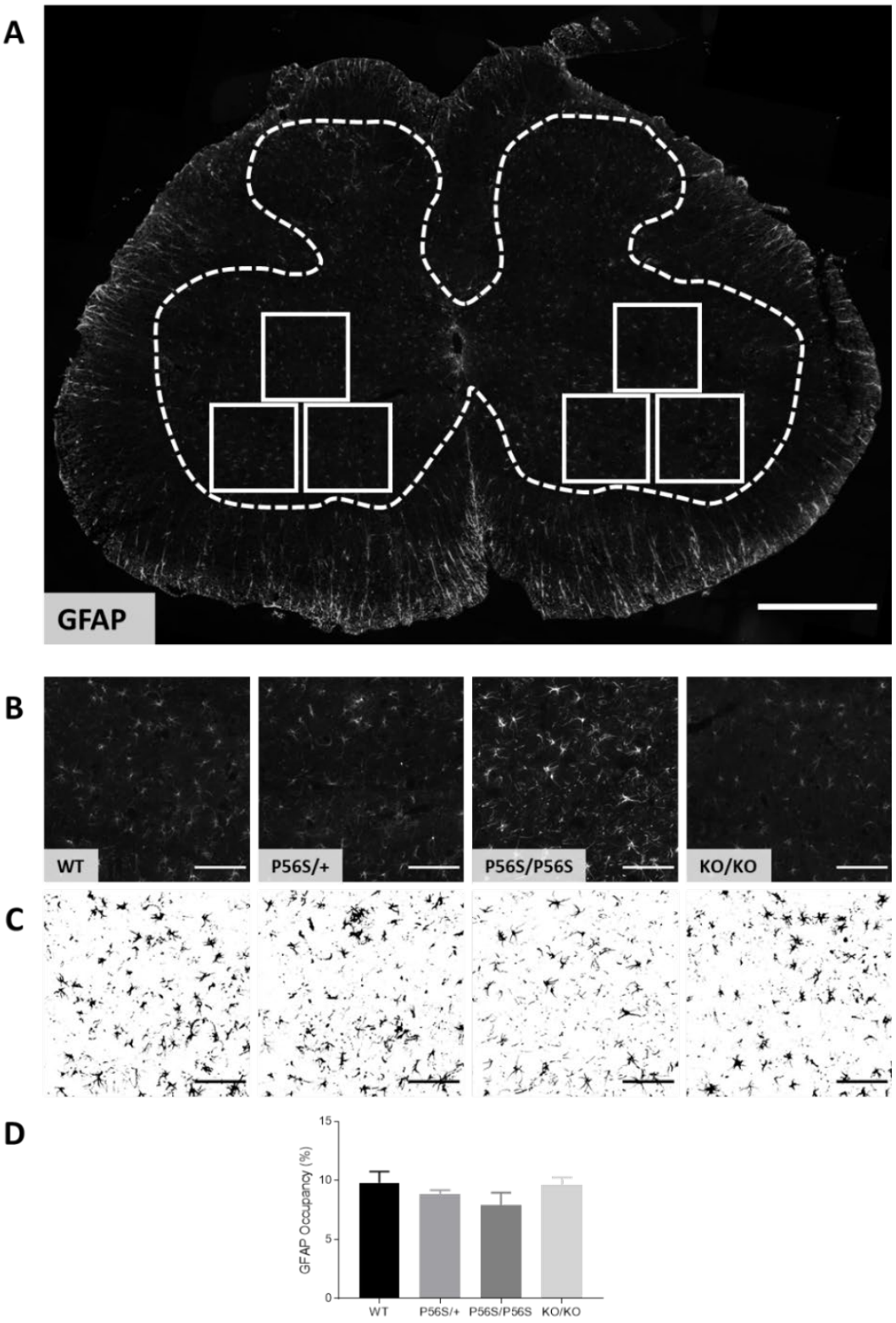

Figure 6.7: Analysis of astrocyte activation in lumbar spinal cord.
A: The same 300µm x 300µm regions of interest (solid line squares) were applied to each section, and percentage occupancy of astrocytes was measured. Scale bar 500µm. **B**: Representative images of ROI from each genotype. Scale bar 100µm. **C**: ROI thresholded. Percentage occupancy calculated from thresholded images through FIJI/ImageJ. Scale bar 100µm. **D**: Average astrocyte occupancy of ROI across genotypes. One-way ANOVA with Dunnett's post-hoc test applied. 3 sections per animal, and 3–4 animals per genotype included in analysis.

As GFAP expression changes under pathological conditions concurrent with astrocyte activation (Eng and Ghirnikar, 1994, Kamphuis et al., 2012), relative expression of GFAP was also analysed by probing homogenates of LSC form 17 – 18 month old rats with an anti-GFAP antibody. There was no change in the relative expression of GFAP in LSC homogenates (Figure 6.8 A and B)

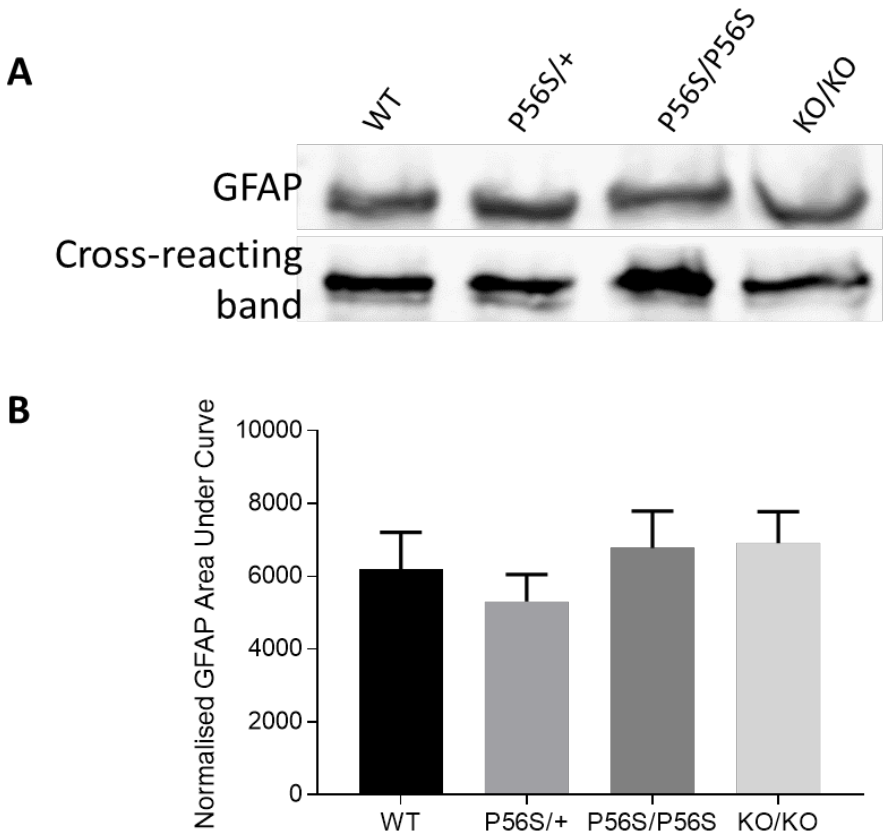

Figure 6.8: Relative expression of GFAP in LSC.
A: Immunoblot of LSC homogenate probed for GFAP. **B**: Relative expression of GFAP expressed as normalised area under the curve for each band normalised to cross-reacting band at 170kDa. Homogenates from 2 – 3 animals per genotype included in analysis.

6.4 No change in microglial number in lumbar spinal cord

Microgliosis was analysed similarly to astrogliosis in that morphology was assessed through histological techniques (Spiller et al., 2018), or expression profiles where changes indicated an activated state (Maniatis et al., 2019, Hammond et al., 2019). To see if microglia were activated in this model, LSC sections from 17 – 18 month old animals were probed with an antibody against Iba1 and images were captured. ROIs were outlined (Figure 6.9 A and B) and

cells with visible soma were counted (Figure 6.9 C). The number of microglia in LSC was similar across genotypes (Figure 6.9 D).

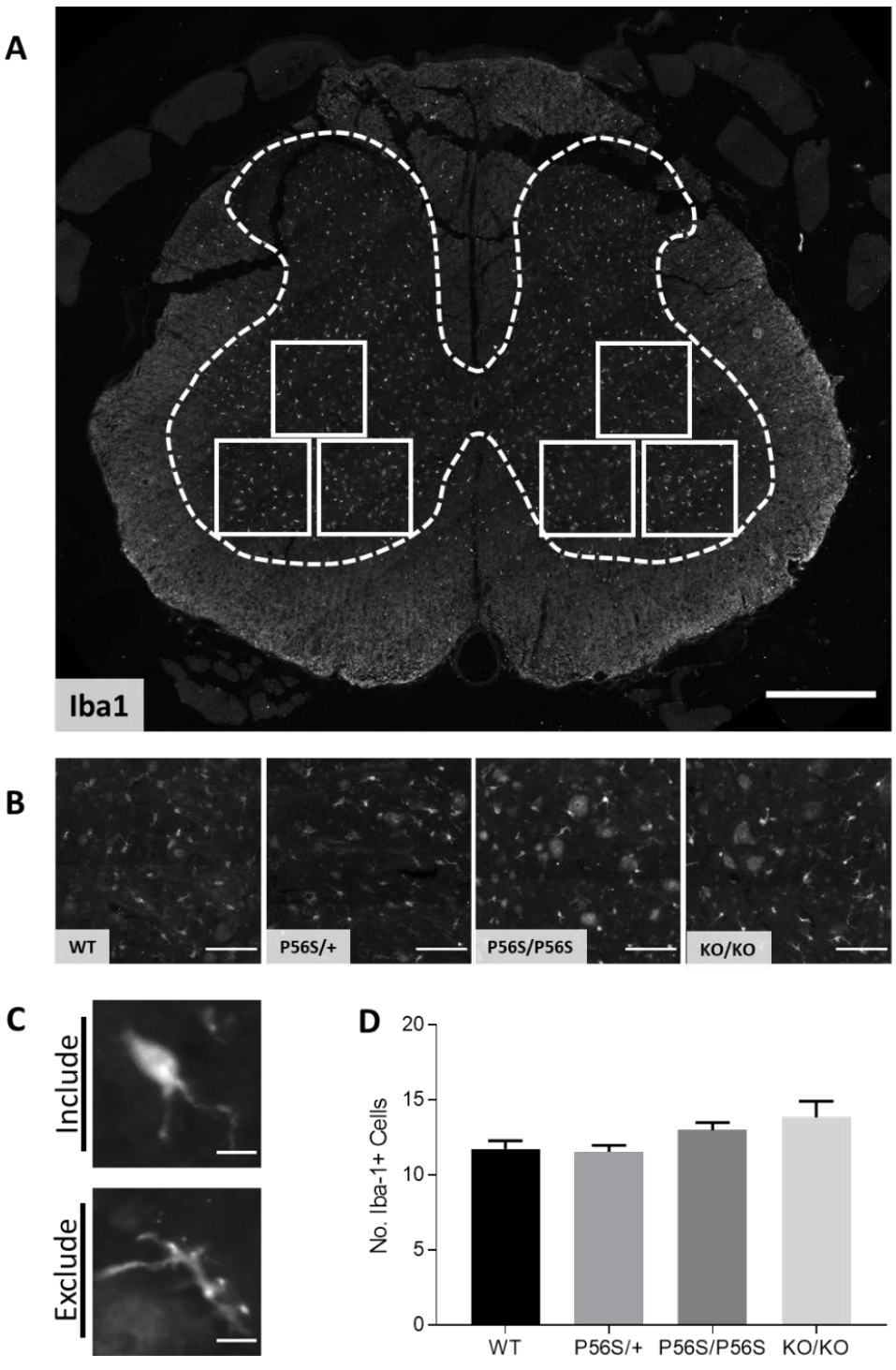

Figure 6.9: Analysis of Iba-1 + cell number.
A: Cells counted in each 300µm x 300µm region of interest for average number of microglia. Scale Bar 500um. **B**: Close-up of ROI, scale bar 100um. **C**: Examples of cells included in count and structures excluded due to lack of discernible soma, scale bar 10um. **D**: Average number of Iba1-positive cells per ROI. One-way ANOVA with Dunnett's post-hoc test applied. 3 sections per animal, and 3 – 4 animals per genotype included in analysis.

Changes in morphology of microglia help to indicate microglial activation where they adopt an amoeboid form by retracting their processes and enlarging their soma (Davalos et al., 2005b, Jonas et al., 2012). Images captured on the Axio Scan slide scanner struggled to capture tiles that were in-focus across all sections, so microglial morphology was difficult to analyse. However, some sections were in-focus and were used for a very preliminary analysis of morphology. The same ROIs used for cell counts were used for this. Microglia within these ROIs were separated into two groups: Complex (3 or more processes from cell coma) to reflect microglia in "resting" state, and Non-Complex (2 or fewer processes from cell soma) to reflect activated microglia. This simplistic method of quantifying morphology did not take note of branch complexity or soma morphology. Although there were no statistically significant changes in the numbers of either cell population, there do appear to be more non-complex microglia in vapB$^{P56S/+}$ and vapB$^{P56S/P56S}$ than vapB (Figure 6.10 A and B). Data from vapB$^{-/-}$ images was not collected as there were too few images that were suitable for analysis.

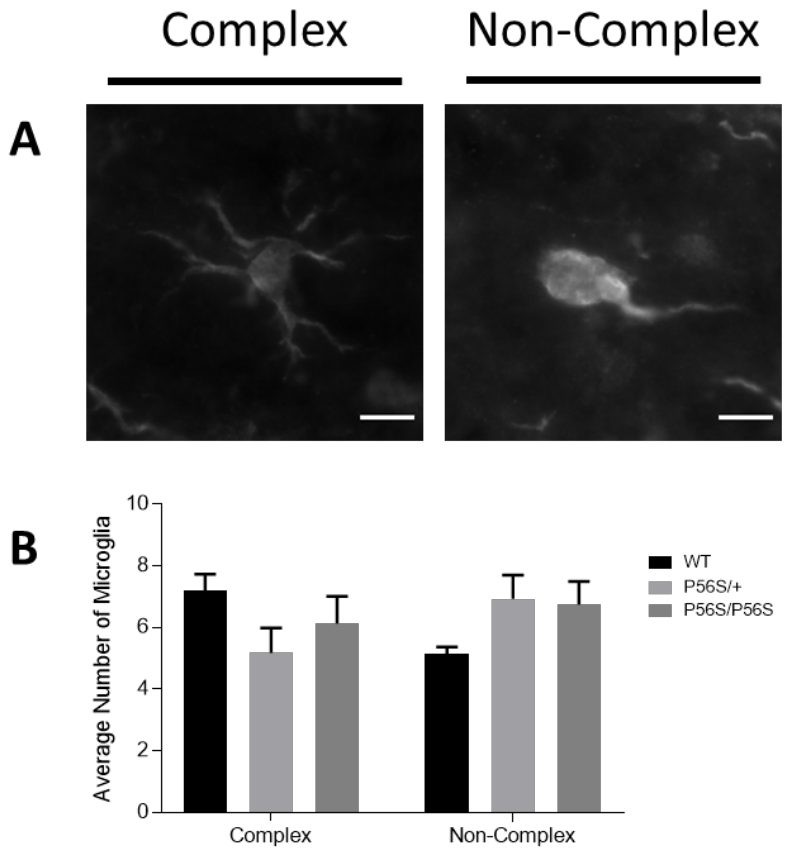

Figure 6.10: Pilot study of microglial morphology.
A: Examples of Complex (3 or more branches from soma), and Non-Complex (fewer than 3 branches from soma) microglia. Scale bar 10µm. **B**: Average number of complex and non-complex microglia. Two-way ANOVA with Dunnett's post-hoc test applied. 3 sections per genotype included in analysis.

6.5 Discussion and Future Work

The loss of MN in vapB$^{P56S/+}$ and vapB$^{P56S/P56S}$ lumbar spinal cord in this model reflect the loss of MN seen in other rodent models of ALS (Scekic-Zahirovic et al., 2016, Dong et al., 2021, Dong et al., 2020, Feeney et al., 2001, Huang et al., 2020), but was contrary to murine models of ALS8 which detected no loss in spinal motor neurons (Kuijpers et al., 2013a, Tudor et al., 2010, Qiu et al., 2013, Larroquette et al., 2015). One mouse model did have a loss in corticospinal MNs (CSMN) where human vapB was over-expressed (Aliaga et al., 2013), and the loss of MN in an SOD1^{G93A} mouse model was slightly alleviated by vapB over-expression (Kim et al., 2016). CSMNs were not studied in this project as all ALS8 patients show signs of lower MN loss (Nishimura et al., 2004a), so spinal MN were prioritised for analysis. However, due to the heterogeneity of ALS8 patients carrying the P56S mutation, and that some patients show upper signs, it could be worth looking at CSMNs in this model to see if there were any changes in upper motor neurons, reflecting what was found in the human vapB-expressing mouse model. It would also be worth using vapB#38 antibody against the C-terminal truncated form of vapB (containing the CCD and TMD) to see if distribution in MNs change as result of mutation, or if distribution was different to that seen in this project where vapB-MSP was labelled. There was evidence of vapB and vapA localising in different parts of cells (Gkogkas et al., 2008), but this was not replicated here due to time restraints. Co-labelling vapA and vapB would offer insight into how protein distribution was affected by the mutation.

The discrepancy of MN number between mouse models and this rat model may be linked to the majority of murine ALS8 models over-expressing vapB, however, a knock-in vapB^{P56S} model in the mouse did not show changes in the number of motor neurons in the spinal cord (Larroquette et al., 2015). This contradiction might be due to species-specific differences (Brozzi et al., 2015), or other proteins of the VAP family of proteins, vapA as well as MOSPD1, MOSPD2, or MOSPD3, could be enough to compensate for changes to vapB in the knock-in mouse model to inhibit neurodegeneration (Di Mattia et al., 2018). Whilst the size and morphologies of MNs were not reported in ALS8 models, the SOD1 G93A mouse had larger MNs than wild type controls (Shoenfeld et al., 2014), completely contrary to findings here. This model could be an accurate tool for studying motor neuron degeneration as it reflects the loss of MN in the spinal cord. Further investigation into CSMN could potentially open the door to insight into heterogeneity seen in the human disease.

Another difference seen in MN from this project was vapB$^{-/-}$ MN having an elevated cytoplasmic TDP-43 signal compared to vapB, but no significant change in nuclear TDP-43 signal from vapB. Under normal conditions, TDP-43 was trafficked between the nucleus and cytoplasm (Ayala et al., 2008). TDP-43 pathology was widely accepted as abnormal truncated forms of the protein mislocalising to the cytoplasm and recruiting normal nuclear TDP-43 to aggregates, leading to a change in TDP-43 distribution rather than up-regulation of protein expression (Arai et al., 2006, Neumann et al., 2006). TDP-43 pathology in vapB$^{-/-}$ LSC could indicate changes to calcium homeostasis as TDP-43 has been shown to interfere with vapB-PTPIP51 ER-mitochondrial tethering via GSK3β activation, and affecting calcium homeostasis between the two organelles (Stoica et al., 2014a, Stoica et al., 2016). There was already evidence for mitochondrial calcium uptake being reduced when vapB was knocked out of HEK293 cells (De Vos et al., 2012), pathogenic mutations that increase cytoplasmic localisation of TDP-43 affects ER calcium signalling in MN, and ER stress induces TDP-43 mislocalisation to the cytoplasm (Mutihac et al., 2015), and interrupting localisation to the nucleus or export to the cytoplasm leads to the formation of aggregates in the cytoplasm or nucleus respectively (Winton et al., 2008). The vapB$^{-/-}$ model could offer insights into how the absence of functional vapB contributes to TDP-43 pathology, potentially affecting trafficking into and out of the nucleus, and its role in ALS. As the number of MN in vapB$^{-/-}$ is not significantly different from wild type, neurodegeneration may not entirely depend upon TDP-43 pathology in this model. There is no evidence in literature to date of TDP-43 pathology in models or patient samples as they have not been mentioned in studies to date.

There was no evidence of glial activation at 17 – 18 months in this model, which was contrary to evidence in literature where reactive astrocytes become hypertrophic with complex networks of extended processes in the spinal cord of ALS patients (Schiffer et al., 1996, Bruijn et al., 1997), and evidence has been collected, mainly from SOD1 models or tissue from patients carrying mutations in SOD1, pointing to multiple roles for astrocytes in ALS. Astrocytes in SOD1 mouse models show signs of irregular protein homeostasis such as protein inclusions (Bruijn et al., 1997), and even signs of astrocyte sub-populations degenerating over the course of disease progression (Rossi et al., 2008). Reducing astrocyte SOD1G93A expression delayed the activation of microglia, slowing disease progression and showing how both glial populations interact in an ALS model (Yamanaka et al., 2008). Astrocytes carrying

the SOD1G93A mutation were toxic to neighbouring neurons, specifically motor neurons in iPSC co-cultures (Di Giorgio et al., 2007, Nagai et al., 2007), and wild type astrocytes extend MN survival in SOD1 mice (Clement et al., 2003). Astrocytes assist in neurotransmission in synapses between neurons by taking up glutamate to prevent excitotoxicity. Under pathological conditions, glutamate uptake was reduced due to reduced expression of glutamate re-uptake transporters such as GLT-1 and excitotoxicity occurs (Bruijn et al., 1997), which motor neurons were particularly susceptible to (Saroff et al., 2000, Vandenberghe et al., 2000).

Although there were no changes in astrocyte occupancy of ROIs in LSC, and no change in GFAP expression in LSC, activated astrocytes also release inflammatory markers such as inducible nitric oxide synthase (iNOS) (Sasaki et al., 2000b) and cyclooxygenase (Maihöfner et al., 2003), and also downregulate glutamate transporters such as GLT1, which was reduced in the spinal cord of ALS patients (Sasaki et al., 2000a, Rothstein et al., 1995). The lack of changes in GFAP expression could reflect differing observations in various ALS models where GFAP has either increased or decreased (Díaz-Amarilla et al., 2011, Cunha et al., 2018, Tripathi et al., 2017, Almer et al., 1999) and so may not be a reliable marker of astrocyte activation. Looking into the expression of markers released by astrocytes may provide more subtle mechanisms being employed by astrocytes in vapB$^{P56S/+}$ and vapB$^{P56S/P56S}$, as the reduction in MN number point to some sort of neurodegenerative mechanism taking place.

There were also no changes in the number of microglia in LSC in this model. Microglia have been shown to activate in ALS through proliferation, and through changes in morphology where a cell soma with stellate processes becomes amoeboid with fewer processes extending from the soma (Spiller et al., 2018, Kreutzberg, 1996, Ohgomori et al., 2016). This formed the basis of the pilot analysis of microglial morphology where there were no differences in the number of microglial with amoeboid or “non-complex” morphology. However, there do appear to be more amoeboid cells in vapB$^{P56S/+}$ and vapB$^{P56S/P56S}$, even if this as not to statistical significance. Future work should focus on sampling cell bodies form the spinal cord and employing Z-stacks to produce detailed images of microglia, and determine if changes in morphology were present. This was worth focusing on as there was evidence of morphology taking precedence over the number of microglia during microgliosis (Gowing et al., 2008). The number of microglia in spinal cord differs depending on the model, for example, the number

of resident microglia in the spinal cord of ALS patients being reduced (Butovsky et al., 2012), although this was not consistent due to the heterogeneity of ALS (Tam et al., 2019). Microglial gene expression also changes during normal ageing (Soreq et al., 2017), potentially affecting signs of activation in ALS as it was a late-onset disease. However, increased neuro-inflammation has been observed in the motor cortices of ALS patients (Alshikho et al., 2018, Corcia et al., 2012), and evidence from animal models all point to microglia having a role to play in ALS. This makes investigation into microglial activity in this rat model key in understanding non-autonomous features of the neurodegeneration seen in vapB$^{P56S/+}$ and vapB$^{P56S/P56S}$ MN.

7 General Discussion and Concluding Remarks

ALS8 is a late-onset slowly progressive disease caused by vapB^{P56S} mutation. In rats the P56S mutation and knock out were inherited in Mendelian proportions, and in the rat spinal cord, vapB$^{P56S/+}$ protein was expressed to the same degree as in vapB$^{-/-}$ in immunoblots of lumbar spinal cord. This reduction in vapB expression reflects the reduced expression of vapB in ALS patient spinal cord (Anagnostou et al., 2010), and in the vapB knock-in mouse model (Larroquette et al., 2015). Such observations have led groups to theorise that the vapB^{P56S} mutation causes loss-of-function, either by sequestering functional wild type vapB into vapB^{P56S} cytoplasmic aggregates (Teuling et al., 2007) along with proteins involved in key processes such as ERAD pathway proteins (Kuijpers et al., 2013a). Aggregates appeared to be reversible in transfected cells and were easily cleared by the proteasome in cell culture (Papiani et al., 2012), iPSCs from ALS patients adopted mitigating transcriptomes to cope with reduced availability of functional vapB (Oliveira et al., 2020), and aggregated misfolded vapB is isolated in a protective ER compartment in transgenic mice (Kuijpers et al., 2013a). Reduction of functional vapB has been shown to affect phosphoinositide homeostasis (Dong et al., 2016, Mao et al., 2019), calcium signalling (De Vos et al., 2012, Gomez-Suaga et al., 2017b), ion transport (Silbernagel et al., 2018), neurite extension (Genevini et al., 2019), and ER stress (Kanekura et al., 2006).

It is possible that, like TDP-43, vapB is toxic at high levels, as seen in over-expression mouse models, and that low levels are insupportable (Stribl et al., 2014). Other groups have argued that the presence of aggregates indicated toxic-gain-of function as seen in other neurodegenerative diseases such as amyloid-β plaques in Alzheimer's disease (Shankar et al., 2008). Aggregates of mutant vapB have been observed in animal models (Larroquette et al., 2015) and in human samples (Cadoni et al., 2020, Tripathi et al., 2017), however they were not overtly present in MN from this rat model. Instead, the cytoplasmic signal distribution of vapB was unchanged, but vapB$^{P56S/P56S}$ MN expressing vapA in a homogenous manner covered a larger area of the soma than wild type MNs. This may indicate compensatory changes in vapA distribution within the cell, as vapB and vapA have been shown to localise to different parts of cell soma (Gkogkas et al., 2008). Co-localisation studies of vapB and vapA in the same cells would help to confirm this, and would utilise vapB#84 in-house antibody which

recognises a motif in the CCD of vapB. As the antibody used in this study recognises vapB-MSP, it is more likely for vapB-MSP and vapA to be distributed differently within cells as the MSP domain is cleaved and secreted as a signalling molecule (Tsuda et al., 2008). Co-localising vapA with vapB-CCD would offer a clearer picture of how both whole proteins are distributed in cells. The lack of aggregates in this model may point to aggregate formation in mouse models being products of over-expression as in SOD1 and TDP-43 models of ALS (Zwiegers et al., 2014, Xu et al., 2010, Xu et al., 2011), however the knock-in model and ALS patients offer the same observation. This is another issue that could be investigated using vapB#84 as there is no evidence of the MSP domain alone forming aggregates in patient or model tissue.

Male vapB$^{P56S/P56S}$ and vapB$^{-/-}$ gained more weight than vapB from 7 months onwards. This is contrary to ALS patients and other rodent models which all report reduction in mass. One TDP-43 model gained weight, potentially from hyperphagia linked to FTLD (White et al., 2018), or increasing fat deposits in muscle due to altered Glut4 receptor location (Stallings et al., 2013). Hypermetabolism has been linked to poor clinical prognosis in ALS patients (Steyn et al., 2018), with hypometabolism was seen as slowing progression (Cattaneo et al., 2021). If behavioural changes underlay this weight gain, it would support evidence of ALS8 not being a pure motor disease and that some cognitive changes might also occur in this model (de Alcântara et al., 2019). Cognitive tests on male vapB$^{P56S/P56S}$ and vapB$^{-/-}$ animals at 7 months would help to investigate any changes in behaviour. Otherwise, lipid metabolism or energy expenditure could also be compromised in this model as vapB interacts with proteins involved in lipid transport (Furuita et al., 2010). Lipid metabolism was not investigated here, but pilot mitochondrial stress tests show that mitochondria of vapB$^{P56S/+}$ hippocampal cultures from P0 – P1 pups were less able to cope in a stressful environment and had less non-mitochondrial oxygen consumption. This points to altered mitochondrial function in the homozygous mutant, but further studies from 7 months onward could help to determine if this could contribute to weight gain in vapB$^{P56S/P56S}$ and vapB$^{-/-}$ male rats. A pilot immunoblot showed that Mitofusin 2 expression was reduced in all genotypes, but quantitation using multiple samples per genotype could help to determine to what the degree of reduction and if any genotypes were affected more than others. Given its role in mitochondrial fusion and metabolism (de Brito and Scorrano, 2008, Chen et al., 2003), it could offer more information about the state of mitochondria in vapB$^{P56S/+}$ MN. Proteins that interact with vapB in lipid

metabolism, such as Osbp, should also be investigated for changes in expression or function. This would be beneficial to the wider field as hypometabolism in ALS patients has been linked to delayed need for ventilation (Körner et al., 2013). As the male vapB$^{P56S/P56S}$ rats only had reductions in paw pressure, whereas female rats had reduced paw pressure and size, and that the MNs of vapB$^{P56S/P56S}$ are fewer and smaller than wild type, it is possible that fat accumulation could be having a mitigating protective effect in these rats. However, the vapB rats do not have the same changes in gait but do have the same changes in weight gain and also have fewer MNs in lumbar spinal cord.

TDP-43 pathology was observed in vapB$^{-/-}$ MNs. There is evidence of the vapB-PTPIP51 interaction being disrupted by TDP-43 (Stoica et al., 2014b), but it is possible that absence of functional vapB also leads to disrupted TDP-43 homeostasis. As vapB is expressed at the same levels in vapB$^{P56S/+}$ and vapB$^{-/-}$, but there was no TDP-43 pathology in vapB$^{P56S/+}$ MNs, it is possible that expression of vapB alone may be the main driver for TDP-43 pathology in this model. Investigating the effect of reduced vapB expression on TDP-43 localisation in cell culture could indicate how the presence or lack of the P56S mutation might affect TDP-43 homeostasis.

Pilot blood analysis indicated changes to erythrocyte morphology and mild anaemia in male vapB$^{-/-}$. Given that vapB has a role in regulating autophagy (Gómez-Suaga et al., 2019, Tripathi et al., 2021b), its absence in vapB$^{-/-}$ could affect erythroblasts ability to expel organelles during erythropoiesis, and leading to the wide variation in erythrocyte diameters seen in male vapB$^{-/-}$ rats. This is supported by syntaxin expression being reduced in vapB$^{P56S/P56S}$ spinal cord. Syntaxin is part of the SNARE complex which is key in the fusion of vesicles, which is a key step in autophagy due to membrane fusion between lysosomes and autophagosomes for cell debris degradation and recycling (Wang et al., 2016).

Altering autophagy or investigating markers of autophagy, such as p62 and LC3, in this model, or examining erythrocyte ultrastructure may help to confirm whether a lack of vapB could lead to erythrocyte morphological changes.

The phenotypes exhibited by mutant and knock out animals in this study demonstrated the myriad of cellular function vapB is involved in, and the avenues of enquiry that this model opens up. Future work on this model will help to link changes in these cellular functions to ALS8, and provides a strong model on which to develop treatments.

8 Bibliography

ABE, K., ITOYAMA, Y., SOBUE, G., TSUJI, S., AOKI, M., DOYU, M., HAMADA, C., KONDO, K., YONEOKA, T., AKIMOTO, M., YOSHINO, H. & EDARAVONE, A. L. S. S. G. 2014. Confirmatory double-blind, parallel-group, placebo-controlled study of efficacy and safety of edaravone (MCI-186) in amyotrophic lateral sclerosis patients. *Amyotrophic lateral sclerosis & frontotemporal degeneration,* 15**,** 610-617.

ABE, K., PAN, L. H., WATANABE, M., KATO, T. & ITOYAMA, Y. 1995. Induction of nitrotyrosine-like immunoreactivity in the lower motor neuron of amyotrophic lateral sclerosis. *Neuroscience Letters,* 199**,** 152-154.

ABELIOVICH, H., DUNN, W. A., JR., KIM, J. & KLIONSKY, D. J. 2000. Dissection of Autophagosome Biogenesis into Distinct Nucleation and Expansion Steps. *Journal of Cell Biology,* 151**,** 1025-1034.

ACUÑA, E., FORNES, R., FERNANDOIS, D., GARRIDO, M. P., GREINER, M., LARA, H. E. & PAREDES, A. H. 2009. Increases in norepinephrine release and ovarian cyst formation during ageing in the rat. *Reproductive Biology and Endocrinology,* 7**,** 64.

AHMED, R. M., STEYN, F. & DUPUIS, L. 2021. Hypothalamus and weight loss in amyotrophic lateral sclerosis. *Handb Clin Neurol,* 180**,** 327-338.

AJMONE-CAT, M. A., ONORI, A., TOSELLI, C., STRONATI, E., MORLANDO, M., BOZZONI, I., MONNI, E., KOKAIA, Z., LUPO, G., MINGHETTI, L., BIAGIONI, S. & CACCI, E. 2019. Increased FUS levels in astrocytes leads to astrocyte and microglia activation and neuronal death. *Sci Rep,* 9**,** 4572.

AKGUN, O., AKAN, A., DEMIR, H. & AKINCI, T. C. 2018. Analysis of Gait Dynamics of ALS Disease and Classification of Artificial Neural Networks. *Tehnicki Vjesnik - Technical Gazette,* 25**,** 183+.

ALBRECHT, P. J., MURTIE, J. C., NESS, J. K., REDWINE, J. M., ENTERLINE, J. R., ARMSTRONG, R. C. & LEVISON, S. W. 2003. Astrocytes produce CNTF during the remyelination phase of viral-induced spinal cord demyelination to stimulate FGF-2 production. *Neurobiology of Disease,* 13**,** 89-101.

ALIAGA, L., LAI, C., YU, J., CHUB, N., SHIM, H., SUN, L., XIE, C., YANG, W.-J., LIN, X., O'DONOVAN, M. J. & CAI, H. 2013. Amyotrophic lateral sclerosis-related VAPB P56S mutation differentially affects the function and survival of corticospinal and spinal motor neurons. *Human Molecular Genetics,* 22**,** 4293-4305.

ALLEN, S. P., RAJAN, S., DUFFY, L., MORTIBOYS, H., HIGGINBOTTOM, A., GRIERSON, A. J. & SHAW, P. J. 2014. Superoxide dismutase 1 mutation in a cellular model of amyotrophic lateral sclerosis shifts energy generation from oxidative phosphorylation to glycolysis. *Neurobiology of Aging,* 35**,** 1499-1509.

ALLODI, I., MONTAÑANA-ROSELL, R., SELVAN, R., LÖW, P. & KIEHN, O. 2021. Locomotor deficits in a mouse model of ALS are paralleled by loss of V1-interneuron connections onto fast motor neurons. *Nature Communications,* 12**,** 3251.

ALMER, G., VUKOSAVIC, S., ROMERO, N. & PRZEDBORSKI, S. 1999. Inducible nitric oxide synthase up-regulation in a transgenic mouse model of familial amyotrophic lateral sclerosis. *J Neurochem,* 72**,** 2415-25.

ALSHIKHO, M. J., ZÜRCHER, N. R., LOGGIA, M. L., CERNASOV, P., REYNOLDS, B., PIJANOWSKI, O., CHONDE, D. B., IZQUIERDO GARCIA, D., MAINERO, C., CATANA, C., CHAN, J., BABU, S., PAGANONI, S., HOOKER, J. M. & ATASSI, N. 2018. Integrated magnetic resonance

imaging and [(11) C]-PBR28 positron emission tomographic imaging in amyotrophic lateral sclerosis. *Annals of neurology,* 83**,** 1186-1197.

AMARILIO, R., RAMACHANDRAN, S., SABANAY, H. & LEV, S. 2005. Differential Regulation of Endoplasmic Reticulum Structure through VAP-Nir Protein Interaction. *Journal of Biological Chemistry,* 280**,** 5934-5944.

ANAGNOSTOU, G., AKBAR, M. T., PAUL, P., ANGELINETTA, C., STEINER, T. J. & DE BELLEROCHE, J. 2010. Vesicle associated membrane protein B (VAPB) is decreased in ALS spinal cord. *Neurobiology of Aging,* 31**,** 969-985.

ANAN'INA, T., KISEL, A., KUDABAEVA, M., CHERNYSHEVA, G., SMOLYAKOVA, V., USOV, K., KRUTENKOVA, E., PLOTNIKOV, M. & KHODANOVICH, M. 2020. Neurodegeneration, Myelin Loss and Glial Response in the Three-Vessel Global Ischemia Model in Rat. *International Journal of Molecular Sciences,* 21**,** 6246.

ANDERSEN, P. M., BORASIO, G. D., DENGLER, R., HARDIMAN, O., KOLLEWE, K., LEIGH, P. N., PRADAT, P.-F., SILANI, V. & TOMIK, B. 2005. EFNS task force on management of amyotrophic lateral sclerosis: guidelines for diagnosing and clinical care of patients and relatives. *European Journal of Neurology,* 12**,** 921-938.

ANDERSEN, P. M., FORSGREN, L., BINZER, M., NILSSON, P., ALA-HURULA, V., KERÄNEN, M.-L., BERGMARK, L., SAARINEN, A., HALTIA, T., TARVAINEN, I., KINNUNEN, E., UDD, B. & MARKLUND, S. L. 1996. Autosomal recessive adult-onset amyotrophic lateral sclerosis associated with homozygosity for Asp90Ala CuZn-superoxide dismutase mutation: A clinical and genealogical study of 36 patients. *Brain,* 119**,** 1153-1172.

ANTOINE, M., PATRICK, K. L., SORET, J., DUC, P., RAGE, F., CACCIOTTOLO, R., NISSEN, K. E., CAUCHI, R. J., KROGAN, N. J., GUTHRIE, C., GACHET, Y. & BORDONNÉ, R. 2020. Splicing Defects of the Profilin Gene Alter Actin Dynamics in an S. pombe SMN Mutant. *iScience,* 23**,** 100809.

ANTONINI, A., LEENDERS, K., SPIEGEL, R., MEIER, D., VONTOBEL, P., WEIGELL-WEBER, M., SANCHEZ-PERNAUTE, R., DE YEBENEZ, J., BOESIGER, P. & WEINDL, A. 1996. Striatal glucose metabolism and dopamine D2 receptor binding in asymptomatic gene carriers and patients with Huntington's disease. *Brain,* 119**,** 2085-2095.

ARAI, T., HASEGAWA, M., AKIYAMA, H., IKEDA, K., NONAKA, T., MORI, H., MANN, D., TSUCHIYA, K., YOSHIDA, M., HASHIZUME, Y. & ODA, T. 2006. TDP-43 is a component of ubiquitin-positive tau-negative inclusions in frontotemporal lobar degeneration and amyotrophic lateral sclerosis. *Biochemical and Biophysical Research Communications,* 351**,** 602-611.

ARAN, F. 1850. Recherches sur une maladie non encore décrite du système musculaire (atrophie musculaire progressive). *Arch Gen Med,* 24**,** 172.

ARIAS, C., MONTIEL, T., QUIROZ-BÁEZ, R. & MASSIEU, L. 2002. β-Amyloid neurotoxicity is exacerbated during glycolysis inhibition and mitochondrial impairment in the rat hippocampus in vivo and in isolated nerve terminals: implications for Alzheimer's disease. *Experimental neurology,* 176**,** 163-174.

ARRIGO, A. P., TANAKA, K., GOLDBERG, A. L. & WELCH, W. J. 1988. Identity of the 19S 'prosome' particle with the large multifunctional protease complex of mammalian cells (the proteasome). *Nature,* 331**,** 192-4.

AWAI, M., OKADA, S., TAKEBAYASHI, J., KUBO, T., INOUE, M. & SENO, S. 1968. Studies on the mechanism of denucleation of the erythroblast. *Acta Haematol,* 39**,** 193-202.

AYALA, Y. M., MISTELI, T. & BARALLE, F. E. 2008. TDP-43 regulates retinoblastoma protein phosphorylation through the repression of cyclin-dependent kinase 6 expression.

Proceedings of the National Academy of Sciences of the United States of America, 105**,** 3785-3789.

BALDRIDGE, R. D. & RAPOPORT, T. A. 2016. Autoubiquitination of the Hrd1 Ligase Triggers Protein Retrotranslocation in ERAD. *Cell,* 166**,** 394-407.

BANIASADI, M., MANAHEJI, H., MAGHSOUDI, N., DANYALI, S., ZAKERI, Z., MAGHSOUDI, A. & ZARINGHALAM, J. 2020. Microglial-induced apoptosis is potentially responsible for hyperalgesia variations during CFA-induced inflammation. *Inflammopharmacology,* 28**,** 475-485.

BANKHEAD, P. E. A. 2017. QuPath: Open source software for digital pathology image analysis. *Scientific Reports*.

BARBER, R. P., PHELPS, P. E., HOUSER, C. R., CRAWFORD, G. D., SALVATERRA, P. M. & VAUGHN, J. E. 1984. The morphology and distribution of neurons containing choline acetyltransferase in the adult rat spinal cord: An immunocytochemical study. *Journal of Comparative Neurology,* 229**,** 329-346.

BARCIA, C., ROS, C. M., ANNESE, V., GÓMEZ, A., ROS-BERNAL, F., AGUADO-LLERA, D., MARTÍNEZ-PAGÁN, M. E., DE PABLOS, V., FERNANDEZ-VILLALBA, E. & HERRERO, M. T. 2011. IFN-γ signaling, with the synergistic contribution of TNF-α, mediates cell specific microglial and astroglial activation in experimental models of Parkinson's disease. *Cell Death & Disease,* 2**,** e142-e142.

BARMADA, S. J., SKIBINSKI, G., KORB, E., RAO, E. J., WU, J. Y. & FINKBEINER, S. 2010. Cytoplasmic mislocalization of TDP-43 is toxic to neurons and enhanced by a mutation associated with familial amyotrophic lateral sclerosis. *Journal of Neuroscience,* 30**,** 639-649.

BARON, Y., PEDRIOLI, P. G., TYAGI, K., JOHNSON, C., WOOD, N. T., FOUNTAINE, D., WIGHTMAN, M. & ALEXANDRU, G. 2014. VAPB/ALS8 interacts with FFAT-like proteins including the p97 cofactor FAF1 and the ASNA1 ATPase. *BMC biology,* 12**,** 39-39.

BARTOLOME, F., WU, H.-C., BURCHELL, VICTORIA S., PREZA, E., WRAY, S., MAHONEY, COLIN J., FOX, NICK C., CALVO, A., CANOSA, A., MOGLIA, C., MANDRIOLI, J., CHIÒ, A., ORRELL, RICHARD W., HOULDEN, H., HARDY, J., ABRAMOV, ANDREY Y. & PLUN-FAVREAU, H. 2013. Pathogenic VCP Mutations Induce Mitochondrial Uncoupling and Reduced ATP Levels. *Neuron,* 78**,** 57-64.

BATKA, R. J., BROWN, T. J., MCMILLAN, K. P., MEADOWS, R. M., JONES, K. J. & HAULCOMB, M. M. 2014. The Need for Speed in Rodent Locomotion Analyses. *The Anatomical Record,* 297**,** 1839-1864.

BEAL, M. F., FERRANTE, R. J., BROWNE, S. E., MATTHEWS, R. T., KOWALL, N. W. & BROWN JR, R. H. 1997. Increased 3-nitrotyrosine in both sporadic and familial amyotrophic lateral sclerosis. *Annals of Neurology,* 42**,** 644-654.

BEERS, D. R., ZHAO, W., WANG, J., ZHANG, X., WEN, S., NEAL, D., THONHOFF, J. R., ALSULIMAN, A. S., SHPALL, E. J. & REZVANI, K. 2017. ALS patients' regulatory T lymphocytes are dysfunctional, and correlate with disease progression rate and severity. *JCI insight,* 2.

BENSIMON, G., LACOMBLEZ, L. & MEININGER, V. 1994. A controlled trial of riluzole in amyotrophic lateral sclerosis. ALS/Riluzole Study Group. *N Engl J Med,* 330**,** 585-91.

BERCOVICH, B., STANCOVSKI, I., MAYER, A., BLUMENFELD, N., LASZLO, A., SCHWARTZ, A. L. & CIECHANOVER, A. 1997. Ubiquitin-dependent Degradation of Certain Protein Substrates in Vitro Requires the Molecular Chaperone Hsc70 *. *Journal of Biological Chemistry,* 272**,** 9002-9010.

BERGHOFF, S. A., SPIETH, L., SUN, T., HOSANG, L., DEPP, C., SASMITA, A. O., VASILEVA, M. H., SCHOLZ, P., ZHAO, Y., KRUEGER-BURG, D., WICHERT, S., BROWN, E. R., MICHAIL, K., NAVE, K.-A., BONN, S., ODOARDI, F., ROSSNER, M., ISCHEBECK, T., EDGAR, J. M. & SAHER, G. 2021. Neuronal cholesterol synthesis is essential for repair of chronically demyelinated lesions in mice. *Cell Reports,* 37**,** 109889.

BHAGWANDIN, A., FUXE, K. & MANGER, P. R. 2006. Choline acetyltransferase immunoreactive cortical interneurons do not occur in all rodents: A study of the phylogenetic occurrence of this neural characteristic. *Journal of Chemical Neuroanatomy,* 32**,** 208-216.

BI, F., HUANG, C., TONG, J., QIU, G., HUANG, B., WU, Q., LI, F., XU, Z., BOWSER, R., XIA, X.-G. & ZHOU, H. 2013. Reactive astrocytes secrete lcn2 to promote neuron death. *Proceedings of the National Academy of Sciences of the United States of America,* 110**,** 4069-4074.

BOLOTINA, V., OMELYANENKO, V., HEYES, B., RYAN, U. & BREGESTOVSKI, P. 1989. Variations of membrane cholesterol alter the kinetics of Ca2(+)-dependent K+ channels and membrane fluidity in vascular smooth muscle cells. *Pflugers Arch,* 415**,** 262-8.

BORGES, L. F. & IVERSEN, S. D. 1986. Topography of choline acetyltransferase Immunoreactive Neurons and fibers in the rat spinal cord. *Brain Research,* 362**,** 140-148.

BORGESE, N., NAVONE, F., NUKINA, N. & YAMANAKA, T. 2021. Mutant VAPB: Culprit or Innocent Bystander of Amyotrophic Lateral Sclerosis? *Contact,* 4**,** 25152564211022515.

BOVERIS, A. & CHANCE, B. 1973. The mitochondrial generation of hydrogen peroxide. General properties and effect of hyperbaric oxygen. *The Biochemical journal,* 134**,** 707-716.

BOVERIS, A., OSHINO, N. & CHANCE, B. 1972. The cellular production of hydrogen peroxide. *Biochem J,* 128**,** 617-30.

BRETTSCHNEIDER, J., TOLEDO, J. B., VAN DEERLIN, V. M., ELMAN, L., MCCLUSKEY, L., LEE, V. M. & TROJANOWSKI, J. Q. 2012. Microglial activation correlates with disease progression and upper motor neuron clinical symptoms in amyotrophic lateral sclerosis. *PLoS One,* 7**,** e39216.

BROOKS, B. R. 1994. El Escorial World Federation of Neurology criteria for the diagnosis of amyotrophic lateral sclerosis. Subcommittee on Motor Neuron Diseases/Amyotrophic Lateral Sclerosis of the World Federation of Neurology Research Group on Neuromuscular Diseases and the El Escorial "Clinical limits of amyotrophic lateral sclerosis" workshop contributors. *J Neurol Sci,* 124 Suppl**,** 96-107.

BROOKS, B. R., MILLER, R. G., SWASH, M. & MUNSAT, T. L. 2000. El Escorial revisited: Revised criteria for the diagnosis of amyotrophic lateral sclerosis. *Amyotrophic Lateral Sclerosis and Other Motor Neuron Disorders,* 1**,** 293-299.

BROOKS, G. 1985. Lactate: glycolytic end product and oxidative substrate during sustained exercise in mammals—the “lactate shuttle”. *Circulation, Respiration, and Metabolism.* Springer.

BROWN, R. H. & AL-CHALABI, A. 2017. Amyotrophic Lateral Sclerosis. *N Engl J Med,* 377**,** 162-172.

BROWN, W. F. & JAATOUL, N. 1974. Amyotrophic Lateral Sclerosis: Electrophysiologic Study (Number of Motor Units and Rate of Decay of Motor Units). *Archives of Neurology,* 30**,** 242-248.

BROZZI, F., NARDELLI, T. R., LOPES, M., MILLARD, I., BARTHSON, J., IGOILLO-ESTEVE, M., GRIECO, F. A., VILLATE, O., OLIVEIRA, J. M., CASIMIR, M., BUGLIANI, M., ENGIN, F.,

HOTAMISLIGIL, G. S., MARCHETTI, P. & EIZIRIK, D. L. 2015. Cytokines induce endoplasmic reticulum stress in human, rat and mouse beta cells via different mechanisms. *Diabetologia,* 58**,** 2307-16.

BRUGMAN, F., WOKKE, J. H. J., VIANNEY DE JONG, J. M. B., FRANSSEN, H., FABER, C. G. & VAN DEN BERG, L. H. 2005. Primary lateral sclerosis as a phenotypic manifestation of familial ALS. *Neurology,* 64**,** 1778-1779.

BRUIJN, L. I., BECHER, M. W., LEE, M. K., ANDERSON, K. L., JENKINS, N. A., COPELAND, N. G., SISODIA, S. S., ROTHSTEIN, J. D., BORCHELT, D. R., PRICE, D. L. & CLEVELAND, D. W. 1997. ALS-Linked SOD1 Mutant G85R Mediates Damage to Astrocytes and Promotes Rapidly Progressive Disease with SOD1-Containing Inclusions. *Neuron,* 18**,** 327-338.

BRYAN, J. 2013, 0:54. Rotarod Test.

BUCHAN, L., ST AUBIN, C. R., FISHER, A. L., HELLINGS, A., CASTRO, M., AL-NAKKASH, L., BRODERICK, T. L. & PLOCHOCKI, J. H. 2018. High-fat, high-sugar diet induces splenomegaly that is ameliorated with exercise and genistein treatment. *BMC research notes,* 11**,** 752-752.

BURKE, D., GASDASKA, P. & HARTWELL, L. 1989. Dominant effects of tubulin overexpression in Saccharomyces cerevisiae. *Mol Cell Biol,* 9**,** 1049-59.

BURNETT, B. G., MUÑOZ, E., TANDON, A., KWON, D. Y., SUMNER, C. J. & FISCHBECK, K. H. 2009. Regulation of SMN protein stability. *Molecular and cellular biology,* 29**,** 1107-1115.

BUTOVSKY, O., SIDDIQUI, S., GABRIELY, G., LANSER, A. J., DAKE, B., MURUGAIYAN, G., DOYKAN, C. E., WU, P. M., GALI, R. R., IYER, L. K., LAWSON, R., BERRY, J., KRICHEVSKY, A. M., CUDKOWICZ, M. E. & WEINER, H. L. 2012. Modulating inflammatory monocytes with a unique microRNA gene signature ameliorates murine ALS. *The Journal of clinical investigation,* 122**,** 3063-3087.

BUTTS, C. L., SHUKAIR, S. A., DUNCAN, K. M., BOWERS, E., HORN, C., BELYAVSKAYA, E., TONELLI, L. & STERNBERG, E. M. 2007. Progesterone inhibits mature rat dendritic cells in a receptor-mediated fashion. *Int Immunol,* 19**,** 287-96.

CABUKUSTA, B., BERLIN, I., VAN ELSLAND, D. M., FORKINK, I., SPITS, M., DE JONG, A. W. M., AKKERMANS, J. J. L. L., WIJDEVEN, R. H. M., JANSSEN, G. M. C., VAN VEELEN, P. A. & NEEFJES, J. 2020. Human VAPome Analysis Reveals MOSPD1 and MOSPD3 as Membrane Contact Site Proteins Interacting with FFAT-Related FFNT Motifs. *Cell Reports,* 33**,** 108475.

CADONI, M. P. L., BIGGIO, M. L., ARRU, G., SECCHI, G., ORRÙ, N., CLEMENTE, M. G., SECHI, G., YAMOAH, A., TRIPATHI, P., ORRÙ, S., MANETTI, R. & GALLERI, G. 2020. VAPB ER-Aggregates, A Possible New Biomarker in ALS Pathology. *Cells,* 9**,** 164.

CAIRNS, N. J., NEUMANN, M., BIGIO, E. H., HOLM, I. E., TROOST, D., HATANPAA, K. J., FOONG, C., WHITE, C. L., 3RD, SCHNEIDER, J. A., KRETZSCHMAR, H. A., CARTER, D., TAYLOR-REINWALD, L., PAULSMEYER, K., STRIDER, J., GITCHO, M., GOATE, A. M., MORRIS, J. C., MISHRA, M., KWONG, L. K., STIEBER, A., XU, Y., FORMAN, M. S., TROJANOWSKI, J. Q., LEE, V. M. Y. & MACKENZIE, I. R. A. 2007. TDP-43 in familial and sporadic frontotemporal lobar degeneration with ubiquitin inclusions. *The American journal of pathology,* 171**,** 227-240.

CAMPBELL, F. R. 1968. Nuclear elimination from the normoblast of fetal guinea pig liver as studied with electron microscopy and serial sectioning techniques. *Anat Rec,* 160**,** 539-54.

CATTANEO, M., JESUS, P., LIZIO, A., FAYEMENDY, P., GUANZIROLI, N., CORRADI, E., SANSONE, V., LEOCANI, L., FILIPPI, M., RIVA, N., CORCIA, P., COURATIER, P. & LUNETTA, C. 2021. The hypometabolic state: a good predictor of a better prognosis in amyotrophic lateral sclerosis. *J Neurol Neurosurg Psychiatry*.

CHA-MOLSTAD, H., YU, J. E., FENG, Z., LEE, S. H., KIM, J. G., YANG, P., HAN, B., SUNG, K. W., YOO, Y. D., HWANG, J., MCGUIRE, T., SHIM, S. M., SONG, H. D., GANIPISETTI, S., WANG, N., JANG, J. M., LEE, M. J., KIM, S. J., LEE, K. H., HONG, J. T., CIECHANOVER, A., MOOK-JUNG, I., KIM, K. P., XIE, X.-Q., KWON, Y. T. & KIM, B. Y. 2017. p62/SQSTM1/Sequestosome-1 is an N-recognin of the N-end rule pathway which modulates autophagosome biogenesis. *Nature Communications,* 8**,** 102.

CHA, M.-Y., CHO, H. J., KIM, C., JUNG, Y. O., KANG, M. J., MURRAY, M. E., HONG, H. S., CHOI, Y.-J., CHOI, H. & KIM, D. K. 2015. Mitochondrial ATP synthase activity is impaired by suppressed O-GlcNAcylation in Alzheimer's disease. *Human molecular genetics,* 24**,** 6492-6504.

CHADI, G., MAXIMINO, J. R., JORGE, F. M. D. H., BORBA, F. C. D., GILIO, J. M., CALLEGARO, D., LOPES, C. G., SANTOS, S. N. D. & REBELO, G. N. S. 2017. Genetic analysis of patients with familial and sporadic amyotrophic lateral sclerosis in a Brazilian Research Center. *Amyotrophic Lateral Sclerosis and Frontotemporal Degeneration,* 18**,** 249-255.

CHAN, G., VAN HUMMEL, A., VAN DER HOVEN, J., ITTNER, L. M. & KE, Y. D. 2020. Neurodegeneration and Motor Deficits in the Absence of Astrogliosis upon Transgenic Mutant TDP-43 Expression in Mature Mice. *Am J Pathol,* 190**,** 1713-1722.

CHANDEL, N. S., TRZYNA, W. C., MCCLINTOCK, D. S. & SCHUMACKER, P. T. 2000. Role of Oxidants in NF-κB Activation and TNF-α Gene Transcription Induced by Hypoxia and Endotoxin. *The Journal of Immunology,* 165**,** 1013-1021.

CHARCOT, J. M. 1869. Deux cas d'atrophie musculaire progressive avec lesions de la substance grise et des faisceaux anterolateraux de la moelle epiniere. *Archives de Pathologie Normale et Pathologique,* 2**,** 744-760.

CHARI, A., GOLAS, M. M., KLINGENHÄGER, M., NEUENKIRCHEN, N., SANDER, B., ENGLBRECHT, C., SICKMANN, A., STARK, H. & FISCHER, U. 2008. An assembly chaperone collaborates with the SMN complex to generate spliceosomal SnRNPs. *Cell,* 135**,** 497-509.

CHEN, A. K.-H., LIN, R. Y.-Y., HSIEH, E. Z.-J., TU, P.-H., CHEN, R. P.-Y., LIAO, T.-Y., CHEN, W., WANG, C.-H. & HUANG, J. J.-T. 2010a. Induction of amyloid fibrils by the C-terminal fragments of TDP-43 in amyotrophic lateral sclerosis. *Journal of the American Chemical Society,* 132**,** 1186-1187.

CHEN, A. Q., FANG, Z., CHEN, X. L., YANG, S., ZHOU, Y. F., MAO, L., XIA, Y. P., JIN, H. J., LI, Y. N., YOU, M. F., WANG, X. X., LEI, H., HE, Q. W. & HU, B. 2019. Microglia-derived TNF-α mediates endothelial necroptosis aggravating blood brain-barrier disruption after ischemic stroke. *Cell Death Dis,* 10**,** 487.

CHEN, H.-J., ANAGNOSTOU, G., CHAI, A., WITHERS, J., MORRIS, A., ADHIKAREE, J., PENNETTA, G. & DE BELLEROCHE, J. S. 2010b. Characterization of the Properties of a Novel Mutation in VAPB in Familial Amyotrophic Lateral Sclerosis. *The Journal of Biological Chemistry,* 285**,** 40266-40281.

CHEN , H., DETMER , S. A., EWALD , A. J., GRIFFIN , E. E., FRASER , S. E. & CHAN , D. C. 2003. Mitofusins Mfn1 and Mfn2 coordinately regulate mitochondrial fusion and are essential for embryonic development. *Journal of Cell Biology,* 160**,** 189-200.

CHEN, Y.-Z., BENNETT, C. L., HUYNH, H. M., BLAIR, I. P., PULS, I., IROBI, J., DIERICK, I., ABEL, A., KENNERSON, M. L., RABIN, B. A., NICHOLSON, G. A., AUER-GRUMBACH, M., WAGNER,

K., DE JONGHE, P., GRIFFIN, J. W., FISCHBECK, K. H., TIMMERMAN, V., CORNBLATH, D. R. & CHANCE, P. F. 2004. DNA/RNA helicase gene mutations in a form of juvenile amyotrophic lateral sclerosis (ALS4). *American journal of human genetics,* 74**,** 1128-1135.

CHEW, J., GENDRON, T. F., PRUDENCIO, M., SASAGURI, H., ZHANG, Y.-J., CASTANEDES-CASEY, M., LEE, C. W., JANSEN-WEST, K., KURTI, A., MURRAY, M. E., BIENIEK, K. F., BAUER, P. O., WHITELAW, E. C., ROUSSEAU, L., STANKOWSKI, J. N., STETLER, C., DAUGHRITY, L. M., PERKERSON, E. A., DESARO, P., JOHNSTON, A., OVERSTREET, K., EDBAUER, D., RADEMAKERS, R., BOYLAN, K. B., DICKSON, D. W., FRYER, J. D. & PETRUCELLI, L. 2015. C9ORF72 repeat expansions in mice cause TDP-43 pathology, neuronal loss, and behavioral deficits. *Science,* 348**,** 1151-1154.

CHIANG, P. M., LING, J., JEONG, Y. H., PRICE, D. L., AJA, S. M. & WONG, P. C. 2010. Deletion of TDP-43 down-regulates Tbc1d1, a gene linked to obesity, and alters body fat metabolism. *Proc Natl Acad Sci U S A,* 107**,** 16320-4.

CHIÒ, A., RESTAGNO, G., BRUNETTI, M., OSSOLA, I., CALVO, A., CANOSA, A., MOGLIA, C., FLORIS, G., TACCONI, P., MARROSU, F., MARROSU, M. G., MURRU, M. R., MAJOUNIE, E., RENTON, A. E., ABRAMZON, Y., PUGLIATTI, M., SOTGIU, M. A., TRAYNOR, B. J. & BORGHERO, G. 2012. ALS/FTD phenotype in two Sardinian families carrying both C9ORF72 and TARDBP mutations. *J Neurol Neurosurg Psychiatry,* 83**,** 730-3.

CHOI, D., KOH, J. & PETERS, S. 1988. Pharmacology of glutamate neurotoxicity in cortical cell culture: attenuation by NMDA antagonists. *The Journal of Neuroscience,* 8**,** 185-196.

CHOTHIA, C. & JANIN, J. 1975. Principles of protein–protein recognition. *Nature,* 256**,** 705-708.

CHUNG, Y. H., JUN, H. S., SON, M., BAO, M., BAE, H. Y., KANG, Y. & YOON, J. W. 2000. Cellular and molecular mechanism for Kilham rat virus-induced autoimmune diabetes in DR-BB rats. *J Immunol,* 165**,** 2866-76.

CIECHANOVER, A., LASZLO, A., BERCOVICH, B., STANCOVSKI, I., ALKALAY, I., BEN-NERIAH, Y. & ORIAN, A. 1995. The ubiquitin-mediated proteolytic system: involvement of molecular chaperones, degradation of oncoproteins, and activation of transcriptional regulators. *Cold Spring Harb Symp Quant Biol,* 60**,** 491-501.

CLEMENT, A. M., NGUYEN, M. D., ROBERTS, E. A., GARCIA, M. L., BOILLÉE, S., RULE, M., MCMAHON, A. P., DOUCETTE, W., SIWEK, D., FERRANTE, R. J., BROWN, R. H., JR., JULIEN, J. P., GOLDSTEIN, L. S. & CLEVELAND, D. W. 2003. Wild-type nonneuronal cells extend survival of SOD1 mutant motor neurons in ALS mice. *Science,* 302**,** 113-7.

COOK, C. N., WU, Y., ODEH, H. M., GENDRON, T. F., JANSEN-WEST, K., DEL ROSSO, G., YUE, M., JIANG, P., GOMES, E., TONG, J., DAUGHRITY, L. M., AVENDANO, N. M., CASTANEDES-CASEY, M., SHAO, W., OSKARSSON, B., TOMASSY, G. S., MCCAMPBELL, A., RIGO, F., DICKSON, D. W., SHORTER, J., ZHANG, Y. J. & PETRUCELLI, L. 2020. C9orf72 poly(GR) aggregation induces TDP-43 proteinopathy. *Sci Transl Med,* 12.

CORCIA, P., TAUBER, C., VERCOULLIE, J., ARLICOT, N., PRUNIER, C., PRALINE, J., NICOLAS, G., VENEL, Y., HOMMET, C., BAULIEU, J.-L., COTTIER, J.-P., ROUSSEL, C., KASSIOU, M., GUILLOTEAU, D. & RIBEIRO, M.-J. 2012. Molecular imaging of microglial activation in amyotrophic lateral sclerosis. *PloS one,* 7**,** e52941-e52941.

CORRIGAN, C., SUBRAMANIAN, R. & MILLER, M. A. 2005. Eph and NMDA receptors control Ca2+/calmodulin-dependent protein kinase II activation during C. elegans oocyte meiotic maturation. *Development,* 132**,** 5225-37.

COSTELLO, J. L., CASTRO, I. G., HACKER, C., SCHRADER, T. A., METZ, J., ZEUSCHNER, D., AZADI, A. S., GODINHO, L. F., COSTINA, V., FINDEISEN, P., MANNER, A., ISLINGER, M. & SCHRADER, M. 2017a. ACBD5 and VAPB mediate membrane associations between peroxisomes and the ER. *The Journal of cell biology,* 216**,** 331-342.

COSTELLO, J. L., CASTRO, I. G., SCHRADER, T. A., ISLINGER, M. & SCHRADER, M. 2017b. Peroxisomal ACBD4 interacts with VAPB and promotes ER-peroxisome associations. *Cell cycle (Georgetown, Tex.),* 16**,** 1039-1045.

COURI, B. M., LENIS, A. T., BORAZJANI, A., PARAISO, M. F. R. & DAMASER, M. S. 2012. Animal models of female pelvic organ prolapse: lessons learned. *Expert review of obstetrics & gynecology,* 7**,** 249-260.

CRIPPA, V., CICARDI, M. E., RAMESH, N., SEGUIN, S. J., GANASSI, M., BIGI, I., DIACCI, C., ZELOTTI, E., BARATASHVILI, M., GREGORY, J. M., DOBSON, C. M., CEREDA, C., PANDEY, U. B., POLETTI, A. & CARRA, S. 2016. The chaperone HSPB8 reduces the accumulation of truncated TDP-43 species in cells and protects against TDP-43-mediated toxicity. *Hum Mol Genet,* 25**,** 3908-3924.

CUERVO, A. M. & DICE, J. F. 1996. A Receptor for the Selective Uptake and Degradation of Proteins by Lysosomes. *Science,* 273**,** 501-503.

CUNHA, C., SANTOS, C., GOMES, C., FERNANDES, A., CORREIA, A. M., SEBASTIÃO, A. M., VAZ, A. R. & BRITES, D. 2018. Downregulated Glia Interplay and Increased miRNA-155 as Promising Markers to Track ALS at an Early Stage. *Molecular Neurobiology,* 55**,** 4207-4224.

D'AMICO, E., GROSSO, G., NIEVES, J. W., ZANGHÌ, A., FACTOR-LITVAK, P. & MITSUMOTO, H. 2021. Metabolic Abnormalities, Dietary Risk Factors and Nutritional Management in Amyotrophic Lateral Sclerosis. *Nutrients,* 13.

DANTES, M. & MCCOMAS, A. 1991. The extent and time course of motoneuron involvement in amyotrophic lateral sclerosis. *Muscle & Nerve,* 14**,** 416-421.

DARBYSON, A. & NGSEE, J. K. 2016. Oxysterol-binding protein ORP3 rescues the Amyotrophic Lateral Sclerosis-linked mutant VAPB phenotype. *Experimental Cell Research,* 341**,** 18-31.

DAS SARMA, S., CHATTERJEE, K., DINDA, H., CHATTERJEE, D. & DAS SARMA, J. 2013. Cytomorphological and cytochemical identification of microglia. *International Scholarly Research Notices,* 2013.

DAVALOS, D., GRUTZENDLER, J., YANG, G., KIM, J. V., ZUO, Y., JUNG, S., LITTMAN, D. R., DUSTIN, M. L. & GAN, W.-B. 2005a. ATP mediates rapid microglial response to local brain injury in vivo. *Nature Neuroscience,* 8**,** 752-758.

DAVALOS, D., GRUTZENDLER, J., YANG, G., KIM, J. V., ZUO, Y., JUNG, S., LITTMAN, D. R., DUSTIN, M. L. & GAN, W. B. 2005b. ATP mediates rapid microglial response to local brain injury in vivo. *Nat Neurosci,* 8**,** 752-8.

DAVIDSON, Y., KELLEY, T., MACKENZIE, I. R., PICKERING-BROWN, S., DU PLESSIS, D., NEARY, D., SNOWDEN, J. S. & MANN, D. M. 2007. Ubiquitinated pathological lesions in frontotemporal lobar degeneration contain the TAR DNA-binding protein, TDP-43. *Acta Neuropathol,* 113**,** 521-33.

DE ALCÂNTARA, C., CRUZEIRO, M. M., FRANÇA, M. C., CAMARGOS, S. T. & DE SOUZA, L. C. 2019. Amyotrophic lateral sclerosis type 8 is not a pure motor disease: evidence from a neuropsychological and behavioural study. *Journal of Neurology,* 266**,** 1980-1987.

DE BRITO, O. M. & SCORRANO, L. 2008. Mitofusin 2 tethers endoplasmic reticulum to mitochondria. *Nature,* 456**,** 605-610.

DE CARVALHO, M., DENGLER, R., EISEN, A., ENGLAND, J. D., KAJI, R., KIMURA, J., MILLS, K., MITSUMOTO, H., NODERA, H., SHEFNER, J. & SWASH, M. 2008. Electrodiagnostic criteria for diagnosis of ALS. *Clinical Neurophysiology,* 119**,** 497-503.

DE VOS, K. J., MÓROTZ, G. M., STOICA, R., TUDOR, E. L., LAU, K.-F., ACKERLEY, S., WARLEY, A., SHAW, C. E. & MILLER, C. C. J. 2012. VAPB interacts with the mitochondrial protein PTPIP51 to regulate calcium homeostasis. *Human molecular genetics,* 21**,** 1299-1311.

DEIDDA, I., GALIZZI, G., PASSANTINO, R., CASCIO, C., RUSSO, D., COLLETTI, T., LA BELLA, V. & GUARNERI, P. 2014. Expression of vesicle-associated membrane-protein-associated protein B cleavage products in peripheral blood leukocytes and cerebrospinal fluid of patients with sporadic amyotrophic lateral sclerosis. *European Journal of Neurology,* 21**,** 478-485.

DEJESUS-HERNANDEZ, M., MACKENZIE, I. R., BOEVE, B. F., BOXER, A. L., BAKER, M., RUTHERFORD, N. J., NICHOLSON, A. M., FINCH, N. A., FLYNN, H., ADAMSON, J., KOURI, N., WOJTAS, A., SENGDY, P., HSIUNG, G.-Y. R., KARYDAS, A., SEELEY, W. W., JOSEPHS, K. A., COPPOLA, G., GESCHWIND, D. H., WSZOLEK, Z. K., FELDMAN, H., KNOPMAN, D. S., PETERSEN, R. C., MILLER, B. L., DICKSON, D. W., BOYLAN, K. B., GRAFF-RADFORD, N. R. & RADEMAKERS, R. 2011. Expanded GGGGCC hexanucleotide repeat in noncoding region of C9ORF72 causes chromosome 9p-linked FTD and ALS. *Neuron,* 72**,** 245-256.

DEMURO, A., MINA, E., KAYED, R., MILTON, S. C., PARKER, I. & GLABE, C. G. 2005. Calcium dysregulation and membrane disruption as a ubiquitous neurotoxic mechanism of soluble amyloid oligomers. *J Biol Chem,* 280**,** 17294-300.

DENG, J., YANG, M., CHEN, Y., CHEN, X., LIU, J., SUN, S., CHENG, H., LI, Y., BIGIO, E. H., MESULAM, M., XU, Q., DU, S., FUSHIMI, K., ZHU, L. & WU, J. Y. 2015. FUS Interacts with HSP60 to Promote Mitochondrial Damage. *PLOS Genetics,* 11**,** e1005357.

DESPORT, J. C., PREUX, P. M., TRUONG, T. C., VALLAT, J. M., SAUTEREAU, D. & COURATIER, P. 1999. Nutritional status is a prognostic factor for survival in ALS patients. *Neurology,* 53**,** 1059-63.

DI GIORGIO, F. P., CARRASCO, M. A., SIAO, M. C., MANIATIS, T. & EGGAN, K. 2007. Non-cell autonomous effect of glia on motor neurons in an embryonic stem cell-based ALS model. *Nature neuroscience,* 10**,** 608-614.

DI, L., CHEN, H., DA, Y., WANG, S. & SHEN, X.-M. 2016. Atypical familial amyotrophic lateral sclerosis with initial symptoms of pain or tremor in a Chinese family harboring VAPB-P56S mutation. *Journal of Neurology,* 263**,** 263-268.

DI MATTIA, T., WILHELM, L. P., IKHLEF, S., WENDLING, C., SPEHNER, D., NOMINÉ, Y., GIORDANO, F., MATHELIN, C., DRIN, G., TOMASETTO, C. & ALPY, F. 2018. Identification of MOSPD2, a novel scaffold for endoplasmic reticulum membrane contact sites. *EMBO reports,* 19**,** e45453.

DÍAZ-AMARILLA, P., OLIVERA-BRAVO, S., TRIAS, E., CRAGNOLINI, A., MARTÍNEZ-PALMA, L., CASSINA, P., BECKMAN, J. & BARBEITO, L. 2011. Phenotypically aberrant astrocytes that promote motoneuron damage in a model of inherited amyotrophic lateral sclerosis. *Proceedings of the National Academy of Sciences,* 108**,** 18126-18131.

DOLS-ICARDO, O., MONTAL, V., SIRISI, S., LÓPEZ-PERNAS, G., CERVERA-CARLES, L., QUEROL-VILASECA, M., MUÑOZ, L., BELBIN, O., ALCOLEA, D., MOLINA-PORCEL, L., PEGUEROLES, J., TURÓN-SANS, J., BLESA, R., LLEÓ, A., FORTEA, J., ROJAS-GARCÍA, R. & CLARIMÓN, J. 2020. Motor cortex transcriptome reveals microglial key events in

amyotrophic lateral sclerosis. *Neurology - Neuroimmunology Neuroinflammation,* 7**,** e829.

DONG, R., SAHEKI, Y., SWARUP, S., LUCAST, L., HARPER, J. W. & DE CAMILLI, P. 2016. Endosome-ER Contacts Control Actin Nucleation and Retromer Function through VAP-Dependent Regulation of PI4P. *Cell,* 166**,** 408-423.

DONG, W., MA, Y., GUAN, F., ZHANG, X., CHEN, W., ZHANG, L. & ZHANG, L. 2021. Ablation of C9orf72 together with excitotoxicity induces ALS in rats. *The FEBS Journal,* 288**,** 1712-1723.

DONG, W., ZHANG, L., SUN, C., GAO, X., GUAN, F., LI, J., CHEN, W., MA, Y. & ZHANG, L. 2020. Knock in of a hexanucleotide repeat expansion in the C9orf72 gene induces ALS in rats. *Animal Models and Experimental Medicine,* 3**,** 237-244.

DORMANN, D., RODDE, R., EDBAUER, D., BENTMANN, E., FISCHER, I., HRUSCHA, A., THAN, M. E., MACKENZIE, I. R., CAPELL, A. & SCHMID, B. 2010. ALS-associated fused in sarcoma (FUS) mutations disrupt Transportin-mediated nuclear import. *The EMBO journal,* 29**,** 2841-2857.

DUAN, W., LI, X., SHI, J., GUO, Y., LI, Z. & LI, C. 2010. Mutant TAR DNA-binding protein-43 induces oxidative injury in motor neuron-like cell. *Neuroscience,* 169**,** 1621-1629.

DUCHENNE DE BOULOGNE, G. 1851. Recherches électro-physiologiques et thérapeutiques. *Comp Rend Seances Acad Sci,* 32**,** 506.

DUDEK, J., BENEDIX, J., CAPPEL, S., GREINER, M., JALAL, C., MÜLLER, L. & ZIMMERMANN, R. 2009. Functions and pathologies of BiP and its interaction partners. *Cellular and Molecular Life Sciences,* 66**,** 1556-1569.

EDEN, E. R., SANCHEZ-HERAS, E., TSAPARA, A., SOBOTA, A., LEVINE, T. P. & FUTTER, C. E. 2016. Annexin A1 Tethers Membrane Contact Sites that Mediate ER to Endosome Cholesterol Transport. *Developmental cell,* 37**,** 473-483.

EHRLICH, P. 1885. Das sauerstoff-bedurfnis des organismus. *Eine farbenanalytische studie*.

ELLERMAN, K. E., RICHARDS, C. A., GUBERSKI, D. L., SHEK, W. R. & LIKE, A. A. 1996. Kilham Rat Virus Triggers T-Cell–Dependent Autoimmune Diabetes in Multiple Strains of Rat. *Diabetes,* 45**,** 557-562.

ENG, L. F. & GHIRNIKAR, R. S. 1994. GFAP and Astrogliosis. *Brain Pathology,* 4**,** 229-237.

FAGAN, A. M., BU, G., SUN, Y., DAUGHERTY, A. & HOLTZMAN, D. M. 1996. Apolipoprotein E-containing high density lipoprotein promotes neurite outgrowth and is a ligand for the low density lipoprotein receptor-related protein. *J Biol Chem,* 271**,** 30121-5.

FALLINI, C., ZHANG, H., SU, Y., SILANI, V., SINGER, R. H., ROSSOLL, W. & BASSELL, G. J. 2011. The survival of motor neuron (SMN) protein interacts with the mRNA-binding protein HuD and regulates localization of poly (A) mRNA in primary motor neuron axons. *Journal of Neuroscience,* 31**,** 3914-3925.

FANG, C., BOURDETTE, D. & BANKER, G. 2012. Oxidative stress inhibits axonal transport: implications for neurodegenerative diseases. *Molecular Neurodegeneration,* 7**,** 29.

FEENEY, S. J., MCKELVIE, P. A., AUSTIN, L., JEAN-FRANCOIS, M. J., KAPSA, R., TOMBS, S. M. & BYRNE, E. 2001. Presymptomatic motor neuron loss and reactive astrocytosis in the SOD1 mouse model of amyotrophic lateral sclerosis. *Muscle Nerve,* 24**,** 1510-9.

FELIX, J. P., NASCIMENTO, H. A. D. D., GUIMARÃES, N. N., PIRES, E. D. O., FONSECA, A. U. D. & VIEIRA, G. D. S. Automatic Classification of Amyotrophic Lateral Sclerosis through Gait Dynamics. 2021 IEEE 45th Annual Computers, Software, and Applications Conference (COMPSAC), 12-16 July 2021 2021. 1942-1947.

FENN, A. M., HALL, J. C. E., GENSEL, J. C., POPOVICH, P. G. & GODBOUT, J. P. 2014. IL-4 Signaling Drives a Unique Arginase⁺/IL-1β⁺ Microglia Phenotype and Recruits Macrophages to the Inflammatory CNS: Consequences of Age-Related Deficits in IL-4Rα after Traumatic Spinal Cord Injury. *The Journal of Neuroscience,* 34**,** 8904-8917.

FERRANTE, R. J., BROWNE, S. E., SHINOBU, L. A., BOWLING, A. C., BAIK, M. J., MACGARVEY, U., KOWALL, N. W., BROWN JR., R. H. & BEAL, M. F. 1997. Evidence of Increased Oxidative Damage in Both Sporadic and Familial Amyotrophic Lateral Sclerosis. *Journal of Neurochemistry,* 69**,** 2064-2074.

FERREIRA-NUÑO, A., MORALES-OTAL, A., PAREDES, R. G. & VELÁZQUEZ-MOCTEZUMA, J. 2005. Sexual behavior of female rats in a multiple-partner preference test. *Hormones and Behavior,* 47**,** 290-296.

FERRUCCI, M., LAZZERI, G., FLAIBANI, M., BIAGIONI, F., CANTINI, F., MADONNA, M., BUCCI, D., LIMANAQI, F., SOLDANI, P. & FORNAI, F. 2018. In search for a gold-standard procedure to count motor neurons in the spinal cord. *Histol Histopathol,* 33**,** 1021-1046.

FINKEL, R. S., MCDERMOTT, M. P., KAUFMANN, P., DARRAS, B. T., CHUNG, W. K., SPROULE, D. M., KANG, P. B., FOLEY, A. R., YANG, M. L. & MARTENS, W. B. 2014. Observational study of spinal muscular atrophy type I and implications for clinical trials. *Neurology,* 83**,** 810-817.

FLEMING, J. C., NORENBERG, M. D., RAMSAY, D. A., DEKABAN, G. A., MARCILLO, A. E., SAENZ, A. D., PASQUALE-STYLES, M., DIETRICH, W. D. & WEAVER, L. C. 2006. The cellular inflammatory response in human spinal cords after injury. *Brain,* 129**,** 3249-3269.

FLOREA, S. M. & BLATTER, L. A. 2008. The effect of oxidative stress on Ca2+ release and capacitative Ca2+ entry in vascular endothelial cells. *Cell Calcium,* 43**,** 405-415.

FOSTER, L. J., WEIR, M. L., LIM, D. Y., LIU, Z., TRIMBLE, W. S. & KLIP, A. 2000. A Functional Role for VAP-33 in Insulin-Stimulated GLUT4 Traffic. *Traffic,* 1**,** 512-521.

FRAIWAN, L. & HASSANIN, O. 2021. Computer-aided identification of degenerative neuromuscular diseases based on gait dynamics and ensemble decision tree classifiers. *PLOS ONE,* 16**,** e0252380.

FRANCIS, C., NATARAJAN, S., LEE, M. T., KHALADKAR, M., BUCKLEY, P. T., SUL, J. Y., EBERWINE, J. & KIM, J. 2014. Divergence of RNA localization between rat and mouse neurons reveals the potential for rapid brain evolution. *BMC Genomics,* 15**,** 883.

FRANCO, A., KITSIS, R. N., FLEISCHER, J. A., GAVATHIOTIS, E., KORNFELD, O. S., GONG, G., BIRIS, N., BENZ, A., QVIT, N., DONNELLY, S. K., CHEN, Y., MENNERICK, S., HODGSON, L., MOCHLY-ROSEN, D. & DORN, G. W. 2016. Correcting mitochondrial fusion by manipulating mitofusin conformations. *Nature,* 540**,** 74-79.

FRATTA, P., SIVAKUMAR, P., HUMPHREY, J., LO, K., RICKETTS, T., OLIVEIRA, H., BRITO-ARMAS, J. M., KALMAR, B., ULE, A., YU, Y., BIRSA, N., BODO, C., COLLINS, T., CONICELLA, A. E., MEJIA MAZA, A., MARRERO-GAGLIARDI, A., STEWART, M., MIANNE, J., CORROCHANO, S., EMMETT, W., CODNER, G., GROVES, M., FUKUMURA, R., GONDO, Y., LYTHGOE, M., PAUWS, E., PESKETT, E., STANIER, P., TEBOUL, L., HALLEGGER, M., CALVO, A., CHIÒ, A., ISAACS, A. M., FAWZI, N. L., WANG, E., HOUSMAN, D. E., BARALLE, F., GREENSMITH, L., BURATTI, E., PLAGNOL, V., FISHER, E. M. & ACEVEDO-AROZENA, A. 2018. Mice with endogenous TDP-43 mutations exhibit gain of splicing function and characteristics of amyotrophic lateral sclerosis. *The EMBO Journal,* 37**,** e98684.

FRIDOVICH, I. 1986. Superoxide dismutases. *Adv Enzymol Relat Areas Mol Biol,* 58**,** 61-97.

FUJII, R. & TAKUMI, T. 2005. TLS facilitates transport of mRNA encoding an actin-stabilizing protein to dendritic spines. *Journal of cell science,* 118**,** 5755-5765.

FUNIKOV, S. Y., REZVYKH, A. P., MAZIN, P. V., MOROZOV, A. V., MALTSEV, A. V., CHICHEVA, M. M., VIKHAREVA, E. A., EVGEN'EV, M. B. & USTYUGOV, A. A. 2018. FUS(1-359) transgenic mice as a model of ALS: pathophysiological and molecular aspects of the proteinopathy. *neurogenetics,* 19**,** 189-204.

FUNKE, A. D., ESSER, M., KRÜTTGEN, A., WEIS, J., MITNE-NETO, M., LAZAR, M., NISHIMURA, A. L., SPERFELD, A. D., TRILLENBERG, P., SENDEREK, J., KRASNIANSKI, M., ZATZ, M., ZIERZ, S. & DESCHAUER, M. 2010. The p.P56S mutation in the VAPB gene is not due to a single founder: the first European case. *Clinical Genetics,* 77**,** 302-303.

FURUITA, K., JEE, J., FUKADA, H., MISHIMA, M. & KOJIMA, C. 2010. Electrostatic Interaction between Oxysterol-binding Protein and VAMP-associated Protein A Revealed by NMR and Mutagenesis Studies. *The Journal of Biological Chemistry,* 285**,** 12961-12970.

G.M., C. 2000. *The Cell: A Molecular Approach,* Sunderland (MA), Sinauer Associates.

GAMBERINO, W. C., BERKICH, D. A., LYNCH, C. J., XU, B. & LANOUE, K. F. 1997. Role of Pyruvate Carboxylase in Facilitation of Synthesis of Glutamate and Glutamine in Cultured Astrocytes. *Journal of Neurochemistry,* 69**,** 2312-2325.

GENEVINI, P., COLOMBO, M. N., VENDITTI, R., MARCUZZO, S., COLOMBO, S. F., BERNASCONI, P., DE MATTEIS, M. A., BORGESE, N. & NAVONE, F. 2019. VAPB depletion alters neuritogenesis and phosphoinositide balance in motoneuron-like cells: relevance to VAPB-linked ALS. *Journal of Cell Science***,** jcs.220061.

GERBER, Y. N., SABOURIN, J.-C., RABANO, M., VIVANCO, M. D. M. & PERRIN, F. E. 2012. Early functional deficit and microglial disturbances in a mouse model of amyotrophic lateral sclerosis. *PloS one,* 7**,** e36000-e36000.

GHASEMI, M. & BROWN, R. H., JR. 2018. Genetics of Amyotrophic Lateral Sclerosis. *Cold Spring Harb Perspect Med,* 8.

GIJSELINCK, I., VAN LANGENHOVE, T., VAN DER ZEE, J., SLEEGERS, K., PHILTJENS, S., KLEINBERGER, G., JANSSENS, J., BETTENS, K., VAN CAUWENBERGHE, C. & PERESON, S. 2012. A C9orf72 promoter repeat expansion in a Flanders-Belgian cohort with disorders of the frontotemporal lobar degeneration-amyotrophic lateral sclerosis spectrum: a gene identification study. *The Lancet Neurology,* 11**,** 54-65.

GKOGKAS, C., MIDDLETON, S., KREMER, A. M., WARDROPE, C., HANNAH, M., GILLINGWATER, T. H. & SKEHEL, P. 2008. VAPB interacts with and modulates the activity of ATF6. *Human Molecular Genetics,* 17**,** 1517-1526.

GKOGKAS, C., WARDROPE, C., HANNAH, M. & SKEHEL, P. 2011. The ALS8-associated mutant VAPBP56S is resistant to proteolysis in neurons. *Journal of Neurochemistry,* 117**,** 286-294.

GLANCY, B., WILLIS, W. T., CHESS, D. J. & BALABAN, R. S. 2013. Effect of calcium on the oxidative phosphorylation cascade in skeletal muscle mitochondria. *Biochemistry,* 52**,** 2793-2809.

GOLDFARB, B. J. & SIMON, S. R. 1984. Gait patterns in patients with amyotrophic lateral sclerosis. *Arch Phys Med Rehabil,* 65**,** 61-5.

GOLTZSCH, W. & CLAUSS, T. 1990. [Age-dependent reproductive performance of Shoe:WIST rats]. *Zeitschrift fur Versuchstierkunde,* 33**,** 137-139.

GOMES-TROLIN, C., NYGREN, I., AQUILONIUS, S. M. & ASKMARK, H. 2002. Increased red blood cell polyamines in ALS and Parkinson's disease. *Exp Neurol,* 177**,** 515-20.

GOMEZ-SUAGA, P., PAILLUSSON, S. & MILLER, C. C. J. 2017a. ER-mitochondria signaling regulates autophagy. *Autophagy,* 13**,** 1250-1251.

GOMEZ-SUAGA, P., PAILLUSSON, S., STOICA, R., NOBLE, W., HANGER, D. P. & MILLER, C. C. J. 2017b. The ER-Mitochondria Tethering Complex VAPB-PTPIP51 Regulates Autophagy. *Current biology : CB,* 27**,** 371-385.

GÓMEZ-SUAGA, P., PÉREZ-NIEVAS, B. G., GLENNON, E. B., LAU, D. H. W., PAILLUSSON, S., MÓROTZ, G. M., CALÌ, T., PIZZO, P., NOBLE, W. & MILLER, C. C. J. 2019. The VAPB-PTPIP51 endoplasmic reticulum-mitochondria tethering proteins are present in neuronal synapses and regulate synaptic activity. *Acta Neuropathologica Communications,* 7**,** 35.

GOTTIPATI, M. K., KALININA, I., BEKYAROVA, E., HADDON, R. C. & PARPURA, V. 2012. Chemically Functionalized Water-Soluble Single-Walled Carbon Nanotubes Modulate Morpho-Functional Characteristics of Astrocytes. *Nano Letters,* 12**,** 4742-4747.

GOULD, R. G., TAYLOR, C. B., HAGGERMAN, J., WARNER, I. & CAMPBELL, D. J. 1953. Cholesterol metabolism. 1. Effect of dietary cholesterol on the synthesis of cholesterol in dog tissue in vitro. *Journal of Biological Chemistry,* 201**,** 519-528.

GOWING, G., PHILIPS, T., VAN WIJMEERSCH, B., AUDET, J.-N., DEWIL, M., VAN DEN BOSCH, L., BILLIAU, A. D., ROBBERECHT, W. & JULIEN, J.-P. 2008. Ablation of proliferating microglia does not affect motor neuron degeneration in amyotrophic lateral sclerosis caused by mutant superoxide dismutase. *The Journal of neuroscience : the official journal of the Society for Neuroscience,* 28**,** 10234-10244.

GRAFFMO, K. S., FORSBERG, K., BERGH, J., BIRVE, A., ZETTERSTRÖM, P., ANDERSEN, P. M., MARKLUND, S. L. & BRÄNNSTRÖM, T. 2012. Expression of wild-type human superoxide dismutase-1 in mice causes amyotrophic lateral sclerosis. *Human Molecular Genetics,* 22**,** 51-60.

GRECO, A., CHIESA, M. R., DA PRATO, I., ROMANELLI, A. M., DOLCIOTTI, C., CAVALLINI, G., MASCIANDARO, S. M., SCILINGO, E. P., DEL CARRATORE, R. & BONGIOANNI, P. 2021. Using blood data for the differential diagnosis and prognosis of motor neuron diseases: a new dataset for machine learning applications. *Scientific Reports,* 11**,** 3371.

GRIFFITHS, W. J., ABDEL-KHALIK, J., MOORE, S. F., WIJEYEKOON, R. S., CRICK, P. J., YUTUC, E., FARRELL, K., BREEN, D. P., WILLIAMS-GRAY, C. H., THEOFILOPOULOS, S., ARENAS, E., TRUPP, M., BARKER, R. A. & WANG, Y. 2021. The Cerebrospinal Fluid Profile of Cholesterol Metabolites in Parkinson's Disease and Their Association With Disease State and Clinical Features. *Front Aging Neurosci,* 13**,** 685594.

GRODZKI, A. C. & BERENSTEIN, E. 2010. Antibody Purification: Ammonium Sulfate Fractionation or Gel Filtration. *In:* OLIVER, C. & JAMUR, M. C. (eds.) *Immunocytochemical Methods and Protocols.* Totowa, NJ: Humana Press.

GRUNDKE-IQBAL, I., IQBAL, K., TUNG, Y., QUINLAN, M., WISNIEWSKI, H. & BINDER, L. 1987. Abnormal phosphorylation of the microtubule-associated protein?(tau) in Alzheimer cytoskeletal pathology. *Alzheimer Disease & Associated Disorders,* 1**,** 202.

GRUNSEICH, C. & FISCHBECK, K. H. 2015. Spinal and Bulbar Muscular Atrophy. *Neurologic clinics,* 33**,** 847-854.

GRUPE, M., MYERS, G., PENNER, R. & FLEIG, A. 2010. Activation of store-operated I(CRAC) by hydrogen peroxide. *Cell calcium,* 48**,** 1-9.

GRUZMAN, A., WOOD, W. L., ALPERT, E., PRASAD, M. D., MILLER, R. G., ROTHSTEIN, J. D., BOWSER, R., HAMILTON, R., WOOD, T. D., CLEVELAND, D. W., LINGAPPA, V. R. & LIU, J. 2007. Common molecular signature in SOD1 for both sporadic and familial

amyotrophic lateral sclerosis. *Proceedings of the National Academy of Sciences,* 104**,** 12524-12529.

GUAN, K. & DIXON, J. E. 1991. Eukaryotic proteins expressed in Escherichia coli: An improved thrombin cleavage and purification procedure of fusion proteins with glutathione S-transferase. *Analytical Biochemistry,* 192**,** 262-267.

GUBER, R. D., SCHINDLER, A. B., BUDRON, M. S., CHEN, K.-L., LI, Y., FISCHBECK, K. H. & GRUNSEICH, C. 2018. Nucleocytoplasmic transport defect in a North American patient with ALS8. *Annals of clinical and translational neurology,* 5**,** 369-375.

GUBERSKI, D. L., THOMAS, V. A., SHEK, W. R., LIKE, A. A., HANDLER, E. S., ROSSINI, A. A., WALLACE, J. E. & WELSH, R. M. 1991. Induction of Type I Diabetes by Kilham's Rat Virus in Diabetes-Resistant BB/Wor Rats. *Science,* 254**,** 1010-1013.

GUILLOT, S. J., BOLBOREA, M. & DUPUIS, L. 2021. Dysregulation of energy homeostasis in amyotrophic lateral sclerosis. *Curr Opin Neurol*.

GURNEY, M., PU, H., CHIU, A., DAL CANTO, M., POLCHOW, C., ALEXANDER, D., CALIENDO, J., HENTATI, A., KWON, Y., DENG, H. & ET, A. 1994a. Motor neuron degeneration in mice that express a human Cu,Zn superoxide dismutase mutation. *Science,* 264**,** 1772-1775.

GURNEY, M. E., PU, H., CHIU, A. Y., DAL CANTO, M. C., POLCHOW, C. Y., ALEXANDER, D. D., CALIENDO, J., HENTATI, A., KWON, Y. W., DENG, H. X. & ET AL. 1994b. Motor neuron degeneration in mice that express a human Cu,Zn superoxide dismutase mutation. *Science,* 264**,** 1772-5.

HAIDET-PHILLIPS, A. M., HESTER, M. E., MIRANDA, C. J., MEYER, K., BRAUN, L., FRAKES, A., SONG, S., LIKHITE, S., MURTHA, M. J., FOUST, K. D., RAO, M., EAGLE, A., KAMMESHEIDT, A., CHRISTENSEN, A., MENDELL, J. R., BURGHES, A. H. M. & KASPAR, B. K. 2011. Astrocytes from familial and sporadic ALS patients are toxic to motor neurons. *Nature biotechnology,* 29**,** 824-828.

HALBLEIB, K., PESEK, K., COVINO, R., HOFBAUER, H. F., WUNNICKE, D., HÄNELT, I., HUMMER, G. & ERNST, R. 2017. Activation of the Unfolded Protein Response by Lipid Bilayer Stress. *Molecular Cell,* 67**,** 673-684.e8.

HAMERS, F. P. T., KOOPMANS, G. C. & JOOSTEN, E. A. J. 2006. CatWalk-Assisted Gait Analysis in the Assessment of Spinal Cord Injury. *Journal of Neurotrauma,* 23**,** 537-548.

HAMERS, F. P. T., LANKHORST, A. J., VAN LAAR, T. J., VELDHUIS, W. B. & GISPEN, W. H. 2001. Automated Quantitative Gait Analysis During Overground Locomotion in the Rat: Its Application to Spinal Cord Contusion and Transection Injuries. *Journal of Neurotrauma,* 18**,** 187-201.

HAMMER, R. P., TOMIYASU, U. & SCHEIBEL, A. B. 1979. Degeneration of the human Betz cell due to amyotrophic lateral sclerosis. *Experimental Neurology,* 63**,** 336-346.

HAMMOND, T. R., DUFORT, C., DISSING-OLESEN, L., GIERA, S., YOUNG, A., WYSOKER, A., WALKER, A. J., GERGITS, F., SEGEL, M., NEMESH, J., MARSH, S. E., SAUNDERS, A., MACOSKO, E., GINHOUX, F., CHEN, J., FRANKLIN, R. J. M., PIAO, X., MCCARROLL, S. A. & STEVENS, B. 2019. Single-Cell RNA Sequencing of Microglia throughout the Mouse Lifespan and in the Injured Brain Reveals Complex Cell-State Changes. *Immunity,* 50**,** 253-271.e6.

HAMPTON, T. G. & AMENDE, I. 2009. Treadmill Gait Analysis Characterizes Gait Alterations in Parkinson's Disease and Amyotrophic Lateral Sclerosis Mouse Models. *Journal of Motor Behavior,* 42**,** 1-4.

HAN, S. M., EL OUSSINI, H., SCEKIC-ZAHIROVIC, J., VIBBERT, J., COTTEE, P., PRASAIN, J. K., BELLEN, H. J., DUPUIS, L. & MILLER, M. A. 2013. VAPB/ALS8 MSP ligands regulate

striated muscle energy metabolism critical for adult survival in caenorhabditis elegans. *PLoS genetics,* 9**,** e1003738-e1003738.

HAN, S. M., TSUDA, H., YANG, Y., VIBBERT, J., COTTEE, P., LEE, S.-J., WINEK, J., HAUETER, C., BELLEN, H. J. & MILLER, M. A. 2012. Secreted VAPB/ALS8 major sperm protein domains modulate mitochondrial localization and morphology via growth cone guidance receptors. *Developmental Cell,* 22**,** 348-362.

HANNAFORD, A., PAVEY, N., VAN DEN BOS, M., GEEVASINGA, N., MENON, P., SHEFNER, J. M., KIERNAN, M. C. & VUCIC, S. 2021. Diagnostic Utility of Gold Coast Criteria in Amyotrophic Lateral Sclerosis. *Annals of Neurology,* 89**,** 979-986.

HANNAH, M. F., BAJIC, V. B. & KLEIN, S. L. 2008. Sex differences in the recognition of and innate antiviral responses to Seoul virus in Norway rats. *Brain Behav Immun,* 22**,** 503-16.

HAREL, T., PEHLIVAN, D., CASKEY, C. T. & LUPSKI, J. R. 2015. Chapter 1 - Mendelian, Non-Mendelian, Multigenic Inheritance, and Epigenetics. *In:* ROSENBERG, R. N. & PASCUAL, J. M. (eds.) *Rosenberg's Molecular and Genetic Basis of Neurological and Psychiatric Disease (Fifth Edition).* Boston: Academic Press.

HARLOW, E. & LANE, D. 1988. A laboratory manual. *New York: Cold Spring Harbor Laboratory,* 579.

HATANAKA, Y., UMEDA, T., SHIGEMORI, K., TAKEUCHI, T., NAGAI, Y. & TOMIYAMA, T. 2022. C9orf72 Hexanucleotide Repeat Expansion-Related Neuropathology Is Attenuated by Nasal Rifampicin in Mice. *Biomedicines,* 10**,** 1080.

HATZIPETROS, T., BOGDANIK, L. P., TASSINARI, V. R., KIDD, J. D., MORENO, A. J., DAVIS, C., OSBORNE, M., AUSTIN, A., VIEIRA, F. G. & LUTZ, C. 2014. C57BL/6J congenic Prp-TDP43A315T mice develop progressive neurodegeneration in the myenteric plexus of the colon without exhibiting key features of ALS. *Brain research,* 1584**,** 59-72.

HAULCOMB, M. M., MEADOWS, R. M., MILLER, W. M., MCMILLAN, K. P., HILSMEYER, M. J., WANG, X., BEAULIEU, W. T., DICKINSON, S. L., BROWN, T. J., SANDERS, V. M. & JONES, K. J. 2017. Locomotor analysis identifies early compensatory changes during disease progression and subgroup classification in a mouse model of amyotrophic lateral sclerosis. *Neural Regen Res,* 12**,** 1664-1679.

HAUSDORFF, J. M., LERTRATANAKUL, A., CUDKOWICZ, M. E., PETERSON, A. L., KALITON, D. & GOLDBERGER, A. L. 2000. Dynamic markers of altered gait rhythm in amyotrophic lateral sclerosis. *Journal of Applied Physiology,* 88**,** 2045-2053.

HAYAKAWA, K., PHAM, L.-D. D., ARAI, K. & LO, E. H. 2014. Reactive astrocytes promote adhesive interactions between brain endothelium and endothelial progenitor cells via HMGB1 and beta-2 integrin signaling. *Stem Cell Research,* 12**,** 531-538.

HEFFERNAN, C., JENKINSON, C., HOLMES, T., FEDER, G., KUPFER, R., LEIGH, P. N., MCGOWAN, S., RIO, A. & SIDHU, P. 2004. Nutritional management in MND/ALS patients: an evidence based review. *Amyotroph Lateral Scler Other Motor Neuron Disord,* 5**,** 72-83.

HEID, M. E., KEYEL, P. A., KAMGA, C., SHIVA, S., WATKINS, S. C. & SALTER, R. D. 2013. Mitochondrial Reactive Oxygen Species Induces NLRP3-Dependent Lysosomal Damage and Inflammasome Activation. *The Journal of Immunology,* 191**,** 5230-5238.

HENKEL, J. S., BEERS, D. R., WEN, S., RIVERA, A. L., TOENNIS, K. M., APPEL, J. E., ZHAO, W., MOORE, D. H., POWELL, S. Z. & APPEL, S. H. 2013. Regulatory T-lymphocytes mediate amyotrophic lateral sclerosis progression and survival. *EMBO Molecular Medicine,* 5**,** 64-79.

HENKEL, J. S., ENGELHARDT, J. I., SIKLÓS, L., SIMPSON, E. P., KIM, S. H., PAN, T., GOODMAN, J. C., SIDDIQUE, T., BEERS, D. R. & APPEL, S. H. 2004. Presence of dendritic cells, MCP-1, and activated microglia/macrophages in amyotrophic lateral sclerosis spinal cord tissue. *Ann Neurol,* 55**,** 221-35.

HERST, P. M. & BERRIDGE, M. V. 2007. Cell surface oxygen consumption: A major contributor to cellular oxygen consumption in glycolytic cancer cell lines. *Biochimica et Biophysica Acta (BBA) - Bioenergetics,* 1767**,** 170-177.

HERTZ, L. & HERTZ, E. 2003. Cataplerotic TCA cycle flux determined as glutamate-sustained oxygen consumption in primary cultures of astrocytes. *Neurochemistry International,* 43**,** 355-361.

HERTZ, L. & ROTHMAN, D. L. 2016. Glucose, lactate, β-hydroxybutyrate, acetate, GABA, and succinate as substrates for synthesis of glutamate and GABA in the glutamine–glutamate/GABA cycle. *The Glutamate/GABA-Glutamine Cycle.* Springer.

HO, R., WORKMAN, M. J., MATHKAR, P., WU, K., KIM, K. J., O'ROURKE, J. G., KELLOGG, M., MONTEL, V., BANUELOS, M. G., AROGUNDADE, O. A., DIAZ-GARCIA, S., OHEB, D., HUANG, S., KHREBTUKOVA, I., WATSON, L., RAVITS, J., TAYLOR, K., BALOH, R. H. & SVENDSEN, C. N. 2021. Cross-Comparison of Human iPSC Motor Neuron Models of Familial and Sporadic ALS Reveals Early and Convergent Transcriptomic Disease Signatures. *Cell Syst,* 12**,** 159-175.e9.

HOLM, T., MAIER, A., WICKS, P., LANG, D., LINKE, P., MÜNCH, C., STEINFURTH, L., MEYER, R. & MEYER, T. 2013. Severe loss of appetite in amyotrophic lateral sclerosis patients: online self-assessment study. *Interact J Med Res,* 2**,** e8.

HONDA, D., ISHIGAKI, S., IGUCHI, Y., FUJIOKA, Y., UDAGAWA, T., MASUDA, A., OHNO, K., KATSUNO, M. & SOBUE, G. 2013. The ALS/FTLD-related RNA-binding proteins TDP-43 and FUS have common downstream RNA targets in cortical neurons. *FEBS open bio,* 4**,** 1-10.

HONG, K., LI, Y., DUAN, W., GUO, Y., JIANG, H., LI, W. & LI, C. 2012. Full-length TDP-43 and its C-terminal fragments activate mitophagy in NSC34 cell line. *Neuroscience Letters,* 530**,** 144-149.

HOUSER, C. R., BARBER, R. P., CRAWFORD, G. D., MATTHEWS, D. A., PHELPS, P. E., SALVATERRA, P. M. & VAUGHN, J. E. 1984. Species-specific second antibodies reduce spurious staining in immunocytochemistry. *Journal of Histochemistry & Cytochemistry,* 32**,** 395-402.

HOWLAND, D. S., LIU, J., SHE, Y., GOAD, B., MARAGAKIS, N. J., KIM, B., ERICKSON, J., KULIK, J., DEVITO, L., PSALTIS, G., DEGENNARO, L. J., CLEVELAND, D. W. & ROTHSTEIN, J. D. 2002. Focal loss of the glutamate transporter EAAT2 in a transgenic rat model of SOD1 mutant-mediated amyotrophic lateral sclerosis (ALS). *Proceedings of the National Academy of Sciences of the United States of America,* 99**,** 1604-1609.

HUANG, C., TONG, J., BI, F., ZHOU, H. & XIA, X. G. 2012. Mutant TDP-43 in motor neurons promotes the onset and progression of ALS in rats. *J Clin Invest,* 122**,** 107-18.

HUANG, S.-L., WU, L.-S., LEE, M., CHANG, C.-W., CHENG, W.-C., FANG, Y.-S., CHEN, Y.-R., CHENG, P.-L. & SHEN, C.-K. J. 2020. A robust TDP-43 knock-in mouse model of ALS. *Acta Neuropathologica Communications,* 8**,** 3.

HUDSON, A. J. 1981. Amyotrophic lateral sclerosis and its association with dementia, parkinsonism and other neurological disorders: a review. *Brain,* 104**,** 217-47.

IANGONE, J. J. 1982. Protein A of Staphylococcus uureus and Related lrnmunog lobul in Receptors Produced by Streptococci and Pneumonococci. *In:* DIXON, F. J. & KUNKEL, H. G. (eds.) *Advances in Immunology.* Academic Press.

IGUCHI, Y., KATSUNO, M., NIWA, J.-I., TAKAGI, S., ISHIGAKI, S., IKENAKA, K., KAWAI, K., WATANABE, H., YAMANAKA, K. & TAKAHASHI, R. 2013. Loss of TDP-43 causes age-dependent progressive motor neuron degeneration. *Brain,* 136**,** 1371-1382.

IKEMOTO, A., NAKAMURA, S., AKIGUCHI, I. & HIRANO, A. 2002. Differential expression between synaptic vesicle proteins and presynaptic plasma membrane proteins in the anterior horn of amyotrophic lateral sclerosis. *Acta Neuropathologica,* 103**,** 179-187.

ILIEVA, E. V., AYALA, V., JOVÉ, M., DALFÓ, E., CACABELOS, D., POVEDANO, M., BELLMUNT, M. J., FERRER, I., PAMPLONA, R. & PORTERO-OTÍN, M. 2007. Oxidative and endoplasmic reticulum stress interplay in sporadic amyotrophic lateral sclerosis. *Brain,* 130**,** 3111-3123.

IOANNIDES, Z. A., NGO, S. T., HENDERSON, R. D., MCCOMBE, P. A. & STEYN, F. J. 2017. Hypermetabolism in motor neurone disease is associated with a greater functional decline but not weight loss. *Journal of Neurology, Neurosurgery & Psychiatry,* 88**,** e1-e1.

IOANNOU, M. S., JACKSON, J., SHEU, S.-H., CHANG, C.-L., WEIGEL, A. V., LIU, H., PASOLLI, H. A., XU, C. S., PANG, S. & HESS, H. F. 2018. Neuron-astrocyte metabolic coupling during neuronal stimulation protects against fatty acid toxicity. *Biorxiv***,** 465237.

ITALIANO, J. E., ROBERTS, T. M., STEWART, M. & FONTANA, C. A. 1996. Reconstitution In Vitro of the Motile Apparatus from the Amoeboid Sperm of Ascaris Shows That Filament Assembly and Bundling Move Membranes. *Cell,* 84**,** 105-114.

JACK, G. W. 1994. Immunoaffinity chromatography. *Molecular Biotechnology,* 1**,** 59-86.

JAKOBSDOTTIR, G., XU, J., MOLIN, G., AHRNÉ, S. & NYMAN, M. 2013. High-fat diet reduces the formation of butyrate, but increases succinate, inflammation, liver fat and cholesterol in rats, while dietary fibre counteracts these effects. *PLoS One,* 8**,** e80476.

JAKOBY, P., SCHMIDT, E., RUMINOT, I., GUTIÉRREZ, R., BARROS, L. F. & DEITMER, J. W. 2012. Higher Transport and Metabolism of Glucose in Astrocytes Compared with Neurons: A Multiphoton Study of Hippocampal and Cerebellar Tissue Slices. *Cerebral Cortex,* 24**,** 222-231.

JAMES, C. & KEHLENBACH, R. H. 2021. The Interactome of the VAP Family of Proteins: An Overview. *Cells,* 10**,** 1780.

JAMES, C., LENZ, C., URLAUB, H. & KEHLENBACH, R. H. 2021. Sequestosome 1 Is Part of the Interaction Network of VAPB. *Int J Mol Sci,* 22.

JANSEN, M., OHSAKI, Y., REGA, L. R., BITTMAN, R., OLKKONEN, V. M. & IKONEN, E. 2011. Role of ORPs in sterol transport from plasma membrane to ER and lipid droplets in mammalian cells. *Traffic,* 12**,** 218-31.

JIANG, J., ZHU, Q., GENDRON, T. F., SABERI, S., MCALONIS-DOWNES, M., SEELMAN, A., STAUFFER, J. E., JAFAR-NEJAD, P., DRENNER, K. & SCHULTE, D. 2016. Gain of toxicity from ALS/FTD-linked repeat expansions in C9ORF72 is alleviated by antisense oligonucleotides targeting GGGGCC-containing RNAs. *Neuron,* 90**,** 535-550.

JIN, M., GÜNTHER, R., AKGÜN, K., HERMANN, A. & ZIEMSSEN, T. 2020. Peripheral proinflammatory Th1/Th17 immune cell shift is linked to disease severity in amyotrophic lateral sclerosis. *Scientific Reports,* 10**,** 5941.

JOHNSON, B. S., MCCAFFERY, J. M., LINDQUIST, S. & GITLER, A. D. 2008. A yeast TDP-43 proteinopathy model: Exploring the molecular determinants of TDP-43 aggregation

and cellular toxicity. *Proceedings of the National Academy of Sciences of the United States of America,* 105**,** 6439-6444.

JOHNSON, D. T., HARRIS, R. A., BLAIR, P. V. & BALABAN, R. S. 2007a. Functional consequences of mitochondrial proteome heterogeneity. *American Journal of Physiology-Cell Physiology,* 292**,** C698-C707.

JOHNSON, D. T., HARRIS, R. A., FRENCH, S., BLAIR, P. V., YOU, J., BEMIS, K. G., WANG, M. & BALABAN, R. S. 2007b. Tissue heterogeneity of the mammalian mitochondrial proteome. *American Journal of Physiology-Cell Physiology,* 292**,** C689-C697.

JONAS, R. A., YUAN, T.-F., LIANG, Y.-X., JONAS, J. B., TAY, D. K. C. & ELLIS-BEHNKE, R. G. 2012. The spider effect: morphological and orienting classification of microglia in response to stimuli in vivo. *PloS one,* 7**,** e30763-e30763.

JUNG, C., HIGGINS, C. M. J. & XU, Z. 2002. Mitochondrial electron transport chain complex dysfunction in a transgenic mouse model for amyotrophic lateral sclerosis. *Journal of Neurochemistry,* 83**,** 535-545.

KABASHI, E., EL OUSSINI, H., BERCIER, V., GROS-LOUIS, F., VALDMANIS, P. N., MCDEARMID, J., MEJIER, I. A., DION, P. A., DUPRE, N., HOLLINGER, D., SINNIGER, J., DIRRIG-GROSCH, S., CAMU, W., MEININGER, V., LOEFFLER, J.-P., RENÉ, F., DRAPEAU, P., ROULEAU, G. A. & DUPUIS, L. 2013. Investigating the contribution of VAPB/ALS8 loss of function in amyotrophic lateral sclerosis. *Human Molecular Genetics,* 22**,** 2350-2360.

KABASHI, E., LIN, L., TRADEWELL, M. L., DION, P. A., BERCIER, V., BOURGOUIN, P., ROCHEFORT, D., BEL HADJ, S., DURHAM, H. D. & VELDE, C. V. 2010. Gain and loss of function of ALS-related mutations of TARDBP (TDP-43) cause motor deficits in vivo. *Human molecular genetics,* 19**,** 671-683.

KAISER, S. E., BRICKNER, J. H., REILEIN, A. R., FENN, T. D., WALTER, P. & BRUNGER, A. T. 2005. Structural Basis of FFAT Motif-Mediated ER Targeting. *Structure,* 13**,** 1035-1045.

KAMPHUIS, W., MAMBER, C., MOETON, M., KOOIJMAN, L., SLUIJS, J. A., JANSEN, A. H. P., VERVEER, M., DE GROOT, L. R., SMITH, V. D., RANGARAJAN, S., RODRÍGUEZ, J. J., ORRE, M. & HOL, E. M. 2012. GFAP Isoforms in Adult Mouse Brain with a Focus on Neurogenic Astrocytes and Reactive Astrogliosis in Mouse Models of Alzheimer Disease. *PLOS ONE,* 7**,** e42823.

KANEKURA, K., NISHIMOTO, I., AISO, S. & MATSUOKA, M. 2006. Characterization of Amyotrophic Lateral Sclerosis-linked P56S Mutation of Vesicle-associated Membrane Protein-associated Protein B (VAPB/ALS8). *Journal of Biological Chemistry,* 281**,** 30223-30233.

KAUFMANN, P., MCDERMOTT, M. P., DARRAS, B. T., FINKEL, R., KANG, P., OSKOUI, M., CONSTANTINESCU, A., SPROULE, D. M., FOLEY, A. R. & YANG, M. 2011. Observational study of spinal muscular atrophy type 2 and 3: functional outcomes over 1 year. *Archives of neurology,* 68**,** 779-786.

KAWANO, M., KUMAGAI, K., NISHIJIMA, M. & HANADA, K. 2006. Efficient Trafficking of Ceramide from the Endoplasmic Reticulum to the Golgi Apparatus Requires a VAMP-associated Protein-interacting FFAT Motif of CERT. *Journal of Biological Chemistry,* 281**,** 30279-30288.

KIERNAN, J. A. & HUDSON, A. J. 1994. Frontal lobe atrophy in motor neuron diseases. *Brain,* 117 (Pt 4)**,** 747-57.

KIM, J.-Y., JANG, A., REDDY, R., YOON, W. H. & JANKOWSKY, J. L. 2016. Neuronal overexpression of human VAPB slows motor impairment and neuromuscular denervation in a mouse model of ALS. *Human molecular genetics,* 25**,** 4661-4673.

KIM, S.-M., KIM, H., KIM, J.-E., PARK, K. S., SUNG, J.-J., KIM, S. H. & LEE, K.-W. 2011. Amyotrophic lateral sclerosis is associated with hypolipidemia at the presymptomatic stage in mice. *PloS one,* 6**,** e17985-e17985.

KIM, S., LEAL, S. S., BEN HALEVY, D., GOMES, C. M. & LEV, S. 2010. Structural requirements for VAP-B oligomerization and their implication in amyotrophic lateral sclerosis-associated VAP-B(P56S) neurotoxicity. *The Journal of biological chemistry,* 285**,** 13839-13849.

KIRKINEZOS, I. G., BACMAN, S. R., HERNANDEZ, D., OCA-COSSIO, J., ARIAS, L. J., PEREZ-PINZON, M. A., BRADLEY, W. G. & MORAES, C. T. 2005. Cytochrome c Association with the Inner Mitochondrial Membrane Is Impaired in the CNS of G93A-SOD1 Mice. *The Journal of Neuroscience,* 25**,** 164-172.

KLEIN, S. L., BIRD, B. H. & GLASS, G. E. 2001. Sex differences in immune responses and viral shedding following Seoul virus infection in Norway rats. *The American journal of tropical medicine and hygiene Am J Trop Med Hyg Am. J. Trop. Med. Hyg.,* 65**,** 57-63.

KONG, L., WANG, X., CHOE, D. W., POLLEY, M., BURNETT, B. G., BOSCH-MARCÉ, M., GRIFFIN, J. W., RICH, M. M. & SUMNER, C. J. 2009. Impaired synaptic vesicle release and immaturity of neuromuscular junctions in spinal muscular atrophy mice. *J Neurosci,* 29**,** 842-51.

KÖRNER, S., HENDRICKS, M., KOLLEWE, K., ZAPF, A., DENGLER, R., SILANI, V. & PETRI, S. 2013. Weight loss, dysphagia and supplement intake in patients with amyotrophic lateral sclerosis (ALS): impact on quality of life and therapeutic options. *BMC neurology,* 13**,** 84-84.

KOROBEYNIKOV, V. A., LYASHCHENKO, A. K., BLANCO-REDONDO, B., JAFAR-NEJAD, P. & SHNEIDER, N. A. 2022. Antisense oligonucleotide silencing of FUS expression as a therapeutic approach in amyotrophic lateral sclerosis. *Nature Medicine,* 28**,** 104-116.

KOSYREVA, A. M., DZHALILOVA, D. S., MAKAROVA, O. V., TSVETKOV, I. S., ZOLOTOVA, N. A., DIATROPTOVA, M. A., PONOMARENKO, E. A., MKHITAROV, V. A., KHOCHANSKIY, D. N. & MIKHAILOVA, L. P. 2020. Sex differences of inflammatory and immune response in pups of Wistar rats with SIRS. *Scientific Reports,* 10**,** 15884.

KRAEMER, B. C., SCHUCK, T., WHEELER, J. M., ROBINSON, L. C., TROJANOWSKI, J. Q., LEE, V. M. Y. & SCHELLENBERG, G. D. 2010. Loss of murine TDP-43 disrupts motor function and plays an essential role in embryogenesis. *Acta neuropathologica,* 119**,** 409-419.

KREUTZBERG, G. W. 1996. Microglia: a sensor for pathological events in the CNS. *Trends in Neurosciences,* 19**,** 312-318.

KRISHER, R. L. & PRATHER, R. S. 2012. A role for the Warburg effect in preimplantation embryo development: Metabolic modification to support rapid cell proliferation. *Molecular Reproduction and Development,* 79**,** 311-320.

KRISHNAN, N., FU, C., PAPPIN, D. J. & TONKS, N. K. 2011. H2S-Induced sulfhydration of the phosphatase PTP1B and its role in the endoplasmic reticulum stress response. *Sci Signal,* 4**,** ra86.

KUIJPERS, M., VAN DIS, V., HAASDIJK, E. D., HARTERINK, M., VOCKING, K., POST, J. A., SCHEPER, W., HOOGENRAAD, C. C. & JAARSMA, D. 2013a. Amyotrophic lateral sclerosis (ALS)-associated VAPB-P56S inclusions represent an ER quality control compartment. *Acta neuropathologica communications,* 1**,** 24-24.

KUIJPERS, M., YU, K. L., TEULING, E., AKHMANOVA, A., JAARSMA, D. & HOOGENRAAD, C. C. 2013b. The ALS8 protein VAPB interacts with the ER-Golgi recycling protein YIF1A and regulates membrane delivery into dendrites. *The EMBO journal,* 32**,** 2056-2072.

KUIPERS-UPMEIJER, J., DE JAGER, A. E. J., HEW, J. M., SNOEK, J. W. & VAN WEERDEN, T. W. 2001. Primary lateral sclerosis: clinical, neurophysiological, and magnetic resonance findings. *Journal of Neurology, Neurosurgery & Psychiatry,* 71**,** 615-620.

KUWERT, T., LANGE, H. W., LANGEN, K.-J., HERZOG, H., AULICH, A. & FEINENDEGEN, L. E. 1990. Cortical and subcortical glucose consumption measured by PET in patients with Huntington's disease. *Brain,* 113**,** 1405-1423.

KWIATKOWSKI, T. J., JR., BOSCO, D. A., LECLERC, A. L., TAMRAZIAN, E., VANDERBURG, C. R., RUSS, C., DAVIS, A., GILCHRIST, J., KASARSKIS, E. J., MUNSAT, T., VALDMANIS, P., ROULEAU, G. A., HOSLER, B. A., CORTELLI, P., DE JONG, P. J., YOSHINAGA, Y., HAINES, J. L., PERICAK-VANCE, M. A., YAN, J., TICOZZI, N., SIDDIQUE, T., MCKENNA-YASEK, D., SAPP, P. C., HORVITZ, H. R., LANDERS, J. E. & BROWN, R. H., JR. 2009. Mutations in the FUS/TLS gene on chromosome 16 cause familial amyotrophic lateral sclerosis. *Science,* 323**,** 1205-8.

LAGIER-TOURENNE, C., POLYMENIDOU, M., HUTT, K. R., VU, A. Q., BAUGHN, M., HUELGA, S. C., CLUTARIO, K. M., LING, S.-C., LIANG, T. Y. & MAZUR, C. 2012. Divergent roles of ALS-linked proteins FUS/TLS and TDP-43 intersect in processing long pre-mRNAs. *Nature neuroscience,* 15**,** 1488-1497.

LARDINOIS, O., KIRBY, P. J., MORGAN, D. L., SILLS, R. C., TOMER, K. B. & DETERDING, L. J. 2014. Mass spectrometric analysis of rat cerebrospinal fluid proteins following exposure to the neurotoxicant carbonyl sulfide. *Rapid communications in mass spectrometry : RCM,* 28**,** 2531-2538.

LARRAMONA-ARCAS, R., GONZÁLEZ-ARIAS, C., PEREA, G., GUTIÉRREZ, A., VITORICA, J., GARCÍA-BARRERA, T., GÓMEZ-ARIZA, J. L., PASCUA-MAESTRO, R., GANFORNINA, M. D., KARA, E., HUDRY, E., MARTINEZ-VICENTE, M., VILA, M., GALEA, E. & MASGRAU, R. 2020. Sex-dependent calcium hyperactivity due to lysosomal-related dysfunction in astrocytes from APOE4 versus APOE3 gene targeted replacement mice. *Mol Neurodegener,* 15**,** 35.

LARROQUETTE, F., SETO, L., GAUB, P. L., KAMAL, B., WALLIS, D., LARIVIERE, R., VALLEE, J., ROBITAILLE, R. & TSUDA, H. 2015. Vapb/Amyotrophic lateral sclerosis 8 knock-in mice display slowly progressive motor behavior defects accompanying ER stress and autophagic response. *Hum Mol Genet,* 24**,** 6515-29.

LAWSON, L. J., PERRY, V. H., DRI, P. & GORDON, S. 1990. Heterogeneity in the distribution and morphology of microglia in the normal adult mouse brain. *Neuroscience,* 39**,** 151-70.

LEE, A. S. 2005. The ER chaperone and signaling regulator GRP78/BiP as a monitor of endoplasmic reticulum stress. *Methods,* 35**,** 373-381.

LEE, I., KAZAMEL, M., MCPHERSON, T., MCADAM, J., BAMMAN, M., AMARA, A., SMITH, D. L., JR. & KING, P. H. 2021. Fat mass loss correlates with faster disease progression in amyotrophic lateral sclerosis patients: Exploring the utility of dual-energy x-ray absorptiometry in a prospective study. *PLOS ONE,* 16**,** e0251087.

LEE, Y.-B., CHEN, H.-J., PERES, J. N., GOMEZ-DEZA, J., ATTIG, J., ŠTALEKAR, M., TROAKES, C., NISHIMURA, A. L., SCOTTER, E. L. & VANCE, C. 2013. Hexanucleotide repeats in ALS/FTD form length-dependent RNA foci, sequester RNA binding proteins, and are neurotoxic. *Cell reports,* 5**,** 1178-1186.

LEFEBVRE, S., BÜRGLEN, L., REBOULLET, S., CLERMONT, O., BURLET, P., VIOLLET, L., BENICHOU, B., CRUAUD, C., MILLASSEAU, P. & ZEVIANI, M. 1995. Identification and characterization of a spinal muscular atrophy-determining gene. *Cell,* 80**,** 155-165.

LEIGH, P. N., ANDERTON, B. H., DODSON, A., GALLO, J. M., SWASH, M. & POWER, D. M. 1988. Ubiquitin deposits in anterior horn cells in motor neurone disease. *Neurosci Lett,* 93**,** 197-203.

LENZI, J., DE SANTIS, R., DE TURRIS, V., MORLANDO, M., LANEVE, P., CALVO, A., CALIENDO, V., CHIÒ, A., ROSA, A. & BOZZONI, I. 2015. ALS mutant FUS proteins are recruited into stress granules in induced pluripotent stem cell-derived motoneurons. *Disease models & mechanisms,* 8**,** 755-766.

LI, Q., VANDE VELDE, C., ISRAELSON, A., XIE, J., BAILEY, A. O., DONG, M.-Q., CHUN, S.-J., ROY, T., WINER, L., YATES, J. R., CAPALDI, R. A., CLEVELAND, D. W. & MILLER, T. M. 2010. ALS-linked mutant superoxide dismutase 1 (SOD1) alters mitochondrial protein composition and decreases protein import. *Proceedings of the National Academy of Sciences,* 107**,** 21146-21151.

LIAN, H., YANG, L., COLE, A., SUN, L., CHIANG, ANGIE C. A., FOWLER, STEPHANIE W., SHIM, DAVID J., RODRIGUEZ-RIVERA, J., TAGLIALATELA, G., JANKOWSKY, JOANNA L., LU, H.-C. & ZHENG, H. 2015. NFκB-Activated Astroglial Release of Complement C3 Compromises Neuronal Morphology and Function Associated with Alzheimer's Disease. *Neuron,* 85**,** 101-115.

LIDDELOW, S. A., GUTTENPLAN, K. A., CLARKE, L. E., BENNETT, F. C., BOHLEN, C. J., SCHIRMER, L., BENNETT, M. L., MÜNCH, A. E., CHUNG, W.-S., PETERSON, T. C., WILTON, D. K., FROUIN, A., NAPIER, B. A., PANICKER, N., KUMAR, M., BUCKWALTER, M. S., ROWITCH, D. H., DAWSON, V. L., DAWSON, T. M., STEVENS, B. & BARRES, B. A. 2017. Neurotoxic reactive astrocytes are induced by activated microglia. *Nature,* 541**,** 481-487.

LIEDTKE, W., EDELMANN, W., CHIU, F. C., KUCHERLAPATI, R. & RAINE, C. S. 1998. Experimental autoimmune encephalomyelitis in mice lacking glial fibrillary acidic protein is characterized by a more severe clinical course and an infiltrative central nervous system lesion. *Am J Pathol,* 152**,** 251-9.

LIMA, C., PINTO, S., NAPOLEÃO, P., PRONTO-LABORINHO, A. C., BARROS, M. A., FREITAS, T., DE CARVALHO, M. & SALDANHA, C. 2016. Identification of erythrocyte biomarkers in amyotrophic lateral sclerosis. *Clin Hemorheol Microcirc,* 63**,** 423-437.

LIN, P.-Y., SIMON, S. M., KOH, W. K., FOLORUNSO, O., UMBAUGH, C. S. & PIERCE, A. 2013. Heat shock factor 1 over-expression protects against exposure of hydrophobic residues on mutant SOD1 and early mortality in a mouse model of amyotrophic lateral sclerosis. *Molecular Neurodegeneration,* 8**,** 43.

LING, S. C., DASTIDAR, S. G., TOKUNAGA, S., HO, W. Y., LIM, K., ILIEVA, H., PARONE, P. A., TYAN, S. H., TSE, T. M., CHANG, J. C., PLATOSHYN, O., BUI, N. B., BUI, A., VETTO, A., SUN, S., MCALONIS-DOWNES, M., HAN, J. S., SWING, D., KAPELI, K., YEO, G. W., TESSAROLLO, L., MARSALA, M., SHAW, C. E., TUCKER-KELLOGG, G., LA SPADA, A. R., LAGIER-TOURENNE, C., DA CRUZ, S. & CLEVELAND, D. W. 2019. Overriding FUS autoregulation in mice triggers gain-of-toxic dysfunctions in RNA metabolism and autophagy-lysosome axis. *Elife,* 8.

LIU, G. T., HWANG, C. S., HSIEH, C. H., LU, C. H., CHANG, S. L., LEE, J. C., HUANG, C. F. & CHANG, H. T. 2013. Eosinophil-derived neurotoxin is elevated in patients with amyotrophic lateral sclerosis. *Mediators Inflamm,* 2013**,** 421389.

LIU, Y., PATTAMATTA, A., ZU, T., REID, T., BARDHI, O., BORCHELT, D. R., YACHNIS, A. T. & RANUM, L. P. 2016. C9orf72 BAC Mouse Model with Motor Deficits and Neurodegenerative Features of ALS/FTD. *Neuron,* 90**,** 521-34.

LOEWEN, C. J. R. & LEVINE, T. P. 2005. A Highly Conserved Binding Site in Vesicle-associated Membrane Protein-associated Protein (VAP) for the FFAT Motif of Lipid-binding Proteins*. *Journal of Biological Chemistry,* 280**,** 14097-14104.

LOEWEN, C. J. R., ROY, A. & LEVINE, T. P. 2003. A conserved ER targeting motif in three families of lipid binding proteins and in Opi1p binds VAP. *The EMBO Journal,* 22**,** 2025-2035.

LOGAN, R., DUBEL-HAAG, J., SCHCOLNICOV, N. & MILLER, S. J. 2022. Novel Genetic Signatures Associated With Sporadic Amyotrophic Lateral Sclerosis. *Frontiers in Genetics,* 13.

LÓPEZ-GÓMEZ, J. J., BALLESTEROS-POMAR, M. D., GÓMEZ-HOYOS, E., PINTOR DE LA MAZA, B., PENACHO-LÁZARO, M., PALACIO-MURES, J. M., ABREU-PADÍN, C., SANZ GALLEGO, I. & DE LUIS-ROMÁN, D. A. 2021. Effect of the type of specialized nutrition support on the course of the patient with amyotrophic lateral sclerosis (ALS). Interhospital registry SCLEDyN. *Endocrinol Diabetes Nutr (Engl Ed)*.

LOVELL, J. L., DIEHL, A., JOYCE, E., COHN, J., LOPEZ, J. & GUARRACI, F. A. 2007. "Some guys have all the luck": Mate preference influences paced-mating behavior in female rats. *Physiology & Behavior,* 90**,** 537-544.

LOWE, J., LENNOX, G., JEFFERSON, D., MORRELL, K., MCQUIRE, D., GRAY, T., LANDON, M., DOHERTY, F. J. & MAYER, R. J. 1988. A filamentous inclusion body within anterior horn neurones in motor neurone disease defined by immunocytochemical localisation of ubiquitin. *Neurosci Lett,* 94**,** 203-10.

LU, J., DUAN, W., GUO, Y., JIANG, H., LI, Z., HUANG, J., HONG, K. & LI, C. 2012. Mitochondrial dysfunction in human TDP-43 transfected NSC34 cell lines and the protective effect of dimethoxy curcumin. *Brain Research Bulletin,* 89**,** 185-190.

LUIGETTI, M., LATTANTE, S., ZOLLINO, M., CONTE, A., MARANGI, G., DEL GRANDE, A. & SABATELLI, M. 2011. SOD1 G93D sporadic amyotrophic lateral sclerosis (SALS) patient with rapid progression and concomitant novel ANG variant. *Neurobiol Aging,* 32**,** 1924.e15-8.

MACHADO, A. S., DARMOHRAY, D. M., FAYAD, J., MARQUES, H. G. & CAREY, M. R. 2015. A quantitative framework for whole-body coordination reveals specific deficits in freely walking ataxic mice. *eLife,* 4**,** e07892.

MACKENZIE, I. R., BIGIO, E. H., INCE, P. G., GESER, F., NEUMANN, M., CAIRNS, N. J., KWONG, L. K., FORMAN, M. S., RAVITS, J. & STEWART, H. 2007a. Pathological TDP-43 distinguishes sporadic amyotrophic lateral sclerosis from amyotrophic lateral sclerosis with SOD1 mutations. *Annals of Neurology: Official Journal of the American Neurological Association and the Child Neurology Society,* 61**,** 427-434.

MACKENZIE, I. R., BIGIO, E. H., INCE, P. G., GESER, F., NEUMANN, M., CAIRNS, N. J., KWONG, L. K., FORMAN, M. S., RAVITS, J., STEWART, H., EISEN, A., MCCLUSKY, L., KRETZSCHMAR, H. A., MONORANU, C. M., HIGHLEY, J. R., KIRBY, J., SIDDIQUE, T., SHAW, P. J., LEE, V. M. & TROJANOWSKI, J. Q. 2007b. Pathological TDP-43 distinguishes sporadic amyotrophic lateral sclerosis from amyotrophic lateral sclerosis with SOD1 mutations. *Ann Neurol,* 61**,** 427-34.

MACKENZIE, I. R. A. & BRIEMBERG, H. 2020. TDP-43 pathology in primary lateral sclerosis. *Amyotrophic Lateral Sclerosis and Frontotemporal Degeneration,* 21**,** 52-58.

MAGISTRETTI, P. J. & CHATTON, J. Y. 2005. Relationship between L-glutamate-regulated intracellular Na+ dynamics and ATP hydrolysis in astrocytes. *Journal of Neural Transmission,* 112**,** 77-85.

MAIHÖFNER, C., PROBST-COUSIN, S., BERGMANN, M., NEUHUBER, W., NEUNDÖRFER, B. & HEUSS, D. 2003. Expression and localization of cyclooxygenase-1 and -2 in human

sporadic amyotrophic lateral sclerosis. *European Journal of Neuroscience,* 18**,** 1527-1534.

MALIK, B., NIRMALANANTHAN, N., GRAY, A. L., LA SPADA, A. R., HANNA, M. G. & GREENSMITH, L. 2013. Co-induction of the heat shock response ameliorates disease progression in a mouse model of human spinal and bulbar muscular atrophy: implications for therapy. *Brain,* 136**,** 926-43.

MANCUSO, R., OLIVÁN, S., OSTA, R. & NAVARRO, X. 2011. Evolution of gait abnormalities in SOD1(G93A) transgenic mice. *Brain Res,* 1406**,** 65-73.

MANES, C. & LAI, N. C. 1995. Nonmitochondrial oxygen utilization by rabbit blastocysts and surface production of superoxide radicals. *Reproduction,* 104**,** 69-75.

MANIATIS, S., ÄIJÖ, T., VICKOVIC, S., BRAINE, C., KANG, K., MOLLBRINK, A., FAGEGALTIER, D., ANDRUSIVOVÁ, Ž., SAARENPÄÄ, S., SAIZ-CASTRO, G., CUEVAS, M., WATTERS, A., LUNDEBERG, J., BONNEAU, R. & PHATNANI, H. 2019. Spatiotemporal dynamics of molecular pathology in amyotrophic lateral sclerosis. *Science,* 364**,** 89-93.

MANTOVANI, S., GARBELLI, S., PASINI, A., ALIMONTI, D., PEROTTI, C., MELAZZINI, M., BENDOTTI, C. & MORA, G. 2009. Immune system alterations in sporadic amyotrophic lateral sclerosis patients suggest an ongoing neuroinflammatory process. *Journal of Neuroimmunology,* 210**,** 73-79.

MAO, D., LIN, G., TEPE, B., ZUO, Z., TAN, K. L., SENTURK, M., ZHANG, S., ARENKIEL, B. R., SARDIELLO, M. & BELLEN, H. J. 2019. VAMP associated proteins are required for autophagic and lysosomal degradation by promoting a PtdIns4P-mediated endosomal pathway. *Autophagy***,** 1-20.

MARQUES, V. D. & MARQUES, W. J. 2008. Neurophysiological Findings of the Late-Onset, Dominant, Proximal Spinal Muscular Atrophies With Dysautonomia Because of the VAPB PRO56SER Mutation. *Journal of Clinical Neurophysiology,* 25**,** 233-235.

MARTENS, G. A. 2015. Species-Related Differences in the Proteome of Rat and Human Pancreatic Beta Cells. *Journal of diabetes research,* 2015**,** 549818-549818.

MASTERS, C. L., SIMMS, G., WEINMAN, N. A., MULTHAUP, G., MCDONALD, B. L. & BEYREUTHER, K. 1985. Amyloid plaque core protein in Alzheimer disease and Down syndrome. *Proceedings of the National Academy of Sciences,* 82**,** 4245-4249.

MATTIAZZI, M., D'AURELIO, M., GAJEWSKI, C. D., MARTUSHOVA, K., KIAEI, M., BEAL, M. F. & MANFREDI, G. 2002. Mutated Human SOD1 Causes Dysfunction of Oxidative Phosphorylation in Mitochondria of Transgenic Mice*. *Journal of Biological Chemistry,* 277**,** 29626-29633.

MAUCH, D. H., NÄGLER, K., SCHUMACHER, S., GÖRITZ, C., MÜLLER, E.-C., OTTO, A. & PFRIEGER, F. W. 2001. CNS Synaptogenesis Promoted by Glia-Derived Cholesterol. *Science,* 294**,** 1354-1357.

MAURER, P. H. & CALLAHAN, H. J. 1980. [2] Proteins and polypeptides as antigens. *Methods in Enzymology.* Academic Press.

MCALARY, L., AQUILINA, J. A. & YERBURY, J. J. 2016. Susceptibility of Mutant SOD1 to Form a Destabilized Monomer Predicts Cellular Aggregation and Toxicity but Not In vitro Aggregation Propensity. *Front Neurosci,* 10**,** 499.

MCCORMACK, J. G. & DENTON, R. M. 1989. The role of Ca2+ ions in the regulation of intramitochondrial metabolism and energy production in rat heart. *Molecular and Cellular Biochemistry,* 89**,** 121-125.

MCGILL, R. B., STEYN, F. J., NGO, S. T., THORPE, K. A., HEGGIE, S., RUITENBERG, M. J., HENDERSON, R. D., MCCOMBE, P. A. & WOODRUFF, T. M. 2020. Monocytes and

neutrophils are associated with clinical features in amyotrophic lateral sclerosis. *Brain Communications,* 2.

MCKENNA, M. C. 2012. Substrate Competition Studies Demonstrate Oxidative Metabolism of Glucose, Glutamate, Glutamine, Lactate and 3-Hydroxybutyrate in Cortical Astrocytes from Rat Brain. *Neurochemical Research,* 37**,** 2613-2626.

MCKISIC, M. D., PATURZO, F. X., GAERTNER, D. J., JACOBY, R. O. & SMITH, A. L. 1995. A nonlethal rat parvovirus infection suppresses rat T lymphocyte effector functions. *J Immunol,* 155**,** 3979-86.

MCMANUS, M. J., MURPHY, M. P. & FRANKLIN, J. L. 2011. The mitochondria-targeted antioxidant MitoQ prevents loss of spatial memory retention and early neuropathology in a transgenic mouse model of Alzheimer's disease. *Journal of Neuroscience,* 31**,** 15703-15715.

MEAD, R. J., BENNETT, E. J., KENNERLEY, A. J., SHARP, P., SUNYACH, C., KASHER, P., BERWICK, J., PETTMANN, B., BATTAGLIA, G., AZZOUZ, M., GRIERSON, A. & SHAW, P. J. 2011. Optimised and rapid pre-clinical screening in the SOD1(G93A) transgenic mouse model of amyotrophic lateral sclerosis (ALS). *PloS one,* 6**,** e23244-e23244.

MENZIES, F. M., COOKSON, M. R., TAYLOR, R. W., TURNBULL, D. M., CHRZANOWSKA-LIGHTOWLERS, Z. M. A., DONG, L., FIGLEWICZ, D. A. & SHAW, P. J. 2002. Mitochondrial dysfunction in a cell culture model of familial amyotrophic lateral sclerosis. *Brain,* 125**,** 1522-1533.

METZ, G. A., CURT, A., VAN DE MEENT, H., KLUSMAN, I., SCHWAB, M. E. & DIETZ, V. 2000. Validation of the weight-drop contusion model in rats: a comparative study of human spinal cord injury. *J Neurotrauma,* 17**,** 1-17.

MEYER, K., FERRAIUOLO, L., MIRANDA, C. J., LIKHITE, S., MCELROY, S., RENUSCH, S., DITSWORTH, D., LAGIER-TOURENNE, C., SMITH, R. A., RAVITS, J., BURGHES, A. H., SHAW, P. J., CLEVELAND, D. W., KOLB, S. J. & KASPAR, B. K. 2014. Direct conversion of patient fibroblasts demonstrates non-cell autonomous toxicity of astrocytes to motor neurons in familial and sporadic ALS. *Proceedings of the National Academy of Sciences of the United States of America,* 111**,** 829-832.

MILLECAMPS, S., SALACHAS, F., CAZENEUVE, C., GORDON, P., BRICKA, B., CAMUZAT, A., GUILLOT-NOËL, L., RUSSAOUEN, O., BRUNETEAU, G., PRADAT, P.-F., LE FORESTIER, N., VANDENBERGHE, N., DANEL-BRUNAUD, V., GUY, N., THAUVIN-ROBINET, C., LACOMBLEZ, L., COURATIER, P., HANNEQUIN, D., SEILHEAN, D., LE BER, I., CORCIA, P., CAMU, W., BRICE, A., ROULEAU, G., LEGUERN, E. & MEININGER, V. 2010. SOD1, ANG, VAPB, TARDBP, and FUS mutations in familial amyotrophic lateral sclerosis: genotype-phenotype correlations. *Journal of Medical Genetics,* 47**,** 554-60.

MIRON, V. E., BOYD, A., ZHAO, J. W., YUEN, T. J., RUCKH, J. M., SHADRACH, J. L., VAN WIJNGAARDEN, P., WAGERS, A. J., WILLIAMS, A., FRANKLIN, R. J. M. & FFRENCH-CONSTANT, C. 2013. M2 microglia and macrophages drive oligodendrocyte differentiation during CNS remyelination. *Nat Neurosci,* 16**,** 1211-1218.

MITCHELL, J. C., MCGOLDRICK, P., VANCE, C., HORTOBAGYI, T., SREEDHARAN, J., ROGELJ, B., TUDOR, E. L., SMITH, B. N., KLASEN, C., MILLER, C. C. J., COOPER, J. D., GREENSMITH, L. & SHAW, C. E. 2013. Overexpression of human wild-type FUS causes progressive motor neuron degeneration in an age- and dose-dependent fashion. *Acta neuropathologica,* 125**,** 273-288.

MITNE-NETO, M., RAMOS, C. R. R., PIMENTA, D. C., LUZ, J. S., NISHIMURA, A. L., GONZALES, F. A., OLIVEIRA, C. C. & ZATZ, M. 2007. A mutation in human VAP-B–MSP domain,

present in ALS patients, affects the interaction with other cellular proteins. *Protein Expression and Purification,* 55**,** 139-146.

MIYASAKA, Y., UNO, Y., YOSHIMI, K., KUNIHIRO, Y., YOSHIMURA, T., TANAKA, T., ISHIKUBO, H., HIRAOKA, Y., TAKEMOTO, N., TANAKA, T., OOGUCHI, Y., SKEHEL, P., AIDA, T., TAKEDA, J. & MASHIMO, T. 2018. CLICK: one-step generation of conditional knockout mice. *BMC Genomics,* 19**,** 318.

MOGLIA, C., CALVO, A., GRASSANO, M., CANOSA, A., MANERA, U., D'OVIDIO, F., BOMBACI, A., BERSANO, E., MAZZINI, L., MORA, G. & CHIÒ, A. 2019. Early weight loss in amyotrophic lateral sclerosis: outcome relevance and clinical correlates in a population-based cohort. *Journal of Neurology, Neurosurgery & Psychiatry,* 90**,** 666-673.

MORI, K., WENG, S.-M., ARZBERGER, T., MAY, S., RENTZSCH, K., KREMMER, E., SCHMID, B., KRETZSCHMAR, H. A., CRUTS, M. & VAN BROECKHOVEN, C. 2013. The C9orf72 GGGGCC repeat is translated into aggregating dipeptide-repeat proteins in FTLD/ALS. *Science,* 339**,** 1335-1338.

MORI, Y., TAKENAKA, K.-I., FUKAZAWA, Y. & TAKAMORI, S. 2021. The endosomal Q-SNARE, Syntaxin 7, defines a rapidly replenishing synaptic vesicle recycling pool in hippocampal neurons. *Communications Biology,* 4**,** 981.

MÓROTZ, G. M., DE VOS, K. J., VAGNONI, A., ACKERLEY, S., SHAW, C. E. & MILLER, C. C. J. 2012. Amyotrophic lateral sclerosis-associated mutant VAPBP56S perturbs calcium homeostasis to disrupt axonal transport of mitochondria. *Human molecular genetics,* 21**,** 1979-1988.

MORTENSEN, M., FERGUSON, D. J. P., EDELMANN, M., KESSLER, B., MORTEN, K. J., KOMATSU, M. & SIMON, A. K. 2010. Loss of autophagy in erythroid cells leads to defective removal of mitochondria and severe anemia in vivo. *Proceedings of the National Academy of Sciences,* 107**,** 832-837.

MURDOCK, B. J., BENDER, D. E., KASHLAN, S. R., FIGUEROA-ROMERO, C., BACKUS, C., CALLAGHAN, B. C., GOUTMAN, S. A. & FELDMAN, E. L. 2016. Increased ratio of circulating neutrophils to monocytes in amyotrophic lateral sclerosis. *Neurology - Neuroimmunology Neuroinflammation,* 3**,** e242.

MUTIHAC, R., ALEGRE-ABARRATEGUI, J., GORDON, D., FARRIMOND, L., YAMASAKI-MANN, M., TALBOT, K. & WADE-MARTINS, R. 2015. TARDBP pathogenic mutations increase cytoplasmic translocation of TDP-43 and cause reduction of endoplasmic reticulum Ca2+ signaling in motor neurons. *Neurobiology of Disease,* 75**,** 64-77.

NAGAI, M., AOKI, M., MIYOSHI, I., KATO, M., PASINELLI, P., KASAI, N., BROWN, R. H., JR. & ITOYAMA, Y. 2001. Rats expressing human cytosolic copper-zinc superoxide dismutase transgenes with amyotrophic lateral sclerosis: associated mutations develop motor neuron disease. *J Neurosci,* 21**,** 9246-54.

NAGAI, M., RE, D. B., NAGATA, T., CHALAZONITIS, A., JESSELL, T. M., WICHTERLE, H. & PRZEDBORSKI, S. 2007. Astrocytes expressing ALS-linked mutated SOD1 release factors selectively toxic to motor neurons. *Nature Neuroscience,* 10**,** 615-622.

NAKAYAMA, Y., SHIMIZU, T., MATSUDA, C., HARAGUCHI, M., HAYASHI, K., BOKUDA, K., NAGAO, M., KAWATA, A., ISHIKAWA-TAKATA, K. & ISOZAKI, E. 2019. Body weight variation predicts disease progression after invasive ventilation in amyotrophic lateral sclerosis. *Scientific Reports,* 9**,** 12262.

NEEFJES, J. & CABUKUSTA, B. 2021. What the VAP: The Expanded VAP Family of Proteins Interacting With FFAT and FFAT-Related Motifs for Interorganellar Contact. *Contact,* 4**,** 25152564211012246.

NEUEDER, A., LANDLES, C., GHOSH, R., HOWLAND, D., MYERS, R. H., FAULL, R. L., TABRIZI, S. J. & BATES, G. P. 2017. The pathogenic exon 1 HTT protein is produced by incomplete splicing in Huntington's disease patients. *Scientific reports,* 7**,** 1-10.

NEUMANN, M., SAMPATHU, D. M., KWONG, L. K., TRUAX, A. C., MICSENYI, M. C., CHOU, T. T., BRUCE, J., SCHUCK, T., GROSSMAN, M., CLARK, C. M., MCCLUSKEY, L. F., MILLER, B. L., MASLIAH, E., MACKENZIE, I. R., FELDMAN, H., FEIDEN, W., KRETZSCHMAR, H. A., TROJANOWSKI, J. Q. & LEE, V. M.-Y. 2006. Ubiquitinated TDP-43 in Frontotemporal Lobar Degeneration and Amyotrophic Lateral Sclerosis. *Science,* 314**,** 130-133.

NGO, S. T., VAN EIJK, R. P. A., CHACHAY, V., VAN DEN BERG, L. H., MCCOMBE, P. A., HENDERSON, R. D. & STEYN, F. J. 2019. Loss of appetite is associated with a loss of weight and fat mass in patients with amyotrophic lateral sclerosis. *Amyotrophic Lateral Sclerosis and Frontotemporal Degeneration,* 20**,** 497-505.

NGUYEN, T. N., PADMAN, B. S., USHER, J., OORSCHOT, V., RAMM, G. & LAZAROU, M. 2016. Atg8 family LC3/GABARAP proteins are crucial for autophagosome–lysosome fusion but not autophagosome formation during PINK1/Parkin mitophagy and starvation. *Journal of Cell Biology,* 215**,** 857-874.

NIEUWENHUYS, R., VOOGD, J. & VAN HUIJZEN, C. 2008. Telencephalon: Neocortex. *In:* NIEUWENHUYS, R., VOOGD, J. & VAN HUIJZEN, C. (eds.) *The Human Central Nervous System.* Berlin, Heidelberg: Springer Berlin Heidelberg.

NIGGESCHULZE, A. & KAST, A. 1994. Maternal age, reproduction and chromosomal aberrations in Wistar derived rats. *Lab Anim,* 28**,** 55-62.

NIMMERJAHN, A., KIRCHHOFF, F. & HELMCHEN, F. 2005. Resting microglial cells are highly dynamic surveillants of brain parenchyma in vivo. *Science,* 308**,** 1314-8.

NIROGI, R., KANDIKERE, V., MUDIGONDA, K., BHYRAPUNENI, G., MUDDANA, N., SARALAYA, R. & BENADE, V. 2009. A simple and rapid method to collect the cerebrospinal fluid of rats and its application for the assessment of drug penetration into the central nervous system. *Journal of Neuroscience Methods,* 178**,** 116-119.

NISHIMURA, A. L., AL-CHALABI, A. & ZATZ, M. 2005. A common founder for amyotrophic lateral sclerosis type 8 (ALS8) in the Brazilian population. *Human Genetics,* 118**,** 499-500.

NISHIMURA, A. L., MITNE-NETO, M., SILVA, H. C. A., OLIVEIRA, J. R. M., VAINZOF, M. & ZATZ, M. 2004a. A novel locus for late onset amyotrophic lateral sclerosis/motor neurone disease variant at 20q13. *Journal of medical genetics,* 41**,** 315-320.

NISHIMURA, A. L., MITNE-NETO, M., SILVA, H. C. A., RICHIERI-COSTA, A., MIDDLETON, S., CASCIO, D., KOK, F., OLIVEIRA, J. R. M., GILLINGWATER, T., WEBB, J., SKEHEL, P. & ZATZ, M. 2004b. A Mutation in the Vesicle-Trafficking Protein VAPB Causes Late-Onset Spinal Muscular Atrophy and Amyotrophic Lateral Sclerosis. *American Journal of Human Genetics,* 75**,** 822-831.

NISHIMURA, Y., HAYASHI, M., INADA, H. & TANAKA, T. 1999. Molecular Cloning and Characterization of Mammalian Homologues of Vesicle-Associated Membrane Protein-Associated (VAMP-Associated) Proteins. *Biochemical and Biophysical Research Communications,* 254**,** 21-26.

NIU, C., ZHANG, J., GAO, F., YANG, L., JIA, M., ZHU, H. & GONG, W. 2012. FUS-NLS/Transportin 1 complex structure provides insights into the nuclear targeting mechanism of FUS and the implications in ALS.

NORENBERG, M. D., SMITH, J. & MARCILLO, A. 2004. The pathology of human spinal cord injury: defining the problems. *J Neurotrauma,* 21**,** 429-40.

O'ROURKE, J. G., BOGDANIK, L., YÁÑEZ, A., LALL, D., WOLF, A. J., MUHAMMAD, A. K., HO, R., CARMONA, S., VIT, J. P., ZARROW, J., KIM, K. J., BELL, S., HARMS, M. B., MILLER, T. M., DANGLER, C. A., UNDERHILL, D. M., GOODRIDGE, H. S., LUTZ, C. M. & BALOH, R. H. 2016. C9orf72 is required for proper macrophage and microglial function in mice. *Science,* 351**,** 1324-9.

O'REGAN, G. C., FARAG, S. H., CASEY, C. S., WOOD-KACZMAR, A., POCOCK, J. M., TABRIZI, S. J. & ANDRE, R. 2021. Human Huntington's disease pluripotent stem cell-derived microglia develop normally but are abnormally hyper-reactive and release elevated levels of reactive oxygen species. *Journal of Neuroinflammation,* 18**,** 94.

OHGOMORI, T., YAMADA, J., TAKEUCHI, H., KADOMATSU, K. & JINNO, S. 2016. Comparative morphometric analysis of microglia in the spinal cord of SOD1(G93A) transgenic mouse model of amyotrophic lateral sclerosis. *Eur J Neurosci,* 43**,** 1340-51.

OLIVEIRA, D., MORALES-VICENTE, D. A., AMARAL, M. S., LUZ, L., SERTIÉ, A. L., LEITE, F. S., NAVARRO, C., KAID, C., ESPOSITO, J., GOULART, E., CAIRES, L., ALVES, L. M., MELO, U. S., FIGUEIREDO, T., MITNE-NETO, M., OKAMOTO, O. K., VERJOVSKI-ALMEIDA, S. & ZATZ, M. 2020. Different gene expression profiles in iPSC-derived motor neurons from ALS8 patients with variable clinical courses suggest mitigating pathways for neurodegeneration. *Human Molecular Genetics,* 29**,** 1465-1475.

OLNEY, J. W. 1971. Glutamate-Induced Neuronal Necrosis in the Infant Mouse Hypothalamus: An Electron Microscopic Study*†. *Journal of Neuropathology & Experimental Neurology,* 30**,** 75-90.

OSKARSSON, B., HORTON, D. K. & MITSUMOTO, H. 2015. Potential Environmental Factors in Amyotrophic Lateral Sclerosis. *Neurologic clinics,* 33**,** 877-888.

OSKOUI, M., DARRAS, B. T. & DE VIVO, D. C. 2017. Chapter 1 - Spinal Muscular Atrophy: 125 Years Later and on the Verge of a Cure. *In:* SUMNER, C. J., PAUSHKIN, S. & KO, C.-P. (eds.) *Spinal Muscular Atrophy.* Academic Press.

OU, S., WU, F., HARRICH, D., GARCÍA-MARTÍNEZ, L. F. & GAYNOR, R. B. 1995. Cloning and characterization of a novel cellular protein, TDP-43, that binds to human immunodeficiency virus type 1 TAR DNA sequence motifs. *Journal of virology,* 69**,** 3584-3596.

OUYANG, Y. B., XU, L. J., EMERY, J. F., LEE, A. S. & GIFFARD, R. G. 2011. Overexpressing GRP78 influences Ca2+ handling and function of mitochondria in astrocytes after ischemia-like stress. *Mitochondrion,* 11**,** 279-86.

OZDINLER, P., BENN, S. & YAMAMOTO, T. Gü zel M, Brown RH, Macklis JD. 2011. Corticospinal motor neurons and related subcerebral projection neurons undergo early and specific neurodegeneration in hSOD1G93A transgenic ALS mice. *Journal of Neuroscience,* 31**,** 4166-4177.

PAILLUSSON, S., GOMEZ-SUAGA, P., STOICA, R., LITTLE, D., GISSEN, P., DEVINE, M. J., NOBLE, W., HANGER, D. P. & MILLER, C. C. J. 2017. α-Synuclein binds to the ER-mitochondria tethering protein VAPB to disrupt Ca(2+) homeostasis and mitochondrial ATP production. *Acta neuropathologica,* 134**,** 129-149.

PANI, B., ONG, H. L., LIU, X., RAUSER, K., AMBUDKAR, I. S. & SINGH, B. B. 2008. Lipid rafts determine clustering of STIM1 in endoplasmic reticulum-plasma membrane junctions and regulation of store-operated Ca2+ entry (SOCE). *J Biol Chem,* 283**,** 17333-40.

PAPIANI, G., RUGGIANO, A., FOSSATI, M., RAIMONDI, A., BERTONI, G., FRANCOLINI, M., BENFANTE, R., NAVONE, F. & BORGESE, N. 2012. Restructured endoplasmic reticulum generated by mutant amyotrophic lateral sclerosis-linked VAPB is cleared by the proteasome. *Journal of Cell Science,* 125**,** 3601-3611.

PARK, K. W., LEE, H. G., JIN, B. K. & LEE, Y. B. 2007. Interleukin-10 endogenously expressed in microglia prevents lipopolysaccharide-induced neurodegeneration in the rat cerebral cortex in vivo. *Experimental & Molecular Medicine,* 39**,** 812-819.

PAULSEN, C. E., TRUONG, T. H., GARCIA, F. J., HOMANN, A., GUPTA, V., LEONARD, S. E. & CARROLL, K. S. 2011. Peroxide-dependent sulfenylation of the EGFR catalytic site enhances kinase activity. *Nat Chem Biol,* 8**,** 57-64.

PELLERIN, L. & MAGISTRETTI, P. J. 1994. Glutamate uptake into astrocytes stimulates aerobic glycolysis: a mechanism coupling neuronal activity to glucose utilization. *Proceedings of the National Academy of Sciences,* 91**,** 10625-10629.

PENG, M.-T. & HUANG, H.-H. 1972. Aging of Hypothalamic-Pituitary-Ovarian Function in the Rat**Supported by Grant M68.88 from the Population Council of New York. *Fertility and Sterility,* 23**,** 535-542.

PENNETTA, G., HIESINGER, P. R., FABIAN-FINE, R., MEINERTZHAGEN, I. A. & BELLEN, H. J. 2002. Drosophila VAP-33A Directs Bouton Formation at Neuromuscular Junctions in a Dosage-Dependent Manner. *Neuron,* 35**,** 291-306.

PERETTI, D., DAHAN, N., SHIMONI, E., HIRSCHBERG, K. & LEV, S. 2008. Coordinated lipid transfer between the endoplasmic reticulum and the Golgi complex requires the VAP proteins and is essential for Golgi-mediated transport. *Molecular biology of the cell,* 19**,** 3871-3884.

PETERS, O. M., CABRERA, G. T., TRAN, H., GENDRON, T. F., MCKEON, J. E., METTERVILLE, J., WEISS, A., WIGHTMAN, N., SALAMEH, J. & KIM, J. 2015. Human C9ORF72 hexanucleotide expansion reproduces RNA foci and dipeptide repeat proteins but not neurodegeneration in BAC transgenic mice. *Neuron,* 88**,** 902-909.

PETERSON, C., GIBSON, G. & BLASS, J. 1985. Altered calcium uptake in cultured skin fibroblasts from patients with Alzheimer's disease. *The New England journal of medicine,* 312**,** 1063-1065.

PHELPS, P. E., BARBER, R. P., HOUSER, C. R., CRAWFORD, G. D., SALVATERRA, P. M. & VAUGHN, J. E. 1984. Postnatal development of neurons containing choline acetyltransferase in rat spinal cord: An immunocytochemical study. *Journal of Comparative Neurology,* 229**,** 347-361.

PICCOLI, C., RIA, R., SCRIMA, R., CELA, O., D'APRILE, A., BOFFOLI, D., FALZETTI, F., TABILIO, A. & CAPITANIO, N. 2005. Characterization of Mitochondrial and Extra-mitochondrial Oxygen Consuming Reactions in Human Hematopoietic Stem Cells: NOVEL EVIDENCE OF THE OCCURRENCE OF NAD(P)H OXIDASE ACTIVITY*. *Journal of Biological Chemistry,* 280**,** 26467-26476.

PITZER, C., KURPIERS, B. & ELTOKHI, A. 2021. Gait performance of adolescent mice assessed by the CatWalk XT depends on age, strain and sex and correlates with speed and body weight. *Scientific Reports,* 11**,** 21372.

PLESCHER, M., SEIFERT, G., HANSEN, J. N., BEDNER, P., STEINHÄUSER, C. & HALLE, A. 2018. Plaque-dependent morphological and electrophysiological heterogeneity of microglia in an A lzheimer's disease mouse model. *Glia,* 66**,** 1464-1480.

POLYMEROPOULOS, M. H., LAVEDAN, C., LEROY, E., IDE, S. E., DEHEJIA, A., DUTRA, A., PIKE, B., ROOT, H., RUBENSTEIN, J. & BOYER, R. 1997. Mutation in the α-synuclein gene identified in families with Parkinson's disease. *science,* 276**,** 2045-2047.

POTTIER, C., BIENIEK, K. F., FINCH, N., VAN DE VORST, M., BAKER, M., PERKERSEN, R., BROWN, P., RAVENSCROFT, T., VAN BLITTERSWIJK, M., NICHOLSON, A. M., DETURE, M., KNOPMAN, D. S., JOSEPHS, K. A., PARISI, J. E., PETERSEN, R. C., BOYLAN, K. B., BOEVE, B. F., GRAFF-RADFORD, N. R., VELTMAN, J. A., GILISSEN, C., MURRAY, M. E., DICKSON, D. W. & RADEMAKERS, R. 2015. Whole-genome sequencing reveals important role for TBK1 and OPTN mutations in frontotemporal lobar degeneration without motor neuron disease. *Acta Neuropathol,* 130**,** 77-92.

POWIS, R. A. & GILLINGWATER, T. H. 2016. Selective loss of alpha motor neurons with sparing of gamma motor neurons and spinal cord cholinergic neurons in a mouse model of spinal muscular atrophy. *Journal of anatomy,* 228**,** 443-451.

PRABHU, P., KARUNAKAR, A. K., ANITHA, H. & PRADHAN, N. 2020. Classification of gait signals into different neurodegenerative diseases using statistical analysis and recurrence quantification analysis. *Pattern Recognition Letters,* 139**,** 10-16.

PRELL, T., LAUTENSCHLÄGER, J., WITTE, O. W., CARRI, M. T. & GROSSKREUTZ, J. 2012. The unfolded protein response in models of human mutant G93A amyotrophic lateral sclerosis. *European Journal of Neuroscience,* 35**,** 652-660.

PRINGLE, C., HUDSON, A., MUNOZ, D., KIERNAN, J., BROWN, W. & EBERS, G. 1992. Primary lateral sclerosis: clinical features, neuropathology and diagnostic criteria. *Brain,* 115**,** 495-520.

PRIOR, T. W., SWOBODA, K. J., SCOTT, H. D. & HEJMANOWSKI, A. Q. 2004. Homozygous SMN1 deletions in unaffected family members and modification of the phenotype by SMN2. *Am J Med Genet A,* 130a**,** 307-10.

PUGA, D. A., TOVAR, C. A., GUAN, Z., GENSEL, J. C., LYMAN, M. S., MCTIGUE, D. M. & POPOVICH, P. G. 2015. Stress exacerbates neuron loss and microglia proliferation in a rat model of excitotoxic lower motor neuron injury. *Brain, Behavior, and Immunity,* 49**,** 246-254.

QIN, X.-Y., ZHANG, S.-P., CAO, C., LOH, Y. P. & CHENG, Y. 2016. Aberrations in Peripheral Inflammatory Cytokine Levels in Parkinson Disease: A Systematic Review and Meta-analysis. *JAMA Neurology,* 73**,** 1316-1324.

QIU, H., LEE, S., SHANG, Y., WANG, W.-Y., AU, K. F., KAMIYA, S., BARMADA, S. J., FINKBEINER, S., LUI, H. & CARLTON, C. E. 2014. ALS-associated mutation FUS-R521C causes DNA damage and RNA splicing defects. *The Journal of clinical investigation,* 124**,** 981-999.

QIU, L., QIAO, T., BEERS, M., TAN, W., WANG, H., YANG, B. & XU, Z. 2013. Widespread aggregation of mutant VAPB associated with ALS does not cause motor neuron degeneration or modulate mutant SOD1 aggregation and toxicity in mice. *Molecular Neurodegeneration,* 8**,** 1.

RADOVANOVIĆ, S., MILIĆEV, M., PERIĆ, S., BASTA, I., KOSTIĆ, V. & STEVIĆ, Z. 2014. Gait in amyotrophic lateral sclerosis: Is gait pattern differently affected in spinal and bulbar onset of the disease during dual task walking? *Amyotrophic Lateral Sclerosis and Frontotemporal Degeneration,* 15**,** 488-493.

RAO, S. D., YIN, H. Z. & WEISS, J. H. 2003. Disruption of glial glutamate transport by reactive oxygen species produced in motor neurons. *The Journal of neuroscience : the official journal of the Society for Neuroscience,* 23**,** 2627-2633.

REDGATE, E. S., DEUTSCH, M. & BOGGS, S. S. 1991. Time of death of CNS tumor-bearing rats can be reliably predicted by body weight-loss patterns. *Lab Anim Sci,* 41**,** 269-73.

REDONDO, P. C., SALIDO, G. M., PARIENTE, J. A. & ROSADO, J. A. 2004. Dual effect of hydrogen peroxide on store-mediated calcium entry in human platelets. *Biochemical Pharmacology,* 67**,** 1065-1076.

REIMAN, E. M., CHEN, K., ALEXANDER, G. E., CASELLI, R. J., BANDY, D., OSBORNE, D., SAUNDERS, A. M. & HARDY, J. 2004. Functional brain abnormalities in young adults at genetic risk for late-onset Alzheimer's dementia. *Proc Natl Acad Sci U S A,* 101**,** 284-9.

REITS, E., GRIEKSPOOR, A., NEIJSSEN, J., GROOTHUIS, T., JALINK, K., VAN VEELEN, P., JANSSEN, H., CALAFAT, J., DRIJFHOUT, J. W. & NEEFJES, J. 2003. Peptide Diffusion, Protection, and Degradation in Nuclear and Cytoplasmic Compartments before Antigen Presentation by MHC Class I. *Immunity,* 18**,** 97-108.

REITS, E., NEIJSSEN, J., HERBERTS, C., BENCKHUIJSEN, W., JANSSEN, L., DRIJFHOUT, J. W. & NEEFJES, J. 2004. A Major Role for TPPII in Trimming Proteasomal Degradation Products for MHC Class I Antigen Presentation. *Immunity,* 20**,** 495-506.

RENTON, A. E., MAJOUNIE, E., WAITE, A., SIMÓN-SÁNCHEZ, J., ROLLINSON, S., GIBBS, J. R., SCHYMICK, J. C., LAAKSOVIRTA, H., VAN SWIETEN, J. C., MYLLYKANGAS, L., KALIMO, H., PAETAU, A., ABRAMZON, Y., REMES, A. M., KAGANOVICH, A., SCHOLZ, S. W., DUCKWORTH, J., DING, J., HARMER, D. W., HERNANDEZ, D. G., JOHNSON, J. O., MOK, K., RYTEN, M., TRABZUNI, D., GUERREIRO, R. J., ORRELL, R. W., NEAL, J., MURRAY, A., PEARSON, J., JANSEN, I. E., SONDERVAN, D., SEELAAR, H., BLAKE, D., YOUNG, K., HALLIWELL, N., CALLISTER, J. B., TOULSON, G., RICHARDSON, A., GERHARD, A., SNOWDEN, J., MANN, D., NEARY, D., NALLS, M. A., PEURALINNA, T., JANSSON, L., ISOVIITA, V.-M., KAIVORINNE, A.-L., HÖLTTÄ-VUORI, M., IKONEN, E., SULKAVA, R., BENATAR, M., WUU, J., CHIÒ, A., RESTAGNO, G., BORGHERO, G., SABATELLI, M., CONSORTIUM, I., HECKERMAN, D., ROGAEVA, E., ZINMAN, L., ROTHSTEIN, J. D., SENDTNER, M., DREPPER, C., EICHLER, E. E., ALKAN, C., ABDULLAEV, Z., PACK, S. D., DUTRA, A., PAK, E., HARDY, J., SINGLETON, A., WILLIAMS, N. M., HEUTINK, P., PICKERING-BROWN, S., MORRIS, H. R., TIENARI, P. J. & TRAYNOR, B. J. 2011. A hexanucleotide repeat expansion in C9ORF72 is the cause of chromosome 9p21-linked ALS-FTD. *Neuron,* 72**,** 257-268.

RENTZOS, M., EVANGELOPOULOS, E., SERETI, E., ZOUVELOU, V., MARMARA, S., ALEXAKIS, T. & EVDOKIMIDIS, I. 2012. Alterations of T cell subsets in ALS: a systemic immune activation? *Acta Neurologica Scandinavica,* 125**,** 260-264.

REUBEN, D. B., MOR, V. & HIRIS, J. 1988. Clinical symptoms and length of survival in patients with terminal cancer. *Arch Intern Med,* 148**,** 1586-91.

ROCHA, A. G., FRANCO, A., KREZEL, A. M., RUMSEY, J. M., ALBERTI, J. M., KNIGHT, W. C., BIRIS, N., ZACHARIOUDAKIS, E., JANETKA, J. W., BALOH, R. H., KITSIS, R. N., MOCHLY-ROSEN, D., TOWNSEND, R. R., GAVATHIOTIS, E. & DORN, G. W. 2018. MFN2 agonists reverse mitochondrial defects in preclinical models of Charcot-Marie-Tooth disease type 2A. *Science,* 360**,** 336-341.

RODRÍGUEZ-GONZÁLEZ, G. L., REYES-CASTRO, L. A., VEGA, C. C., BOECK, L., IBÁÑEZ, C., NATHANIELSZ, P. W., LARREA, F. & ZAMBRANO, E. 2014. Accelerated aging of reproductive capacity in male rat offspring of protein-restricted mothers is associated

with increased testicular and sperm oxidative stress. *Age (Dordrecht, Netherlands),* 36**,** 9721-9721.

ROSEN, D. R., SIDDIQUE, T., PATTERSON, D., FIGLEWICZ, D. A., SAPP, P., HENTATI, A., DONALDSON, D., GOTO, J., O'REGAN, J. P., DENG, H.-X., RAHMANI, Z., KRIZUS, A., MCKENNA-YASEK, D., CAYABYAB, A., GASTON, S. M., BERGER, R., TANZI, R. E., HALPERIN, J. J., HERZFELDT, B., VAN DEN BERGH, R., HUNG, W.-Y., BIRD, T., DENG, G., MULDER, D. W., SMYTH, C., LAING, N. G., SORIANO, E., PERICAK–VANCE, M. A., HAINES, J., ROULEAU, G. A., GUSELLA, J. S., HORVITZ, H. R. & BROWN JR, R. H. 1993a. Mutations in Cu/Zn superoxide dismutase gene are associated with familial amyotrophic lateral sclerosis. *Nature,* 362**,** 59.

ROSEN, D. R., SIDDIQUE, T., PATTERSON, D., FIGLEWICZ, D. A., SAPP, P., HENTATI, A., DONALDSON, D., GOTO, J., O'REGAN, J. P., DENG, H. X. & ET AL. 1993b. Mutations in Cu/Zn superoxide dismutase gene are associated with familial amyotrophic lateral sclerosis. *Nature,* 362**,** 59-62.

RÖSLER, K. M., TRUFFERT, A., HESS, C. W. & MAGISTRIS, M. R. 2000. Quantification of upper motor neuron loss in amyotrophic lateral sclerosis. *Clinical Neurophysiology,* 111**,** 2208-2218.

ROSSAERT, E., POLLARI, E., JASPERS, T., VAN HELLEPUTTE, L., JARPE, M., VAN DAMME, P., DE BOCK, K., MOISSE, M. & VAN DEN BOSCH, L. 2019. Restoration of histone acetylation ameliorates disease and metabolic abnormalities in a FUS mouse model. *Acta Neuropathologica Communications,* 7**,** 107.

ROSSI, D., BRAMBILLA, L., VALORI, C. F., RONCORONI, C., CRUGNOLA, A., YOKOTA, T., BREDESEN, D. E. & VOLTERRA, A. 2008. Focal degeneration of astrocytes in amyotrophic lateral sclerosis. *Cell Death & Differentiation,* 15**,** 1691-1700.

ROTHSTEIN, J. D., MARTIN, L. J. & KUNCL, R. W. 1992. Decreased glutamate transport by the brain and spinal cord in amyotrophic lateral sclerosis. *N Engl J Med,* 326**,** 1464-8.

ROTHSTEIN, J. D., VAN KAMMEN, M., LEVEY, A. I., MARTIN, L. J. & KUNCL, R. W. 1995. Selective loss of glial glutamate transporter GLT-1 in amyotrophic lateral sclerosis. *Annals of Neurology,* 38**,** 73-84.

RUSS, W. P. & ENGELMAN, D. M. 2000. The GxxxG motif: A framework for transmembrane helix-helix association11Edited by G. von Heijne. *Journal of Molecular Biology,* 296**,** 911-919.

RUSTAY, N. R., WAHLSTEN, D. & CRABBE, J. C. 2003. Influence of task parameters on rotarod performance and sensitivity to ethanol in mice. *Behavioural Brain Research,* 141**,** 237-249.

RUTHERFORD, N. J., ZHANG, Y.-J., BAKER, M., GASS, J. M., FINCH, N. A., XU, Y.-F., STEWART, H., KELLEY, B. J., KUNTZ, K., CROOK, R. J. P., SREEDHARAN, J., VANCE, C., SORENSON, E., LIPPA, C., BIGIO, E. H., GESCHWIND, D. H., KNOPMAN, D. S., MITSUMOTO, H., PETERSEN, R. C., CASHMAN, N. R., HUTTON, M., SHAW, C. E., BOYLAN, K. B., BOEVE, B., GRAFF-RADFORD, N. R., WSZOLEK, Z. K., CASELLI, R. J., DICKSON, D. W., MACKENZIE, I. R., PETRUCELLI, L. & RADEMAKERS, R. 2008. Novel mutations in TARDBP (TDP-43) in patients with familial amyotrophic lateral sclerosis. *PLoS genetics,* 4**,** e1000193-e1000193.

SABATELLI, M., CONTE, A. & ZOLLINO, M. 2013. Clinical and genetic heterogeneity of amyotrophic lateral sclerosis. *Clinical Genetics,* 83**,** 408-416.

SAHADEVAN, S., HEMBACH, K. M., TANTARDINI, E., PÉREZ-BERLANGA, M., HRUSKA-PLOCHAN, M., MEGAT, S., WEBER, J., SCHWARZ, P., DUPUIS, L., ROBINSON, M. D., DE ROSSI, P. &

POLYMENIDOU, M. 2021. Synaptic FUS accumulation triggers early misregulation of synaptic RNAs in a mouse model of ALS. *Nature Communications,* 12**,** 3027.

SAIJO, K., WINNER, B., CARSON, C. T., COLLIER, J. G., BOYER, L., ROSENFELD, M. G., GAGE, F. H. & GLASS, C. K. 2009. A Nurr1/CoREST Pathway in Microglia and Astrocytes Protects Dopaminergic Neurons from Inflammation-Induced Death. *Cell,* 137**,** 47-59.

SANJAK, M., LANGFORD, V., HOLSTEN, S., ROZARIO, N., PATTERSON, C. G. M., BRAVVER, E., BOCKENEK, W. L. & BROOKS, B. R. 2017. Six-Minute Walk Test as a Measure of Walking Capacity in Ambulatory Individuals With Amyotrophic Lateral Sclerosis. *Archives of Physical Medicine and Rehabilitation,* 98**,** 2301-2307.

SAROFF, D., DELFS, J., KUZNETSOV, D. & GEULA, C. 2000. Selective vulnerability of spinal cord motor neurons to non-NMDA toxicity. *Neuroreport,* 11**,** 1117-21.

SASAKI, S., KOMORI, T. & IWATA, M. 2000a. Excitatory amino acid transporter 1 and 2 immunoreactivity in the spinal cord in amyotrophic lateral sclerosis. *Acta Neuropathologica,* 100**,** 138-144.

SASAKI, S., SHIBATA, N., KOMORI, T. & IWATA, M. 2000b. iNOS and nitrotyrosine immunoreactivity in amyotrophic lateral sclerosis. *Neuroscience Letters,* 291**,** 44-48.

SATTLER, T. & MAYER, A. 2000. Cell-free reconstitution of microautophagic vacuole invagination and vesicle formation. *J Cell Biol,* 151**,** 529-38.

SCEKIC-ZAHIROVIC, J., SENDSCHEID, O., EL OUSSINI, H., JAMBEAU, M., SUN, Y., MERSMANN, S., WAGNER, M., DIETERLÉ, S., SINNIGER, J., DIRRIG-GROSCH, S., DRENNER, K., BIRLING, M.-C., QIU, J., ZHOU, Y., LI, H., FU, X.-D., ROUAUX, C., SHELKOVNIKOVA, T., WITTING, A., LUDOLPH, A. C., KIEFER, F., STORKEBAUM, E., LAGIER-TOURENNE, C. & DUPUIS, L. 2016. Toxic gain of function from mutant FUS protein is crucial to trigger cell autonomous motor neuron loss. *The EMBO Journal,* 35**,** 1077-1097.

SCHIFFER, D., CORDERA, S., CAVALLA, P. & MIGHELI, A. 1996. Reactive astrogliosis of the spinal cord in amyotrophic lateral sclerosis. *Journal of the Neurological Sciences,* 139**,** 27-33.

SCHINDELIN, J., ARGANDA-CARRERAS, I., FRISE, E., KAYNIG, V., LONGAIR, M., PIETZSCH, T., PREIBISCH, S., RUEDEN, C., SAALFELD, S., SCHMID, B., TINEVEZ, J.-Y., WHITE, D. J., HARTENSTEIN, V., ELICEIRI, K., TOMANCAK, P. & CARDONA, A. 2012. Fiji: an open-source platform for biological-image analysis. *Nature Methods,* 9**,** 676-682.

SCHUBERT, U., ANTÓN, L. C., GIBBS, J., NORBURY, C. C., YEWDELL, J. W. & BENNINK, J. R. 2000. Rapid degradation of a large fraction of newly synthesized proteins by proteasomes. *Nature,* 404**,** 770-774.

SEGATTO, M., TRAPANI, L., DI TUNNO, I., STICOZZI, C., VALACCHI, G., HAYEK, J. & PALLOTTINI, V. 2014. Cholesterol Metabolism Is Altered in Rett Syndrome: A Study on Plasma and Primary Cultured Fibroblasts Derived from Patients. *PLOS ONE,* 9**,** e104834.

SENGUPTA, P. 2011. A scientific review of age determination for a laboratory rat: how old is it in comparison with human age. *Biomed Int,* 2**,** 81-89.

SENGUPTA, P. 2013. The Laboratory Rat: Relating Its Age With Human's. *International journal of preventive medicine,* 4**,** 624-630.

SHAN, X., CHIANG, P. M., PRICE, D. L. & WONG, P. C. 2010. Altered distributions of Gemini of coiled bodies and mitochondria in motor neurons of TDP-43 transgenic mice. *Proc Natl Acad Sci U S A,* 107**,** 16325-30.

SHANKAR, G. M., LI, S., MEHTA, T. H., GARCIA-MUNOZ, A., SHEPARDSON, N. E., SMITH, I., BRETT, F. M., FARRELL, M. A., ROWAN, M. J., LEMERE, C. A., REGAN, C. M., WALSH, D. M., SABATINI, B. L. & SELKOE, D. J. 2008. Amyloid-beta protein dimers isolated directly

from Alzheimer's brains impair synaptic plasticity and memory. *Nature medicine,* 14**,** 837-842.

SHAO, Q., LIANG, C., CHANG, Q., ZHANG, W., YANG, M. & CHEN, J.-F. 2019. C9orf72 deficiency promotes motor deficits of a C9ALS/FTD mouse model in a dose-dependent manner. *Acta neuropathologica communications,* 7**,** 1-3.

SHAO, Y., LI, T., LIU, Z., WANG, X., XU, X., LI, S., XU, G. & LE, W. 2021. Comprehensive metabolic profiling of Parkinson's disease by liquid chromatography-mass spectrometry. *Molecular Neurodegeneration,* 16**,** 4.

SHARMA, A., LYASHCHENKO, A. K., LU, L., NASRABADY, S. E., ELMALEH, M., MENDELSOHN, M., NEMES, A., TAPIA, J. C., MENTIS, G. Z. & SHNEIDER, N. A. 2016. ALS-associated mutant FUS induces selective motor neuron degeneration through toxic gain of function. *Nature communications,* 7**,** 10465-10465.

SHAW, P. J., INCE, P. G., FALKOUS, G. & MANTLE, D. 1995. Oxidative damage to protein in sporadic motor neuron disease spinal cord. *Annals of Neurology,* 38**,** 691-695.

SHEFNER, J. M., AL-CHALABI, A., BAKER, M. R., CUI, L.-Y., DE CARVALHO, M., EISEN, A., GROSSKREUTZ, J., HARDIMAN, O., HENDERSON, R., MATAMALA, J. M., MITSUMOTO, H., PAULUS, W., SIMON, N., SWASH, M., TALBOT, K., TURNER, M. R., UGAWA, Y., VAN DEN BERG, L. H., VERDUGO, R., VUCIC, S., KAJI, R., BURKE, D. & KIERNAN, M. C. 2020. A proposal for new diagnostic criteria for ALS. *Clinical Neurophysiology,* 131**,** 1975-1978.

SHEIKHBAHAEI, S., MORRIS, B., COLLINA, J., ANJUM, S., ZNATI, S., GAMARRA, J., ZHANG, R., GOURINE, A. V. & SMITH, J. C. 2018. Morphometric analysis of astrocytes in brainstem respiratory regions. *Journal of Comparative Neurology,* 526**,** 2032-2047.

SHIMIZU, T., NAKAYAMA, Y., MATSUDA, C., HARAGUCHI, M., BOKUDA, K., ISHIKAWA-TAKATA, K., KAWATA, A. & ISOZAKI, E. 2019. Prognostic significance of body weight variation after diagnosis in ALS: a single-centre prospective cohort study. *Journal of Neurology,* 266**,** 1412-1420.

SHOENFELD, L., WESTENBROEK, R. E., FISHER, E., QUINLAN, K. A., TYSSELING, V. M., POWERS, R. K., HECKMAN, C. J. & BINDER, M. D. 2014. Soma size and Cav1.3 channel expression in vulnerable and resistant motoneuron populations of the SOD1G93A mouse model of ALS. *Physiological Reports,* 2**,** e12113.

SIERRA, A., ENCINAS, J. M., DEUDERO, J. J. P., CHANCEY, J. H., ENIKOLOPOV, G., OVERSTREET-WADICHE, L. S., TSIRKA, S. E. & MALETIC-SAVATIC, M. 2010. Microglia Shape Adult Hippocampal Neurogenesis through Apoptosis-Coupled Phagocytosis. *Cell Stem Cell,* 7**,** 483-495.

SILBERNAGEL, N., WALECKI, M., SCHÄFER, M. K.-H., KESSLER, M., ZOBEIRI, M., RINNÉ, S., KIPER, A. K., KOMADOWSKI, M. A., VOWINKEL, K. S., WEMHÖNER, K., FORTMÜLLER, L., SCHEWE, M., DOLGA, A. M., SCEKIC-ZAHIROVIC, J., MATSCHKE, L. A., CULMSEE, C., BAUKROWITZ, T., MONASSIER, L., ULLRICH, N. D., DUPUIS, L., JUST, S., BUDDE, T., FABRITZ, L. & DECHER, N. 2018. The VAMP-associated protein VAPB is required for cardiac and neuronal pacemaker channel function. *The FASEB Journal,* 32**,** 6159-6173.

SIMONEAU, S., REZAEI, H., SALÈS, N., KAISER-SCHULZ, G., LEFEBVRE-ROQUE, M., VIDAL, C., FOURNIER, J. G., COMTE, J., WOPFNER, F., GROSCLAUDE, J., SCHÄTZL, H. & LASMÉZAS, C. I. 2007. In vitro and in vivo neurotoxicity of prion protein oligomers. *PLoS Pathog,* 3**,** e125.

SIMPSON, C. F. & KLING, J. M. 1967. The mechanism of denucleation in circulating erythroblasts. *J Cell Biol,* 35**,** 237-45.

SINGER, M. A., KOJAN, S., BAROHN, R. J., HERBELIN, L., NATIONS, S. P., TRIVEDI, J. R., JACKSON, C. E., BURNS, D. K., BOYER, P. J. & WOLFE, G. I. 2005. Primary Lateral Sclerosis: Clinical and Laboratory Features in 25 Patients. *Journal of Clinical Neuromuscular Disease,* 7.

SINGER, M. A., STATLAND, J. M., WOLFE, G. I. & BAROHN, R. J. 2007. Primary lateral sclerosis. *Muscle & Nerve,* 35**,** 291-302.

SINGH, N., RAY, S. & SRIVASTAVA, A. 2018. Clinical Mimickers of Amyotrophic Lateral Sclerosis-Conditions We Cannot Afford to Miss. *Annals of Indian Academy of Neurology,* 21**,** 173-178.

SKEHEL, P., MARTIN, K., KANDEL, E. & BARTSCH, D. 1995. A VAMP-binding protein from Aplysia required for neurotransmitter release. *Science,* 269**,** 1580-1583.

SKEHEL, P. A., FABIAN-FINE, R. & KANDEL, E. R. 2000. Mouse VAP33 is associated with the endoplasmic reticulum and microtubules. *Proceedings of the National Academy of Sciences of the United States of America,* 97**,** 1101-1106.

SKUTELSKY, E. & DANON, D. 1967. An electron microscopic study of nuclear elimination from the late erythroblast. *The Journal of cell biology,* 33**,** 625-635.

SKUTELSKY, E. & DANON, D. 1970. Comparative study of nuclear expulsion from the late erythroblast and cytokinesis. *Exp Cell Res,* 60**,** 427-36.

SMITH, D. B. & JOHNSON, K. S. 1988. Single-step purification of polypeptides expressed in Escherichia coli as fusions with glutathione S-transferase. *Gene,* 67**,** 31-40.

SMITH, E. R., STEFANICK, M. L., CLARK, J. T. & DAVIDSON, J. M. 1992. Hormones and sexual behavior in relationship to aging in male rats. *Hormones and Behavior,* 26**,** 110-135.

SONNEWALD, U., WESTERGAARD, N., PETERSEN, S. B., UNSGÅRD, G. & SCHOUSBOE, A. 1993. Metabolism of [U-13C]Glutamate in Astrocytes Studied by 13C NMR Spectroscopy: Incorporation of More Label into Lactate than into Glutamine Demonstrates the Importance of the Tricarboxylic Acid Cycle. *Journal of Neurochemistry,* 61**,** 1179-1182.

SORENSON, E. J., STALKER, A. P., KURLAND, L. T. & WINDEBANK, A. J. 2002. Amyotrophic lateral sclerosis in Olmsted County, Minnesota, 1925 to 1998. *Neurology,* 59**,** 280-282.

SOREQ, L., ROSE, J., SOREQ, E., HARDY, J., TRABZUNI, D., COOKSON, M. R., SMITH, C., RYTEN, M., PATANI, R. & ULE, J. 2017. Major Shifts in Glial Regional Identity Are a Transcriptional Hallmark of Human Brain Aging. *Cell Rep,* 18**,** 557-570.

SPILLER, K. J., RESTREPO, C. R., KHAN, T., DOMINIQUE, M. A., FANG, T. C., CANTER, R. G., ROBERTS, C. J., MILLER, K. R., RANSOHOFF, R. M., TROJANOWSKI, J. Q. & LEE, V. M. Y. 2018. Microglia-mediated recovery from ALS-relevant motor neuron degeneration in a mouse model of TDP-43 proteinopathy. *Nature neuroscience,* 21**,** 329-340.

SREEDHARAN, J., BLAIR, I. P., TRIPATHI, V. B., HU, X., VANCE, C., ROGELJ, B., ACKERLEY, S., DURNALL, J. C., WILLIAMS, K. L., BURATTI, E., BARALLE, F., DE BELLEROCHE, J., MITCHELL, J. D., LEIGH, P. N., AL-CHALABI, A., MILLER, C. C., NICHOLSON, G. & SHAW, C. E. 2008. TDP-43 mutations in familial and sporadic amyotrophic lateral sclerosis. *Science (New York, N.Y.),* 319**,** 1668-1672.

STALLINGS, N. R., PUTTAPARTHI, K., DOWLING, K. J., LUTHER, C. M., BURNS, D. K., DAVIS, K. & ELLIOTT, J. L. 2013. TDP-43, an ALS linked protein, regulates fat deposition and glucose homeostasis. *PloS one,* 8**,** e71793-e71793.

STEPPAN, S., ADKINS, R. & ANDERSON, J. 2004. Phylogeny and divergence-date estimates of rapid radiations in muroid rodents based on multiple nuclear genes. *Syst Biol,* 53**,** 533-53.

STEVENTON, J. J., TRUEMAN, R. C., MA, D., YHNELL, E., BAYRAM-WESTON, Z., MODAT, M., CARDOSO, J., OURSELIN, S., LYTHGOE, M., STEWART, A., ROSSER, A. E. & JONES, D. K.

2016. Longitudinal in vivo MRI in a Huntington's disease mouse model: Global atrophy in the absence of white matter microstructural damage. *Scientific Reports,* 6**,** 32423.

STEYN, F. J., IOANNIDES, Z. A., VAN EIJK, R. P. A., HEGGIE, S., THORPE, K. A., CESLIS, A., HESHMAT, S., HENDERS, A. K., WRAY, N. R., VAN DEN BERG, L. H., HENDERSON, R. D., MCCOMBE, P. A. & NGO, S. T. 2018. Hypermetabolism in ALS is associated with greater functional decline and shorter survival. *Journal of Neurology, Neurosurgery & Psychiatry,* 89**,** 1016-1023.

STOCKER, H., NABERS, A., PERNA, L., MÖLLERS, T., RUJESCU, D., HARTMANN, A., HOLLECZEK, B., SCHÖTTKER, B., GERWERT, K. & BRENNER, H. 2020. Prediction of Alzheimer's disease diagnosis within 14 years through Aβ misfolding in blood plasma compared to APOE4 status, and other risk factors. *Alzheimer's & Dementia,* 16**,** 283-291.

STOICA, R., DE VOS, K. J., PAILLUSSON, S., MUELLER, S., SANCHO, R. M., LAU, K.-F., VIZCAY-BARRENA, G., LIN, W.-L., XU, Y.-F., LEWIS, J., DICKSON, D. W., PETRUCELLI, L., MITCHELL, J. C., SHAW, C. E. & MILLER, C. C. J. 2014a. ER-mitochondria associations are regulated by the VAPB-PTPIP51 interaction and are disrupted by ALS/FTD-associated TDP-43. *Nature communications,* 5**,** 3996-3996.

STOICA, R., DE VOS, K. J., PAILLUSSON, S., MUELLER, S., SANCHO, R. M., LAU, K.-F., VIZCAY-BARRENA, G., LIN, W.-L., XU, Y.-F., LEWIS, J., DICKSON, D. W., PETRUCELLI, L., MITCHELL, J. C., SHAW, C. E. & MILLER, C. C. J. 2014b. ER–mitochondria associations are regulated by the VAPB–PTPIP51 interaction and are disrupted by ALS/FTD-associated TDP-43. *Nature Communications,* 5**,** 3996.

STOICA, R., PAILLUSSON, S., GOMEZ-SUAGA, P., MITCHELL, J. C., LAU, D. H., GRAY, E. H., SANCHO, R. M., VIZCAY-BARRENA, G., DE VOS, K. J., SHAW, C. E., HANGER, D. P., NOBLE, W. & MILLER, C. C. 2016. ALS/FTD-associated FUS activates GSK-3β to disrupt the VAPB-PTPIP51 interaction and ER-mitochondria associations. *EMBO reports,* 17**,** 1326-1342.

STORKEBAUM, E., LAMBRECHTS, D., DEWERCHIN, M., MORENO-MURCIANO, M.-P., APPELMANS, S., OH, H., VAN DAMME, P., RUTTEN, B., MAN, W. Y., DE MOL, M., WYNS, S., MANKA, D., VERMEULEN, K., VAN DEN BOSCH, L., MERTENS, N., SCHMITZ, C., ROBBERECHT, W., CONWAY, E. M., COLLEN, D., MOONS, L. & CARMELIET, P. 2005. Treatment of motoneuron degeneration by intracerebroventricular delivery of VEGF in a rat model of ALS. *Nature Neuroscience,* 8**,** 85-92.

STRIBL, C., SAMARA, A., TRÜMBACH, D., PEIS, R., NEUMANN, M., FUCHS, H., GAILUS-DURNER, V., HRABĚ DE ANGELIS, M., RATHKOLB, B., WOLF, E., BECKERS, J., HORSCH, M., NEFF, F., KREMMER, E., KOOB, S., REICHERT, A. S., HANS, W., ROZMAN, J., KLINGENSPOR, M., AICHLER, M., WALCH, A. K., BECKER, L., KLOPSTOCK, T., GLASL, L., HÖLTER, S. M., WURST, W. & FLOSS, T. 2014. Mitochondrial dysfunction and decrease in body weight of a transgenic knock-in mouse model for TDP-43. *J Biol Chem,* 289**,** 10769-10784.

STROMBERG, P. C., KOCIBA, G. J., GRANTS, I. S., KRAKOWKA, G. S., RINEHART, J. J. & MEZZA, L. E. 1990. Spleen Cell Population Changes and Hemolytic Anemia in F344 Rats with Large Granular Lymphocyte Leukemia. *Veterinary Pathology,* 27**,** 397-403.

STROMBERG, P. C. & VOGTSBERGER, L. M. 1983. Pathology of the mononuclear cell leukemia of Fischer rats. I. Morphologic studies. *Vet Pathol,* 20**,** 698-708.

STROMBERG, P. C., VOGTSBERGER, L. M., MARSH, L. R. & WILSON, F. D. 1983. Pathology of the Mononuclear Cell Leukemia of Fischer Rats. II. Hematology. *Veterinary Pathology,* 20**,** 709-717.

SUGARMAN, E. A., NAGAN, N., ZHU, H., AKMAEV, V. R., ZHOU, Z., ROHLFS, E. M., FLYNN, K., HENDRICKSON, B. C., SCHOLL, T. & SIRKO-OSADSA, D. A. 2012. Pan-ethnic carrier screening and prenatal diagnosis for spinal muscular atrophy: clinical laboratory analysis of> 72 400 specimens. *European journal of human genetics,* 20**,** 27-32.

SUN, Y.-M., DONG, Y., WANG, J., LU, J.-H., CHEN, Y. & WU, J.-J. 2017. A novel mutation of VAPB in one Chinese familial amyotrophic lateral sclerosis pedigree and its clinical characteristics. *Journal of Neurology,* 264**,** 2387-2393.

SUZUKI, K., KIRISAKO, T., KAMADA, Y., MIZUSHIMA, N., NODA, T. & OHSUMI, Y. 2001. The pre-autophagosomal structure organized by concerted functions of APG genes is essential for autophagosome formation. *The EMBO Journal,* 20**,** 5971-5981.

SWINDELL, W. R., KRUSE, C. P. S., LIST, E. O., BERRYMAN, D. E. & KOPCHICK, J. J. 2019. ALS blood expression profiling identifies new biomarkers, patient subgroups, and evidence for neutrophilia and hypoxia. *Journal of Translational Medicine,* 17**,** 170.

SWOBODA, K. J., PRIOR, T. W., SCOTT, C. B., MCNAUGHT, T. P., WRIDE, M. C., REYNA, S. P. & BROMBERG, M. B. 2005. Natural history of denervation in SMA: relation to age, SMN2 copy number, and function. *Annals of Neurology: Official Journal of the American Neurological Association and the Child Neurology Society,* 57**,** 704-712.

SZEBÉNYI, K., WENGER, L. M. D., SUN, Y., DUNN, A. W. E., LIMEGROVER, C. A., GIBBONS, G. M., CONCI, E., PAULSEN, O., MIERAU, S. B., BALMUS, G. & LAKATOS, A. 2021. Human ALS/FTD brain organoid slice cultures display distinct early astrocyte and targetable neuronal pathology. *Nature Neuroscience,* 24**,** 1542-1554.

TAGASHIRA, H., SHINODA, Y., SHIODA, N. & FUKUNAGA, K. 2014. Methyl pyruvate rescues mitochondrial damage caused by SIGMAR1 mutation related to amyotrophic lateral sclerosis. *Biochimica et Biophysica Acta (BBA) - General Subjects,* 1840**,** 3320-3334.

TAM, O. H., ROZHKOV, N. V., SHAW, R., KIM, D., HUBBARD, I., FENNESSEY, S., PROPP, N., CONSORTIUM, N. A., FAGEGALTIER, D., HARRIS, B. T., OSTROW, L. W., PHATNANI, H., RAVITS, J., DUBNAU, J. & GALE HAMMELL, M. 2019. Postmortem Cortex Samples Identify Distinct Molecular Subtypes of ALS: Retrotransposon Activation, Oxidative Stress, and Activated Glia. *Cell reports,* 29**,** 1164-1177.e5.

TAN, C. F., EGUCHI, H., TAGAWA, A., ONODERA, O., IWASAKI, T., TSUJINO, A., NISHIZAWA, M., KAKITA, A. & TAKAHASHI, H. 2007. TDP-43 immunoreactivity in neuronal inclusions in familial amyotrophic lateral sclerosis with or without SOD1 gene mutation. *Acta Neuropathol,* 113**,** 535-42.

TARNARIS, A., TOMA, A. K., CHAPMAN, M. D., PETZOLD, A., KEIR, G., KITCHEN, N. D. & WATKINS, L. D. 2011. Rostrocaudal dynamics of CSF biomarkers. *Neurochem Res,* 36**,** 528-32.

TARTAGLIA, M. C., ROWE, A., FINDLATER, K., ORANGE, J. B., GRACE, G. & STRONG, M. J. 2007. Differentiation Between Primary Lateral Sclerosis and Amyotrophic Lateral Sclerosis: Examination of Symptoms and Signs at Disease Onset and During Follow-up. *Archives of Neurology,* 64**,** 232-236.

TEULING, E., AHMED, S., HAASDIJK, E., DEMMERS, J., STEINMETZ, M. O., AKHMANOVA, A., JAARSMA, D. & HOOGENRAAD, C. C. 2007. Motor Neuron Disease-Associated Mutant Vesicle-Associated Membrane Protein-Associated Protein (VAP) B Recruits Wild-Type VAPs into Endoplasmic Reticulum-Derived Tubular Aggregates. *The Journal of Neuroscience,* 27**,** 9801-9815.

THOMSEN, G. M., GOWING, G., LATTER, J., CHEN, M., VIT, J.-P., STAGGENBORG, K., AVALOS, P., ALKASLASI, M., FERRAIUOLO, L. & LIKHITE, S. 2014. Delayed disease onset and

extended survival in the SOD1G93A rat model of amyotrophic lateral sclerosis after suppression of mutant SOD1 in the motor cortex. *Journal of Neuroscience,* 34**,** 15587-15600.

THONHOFF, J. R., JORDAN, P. M., KARAM, J. R., BASSETT, B. L. & WU, P. 2007. Identification of early disease progression in an ALS rat model. *Neurosci Lett,* 415**,** 264-8.

TONG, J., HUANG, C., BI, F., WU, Q., HUANG, B., LIU, X., LI, F., ZHOU, H. & XIA, X. G. 2013. Expression of ALS-linked TDP-43 mutant in astrocytes causes non-cell-autonomous motor neuron death in rats. *Embo j,* 32**,** 1917-26.

TRILICO, M. L. C., LORENZONI, P. J., KAY, C. S. K., DUCCI, R. D. P., FUSTES, O. J. H., WERNECK, L. C. & SCOLA, R. H. 2020. Characterization of the amyotrophic lateral sclerosis-linked P56S mutation of the VAPB gene in Southern Brazil. *Amyotroph Lateral Scler Frontotemporal Degener,* 21**,** 286-290.

TRIPATHI, P., GUO, H., DRESER, A., YAMOAH, A., SECHI, A., JESSE, C. M., KATONA, I., DOUKAS, P., NIKOLIN, S., ERNST, S., ARONICA, E., GLAß, H., HERMANN, A., STEINBUSCH, H., FELLER, A. C., BERGMANN, M., JAARSMA, D., WEIS, J. & GOSWAMI, A. 2021a. Pathomechanisms of ALS8: altered autophagy and defective RNA binding protein (RBP) homeostasis due to the VAPB P56S mutation. *Cell Death & Disease,* 12**,** 466.

TRIPATHI, P., GUO, H., DRESER, A., YAMOAH, A., SECHI, A., JESSE, C. M., KATONA, I., DOUKAS, P., NIKOLIN, S., ERNST, S., ARONICA, E., GLAß, H., HERMANN, A., STEINBUSCH, H., FELLER, A. C., BERGMANN, M., JAARSMA, D., WEIS, J. & GOSWAMI, A. 2021b. Pathomechanisms of ALS8: altered autophagy and defective RNA binding protein (RBP) homeostasis due to the VAPB P56S mutation. *Cell death & disease,* 12**,** 466-466.

TRIPATHI, P., RODRIGUEZ-MUELA, N., KLIM, J. R., DE BOER, A. S., AGRAWAL, S., SANDOE, J., LOPES, C. S., OGLIARI, K. S., WILLIAMS, L. A., SHEAR, M., RUBIN, L. L., EGGAN, K. & ZHOU, Q. 2017. Reactive Astrocytes Promote ALS-like Degeneration and Intracellular Protein Aggregation in Human Motor Neurons by Disrupting Autophagy through TGF-β1. *Stem Cell Reports,* 9**,** 667-680.

TROTTI, D., ROSSI, D., GJESDAL, O., LEVY, L. M., RACAGNI, G., DANBOLT, N. C. & VOLTERRA, A. 1996. Peroxynitrite inhibits glutamate transporter subtypes. *J Biol Chem,* 271**,** 5976-9.

TSUDA, H., HAN, S. M., YANG, Y., TONG, C., LIN, Y. Q., MOHAN, K., HAUETER, C., ZOGHBI, A., HARATI, Y., KWAN, J., MILLER, M. A. & BELLEN, H. J. 2008. The Amyotrophic Lateral Sclerosis 8 protein VAPB is cleaved, secreted, and acts as a ligand for Eph receptors. *Cell,* 133**,** 963-977.

TUDOR, E. L., GALTREY, C. M., PERKINTON, M. S., LAU, K. F., DE VOS, K. J., MITCHELL, J. C., ACKERLEY, S., HORTOBÁGYI, T., VÁMOS, E., LEIGH, P. N., KLASEN, C., MCLOUGHLIN, D. M., SHAW, C. E. & MILLER, C. C. J. 2010. Amyotrophic lateral sclerosis mutant vesicle-associated membrane protein-associated protein-B transgenic mice develop TAR-DNA-binding protein-43 pathology. *Neuroscience,* 167**,** 774-785.

TURNER, M. R., BAROHN, R. J., CORCIA, P., FINK, J. K., HARMS, M. B., KIERNAN, M. C., RAVITS, J., SILANI, V., SIMMONS, Z., STATLAND, J., VAN DEN BERG, L. H. & MITSUMOTO, H. 2020. Primary lateral sclerosis: consensus diagnostic criteria. *Journal of Neurology, Neurosurgery & Psychiatry,* 91**,** 373-377.

TURNER, M. R., HARDIMAN, O., BENATAR, M., BROOKS, B. R., CHIO, A., DE CARVALHO, M., INCE, P. G., LIN, C., MILLER, R. G., MITSUMOTO, H., NICHOLSON, G., RAVITS, J., SHAW, P. J., SWASH, M., TALBOT, K., TRAYNOR, B. J., VAN DEN BERG, L. H., VELDINK, J. H., VUCIC, S. & KIERNAN, M. C. 2013. Controversies and priorities in amyotrophic lateral sclerosis. *The Lancet Neurology,* 12**,** 310-322.

TURRENS, J. F. 2003. Mitochondrial formation of reactive oxygen species. *J Physiol,* 552**,** 335-44.

TZIORTZOUDA, P., VAN DEN BOSCH, L. & HIRTH, F. 2021. Triad of TDP43 control in neurodegeneration: autoregulation, localization and aggregation. *Nature Reviews Neuroscience,* 22**,** 197-208.

UYSAL, H., BILGE, U., İLHANLI, N., GROMICHO, M., GROSSKREUTZ, J., KUZMA-KOZAKIEWICZ, M., PINTO, S., PETRI, S., SZACKA, K., NIEPORECKI, K. & DE CARVALHO, M. 2021. ALS and fertility: does ALS affect number of children patients have? *Amyotroph Lateral Scler Frontotemporal Degener,* 22**,** 94-100.

VAN BLITTERSWIJK, M., DEJESUS-HERNANDEZ, M., NIEMANTSVERDRIET, E., MURRAY, M. E., HECKMAN, M. G., DIEHL, N. N., BROWN, P. H., BAKER, M. C., FINCH, N. A. & BAUER, P. O. 2013. Association between repeat sizes and clinical and pathological characteristics in carriers of C9ORF72 repeat expansions (Xpansize-72): a cross-sectional cohort study. *The Lancet Neurology,* 12**,** 978-988.

VAN BLITTERSWIJK, M., VAN ES, M. A., HENNEKAM, E. A., DOOIJES, D., VAN RHEENEN, W., MEDIC, J., BOURQUE, P. R., SCHELHAAS, H. J., VAN DER KOOI, A. J., DE VISSER, M., DE BAKKER, P. I., VELDINK, J. H. & VAN DEN BERG, L. H. 2012a. Evidence for an oligogenic basis of amyotrophic lateral sclerosis. *Hum Mol Genet,* 21**,** 3776-84.

VAN BLITTERSWIJK, M., VAN ES, M. A., KOPPERS, M., VAN RHEENEN, W., MEDIC, J., SCHELHAAS, H. J., VAN DER KOOI, A. J., DE VISSER, M., VELDINK, J. H. & VAN DEN BERG, L. H. 2012b. VAPB and C9orf72 mutations in 1 familial amyotrophic lateral sclerosis patient. *Neurobiology of Aging,* 33**,** 2950.e1-2950.e4.

VAN DAMME, P., BOGAERT, E., DEWIL, M., HERSMUS, N., KIRALY, D., SCHEVENEELS, W., BOCKX, I., BRAEKEN, D., VERPOORTEN, N., VERHOEVEN, K., TIMMERMAN, V., HERIJGERS, P., CALLEWAERT, G., CARMELIET, P., VAN DEN BOSCH, L. & ROBBERECHT, W. 2007. Astrocytes regulate GluR2 expression in motor neurons and their vulnerability to excitotoxicity. *Proceedings of the National Academy of Sciences of the United States of America,* 104**,** 14825-14830.

VAN GIJSEL-BONNELLO, M., BARANGER, K., BENECH, P., RIVERA, S., KHRESTCHATISKY, M., DE REGGI, M. & GHARIB, B. 2017. Metabolic changes and inflammation in cultured astrocytes from the 5xFAD mouse model of Alzheimer's disease: alleviation by pantethine. *PloS one,* 12**,** e0175369.

VANCE, C., ROGELJ, B., HORTOBÁGYI, T., DE VOS, K. J., NISHIMURA, A. L., SREEDHARAN, J., HU, X., SMITH, B., RUDDY, D. & WRIGHT, P. 2009a. Mutations in FUS, an RNA processing protein, cause familial amyotrophic lateral sclerosis type 6. *Science,* 323**,** 1208-1211.

VANCE, C., ROGELJ, B., HORTOBÁGYI, T., DE VOS, K. J., NISHIMURA, A. L., SREEDHARAN, J., HU, X., SMITH, B., RUDDY, D., WRIGHT, P., GANESALINGAM, J., WILLIAMS, K. L., TRIPATHI, V., AL-SARAJ, S., AL-CHALABI, A., LEIGH, P. N., BLAIR, I. P., NICHOLSON, G., DE BELLEROCHE, J., GALLO, J.-M., MILLER, C. C. & SHAW, C. E. 2009b. Mutations in FUS, an RNA processing protein, cause familial amyotrophic lateral sclerosis type 6. *Science (New York, N.Y.),* 323**,** 1208-1211.

VANDENBERGHE, W., ROBBERECHT, W. & BRORSON, J. R. 2000. AMPA receptor calcium permeability, GluR2 expression, and selective motoneuron vulnerability. *The Journal of neuroscience : the official journal of the Society for Neuroscience,* 20**,** 123-132.

VEJUX, A., NAMSI, A., NURY, T., MOREAU, T. & LIZARD, G. 2018. Biomarkers of Amyotrophic Lateral Sclerosis: Current Status and Interest of Oxysterols and Phytosterols. *Frontiers in molecular neuroscience,* 11**,** 12-12.

VERDONE, B. M., CICARDI, M. E., WEN, X., SRIRAMOJI, S., RUSSELL, K., MARKANDAIAH, S. S., JENSEN, B. K., KRISHNAMURTHY, K., HAEUSLER, A. R., PASINELLI, P. & TROTTI, D. 2022. A mouse model with widespread expression of the C9orf72-linked glycine–arginine dipeptide displays non-lethal ALS/FTD-like phenotypes. *Scientific Reports,* 12**,** 5644.

VERGOUTS, M., MARINANGELI, C., INGELBRECHT, C., GENARD, G., SCHAKMAN, O., STERNOTTE, A., CALAS, A.-G. & HERMANS, E. 2015. Early ALS-type gait abnormalities in AMP-dependent protein kinase-deficient mice suggest a role for this metabolic sensor in early stages of the disease. *Metabolic Brain Disease,* 30**,** 1369-1377.

VOLTERRA, A., TROTTI, D., TROMBA, C., FLORIDI, S. & RACAGNI, G. 1994. Glutamate uptake inhibition by oxygen free radicals in rat cortical astrocytes. *The Journal of neuroscience : the official journal of the Society for Neuroscience,* 14**,** 2924-2932.

WAKE, H., MOORHOUSE, A. J., JINNO, S., KOHSAKA, S. & NABEKURA, J. 2009. Resting microglia directly monitor the functional state of synapses in vivo and determine the fate of ischemic terminals. *J Neurosci,* 29**,** 3974-80.

WANG, J., FARR, G. W., HALL, D. H., LI, F., FURTAK, K., DREIER, L. & HORWICH, A. L. 2009. An ALS-Linked Mutant SOD1 Produces a Locomotor Defect Associated with Aggregation and Synaptic Dysfunction When Expressed in Neurons of Caenorhabditis elegans. *PLOS Genetics,* 5**,** e1000350.

WANG, W.-Y., PAN, L., SU, S. C., QUINN, E. J., SASAKI, M., JIMENEZ, J. C., MACKENZIE, I. R., HUANG, E. J. & TSAI, L.-H. 2013a. Interaction of FUS and HDAC1 regulates DNA damage response and repair in neurons. *Nature neuroscience,* 16**,** 1383-1391.

WANG, W., LI, L., LIN, W.-L., DICKSON, D. W., PETRUCELLI, L., ZHANG, T. & WANG, X. 2013b. The ALS disease-associated mutant TDP-43 impairs mitochondrial dynamics and function in motor neurons. *Human Molecular Genetics,* 22**,** 4706-4719.

WANG, Y., LI, L., HOU, C., LAI, Y., LONG, J., LIU, J., ZHONG, Q. & DIAO, J. 2016. SNARE-mediated membrane fusion in autophagy. *Seminars in cell & developmental biology,* 60**,** 97-104.

WANG, Y., YE, S., CHEN, L., TANG, L. & FAN, D. 2021. Loss of appetite in patients with amyotrophic lateral sclerosis is associated with weight loss and anxiety/depression. *Sci Rep,* 11**,** 9119.

WANNER, I. B., ANDERSON, M. A., SONG, B., LEVINE, J., FERNANDEZ, A., GRAY-THOMPSON, Z., AO, Y. & SOFRONIEW, M. V. 2013. Glial scar borders are formed by newly proliferated, elongated astrocytes that interact to corral inflammatory and fibrotic cells via STAT3-dependent mechanisms after spinal cord injury. *The Journal of neuroscience : the official journal of the Society for Neuroscience,* 33**,** 12870-12886.

WATKINS, J. A., ALIX, J. J. P., SHAW, P. J. & MEAD, R. J. 2021. Extensive phenotypic characterisation of a human TDP-43Q331K transgenic mouse model of amyotrophic lateral sclerosis (ALS). *Scientific Reports,* 11**,** 16659.

WEGORZEWSKA, I., BELL, S., CAIRNS, N. J., MILLER, T. M. & BALOH, R. H. 2009a. TDP-43 mutant transgenic mice develop features of ALS and frontotemporal lobar degeneration. *Proc Natl Acad Sci U S A,* 106**,** 18809-14.

WEGORZEWSKA, I., BELL, S., CAIRNS, N. J., MILLER, T. M. & BALOH, R. H. 2009b. TDP-43 mutant transgenic mice develop features of ALS and frontotemporal lobar degeneration. *Proceedings of the National Academy of Sciences,* 106**,** 18809-18814.

WEI, Q.-Q., CHEN, Y., CAO, B., OU, R. W., ZHANG, L., HOU, Y., GAO, X. & SHANG, H. 2017. Blood hemoglobin A1c levels and amyotrophic lateral sclerosis survival. *Molecular Neurodegeneration,* 12**,** 69.

WEINSTEIN, B. & SOLOMON, F. 1990. Phenotypic consequences of tubulin overproduction in Saccharomyces cerevisiae: differences between alpha-tubulin and beta-tubulin. *Molecular and cellular biology,* 10**,** 5295-5304.

WEIR, M. L., KLIP, A. & TRIMBLE, W. S. 1998. Identification of a human homologue of the vesicle-associated membrane protein (VAMP)-associated protein of 33 kDa (VAP-33): a broadly expressed protein that binds to VAMP. *Biochemical Journal,* 333**,** 247-251.

WEST, A. P., BRODSKY, I. E., RAHNER, C., WOO, D. K., ERDJUMENT-BROMAGE, H., TEMPST, P., WALSH, M. C., CHOI, Y., SHADEL, G. S. & GHOSH, S. 2011. TLR signalling augments macrophage bactericidal activity through mitochondrial ROS. *Nature,* 472**,** 476-480.

WHITE, M. A., KIM, E., DUFFY, A., ADALBERT, R., PHILLIPS, B. U., PETERS, O. M., STEPHENSON, J., YANG, S., MASSENZIO, F., LIN, Z., ANDREWS, S., SEGONDS-PICHON, A., METTERVILLE, J., SAKSIDA, L. M., MEAD, R., RIBCHESTER, R. R., BARHOMI, Y., SERRE, T., COLEMAN, M. P., FALLON, J. R., BUSSEY, T. J., BROWN, R. H., JR. & SREEDHARAN, J. 2018. TDP-43 gains function due to perturbed autoregulation in a Tardbp knock-in mouse model of ALS-FTD. *Nature neuroscience,* 21**,** 552-563.

WHITE, M. A., LIN, Z., KIM, E., HENSTRIDGE, C. M., PENA ALTAMIRA, E., HUNT, C. K., BURCHILL, E., CALLAGHAN, I., LORETO, A., BROWN-WRIGHT, H., MEAD, R., SIMMONS, C., CASH, D., COLEMAN, M. P. & SREEDHARAN, J. 2019. Sarm1 deletion suppresses TDP-43-linked motor neuron degeneration and cortical spine loss. *Acta neuropathologica communications,* 7**,** 166-166.

WILHELMSSON, U., BUSHONG, E. A., PRICE, D. L., SMARR, B. L., PHUNG, V., TERADA, M., ELLISMAN, M. H. & PEKNY, M. 2006. Redefining the concept of reactive astrocytes as cells that remain within their unique domains upon reaction to injury. *Proceedings of the National Academy of Sciences of the United States of America,* 103**,** 17513-17518.

WILHELMSSON, U., LI, L., PEKNA, M., BERTHOLD, C.-H., BLOM, S., ELIASSON, C., RENNER, O., BUSHONG, E., ELLISMAN, M., MORGAN, T. E. & PEKNY, M. 2004. Absence of Glial Fibrillary Acidic Protein and Vimentin Prevents Hypertrophy of Astrocytic Processes and Improves Post-Traumatic Regeneration. *The Journal of Neuroscience,* 24**,** 5016-5021.

WILS, H., KLEINBERGER, G., JANSSENS, J., PERESON, S., JORIS, G., CUIJT, I., SMITS, V., GROOTE, C. C.-D., BROECKHOVEN, C. V. & KUMAR-SINGH, S. 2010. TDP-43 transgenic mice develop spastic paralysis and neuronal inclusions characteristic of ALS and frontotemporal lobar degeneration. *Proceedings of the National Academy of Sciences,* 107**,** 3858-3863.

WINTON, M. J., IGAZ, L. M., WONG, M. M., KWONG, L. K., TROJANOWSKI, J. Q. & LEE, V. M. Y. 2008. Disturbance of Nuclear and Cytoplasmic TAR DNA-binding Protein (TDP-43) Induces Disease-like Redistribution, Sequestration, and Aggregate Formation *. *Journal of Biological Chemistry,* 283**,** 13302-13309.

WOLBURG, H., NOELL, S., WOLBURG-BUCHHOLZ, K., MACK, A. & FALLIER-BECKER, P. 2009. Agrin, Aquaporin-4, and Astrocyte Polarity as an Important Feature of the Blood-Brain Barrier. *The Neuroscientist,* 15**,** 180-193.

WONG, P. C., PARDO, C. A., BORCHELT, D. R., LEE, M. K., COPELAND, N. G., JENKINS, N. A., SISODIA, S. S., CLEVELAND, D. W. & PRICE, D. L. 1995. An adverse property of a familial ALS-linked SOD1 mutation causes motor neuron disease characterized by vacuolar degeneration of mitochondria. *Neuron,* 14**,** 1105-1116.

WU, L.-S., CHENG, W.-C. & SHEN, C.-K. J. 2012. Targeted depletion of TDP-43 expression in the spinal cord motor neurons leads to the development of amyotrophic lateral sclerosis-like phenotypes in mice. *Journal of Biological Chemistry,* 287**,** 27335-27344.

WU, Y. & KRISHNAN, S. 2009. Computer-aided analysis of gait rhythm fluctuations in amyotrophic lateral sclerosis. *Medical & Biological Engineering & Computing,* 47**,** 1165.

WYLES, J. P., MCMASTER, C. R. & RIDGWAY, N. D. 2002. Vesicle-associated Membrane Protein-associated Protein-A (VAP-A) Interacts with the Oxysterol-binding Protein to Modify Export from the Endoplasmic Reticulum. *Journal of Biological Chemistry,* 277**,** 29908-29918.

XU, T., RAMMNER, B., MARGITTAI, M., ARTALEJO, A. R., NEHER, E. & JAHN, R. 1999. Inhibition of SNARE Complex Assembly Differentially Affects Kinetic Components of Exocytosis. *Cell,* 99**,** 713-722.

XU, Y.-F., GENDRON, T. F., ZHANG, Y.-J., LIN, W.-L., D'ALTON, S., SHENG, H., CASEY, M. C., TONG, J., KNIGHT, J., YU, X., RADEMAKERS, R., BOYLAN, K., HUTTON, M., MCGOWAN, E., DICKSON, D. W., LEWIS, J. & PETRUCELLI, L. 2010. Wild-type human TDP-43 expression causes TDP-43 phosphorylation, mitochondrial aggregation, motor deficits, and early mortality in transgenic mice. *The Journal of neuroscience : the official journal of the Society for Neuroscience,* 30**,** 10851-10859.

XU, Y.-F., ZHANG, Y.-J., LIN, W.-L., CAO, X., STETLER, C., DICKSON, D. W., LEWIS, J. & PETRUCELLI, L. 2011. Expression of mutant TDP-43 induces neuronal dysfunction in transgenic mice. *Molecular neurodegeneration,* 6**,** 73-73.

YAMANAKA, K., CHUN, S. J., BOILLEE, S., FUJIMORI-TONOU, N., YAMASHITA, H., GUTMANN, D. H., TAKAHASHI, R., MISAWA, H. & CLEVELAND, D. W. 2008. Astrocytes as determinants of disease progression in inherited amyotrophic lateral sclerosis. *Nature neuroscience,* 11**,** 251-253.

YAMANAKA, T., NISHIYAMA, R., SHIMOGORI, T. & NUKINA, N. 2020. Proteomics-Based Approach Identifies Altered ER Domain Properties by ALS-Linked VAPB Mutation. *Scientific Reports,* 10**,** 7610.

YANG, C., WANG, H., QIAO, T., YANG, B., ALIAGA, L., QIU, L., TAN, W., SALAMEH, J., MCKENNA-YASEK, D. M., SMITH, T., PENG, L., MOORE, M. J., BROWN, R. H., JR., CAI, H. & XU, Z. 2014. Partial loss of TDP-43 function causes phenotypes of amyotrophic lateral sclerosis. *Proceedings of the National Academy of Sciences of the United States of America,* 111**,** E1121-E1129.

YASUDA, K., ZHANG, H., LOISELLE, D., HAYSTEAD, T., MACARA, I. G. & MILI, S. 2013. The RNA-binding protein Fus directs translation of localized mRNAs in APC-RNP granules. *Journal of Cell Biology,* 203**,** 737-746.

YOSHIDA, H., MATSUI, T., YAMAMOTO, A., OKADA, T. & MORI, K. 2001. XBP1 mRNA Is Induced by ATF6 and Spliced by IRE1 in Response to ER Stress to Produce a Highly Active Transcription Factor. *Cell,* 107**,** 881-891.

YOU, J. S., GELFANOVA, V., KNIERMAN, M. D., WITZMANN, F. A., WANG, M. & HALE, J. E. 2005. The impact of blood contamination on the proteome of cerebrospinal fluid. *Proteomics,* 5**,** 290-6.

YU, Y.-L., LI, H.-Y., ZHANG, P.-X., YIN, X.-F., HAN, N., KOU, Y.-H. & JIANG, B.-G. 2015. Comparison of commonly used retrograde tracers in rat spinal motor neurons. *Neural regeneration research,* 10**,** 1700-1705.

ZAMANIAN, J. L., XU, L., FOO, L. C., NOURI, N., ZHOU, L., GIFFARD, R. G. & BARRES, B. A. 2012. Genomic analysis of reactive astrogliosis. *The Journal of neuroscience : the official journal of the Society for Neuroscience,* 32**,** 6391-6410.

ZHANG, J. 2007. Proteomics of human cerebrospinal fluid – the good, the bad, and the ugly. *PROTEOMICS – Clinical Applications,* 1**,** 805-819.

ZHANG, J., XUE, R., ONG, W. Y. & CHEN, P. 2009. Roles of cholesterol in vesicle fusion and motion. *Biophys J,* 97**,** 1371-80.

ZHANG, R., GASCON, R., MILLER, R. G., GELINAS, D. F., MASS, J., HADLOCK, K., JIN, X., REIS, J., NARVAEZ, A. & MCGRATH, M. S. 2005. Evidence for systemic immune system alterations in sporadic amyotrophic lateral sclerosis (sALS). *Journal of Neuroimmunology,* 159**,** 215-224.

ZHANG, W., COLAVITA, A. & NGSEE, J. K. 2017. Mitigating Motor Neuronal Loss in C. elegans Model of ALS8. *Scientific reports,* 7**,** 11582-11582.

ZHANG, X., WANG, F., HU, Y., CHEN, R., MENG, D., GUO, L., LV, H., GUAN, J. & JIA, Y. 2020. In vivo stress granule misprocessing evidenced in a FUS knock-in ALS mouse model. *Brain,* 143**,** 1350-1367.

ZHANG, Z., ALMEIDA, S., LU, Y., NISHIMURA, A. L., PENG, L., SUN, D., WU, B., KARYDAS, A. M., TARTAGLIA, M. C. & FONG, J. C. 2013. Downregulation of microRNA-9 in iPSC-derived neurons of FTD/ALS patients with TDP-43 mutations. *PloS one,* 8**,** e76055.

ZHAO, W., BEERS, D. R., BELL, S., WANG, J., WEN, S., BALOH, R. H. & APPEL, S. H. 2015. TDP-43 activates microglia through NF-κB and NLRP3 inflammasome. *Exp Neurol,* 273**,** 24-35.

ZHAO, W., BEERS, D. R., HOOTEN, K. G., SIEGLAFF, D. H., ZHANG, A., KALYANA-SUNDARAM, S., TRAINI, C. M., HALSEY, W. S., HUGHES, A. M., SATHE, G. M., LIVI, G. P., FAN, G.-H. & APPEL, S. H. 2017. Characterization of Gene Expression Phenotype in Amyotrophic Lateral Sclerosis Monocytes. *JAMA neurology,* 74**,** 677-685.

ZHAO, Y. G., LIU, N., MIAO, G., CHEN, Y., ZHAO, H. & ZHANG, H. 2018. The ER Contact Proteins VAPA/B Interact with Multiple Autophagy Proteins to Modulate Autophagosome Biogenesis. *Current Biology,* 28**,** 1234-1245.e4.

ZHOU, H., HUANG, C., CHEN, H., WANG, D., LANDEL, C. P., XIA, P. Y., BOWSER, R., LIU, Y.-J. & XIA, X. G. 2010. Transgenic rat model of neurodegeneration caused by mutation in the TDP gene. *PLoS genetics,* 6**,** e1000887.

ZHOU, X., WAHANE, S., FRIEDL, M. S., KLUGE, M., FRIEDEL, C. C., AVRAMPOU, K., ZACHARIOU, V., GUO, L., ZHANG, B., HE, X., FRIEDEL, R. H. & ZOU, H. 2020. Microglia and macrophages promote corralling, wound compaction and recovery after spinal cord injury via Plexin-B2. *Nat Neurosci,* 23**,** 337-350.

ZHU, Q., JIANG, J., GENDRON, T. F., MCALONIS-DOWNES, M., JIANG, L., TAYLOR, A., DIAZ GARCIA, S., GHOSH DASTIDAR, S., RODRIGUEZ, M. J. & KING, P. 2020. Reduced C9ORF72 function exacerbates gain of toxicity from ALS/FTD-causing repeat expansion in C9orf72. *Nature neuroscience,* 23**,** 615-624.

ZINSZNER, H., SOK, J., IMMANUEL, D., YIN, Y. & RON, D. 1997. TLS (FUS) binds RNA in vivo and engages in nucleo-cytoplasmic shuttling. *Journal of cell science,* 110**,** 1741-1750.

ZONDLER, L., MÜLLER, K., KHALAJI, S., BLIEDERHÄUSER, C., RUF, W. P., GROZDANOV, V., THIEMANN, M., FUNDEL-CLEMES, K., FREISCHMIDT, A., HOLZMANN, K., STROBEL, B., WEYDT, P., WITTING, A., THAL, D. R., HELFERICH, A. M., HENGERER, B., GOTTSCHALK, K. E., HILL, O., KLUGE, M., LUDOLPH, A. C., DANZER, K. M. & WEISHAUPT, J. H. 2016.

Peripheral monocytes are functionally altered and invade the CNS in ALS patients. *Acta Neuropathol,* 132**,** 391-411.

ZWIEGERS, P., LEE, G. & SHAW, C. A. 2014. Reduction in hSOD1 copy number significantly impacts ALS phenotype presentation in G37R (line 29) mice: implications for the assessment of putative therapeutic agents. *Journal of Negative Results in BioMedicine,* 13**,** 14.

9 Appendix

			Male - p value change from WT								
			6 Months			12 Months			18 Months		
	Paw	Parameter	P56S/+	P56S/P56S	KO/KO	P56S/+	P56S/P56S	KO/KO	P56S/+	P56S/P56S	KO/KO
Paw Size	LF	Max Contact Area	0.3058	0.7184	0.4039	0.0829	0.2937	0.8503	0.1648	0.1237	0.5918
	RF	Max Contact Area	0.1827	0.9525	0.6159	0.278	0.7973	0.9863	0.1365	0.1997	0.6232
	LH	Max Contact Area	0.0231	0.0612	0.0444	0.9441	0.1057	0.2637	0.1451	0.0746	0.1774
	RH	Max Contact Area	0.0914	0.0395	0.0889	>0.9999	0.2535	0.6962	0.0954	0.0712	0.2944
	LF	Max Contact At	0.934	0.2974	0.6336	0.932	0.3291	0.9062	0.8563	0.2813	0.3254
	RF	Max Contact At	0.6589	0.287	0.543	0.9881	0.5308	0.8127	0.9844	0.9321	0.1052
	LH	Max Contact At	0.6567	0.3657	0.1802	0.4659	0.3612	0.351	0.6855	0.509	0.298
	RH	Max Contact At	0.366	0.779	0.123	0.4203	0.075	0.8679	0.9089	0.4848	0.5095
	LF	Print Area	0.2049	0.5483	0.3006	0.1012	0.233	0.8172	0.1159	0.0749	0.4793
	RF	Print Area	0.114	0.8224	0.4486	0.3412	0.6974	0.9767	0.0901	0.1072	0.3867
	LH	Print Area	0.0291	0.0797	0.063	0.961	0.1683	0.416	0.1426	0.0926	0.1821
	RH	Print Area	0.0437	0.0249	0.0461	>0.9999	0.265	0.7283	0.1185	0.0961	0.2986
	LF	Print Length	0.9975	0.6696	0.3123	0.3627	0.2392	0.5422	0.4214	0.113	0.1412
	RF	Print Length	0.7375	0.7393	0.4143	0.5821	0.4284	0.6962	0.2492	0.1035	0.1206
	LH	Print Length	0.0942	0.0666	0.0532	>0.9999	0.2161	0.6906	0.0714	0.0388	0.1254
	RH	Print Length	0.0107	0.0372	0.0099	>0.9999	0.187	0.6466	0.1882	0.0972	0.3113
	LF	Print Width	0.4923	0.9796	0.3693	0.2176	0.4327	0.2334	0.0348	0.1178	0.1531
	RF	Print Width	0.0722	0.9097	0.1295	0.5528	0.739	0.5766	0.1711	0.1646	0.2407
	LH	Print Width	0.0334	0.1274	0.1719	0.9967	0.175	0.7242	0.2576	0.0972	0.2992
	RH	Print Width	0.2537	0.0977	0.3863	>0.9999	0.2202	0.9307	0.1591	0.135	0.5535
Paw Pressure	LF	Max Contact Max Intensity	0.0209	0.4368	0.2721	0.8766	0.1267	0.3161	0.0482	0.0746	0.2515
	RF	Max Contact Max Intensity	0.0434	0.0743	0.1955	0.9608	0.0468	0.1729	0.1372	0.0251	0.1819
	LH	Max Contact Max Intensity	0.2236	0.0347	0.0451	0.8676	0.0035	0.1338	0.0428	0.0102	0.1916
	RH	Max Contact Max Intensity	0.2259	0.0991	0.0393	0.9904	0.0167	0.401	0.1182	0.0219	0.1034
	LF	Max Contact Mean Intensity	0.6173	0.3569	0.0623	0.9952	0.1533	0.2964	0.0523	0.0058	0.1506
	RF	Max Contact Mean Intensity	0.9845	0.4855	0.1613	0.9006	0.0447	0.2885	0.371	0.0245	0.1608
	LH	Max Contact Mean Intensity	0.5135	0.1836	0.088	0.9053	0.0134	0.3144	0.1081	0.0133	0.3692
	RH	Max Contact Mean Intensity	0.8172	0.1462	0.2959	>0.9999	0.062	0.8953	0.2113	0.023	0.2916
	LF	Max Intensity	0.0107	0.3953	0.1521	0.7639	0.1983	0.4148	0.0484	0.0511	0.2457
	RF	Max Intensity	0.0308	0.0867	0.1848	0.9625	0.0289	0.2207	0.0524	0.006	0.0876
	LH	Max Intensity	0.1919	0.0274	0.0558	0.8797	0.0029	0.1362	0.0226	0.0117	0.1746
	RH	Max Intensity	0.0967	0.0952	0.0238	0.9875	0.0154	0.454	0.1357	0.0215	0.0939
	LF	Max Intensity At	0.4441	0.0834	0.9705	0.9933	0.2146	0.9985	0.7958	0.034	0.3585
	RF	Max Intensity At	0.0601	0.9973	0.1125	0.6987	>0.9999	0.5479	0.7941	0.7605	0.6929
	LH	Max Intensity At	0.9978	0.8935	0.8958	0.9205	0.1515	0.8023	0.7525	0.0203	0.1087
	RH	Max Intensity At	0.0644	0.0378	0.0232	0.9501	0.2543	0.3392	0.6161	0.0117	0.0053
	LF	Mean Intensity	0.6597	0.5715	0.0556	0.894	0.3419	0.4277	0.1004	0.0116	0.2205
	RF	Mean Intensity	0.9926	0.6345	0.1187	0.9636	0.1098	0.4145	0.7116	0.084	0.469
	LH	Mean Intensity	0.7197	0.1633	0.1186	0.8527	0.017	0.2091	0.2645	0.0212	0.3448
	RH	Mean Intensity	0.3336	0.1992	0.1673	0.9908	0.1342	0.643	0.2387	0.0305	0.3892
	LF	Min Intensity	0.002	0.9906	0.0914	0.1742	0.3036	0.4994	0.3071	0.9861	0.9991
	RF	Min Intensity	0.0005	0.9826	0.2434	0.9868	0.0321	0.2818	0.6191	0.7556	0.5063
	LH	Min Intensity	0.0011	0.042	0.0935	0.8304	0.022	0.1162	0.5613	0.0545	0.3322
	RH	Min Intensity	0.001	0.0221	0.0767	0.9768	0.1358	0.6649	0.6476	0.146	0.6257

			Male - p value change from WT								
			6 Months			12 Months			18 Months		
	Paw	Parameter	P56S/+	P56S/P56S	KO/KO	P56S/+	P56S/P56S	KO/KO	P56S/+	P56S/P56S	KO/KO
Support	LF	Duty Cycle	0.3047	0.9219	0.2335	0.2712	0.357	0.9077	0.9879	0.9993	0.9812
	RF	Duty Cycle	0.323	0.8733	0.2995	0.8448	0.454	0.9936	0.9984	0.995	0.9356
	LH	Duty Cycle	0.013	0.924	0.0406	0.998	0.9286	0.6855	0.625	0.7278	0.5597
	RH	Duty Cycle	0.0522	0.5958	0.1116	0.8705	0.922	>0.9999	0.6812	0.7383	0.8718
	LF	Stand	0.5793	0.8012	0.5888	0.5383	0.6006	0.9848	0.9332	0.8658	0.9965
	RF	Stand	0.6424	0.7353	0.6628	0.7475	0.5216	0.9904	0.9898	0.9523	0.9955
	LH	Stand	0.2207	0.9441	0.3872	0.8398	0.9002	0.9907	0.9736	0.9923	0.8641
	RH	Stand	0.2753	0.9986	0.4217	0.5438	0.6081	0.9989	0.9862	0.9995	0.9828
	LF	Swing	0.5827	0.7016	0.6973	0.9925	0.9752	0.9998	0.944	0.629	0.9776
	RF	Swing	0.7784	0.9342	0.8964	0.9547	0.9729	0.9186	0.7284	0.5095	0.9941
	LH	Swing	0.1398	0.2229	0.3114	0.312	0.052	0.346	0.2517	0.1852	0.2747
	RH	Swing	0.0895	0.1709	0.0699	0.8551	0.7865	0.9821	0.2243	0.223	0.5316
		BoS Front	0.7443	0.8852	0.9981	0.8722	0.6834	0.9957	0.8732	0.4913	0.9067
		BoS Hind	0.6937	0.9934	0.714	0.0095	0.0023	0.2551	0.2317	0.0335	0.5528
		Support Diagonal	0.0787	0.953	0.2783	0.9988	0.1179	0.3536	0.8788	0.3486	0.3905
		Support Four	0.3078	0.949	0.7186	0.5613	0.4531	0.9206	0.8344	0.9853	0.981
		Support Girdle	0.9602	0.6919	0.8882	0.9191	0.5601	0.9988	0.4996	0.8325	0.9551
		Support Lateral	0.6429	0.8133	0.9992	0.2115	0.4716	0.6031	0.9917	0.8768	0.8755
		Support Single	0.1356	0.5839	0.4383	0.7038	>0.9999	0.9553	0.5411	0.6522	0.6712
		Support Three	0.066	>0.9999	0.097	0.5151	0.2922	0.8633	0.9902	0.9864	0.9995
		Support Zero	0.7618		0.7586	0.7618	0.72	0.7618	0.6771	0.5921	0.6771
Temporal	LF	Step Cycle	0.8518	0.7322	0.8038	0.8055	0.7851	0.9944	0.9046	0.8347	0.9863
	RF	Step Cycle	0.935	0.7852	0.8738	0.857	0.6115	0.9733	0.9557	0.8906	0.9984
	LH	Step Cycle	0.722	0.8276	0.7334	0.5946	0.4859	0.9994	0.9917	0.9319	0.9886
	RH	Step Cycle	0.7173	0.9413	0.7978	0.5251	0.4889	0.9998	0.9899	0.8907	0.9999
	LF	Swing Speed	0.9849	0.9761	0.9053	0.9961	0.9991	0.7518	0.9926	0.9709	0.6746
	RF	Swing Speed	0.9728	0.9862	0.9345	0.9998	0.8906	0.8443	>0.9999	0.9788	0.892
	LH	Swing Speed	0.9881	0.6208	0.9862	0.7514	0.2965	0.9757	0.8907	0.3788	0.9889
	RH	Swing Speed	0.9912	0.595	0.9834	0.9991	0.8194	0.7665	0.9716	0.689	0.9894
		Average Speed	0.8323	0.9797	0.718	0.9152	0.8635	0.8434	>0.9999	0.9478	0.8764
		Maximum Variation	0.7236	0.8463	0.9795	0.7846	0.7094	>0.9999	0.3096	0.1719	0.9616
		Run Duration	0.7577	0.9305	0.6929	0.6486	0.437	0.9988	0.6117	0.3133	0.9202

			Male - p value change from WT								
			6 Months			12 Months			18 Months		
	Paw	Parameter	P56S/+	P56S/P56S	KO/KO	P56S/+	P56S/P56S	KO/KO	P56S/+	P56S/P56S	KO/KO
Placement	LF	Stride Length	0.5403	0.9945	0.4673	0.9999	0.8652	0.5848	0.9265	0.9999	0.4731
	RF	Stride Length	0.4406	0.9869	0.4548	>0.9999	0.9515	0.6307	0.9292	0.9977	0.5024
	LH	Stride Length	0.3957	0.9791	0.7547	0.9988	0.9525	0.5357	0.932	0.9829	0.6598
	RH	Stride Length	0.4252	0.8793	0.6193	0.9039	0.9749	0.4378	0.8783	0.9982	0.4485
		Print Positions Left	0.9932	>0.9999	0.9951	0.821	0.9985	0.6956	>0.9999	0.9847	0.6203
		Print Positions Right	>0.9999	0.7884	0.895	0.9961	0.9945	0.2484	0.9816	0.9729	0.1134
Coordination		Cadence	0.9348	0.9019	0.7519	0.7057	0.6259	0.9885	0.8393	0.8808	0.985
		Number of Patterns	0.4227	0.9789	0.4879	0.58	0.9916	0.3335	0.9072	0.9986	0.4877
		Phase Dispersions LF->LH	0.9458	0.7215	0.1802	0.7973	0.5861	0.054	0.9465	0.9024	0.9999
		Phase Dispersions LF->RF	0.9868	0.9998	0.9969	0.39	0.593	0.5994	0.9938	0.9466	0.9979
		Phase Dispersions LF->RH	0.7301	0.4019	0.9291	0.6219	0.9822	0.3438	0.9777	0.8959	0.9216
		Phase Dispersions LH->RH	0.9996	0.9981	0.9941	0.4449	0.564	0.3179	0.951	0.9014	0.8968
		Phase Dispersions RF->LH	0.8169	0.319	>0.9999	0.391	0.0974	0.0692	0.5874	0.3355	0.4759
		Phase Dispersions RF->RH	0.6212	0.7688	0.1846	0.2093	0.1516	0.7737	0.9561	0.4457	0.6742
		Regularity Index	0.5056	0.488	0.8214	0.3262	0.5653	0.4382	0.899	0.1085	0.739
		Step Sequence AA									
		Step Sequence AB	>0.9999	0.6996	0.5999	0.3615	0.0575	0.7759	0.9905	0.9538	0.9682
		Step Sequence CA	>0.9999	0.2444	0.9298	0.4482	0.1727	0.7738	0.4217	0.8439	0.991
		Step Sequence CB	0.997	0.9878	0.8635	0.7941	0.3824	0.6393	0.9479	0.9975	0.8839
		Step Sequence RA		0.7586	0.7586	0.7618	0.4552	0.4951			0.7586
		Step Sequence RB	0.7618	0.6347	0.8981	0.9965	0.9197	0.9969			
	LF	Stand Index	0.1818	0.9895	0.2594	0.9372	0.9489	0.942	0.5512	0.9992	0.9933
	RF	Stand Index	0.2112	0.9999	0.2162	0.9881	0.8798	0.968	0.9462	0.8147	0.9992
	LH	Stand Index	0.9877	0.7394	0.9703	0.7353	0.8961	>0.9999	0.8429	0.9858	>0.9999
	RH	Stand Index	0.9489	0.9872	>0.9999	0.44	0.6297	>0.9999	0.5447	0.86	0.4985
Other		Number of Steps	0.4003	0.8999	0.5039	>0.9999	0.9444	0.6372	0.98	>0.9999	0.4073
		Other Statistics Abdomen									
		Other Statistics Genitals	0.4998								
		Other Statistics Left Hip									
		Other Statistics Left Knee									
		Other Statistics Nose	0.6438	0.74	0.988	>0.9999	0.4656	0.9902	0.9934	0.9928	0.9977
		Other Statistics Right Hip									
		Other Statistics Right Knee									
		Other Statistics Tail	0.7618								

Table 9.1: p-values from analysis of Run Statistics parameters produced by CatWalk XT 8.1 software for male animals.

Parameters have been grouped into 7 categories: Paw Size, Paw Pressure, Support, Temporal, Placement, Coordination, and Other. Some parameters were calculated for each individual paw and have been grouped together in the following order: left front (LF), right front (RF), left hind (LH), and right hind (RH). p-values in blue indicate a decrease in value from wild type, and values in red indicate an increase in value from wild type. Figures in chapter 4 represent reductions in paw pressure parameters for vapBP56S/P56S seen here at 18 months.

			Female - p value change from WT								
			6 Months			12 Months			18 Months		
	Paw	Parameter	P56S/+	P56S/P56S	KO/KO	P56S/+	P56S/P56S	KO/KO	P56S/+	P56S/P56S	KO/KO
Paw Size	LF	Max Contact Area	0.883	0.421	0.0968	0.5907	0.9963	0.6822	0.2305	0.0056	0.0075
	RF	Max Contact Area	0.9877	0.9303	0.0537	0.6588	0.4068	0.1903	0.0542	0.0015	0.0013
	LH	Max Contact Area	0.9797	0.7754	0.2631	0.8924	0.9997	0.3507	0.043	<0.0001	0.0019
	RH	Max Contact Area	0.3156	0.1787	0.0198	0.9977	0.9822	0.0037	0.0685	0.0032	0.0273
	LF	Max Contact At	0.7021	0.208	0.9944	0.506	0.152	0.9682	0.0811	0.1048	0.9526
	RF	Max Contact At	0.9645	0.104	0.418	0.616	0.9963	0.2299	0.2342	0.704	0.5747
	LH	Max Contact At	0.7345	0.7276	0.3378	0.9473	0.5503	0.962	0.5307	0.0096	0.0154
	RH	Max Contact At	0.7204	0.2207	0.0347	0.8956	0.0504	0.5218	0.2219	0.0042	0.012
	LF	Print Area	0.8571	0.3511	0.0633	0.6748	>0.9999	0.4386	0.1883	0.0063	0.0091
	RF	Print Area	0.9975	0.693	0.0516	0.6607	0.3819	0.0998	0.0646	0.0011	0.0015
	LH	Print Area	0.913	0.6305	0.0909	0.8767	0.9793	0.2694	0.0422	<0.0001	0.0019
	RH	Print Area	0.3322	0.1333	0.0077	0.9964	>0.9999	0.0513	0.0594	0.0037	0.032
	LF	Print Length	0.7694	0.2724	0.0302	0.9505	0.5789	0.674	0.887	0.0016	0.0013
	RF	Print Length	0.8969	0.2748	0.0773	0.8772	0.8116	0.6529	0.6498	0.0092	0.0084
	LH	Print Length	0.9792	0.8212	0.1158	0.9873	0.4916	0.2517	0.1508	0.0003	0.0062
	RH	Print Length	0.7254	0.0766	0.0041	>0.9999	0.926	0.4483	0.1777	0.0021	<0.0001
	LF	Print Width	0.668	0.3187	0.0345	>0.9999	0.9671	0.9936	0.0169	0.0005	0.0009
	RF	Print Width	0.5632	0.3067	0.0858	0.9978	0.8893	0.8309	0.1263	0.014	0.0281
	LH	Print Width	>0.9999	0.812	0.4928	0.64	0.998	0.6305	0.2882	0.0004	0.0004
	RH	Print Width	0.8978	0.139	0.0126	0.9098	>0.9999	0.0601	0.5661	0.0037	0.0208
Paw Pressure	LF	Max Contact Max Intensity	0.944	0.7119	0.0538	0.9721	0.3428	0.098	0.1072	0.0051	0.0003
	RF	Max Contact Max Intensity	0.4185	0.3177	0.0216	0.8767	0.9929	0.9952	0.1314	0.0106	0.0588
	LH	Max Contact Max Intensity	0.9498	0.9069	0.0611	0.8839	0.9992	0.2005	0.447	0.0025	0.0089
	RH	Max Contact Max Intensity	0.6584	0.0833	0.0061	0.97	0.9996	0.139	0.0755	0.0109	0.0095
	LF	Max Contact Mean Intensity	0.3596	0.7842	0.0294	0.6052	0.3628	0.1271	0.1859	0.0021	0.0019
	RF	Max Contact Mean Intensity	0.9164	0.914	0.0238	0.9482	0.8047	0.4578	0.01	0.0115	0.0073
	LH	Max Contact Mean Intensity	0.2822	0.963	0.2908	0.8885	0.8714	0.1706	0.4426	0.0006	0.0248
	RH	Max Contact Mean Intensity	0.9762	0.5777	0.2963	0.9232	0.9905	0.0321	0.2414	0.007	0.0304
	LF	Max Intensity	0.9774	0.5565	0.022	0.8048	0.1827	0.0403	0.1376	0.0051	0.005
	RF	Max Intensity	0.8962	0.3569	0.0062	0.9689	0.9841	0.8106	0.1376	0.0074	0.0392
	LH	Max Intensity	0.9663	0.8325	0.0641	0.7934	0.9984	0.2476	0.4365	0.0033	0.0083
	RH	Max Intensity	0.7386	0.0811	0.0048	0.9836	0.9984	0.1575	0.1167	0.0111	0.0068
	LF	Max Intensity At	0.5351	0.9034	0.9214	0.8836	0.4054	0.5432	0.8882	0.7651	0.0846
	RF	Max Intensity At	0.8031	0.7385	0.9981	0.7333	0.9226	0.8428	0.9008	0.8905	0.1947
	LH	Max Intensity At	0.9988	0.9276	0.9874	0.4993	0.9756	0.9874	0.97	0.0223	0.6499
	RH	Max Intensity At	0.7836	0.9845	0.7226	0.5385	0.5662	0.9404	0.8941	0.0683	0.2375
	LF	Mean Intensity	0.3112	0.6545	0.0471	0.4529	0.323	0.1627	0.1844	0.004	0.0029
	RF	Mean Intensity	0.7073	>0.9999	0.0754	0.899	0.3466	0.3061	0.0684	0.0176	0.0102
	LH	Mean Intensity	0.2281	0.9584	0.3668	0.817	0.669	0.2095	0.5494	0.0013	0.0149
	RH	Mean Intensity	0.9923	0.6205	0.021	0.924	0.8595	0.0717	0.2348	0.0066	0.0374
	LF	Min Intensity	0.8139	0.2626	0.0409	>0.9999	0.8171	0.9938	0.1618	0.0033	0.0008
	RF	Min Intensity	0.9795	0.586	0.0023	0.9312	0.3026	0.5639	0.2436	0.0246	0.0059
	LH	Min Intensity	0.3494	0.6998	0.0607	0.9981	0.8468	0.9911	0.1235	0.0298	0.1062
	RH	Min Intensity	0.2483	0.3999	0.0027	0.9743	0.3789	0.1089	0.258	0.1115	0.1641

			Female - p value change from WT								
			6 Months			12 Months			18 Months		
	Paw	Parameter	P56S/+	P56S/P56S	KO/KO	P56S/+	P56S/P56S	KO/KO	P56S/+	P56S/P56S	KO/KO
Support	LF	Duty Cycle	0.9981	0.4344	0.0007	0.9153	>0.9999	0.154	0.81	0.0983	0.0482
	RF	Duty Cycle	0.9973	0.9788	0.0285	0.9643	0.7219	0.293	0.3037	0.5759	0.0359
	LH	Duty Cycle	0.9588	0.7631	0.1078	0.6148	>0.9999	0.1584	0.1789	0.1056	0.0581
	RH	Duty Cycle	0.9917	0.63	0.0209	0.5277	0.9979	0.3219	0.0584	0.3735	0.0025
	LF	Stand	0.9613	0.9522	0.017	0.6021	0.9913	0.1214	0.2139	0.9478	0.1132
	RF	Stand	0.9882	0.9989	0.0575	0.6935	0.9933	0.149	0.2684	0.9616	0.191
	LH	Stand	0.9972	0.987	0.3015	0.5561	>0.9999	0.0951	0.2004	0.3358	0.0943
	RH	Stand	0.9998	0.9474	0.3548	0.5388	0.8696	0.1457	0.3226	0.5244	0.1948
	LF	Swing	0.5126	0.8555	0.2916	0.3568	0.6883	0.549	0.3124	0.7653	0.1813
	RF	Swing	0.999	0.9995	0.1983	0.1223	0.1607	0.2117	0.5224	0.742	0.0922
	LH	Swing	0.9092	0.7741	0.8574	0.4954	0.947	0.0699	0.2833	0.0101	0.0689
	RH	Swing	0.8113	0.5637	0.454	0.9789	0.9379	0.2407	0.8261	0.084	0.0663
		BoS Front	0.9839	0.9146	0.0284	0.9988	0.9158	0.0538	0.7841	0.0358	0.0145
		BoS Hind	0.4404	0.9483	0.3487	0.7412	0.6123	0.7999	0.5849	0.6523	0.9994
		Support Diagonal	0.2406	0.3885	0.7965	0.9596	0.4869	0.9991	0.8666	0.1208	0.6525
		Support Four	0.9561	0.8139	0.7432	0.7683	0.7586		0.4436	0.6251	0.4981
		Support Girdle	0.5759	0.2037	0.445	0.9608	0.9769	0.9712	0.2708	0.3768	0.9301
		Support Lateral	0.9185	0.9447	0.0905	0.9986	0.9767	0.7163	0.9908	0.9997	>0.9999
		Support Single	0.9357	0.689	0.0049	0.7949	>0.9999	0.2336	0.1608	0.172	0.0007
		Support Three	0.5044	0.9951	0.2499	0.9996	0.2988	0.8183	0.9816	0.8797	0.3755
		Support Zero		0.4751	0.0878	0.7683		0.4099		0.3762	0.5037
Temporal	LF	Step Cycle	0.8284	0.9902	0.2094	0.4356	0.8936	0.0882	0.1355	0.993	0.2678
	RF	Step Cycle	0.9458	0.9962	0.2808	0.3794	0.937	0.083	0.1555	0.9946	0.4453
	LH	Step Cycle	0.9652	>0.9999	0.5112	0.5101	0.9998	0.0876	0.2549	0.9697	0.4217
	RH	Step Cycle	>0.9999	0.9992	0.543	0.7104	0.9598	0.082	0.6461	0.9199	0.8949
	LF	Swing Speed	0.9301	0.823	0.6621	0.4434	0.5051	0.0186	0.3731	0.9993	0.7784
	RF	Swing Speed	0.9266	0.5996	0.6238	0.3956	0.1564	0.0242	0.3904	>0.9999	0.9674
	LH	Swing Speed	0.9899	0.7565	0.215	0.5921	0.5091	0.0513	0.9113	0.1679	>0.9999
	RH	Swing Speed	0.9546	0.9294	0.4738	0.7639	0.6086	0.0349	0.5937	0.0893	0.9719
		Average Speed	0.9878	0.8297	0.2436	0.5139	0.9737	0.046	0.2826	0.9434	0.2246
		Maximum Variation	0.2281	0.1271	0.2437	0.7762	0.8668	0.6765	0.5785	0.9067	0.9825
		Run Duration	0.8048	0.9364	0.2912	0.247	0.9525	0.0315	0.4571	0.998	0.6419

			Female - p value change from WT								
			6 Months			12 Months			18 Months		
	Paw	Parameter	P56S/+	P56S/P56S	KO/KO	P56S/+	P56S/P56S	KO/KO	P56S/+	P56S/P56S	KO/KO
Placement	LF	Stride Length	0.8007	0.4377	0.0912	0.5388	0.8258	0.0283	0.4829	0.9542	0.1681
	RF	Stride Length	0.9234	0.3518	0.0975	0.7067	0.9029	0.0396	0.4956	0.9712	0.1847
	LH	Stride Length	0.8922	0.323	0.0541	0.6726	0.6284	0.0603	0.4506	0.9983	0.2847
	RH	Stride Length	0.9353	0.4192	0.0408	0.5793	0.6097	0.0161	0.3225	0.9514	0.1467
		Print Positions Left	0.6851	0.478	0.6717	0.4811	0.7106	0.1858	0.2097	0.9979	0.1987
		Print Positions Right	0.6991	0.5952	0.2297	0.2691	0.7077	0.1597	0.2864	0.9928	0.1885
Coordination		Cadence	0.9947	0.9987	0.2742	0.3864	0.9896	0.0756	0.1577	0.906	0.3719
		Number of Patterns	0.9469	0.3963	0.1752	0.8207	0.9395	0.1462	0.6873	0.5933	0.2755
		Phase Dispersions LF->LH	0.5755	0.6935	0.2161	0.5458	0.8522	0.8421	0.9982	0.9656	0.7735
		Phase Dispersions LF->RF	0.8117	>0.9999	0.9909	0.8188	0.7068	0.8348	0.813	>0.9999	>0.9999
		Phase Dispersions LF->RH	0.9668	0.6029	0.0239	0.9912	0.9993	0.4743	0.5106	0.9302	0.9322
		Phase Dispersions LH->RH	0.6407	0.9674	0.2331	0.8616	0.9727	0.9799	>0.9999	0.9993	0.5504
		Phase Dispersions RF->LH	0.8411	0.9997	0.08	0.9464	0.8104	0.9656	0.6742	0.5244	0.9985
		Phase Dispersions RF->RH	0.9987	0.6682	0.532	0.1012	0.8858	0.4729	0.9603	0.5941	0.1984
		Regularity Index	0.7483	0.9991	0.9621	0.6347	0.6643	0.5972	0.4912	0.3212	0.9699
		Step Sequence AA									
		Step Sequence AB	0.2612	0.3433	0.3357	0.9509	>0.9999	0.517	0.9686	0.4342	0.9967
		Step Sequence CA	0.7683	0.7754	0.3	0.9967	0.8495	0.6867	0.6909	0.6769	0.7631
		Step Sequence CB	0.2401	0.1827	0.3758	0.994	0.983	0.9943	0.7415	0.9798	0.9999
		Step Sequence RA	0.7593	0.9976	0.9794	0.9932	0.7683	>0.9999	0.4518	0.9996	0.956
		Step Sequence RB	0.1306	0.5131		0.9967	0.9984	0.8435	0.7683	0.8965	0.7683
	LF	Stand Index	0.9994	0.8761	0.1985	0.1923	0.8688	0.0481	0.5851	0.679	0.1871
	RF	Stand Index	0.9918	0.5325	0.1306	0.5072	0.9939	0.0945	0.9039	0.9532	0.6995
	LH	Stand Index	0.2758	0.6095	0.5387	0.9969	0.3847	0.5131	0.9387	0.8664	0.3289
	RH	Stand Index	0.9417	0.79	0.7644	0.9974	0.5643	0.654	0.6525	0.5597	0.4378
Other		Number of Steps	0.8381	0.4742	0.0694	0.5561	0.6929	0.0684	0.4661	0.9997	0.1952
		Other Statistics Abdomen									
		Other Statistics Genitals				0.7683	0.7683	0.7683			
		Other Statistics Left Hip									
		Other Statistics Left Knee									
		Other Statistics Nose	0.9967	0.9339	0.9533	0.9891	0.3214	0.6793	0.9584	0.9063	0.9951
		Other Statistics Right Hip									
		Other Statistics Right Knee				0.7683	0.7683	0.7683			
		Other Statistics Tail									

Table 9.2: p-values from analysis of Run Statistics parameters produced by CatWalk XT 8.1 software for female animals.

Parameters have been grouped into 7 categories: Paw Size, Paw Pressure, Support, Temporal, Placement, Coordination, and Other. Some parameters were calculated for each individual paw and have been grouped together in the following order: left front (LF), right front (RF), left hind (LH), and right hind (RH). p-values in blue indicate a decrease in value from wild type, and values in red indicate an increase in value from wild type. Figures in chapter 4 represent reductions in paw pressure and paw size parameters for vapBP56S/P56S and vapB-/- seen here at 18 months.

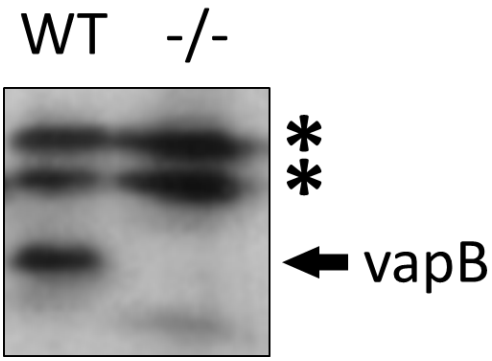

Figure 9.1: vapB#38 against wild type and vapB$^{-/-}$ spinal vapB$^{P56S/+}$ cord homogenates.

Arrow pointing to specific vapB band. Asterisks annotate non-specific cross-reacting band.